Investigation of Potential Organic Markers for Source Apportionment of Ship Emissions via Single-Particle Mass Spectrometry

Cumulative Dissertation

in fulfillment of the requirements for the degree of
doctor rerum naturalium (Dr. rer. nat.)

submitted to
the Faculty of Mathematics and Natural Sciences
of the University of Rostock, Germany

by Lukas Alexander Anders, born on 30th May 1993, in Itzehoe
from Rostock

Rostock, Germany
13th February 2025

https://doi.org/10.18453/rosdok_id00004904

Die vorliegende Arbeit wurde im Arbeitskreis „Analytische Chemie" von Prof. Dr. Ralf Zimmermann am Institut für Chemie an der Universität Rostock angefertigt.

Einreichung der Dissertation:
13.02.2025

Wissenschaftliches Kolloquium:
22.04.2025

1. Gutachter und Betreuer:

Prof. Dr. Ralf Zimmermann, Lehrstuhl für Analytische Chemie, Abteilung Technische und Analytische Chemie, Institut für Chemie, Mathematisch - Naturwissenschaftliche Fakultät, Universität Rostock und Gruppenleiter für Comprehensive Molecular Analytics, Helmholtz Zentrum München

2. Gutachter:

Prof. Dr. Frank Kelly, School of Public Health, Faculty of Medicine, Imperial College London

Rostock, 2025
Place, Date

Signature

"The present is theirs; the future, for which I really worked, is mine."

Nikola Tesla

Kurzzusammenfassung

Die zunehmende Regulierung von Schiffsemissionen durch die Internationale Maritime Organisation (IMO) hinsichtlich gesundheitlicher, ökologischer und klimatischer Aspekte zwingt Reedereien zur Nutzung moderner Treibstoffe. Diese beinhalten oft keine Übergangsmetalle wie Nickel, Eisen oder Vanadium, die ursprünglich zur Quellenidentifizierung von Emissionen des Schiffsverkehrs verwendet wurden. Da diese Emissionen nicht zwangsläufig durch metallische Marker charakterisiert sind, wird ihre Quellenzuordnung erheblich erschwert. Moderne Treibstoffe sind oft teurer und haben trotz der Regulierungsmaßnahmen Auswirkungen auf Gesundheit, Umwelt und Klima. Die vorliegende Dissertation untersucht neuartige organische Marker zur Quellenzuordnung von Schiffsemissionen moderner Treibstoffe. Die Forschungsarbeit fokussiert sich auf die Bestimmung charakteristischer Verteilungen polyzyklischer aromatischer Kohlenwasserstoffe (PAKs) in relevanten Schiffstreibstoffen, insbesondere verschiedener Schweröle (HFOs) und Marine Gasöl (MGO). Zudem wird die Anwendbarkeit von EC/OC-Verhältnissen als potenzielle Schiffsmarker evaluiert. Die Analyse erfolgt mittels moderner Einzelpartikelmassenspektrometrie, die eine simultane Echtzeiterfassung organischer und anorganischer Partikelkomponenten ermöglicht. Diese Methode kombiniert ein bipolares ToF-System mit verschiedenen Laser-Ionisationsmethoden. Die Arbeit demonstriert die erfolgreiche Implementierung dieser Messtechnik in Labor- und Feldexperimenten, identifiziert methodische Limitationen und schlägt Optimierungsansätze für zukünftige Schiffsemissionsmessungen vor.

Abstract

The increasing regulation of ship emissions by the International Maritime Organization (IMO) regarding health, environmental, and climatic aspects compels shipping companies to adopt modern fuels. These often lack transition metals such as nickel, iron, or vanadium, which were traditionally used to identify the source of marine emissions. As these emissions are not necessarily characterized by metallic markers, their source attribution becomes significantly more challenging. Modern fuels are frequently more expensive and continue to impact health, environment, and climate despite regulatory measures. This dissertation investigates novel organic markers for source apportionment of ship emissions from modern fuels. The research focuses on determining characteristic distributions of polycyclic aromatic hydrocarbons (PAHs) in relevant marine fuels, particularly various heavy fuel oils (HFOs) and marine gas oil (MGO). Additionally, the applicability of EC/OC ratios as potential ship markers is evaluated. The analysis employs state-of-the-art single-particle mass spectrometry, enabling simultaneous real-time detection of organic and inorganic particle components. This method combines a bipolar time-of-flight system with laser ionization methods. The study demonstrates the successful implementation of this measurement technology in laboratory and field experiments, identifies methodological limitations, and proposes optimization approaches for future ship emission measurements.

Acknowledgements

Working on single-particles in analytical chemistry with advanced measurement and analysis methods requires a complex scientific understanding of chemistry, physics and the use of various techniques in this field, especially the interpretation of the data. I am grateful to all those who were involved in this work, providing their scientific and non-scientific knowledge as well as help in challenging situations.

First of all, I would like to thank my supervisor, **Professor Dr. Ralf Zimmermann**, for giving me the opportunity to work on such an exciting project. I am also grateful for this instructive time, which has helped me to develop personally. I would also like to thank my co-supervisor **Dr. Johannes Passig**, who provided invaluable ideas and advice to move the work forward. His guidance was instrumental in enabling me to complete this work.

I would also like to thank **Dr. Robert Irsig** and **Thomas Kröger-Badge** for their time, which was often spent discussing theoretical or instrumental issues. Special thanks also for non-scientific discussions to **Marco Schmidt**, **Dr. Haseeb Hakkim**, **Ole Tiemann** and **Dr. Eric Schneider**.

I would like to thank all my friends who have always motivated me to keep going, even in difficult times. I would like to thank **Florian Bauer**, **Thomas Cullot**, **Erika Henell**, **Tom Polte**, **Peter Weinhardt**, **Britta Schäfer**, **Alexander Meinke**, **Jakob Wolansky**, **Helge Dobbertin**, **Nis Meinert**, **Sophie Rhode**, **Eric Meyer**, **Tobias Lipfert**, **Anna-Julia Poser**, **Charlotte Rasch**, **Matthias Scheiter**, **Björn König**, **Martin Preising**, **Katharina Springstein**, **Johanne Nynhuis**, **Ulrike Voßmann**, **Tino Altmann**, **Lisa Zinta**, **Julian Schmidt**, **Anna Graß**, **Jan Ole Stephan**, **Ha-Vy Verbeek**, **Torid Jacob**, **Timea Koch**, **Ann-Christin Maas**, **Vanessa Roßberg**, **Hannes Hollborn** and **Klara Raspe** for being my great friends and supporters! I further have to thank my grandmothers, **Ursula Hytry**, **Marlis Anders** and **Erika Alexander**, without whom I wouldn't have made it this far.

My greatest thank goes to **Paula Bülow** and my sisters **Sarah Rahel Anders** and **Rahel-Katharina Anders**. You are my biggest supporter and motivator, giving me the strength to hold on during my PhD time.

Contents

Contributions to Scientific Publications

Publication 1

Title: Detection of ship emissions from distillate fuel operation via single-particle profiling of polycyclic aromatic hydrocarbons

Authors: Lukas Anders, Julian Schade, Ellen Iva Rosewig, Thomas Kröger-Badge, Robert Irsig, Seongho Jeong, Jan Bendl, Mohammad Reza Saraji-Bozorgzad, Jhih-Hong Huang, Fu-Yi Zhang, Chia C. Wang, Thomas Adam, Martin Sklorz, Uwe Etzien, Bert Buchholz, Hendryk Czech, Thorsten Streibel, Johannes Passig and Ralf Zimmermann

Journal: Environmental Science: Atmospheres

Year: 2023

Contribution: *Lukas Anders participated the measurements, analyzed the data, prepared and designed the figures.*

Publication 2

Title: Polycyclic aromatic hydrocarbons as fuel-dependent markers in ship engine emissions using single-particle mass spectrometry

Authors: Lukas Anders, Julian Schade, Ellen Iva Rosewig, Marco Schmidt, Robert Irsig, Seongho Jeong, Uwe Käfer, Thomas Gröger, Jan Bendl, Mohammad Reza Saraji-Bozorgzad, Thomas Adam, Uwe Etzien, Hendryk Czech, Bert Buchholz, Thorsten Streibel, Johannes Passig and Ralf Zimmermann

Journal: Environmental Science: Atmospheres

Year: 2024

Contribution: *Lukas Anders did the measurements, analyzed the data, prepared and designed the figures and worked on the manuscript.*

Publication 3

Title: Limited Impact of Wet Scrubber Exhaust Treatment on the Chemical Composition of Individual Ship Emission Particles

Authors: Lukas Anders, Martin Bauer, Seongho Jeong, Marco Schmidt, Haseeb Hakkim, Aleksandrs Kalamašņikovs, Ellen Iva Rosewig, Julian Schade, Robert Irsig, Sven Ehlert, Jan Bendl, Mohammad Reza Saraji-Bozorgzad, Martin Sklorz, Uwe Etzien, Bert Buchholz, Thomas Adam, Thorsten Streibel, Hendryk Czech, Johannes Passig and Ralf Zimmermann

Journal: Environmental Chemistry Letters

Year: 2025

Contribution: *Lukas Anders did the investigations, analyzed the data, prepared and designed the figures and worked on the manuscript.*

Publication 4

Title: Impact of Fuel Sulfur Regulations on Carbonaceous Particle Emission from a Marine Engine

Authors: Martin Bauer, Hendryk Czech, Lukas Anders, Johannes Passig, Uwe Etzien, Jan Bendl, Thorsten Streibel, Thomas W. Adam, Bert Buchholz and Ralf Zimmermann

Journal: Npj Climate and Atmospheric Science

Year: 2024

Contribution: *Lukas Anders participated the measurements, analyzed the data, prepared and designed the figure for the single-particle measurement.*

Publication 5

Title: A solid-state IR laser for two-step desorption/ionization processes in single-particle mass spectrometry

Authors: Marco Schmidt, Haseeb Hakkim, Lukas Anders, Aleksandrs Kalamašņikovs, Thomas Kröger-Badge, Robert Irsig, Norbert Graf, Reinhard Kelnberger, Johannes Passig and Ralf Zimmermann

Journal: EGUsphere

Year: 2025

Contibution: *Lukas Anders took part in the measurements and provided technical assistance.*

Abbreviations and Nomenclature

Abbreviations and Nomenclature			
Abbreviation	***Full name***	***Abbreviation***	***Full name***
ART 2-A	Adaptive Resonance Theory 2-A	**BAU**	Business As Usual
BC	Black carbon	**CCN/ IN**	Cloud condensation nuclei/ Ice nuclei
COPD	Chronic obstructive pulmonary disease	**cw**	Continuous wave
DNA	Deoxyribonucleic acid	**DR**	Diagnostic ratio
EC	Elemental carbon	**ECA**	Emission control area
EF	Emission factor	**FHG**	Fourth harmonic generation
FSC	Fuel sulfur content	**GHG**	Greenhouse gas
HFO	Heavy fuel oil	**HVO**	Hydrotreated vegetable oil
ICE	Internal-combustion engine	**IFO**	Intermediate fuel oil
IMO	International Maritime Organization	**LDI**	Laser desorption ionization
LD-REMPI	Laser desorption - resonance-enhanced multiphoton ionization	**MW-TOCA**	Multi-wavelength thermal-optical carbon analysis
LNG	Liquefied Natural Gas	**LSFO**	Low sulfur fuel oil
MCP	Microchannel plate	**MDO**	Marine diesel oil
MGO	Marine gas oil	**NECA**	Nitrogen emission control area
NO_x	Nitrogen oxides	**OC**	Organic carbon
PAH	Polycyclic aromatic hydrocarbon carbon	**PM**	Particulate matter
REMPI	Resonance-enhanced multiphoton ionization	**RF**	Radiative forcing

Abbreviations and Nomenclature			
Abbreviation	***Full name***	***Abbreviation***	***Full name***
Rpm	Revolutions per minute	**ROS**	Reactive oxygen species
SECA	Sulfur emission control area	**SHG**	Second harmonic generation
SO_x	Sulfur oxides	**SPMS**	Single-particle mass spectrometer
ToF	Time-of-flight	**ULSFO**	Ultra-low sulfur fuel oil
VLSFO	Very low sulfur fuel oil	**UV**	Ultraviolet
VOC	Volatile organic compound		

Chapter 1.

Introduction

1.1. Airborne Particles

Aerosols are defined as small solid or liquid particles suspended in a gas, typically in air.[1,2] The term 'particulate matter' (PM) is commonly used to denote particle sizes ranging from 10^{-9} m to several tens of micrometers.[3] PM classification follows size-dependent categories: PM_{10} (coarse particles), $PM_{2.5}$ (fine particles), PM_1 (accumulation mode), and $PM_{0.1}$ (ultrafine particles or Aitken mode). Numerical indices indicate the upper size limit in micrometers (µm).[4,5] An overview of important particle size ranges and definitions of diverse aerosols is shown in Fig. 1.1.

Aerosol particles are produced by two main processes: direct emission to the atmosphere (primary aerosols) and condensation of atmospheric gas-phase species (secondary aerosols formed via gas-to-particle conversion),[3,7] also called 'aerosol precursors'.[6] PM is capable of undergoing dynamic transformations in size and composition through complex physical and chemical processes. In this context, it is particularly noteworthy that particles can coagulate, vapours can condense on particle surfaces, photochemical conversion can occur, and various chemical activation reactions can take place, leading to the formation of cloud- or ice condensation nuclei.[7–9]
Once in the atmosphere, the lifetime of PM is also dependent on its size. $PM_{0.1}$ can remain in the atmosphere for several hours, but typically coagulates and grows into PM_1. These accumulation mode particles can then persist in the atmosphere for several days to weeks, undergoing various processes before being partitioned, oxidized or deposited back onto the Earth's surface.[10,11] In contrast, coarse

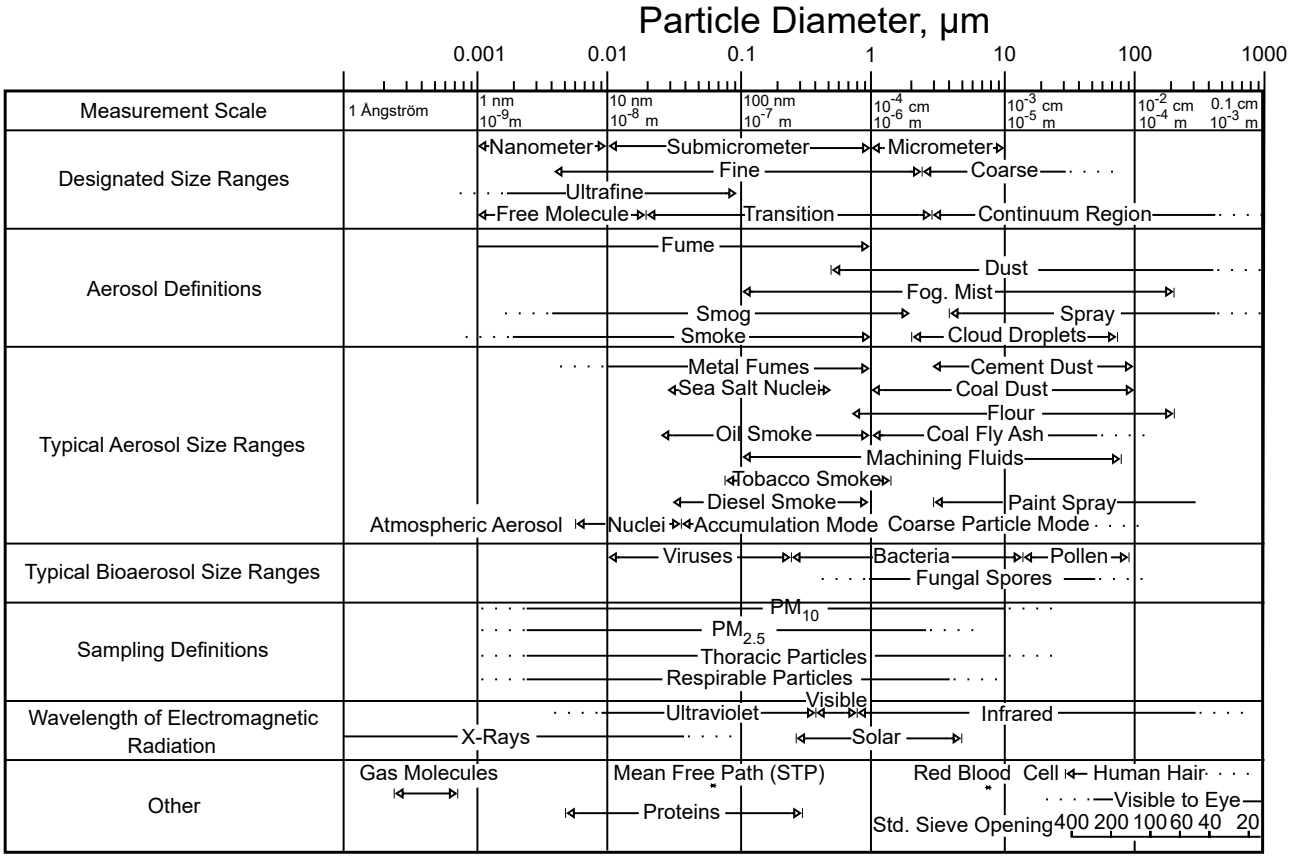

Figure 1.1.: Diverse aerosol type definitions and their size range (modified after Ref. [6]).

mode particles have a relatively short atmospheric lifetime, spanning a period of hours to days before being removed or deposited.[5,12] There is a variety of removal pathways for PM. Among those are oxidation[13,14] and photooxidation,[15,16] hydrolysis[14,17] and removal via atmospheric humidity caused by evapotranspiration,[18] dry deposition and wet deposition evoked by precipitation.[19–21]

Atmospheric particle evolution encompasses complex processes that can vary, including several multiphase reactions such as coagulation, diverse aging processes (photochemical aging, oxidation, photolysis, etc.), the formation of cloud condensation nuclei and ice nuclei (CCN/IN), the removal of PM or CCN/IN by precipitation, and more.[11,22,23] The sources of particles comprise both natural and anthropogenic origins[24] as illustrated in Fig. 1.2. The most common natural sources of PM are volcanic particles, algae, pollen, dust, and soil and sea spray.[5,25] It is noteworthy that the largest contributor of natural primary aerosols (including sea spray) in the atmosphere comes from the marine environment.[25–29] This emphasizes the importance of marine aerosols, as evidenced by Chin et al. (2016) and Dulac et al. (2023).[5,12]
Sources of anthropogenic aerosols include combustion processes of fossil and non-fossil fuels in industry and traffic (e.g. aircraft, cars, and ships), domestic heating and cooling, coal-fired power plants, deforestation, biomass burning, brake and tyre wear, and microplastics among many others.[3,30–32] While natural sources often contribute primary aerosols in the coarse mode, anthropogenic aerosols predominantly occur in the accumulation mode and 'are often of secondary origin'.[12] Consequently, the size range of combustion aerosols is typically smaller than that of non-combustion aerosols, yet they occur in higher concentrations.[33,34] In basic combustion systems or insufficient combustion conditions, the proportion of unburnt particles in the total particle mass can exceed a level of 90 %. Conversely, under optimal combustion conditions, this proportion can decline to a level of less than 1 %.[34]

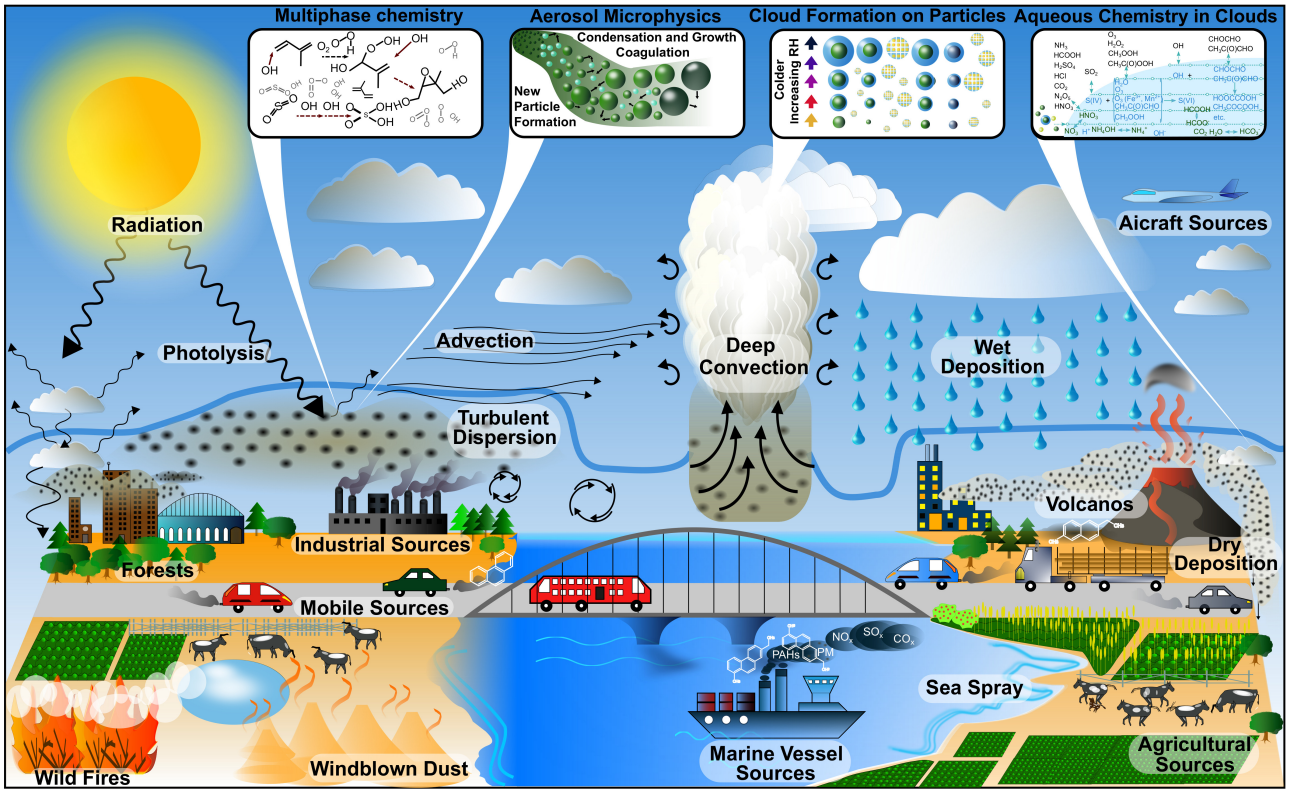

Figure 1.2.: Diverse sources of PM and their processes affecting air quality and atmospheric chemistry (modified after Ref. [35]). Global shipping represents a rapidly expanding and significant source of emissions.[36–38] It accounts for approximately 3 % of greenhouse gas (GHG) emissions,[39,40] with a tendency to increase.[41] Furthermore, ship emissions contribute a range of pollutants to the environment, including soot, sulfur oxides (SO_x), nitrogen oxides (NO_x), and particulate matter (PM).[42,43]

Combustion-derived particles emitted by various sources, including traffic with Otto engines or diesel engines, biomass burning, and wood heating frequently contain a complex mixture of chemicals, including soot (elemental carbon (EC) and organic carbon (OC)), nitrogen oxides (NO_x), sulfur oxides (SO_x), and polycyclic aromatic hydrocarbons (PAHs).[44,45] These chemical compounds can undergo further reactions in the atmosphere. These reactions influence not only meteorological conditions (directly and indirectly) but also air quality and, consequently, human health.[44,46] A more detailed examination of this topic will be provided in Sections 1.2 and 1.3. In this context, the maritime environment is of particular concern. It has a significant impact on the Earth's radiative budget and climate,[12,47] yet a large quantity of natural and combustion-related aerosols are emitted in these environments.[48–51] A considerable portion of anthropogenic aerosols and key pollutants, including PM, soot, volatile organic compounds (VOCs), carbon dioxide (CO_2), NO_x, SO_x, and PAHs originate from global shipping.[42,43] Some compounds of ship emissions arise from the complete combustion process (e.g. CO_2 and SO_x). Others are formed through the oxidation of nitrogen in the intake air (NO_x). However, certain species, such as PAHs, are produced as a result of incomplete combustion of the fuel.[52,53] Since the 1990s, shipping has been identified as one of the fastest-growing sources of greenhouse gases (GHGs) and pollutants, along with aviation. This phenomenon can be attributed to the long-term growth of global shipping.[36,37]

Nowadays, around 90 % of global trade volume is facilitated by maritime transport[54–56] and trends point towards an even higher demand of ships in the future.[38,39,57,58] According to a Business As Usual (BAU) scenario conducted in 2019, the number of ships indexed in 2008 will more than have doubled by 2030.[38] Furthermore, maritime traffic is projected to increase by 240 % to 1,209 % by 2050.[59] This highlights a long-term challenge for governments to reduce greenhouse gas (GHG) emissions, particularly in the context of the Paris Agreement, which came into effect in 2016. The objective of the Paris Agreement is to constrain global warming to 2 °C, preferably to 1.5 °C, through measures aimed at reducing GHG emissions.[41,60] However, global shipping is not unequivocally included,[61] even though ship emissions are known to affect the climate.[62,63] GHGs not only have an adverse impact on the environment; PM emitted in large quantities from ships also contributes to direct and indirect climate effects.[62,64,65]

Today, about 3 % of global emissions can be attributed to ship emissions.[39,40] According to the BAU scenario this fraction may increase to about 10 % by 2050.[38,41] Moreover, in many coastal countries ship emissions already have a significant influence on particle concentrations. Recent calculations show that ships are responsible for at least 10 % of controllable fine particles.[65] Hereinafter, PM can grow through the aforementioned physical and chemical processes. Thus PM can be transported by wind over hundreds of kilometers,[66] affecting not only coastal regions but also ecosystems and people inland, leading to thousands of untimely deaths each year.[67,68] Nowadays, approximately 37 % of the world's population resides within 100 km of the coastline,[69] highlighting a significant concern regarding the global impact of increasing ship emissions.

1.2. Health Impacts of Ship Emissions

Ship emissions, when released into the atmosphere, pose significant concerns due to their impact on human health, ecosystem quality, and climate change.[28,67,70–72] Notably, pollutants such as sulfur oxides (SO_x), nitrogen oxides (NO_x), carbon oxides (CO_x), and high concentrations of $PM_{2.5}$ from ships contribute to various adverse health effects, including cardiorespiratory diseases.[53,73] It is estimated that air pollution, in general, is responsible for approximately seven million untimely deaths annually.[74] Furthermore, sulfur emissions from ships fuel combustion alone have been linked to between 19,000 to 91,000 deaths per year in coastal regions.[75] However, the health consequences cannot be attributed solely to sulfur content. For instance, high sulfur levels in fuels lead to increased PM emissions, which, in turn, have significant health impacts on humans.[76–78]

Depending on its size and surface area, PM from ship emissions, especially $PM_{0.1}$ from combustion, can

penetrate deep into the lungs, reaching alveolar cells, and potentially translocate into the bloodstream (see Fig. 1.3).[79,80] Studies have shown that, in terms of health implications, smaller PM generated by the combustion process tends to have a greater impact than larger PM.[81,82]

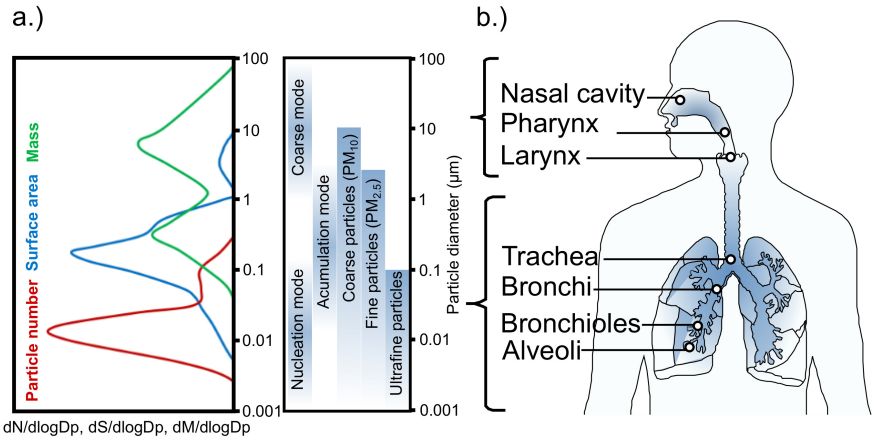

Figure 1.3: a.) The distribution of particle number, surface area, and mass over different size modes (modified after Ref. [4]) provides in b.) insight into the deposition of particles of varying sizes in different regions of the human respiratory tract (modified after Ref. [83]).

Although the human body has mechanisms to clear PM through the mucociliary escalator and the actions of resident macrophages,[84–86] inhaled PM can still induce oxidative stress and pro-inflammatory responses leading to a range of inflammatory reactions and chronic diseases.[87–93] In this context, oxidative stress refers to an imbalance between the production of reactive oxygen species (ROS) and the body's ability to detoxify these reactive intermediates or repair the resulting damage.[94,95] Ship emissions, depending on the type of fuel used, can trigger oxidative stress by carrying metallic constituents such as nickel, iron, and vanadium. For instance, PM containing iron or vanadium interacts with airway cells leading to the formation of free radicals such as superoxide anions (e.g. O_2^-) and hydroxyl radicals ($\bullet$ OH), as well as non-radical molecules like hydrogen peroxide (H_2O_2). These reactive species have the potential to induce oxidative DNA damage, membrane lipid peroxidation, and various metabolic and molecular adverse effects.[96] These effects may differ from those induced by PAHs or other organic PM, which are well known for their mutagenic and carcinogenic potential.[82,97,98]

In mammalian systems, the metabolization of PAHs is primarily regulated by the aryl hydrocarbon receptor (AhR) signalling pathway, which controls xenobiotic metabolizing enzymes such as cytochrome P450 (CYP) enzymes, including CYP1A1 and CYP1B1. These enzymes facilitate the conversion of PAHs into water soluble conjugates for excretion. However, these metabolic processes can also generate reactive intermediates, such as diolepoxides, quinones, and hydroxyalkyl derivates, which are not sufficiently polar for excretion. Instead, they can form covalent adducts with proteins and nucleic acids, leading to oxidative stress, immunotoxicity, genotoxicity, and carcinogenic effects.[99,100] Additionally, other emissions from ships, such as SO_x, pose significant health concerns due to their toxicity.[86,101–103] Marine fuels like heavy fuel oil (HFO), which contain high concentrations of these compounds,[104] are known to be toxic.[102] However, even supposedly cleaner distillate fuels such as marine gas oil (MGO), which contains lower levels of organic compounds, also have the potential to cause acute health effects.[102,105] It is important to note that the interactions of individual particles with the human body vary, leading to different biochemical reactions and a wide range of health effects.[82] Consequently, the resulting damage from PM exposure can result in a range of pathological conditions, resulting in either acute or chronic diseases.[103,106] In the case of acute diseases, the rapid release of inflammatory markers such as cytokines or chemokines leads to an acute inflammatory reaction that can result in increased blood pressure (hypertension), arrhythmias and thrombogenesis, or cardiovascular events such as myocardial infarctions.[107] Conversely, long-term reactions caused by PM result in chronic diseases, including asthma, chronic obstructive pulmonary disease (COPD), lung cancer, atherosclerosis, and others.[108] It is estimated that over 260 million people worldwide are affected by asthma.[109] In 2020, ship emissions were responsible for approximately 265,000 untimely

deaths globally, underscoring the substantial health implications of inhaled PM.[110] A reduction in air pollution, specifically in terms of $PM_{2.5}$ and PM_{10}, has been demonstrated to yield significant benefits, such as increased life expectancy and improved respiratory health.[111] According to Sofiev et al. (2018),[68] the adoption of cleaner marine fuels, such as low-sulfur fuels, in the shipping industry would lead to a 34 % and 54 % reduction in premature mortality and morbidity, respectively. Moreover, cardiovascular and lung cancer deaths would be reduced by a decrease in $PM_{2.5}$. And last but not least, there would be an estimated 3.6 % reduction in childhood asthma.[68] This clearly underlines how marine fuels are linked to human health matters.

1.3. Direct and Indirect Climate Effects

In addition to these health effects, PM from global shipping, particularly $PM_{2.5}$ and PM_{10}, exerts both direct and indirect effects on the climate, as illustrated in Fig. 1.4. They effect the atmosphere, radiative forcing (RF), and cloud formation, thus altering the climate.[70,71] Direct effects through RF is driven by particles absorbing and scattering solar radiation. For instance, RF influenced by soot

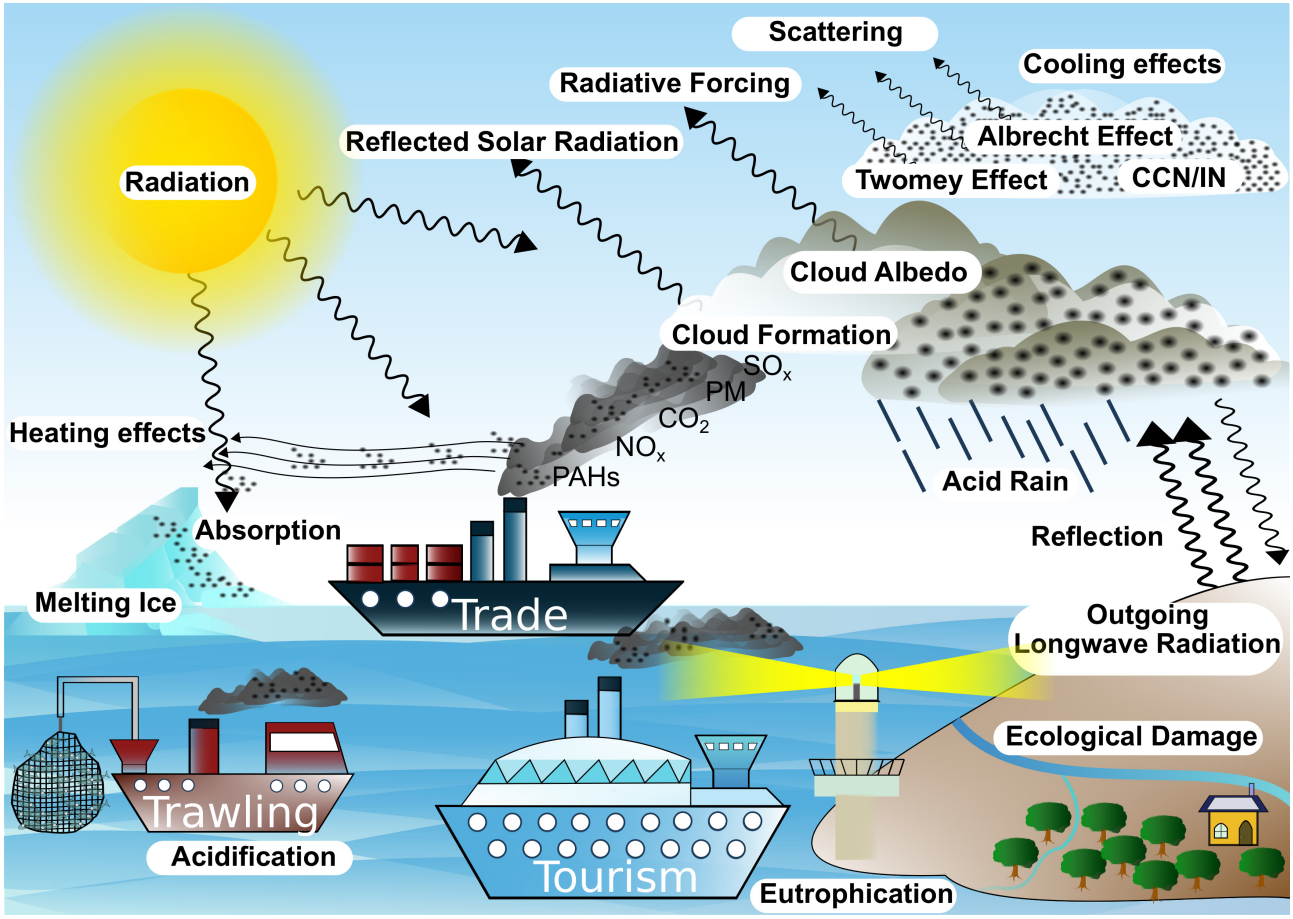

Figure 1.4.: Diverse direct and indirect climate effects evoked by ship emissions. Direct effects: acidification and eutrophication of aquatic systems through particulate matter (PM) containing sulfur or nitrogen;[112,113] Furthermore, the absorption of solar radiation by soot results in a warming effect in the atmosphere and a reduction in the albedo[114] on ice surfaces. Indirect effects: the Twomey effect increases the cloud albedo (reflectance degree) by reducing droplet size due to higher cloud condensation nuclei (CCN) concentrations, such as sulfate aerosols. Smaller droplets enhance solar radiation scattering, resulting in a net cooling effect.[115–117] A cooling effect is also induced by the Albrecht effect, wherein reduced coalescence efficiency leads to an extended cloud lifetime, thereby enhancing prolonged cloud reflectivity.[118]

particles absorbing solar radiation results in localized warming.[119–121] Emitted sulfur, on the other hand, scatters solar radiation and has thus been identified as a potential contributor to cooling of the Earth's surface.[70] As previously stated, PM can act as condensation nuclei, facilitating the formation of water droplets from water vapour.[122,123] An indirect consequence of anthropogenic aerosols from global shipping is the Twomey effect:[115,124] An increase in the aerosol concentrations within the clouds results in a greater number of condensation nuclei. Consequently, an increase in the number of smaller water droplets is observed. This results in a delay in the formation of precipitation. Hence clouds reflect sunlight for longer, increasing the clouds' albedo (reflectance of the clouds' surface), which results in a cooling effect of the Earth's surface.[117,125] Furthermore, a multitude of feedback mechanisms exist, including soil- or surface albedo feedback, black carbon (BC) feedback, albedo-cloud feedback, and so forth. These feedback mechanisms can both reinforce or counteract the aforementioned effects, thereby underscoring the intricate manner in which PM exerts its influence on our climate.[126]
Ship emissions in the form of SO_x and NO_x are significant contributors to atmospheric acidity and influence coastal waters.[112,127] Moreover, sulfurous and nitrogenous compounds possess the capacity to acidify precipitation, potentially causing extensive ecological damage. The acidification of water bodies and soil impacts vegetation, which plays a crucial role for regulating the climate,[70,128] and affects man-made structures.[129] These effects are of high social, health, and environmental concern. Omstedt et al. (2015)[130] demonstrated that the acidification of the Baltic Sea has been decreasing since 1980 by a magnitude of 10^2. This is due to the fact that the emissions leading to an acidification have been reduced in cars and land-based sources. However, the emissions from ships have not been following this trend.[128,130] The increased number of ships underlines the necessity to implement regulations governing ship emissions in order to mitigate the adverse impacts on the environment and human health in the future.

1.4. New Ordinances and the Establishment of Different Emission Control Areas

Despite the well-known environmental and health risks associated with elevated levels of metals, soot, sulfur, and polycyclic aromatic hydrocarbons (PAH) in ship emissions,[53,131] they remain largely unregulated.[132,133] In order to address this discrepancy, the International Maritime Organization (IMO) introduced Annex VI to the MARPOL 73/78 Convention.[134] Its objective is to regulate air pollution by ship emissions, enhancing human health, and aligning with the EU's aspiration to attain climate neutrality by the year 2050.[135,136] The IMO's establishment of Emission Control Areas (ECAs) in proximity to coastal regions is a pivotal aspect of this initiative. These zones impose limitations on the emissions of NO_x for nitrogen emission control areas (NECAs) and SO_x for sulfur emission control areas (SECAs).[137] In contrast, the regulation step Tier III focuses on the total weighted cycle emission limit (g/kW h). The aim is the reduction of engine emissions, which are dependent on the engine's rated speed (revolutions per minute (rpm)). Tier III applies to all marine diesel engines installed on ships constructed after January 1st, 2016. It mandates an approximately 80 % reduction of NO_x emissions compared to Tier I levels. Emissions are required not to exceed 3.4 g/kWh at low engine speeds (less than 130 rpm) and limits emissions at higher engine speeds.[138,139] Conversely, sulfur restrictions directly limit the sulfur content in the fuel.[140] These regulations depicted in Fig. 1.5 have been realized gradually over the past decades. As of January 1st, 2020, ships are required to comply with regulations pertaining to the total fuel sulfur content (FSC), which is prohibited to exceed 0.1 % (w/w) within SECAs and 0.5 % (w/w) outside.[141] Furthermore, Fig. 1.5 depicts the geographical distribution of existing and debated ECAs across the globe, as well as ECAs with additional regulations, such as the Chinese and the Vietnamese SECA. In the latter cases, the FSC is limited to 0.5 % (w/w) and 0.25 % (w/w), respectively. However, in contrast to the Chinese SECA, open-loop scrubbers are permitted within the Vietnamese SECA,[142] a technology that will be discussed subsequently.

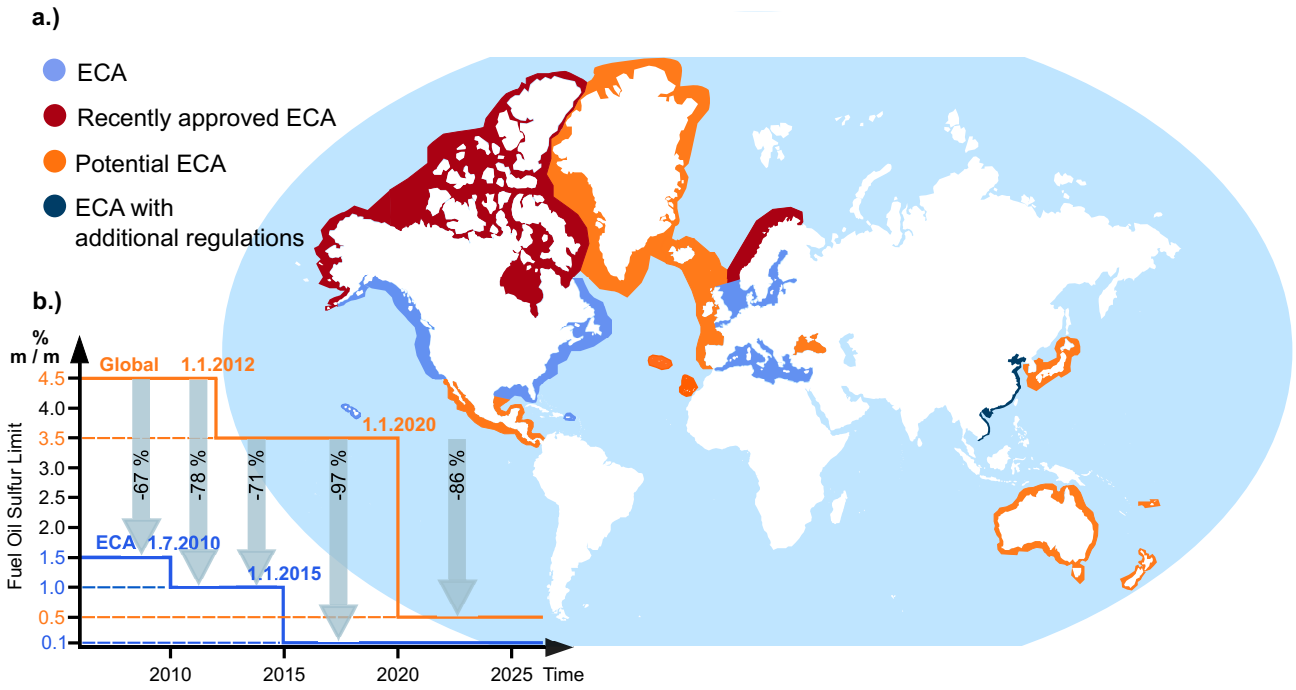

Figure 1.5.: a.) World map (modified after Ref. [143]) showing existing emission control areas (ECAs) (blue), recently approved ECAs (dark red), potential ECAs (orange) and ECAs with additional regulations (dark blue).[142,144–147] b.) The diagram demonstrates the development of permissible fuel sulfur content (FSC) in global and ECA waters (modified after Ref. [137]).

HFO, also known as residual fuel oil, is a cheap and established marine fuel source that has been commonly in use since the 1920s.[148] In order to reach a specific maximum viscosity, 'the vacuum residue of the crude oil refinery' is 'blended by lighter refinery products'.[149] Nevertheless, HFO contains a considerable quantity of heavy metals and sulfur, in form of $PM_{2.5}$, which are released into the atmosphere by combustion.[149] HFOs commonly exceed the compliance limit of 0.1 % (w/w) FSC for SECAs. Consequently, they must be eliminated as a pure fuel solution inside SECAs.[150,151] Therefore, an increasing number of new marine fuels are entering the market complying the ECA standards.[152,153] Alongside low-sulfur bunker fuels, distillates such as marine gas oil (MGO) or marine diesel oil (MDO) are compatible with SECA regulations and are thus becoming an increasingly important fuel in shipping, as evidenced by their increasing use in recent years.[154] A broad market is emerging for a variety of "cleaner" alternatives to HFO, including very low sulfur fuel oil (VLSFO), ultra-low sulfur fuel oil (ULSFO), Methane, Ammonia, liquified natural gas (LNG), hydrotreated vegetable oil (HVO), MGO, and many blends of distillates with bunker fuels such as marine diesel oil (MDO) and other intermediate fuel oils (IFO).[152,153] However, more than 95 % of ships are powered by internal-combustion engines that run on petroleum products (e.g. HFO, MGO, or MDO).[155]
In addition to low-sulfur fuels, technologies that reduce the sulfur content of ship emissions prior to their release into the atmosphere are also permitted and comply with SECA regulations.[141] Exhaust gas scrubbers have been demonstrated to be capable of reducing the sulfur content of exhaust gases in accordance with SECA standards. Moreover, they reduce the particle mass from the exhaust.[156] However, the effectiveness of particulate emissions reduction is contingent upon fuel, engine and scrubber parameters. Recent studies indicate modest effects on particle number and mass emission factors (EF)[157] but the literature does not show consistent results.[156,158,159]

Scrubbers can be operated in two principal modes that are depicted in Fig. 1.6. One is the open-loop mode, where the scrubbed residue of the fuel is released into the sea with the wash water. The second is the closed-loop mode, where the contaminated wash water is collected for disposal on

land. There is also a hybrid mode, where open-loop or closed-loop can be used depending on the shipping lane.[160,161] The prevailing trend in the field is the utilization of open-loop scrubbers, which have been demonstrated to be more cost-effective in a range of scenarios compared to closed-loop systems.[162,163] This implies that there are two potential avenues for regulating ship emissions: either by utilizing slightly more expensive low-sulfur fuels or by continuing to employ inexpensive bunker fuels in conjunction with scrubbers.[160] The implementation of scrubbers can have a profound impact on the environment. The legal use of HFO generally increases emissions. In open-loop systems, these pollutants can have a direct impact on the marine environment.[104,131,164] However, the number of used scrubber systems on the market is predicted to increase.[156,165,166]

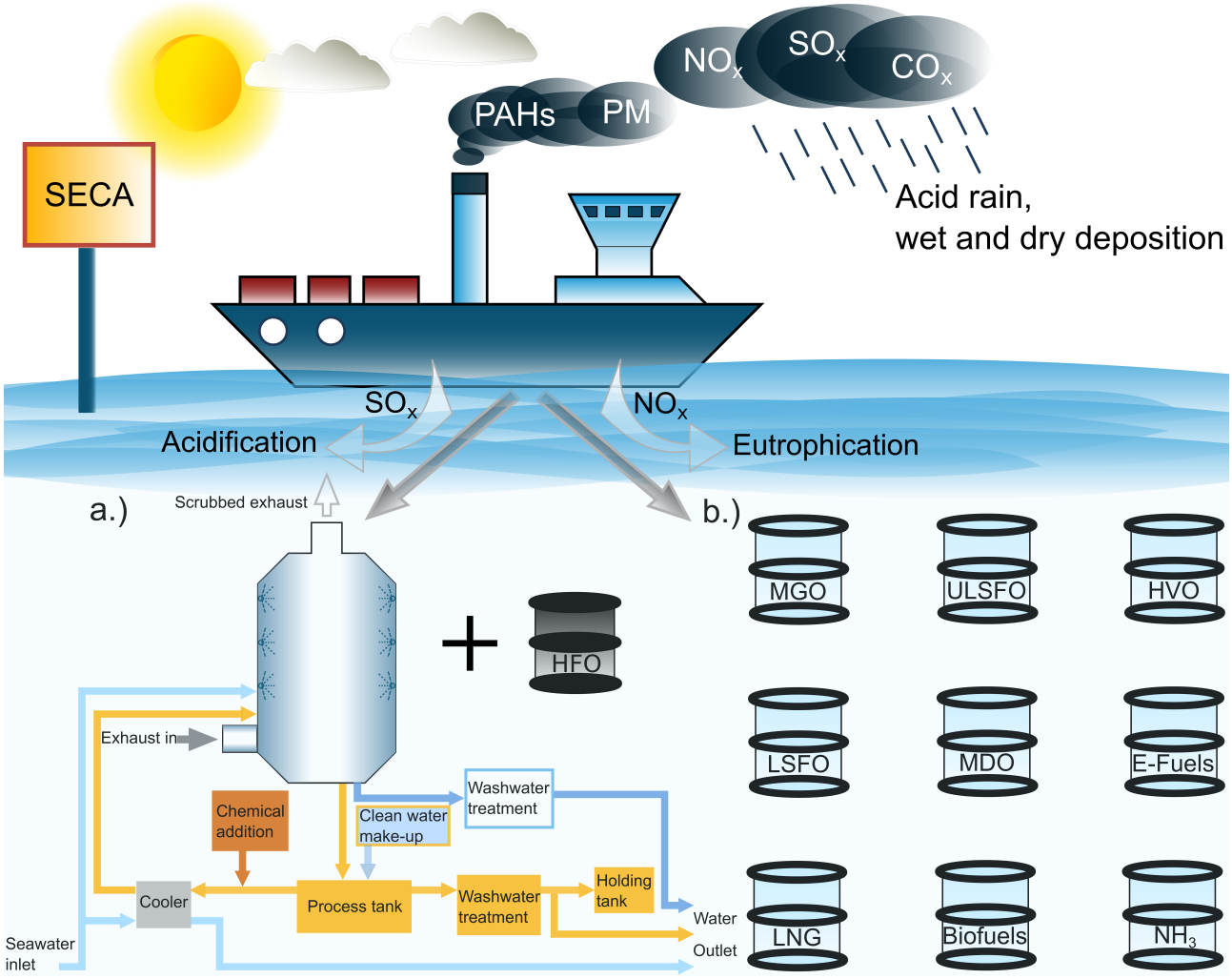

Figure 1.6.: Depicted possibilities for ships to comply with sulfur emission control area (SECA) restrictions. One is illustrated in a.), which depicts a simplified overview of a scrubber in hybrid setup as an alternative solution for low-sulfur fuels. The scrubber can be operated in two modes, either in open-loop (light and dark blue lines) or in closed-loop (yellow lines) (modified after Ref. [164]). In contrast, b.) highlights diverse fuels such as marine gas oil (MGO), ultra-low sulfur fuel oil (ULSFO), hydrotreated vegetable oil (HVO), low sulfur fuel oil (LSFO), marine diesel oil (MDO), e-fuels, liquefied natural gas (LNG), biofuels, and ammonia (NH_3). These fuels can be SECA compliant as a main solution, dependent on the fuels' sulfur content (FSC).

Nevertheless, the transition to "cleaner" fuels, such as distillates or alternatives, is a gradual process that is contingent upon the cost reduction factors of the modern fuels:[155] The estimated cost of "cleaner" HVO is within the range of 140-195 €/MW h, the global average of MGO is approximately 69 €/MW h,[167] while the cost of HFO is around 36 €/MW h.[168] With a total of approximately 60,000 merchant ships in the world fleet in 2023,[169] it is conceivable that the transition will be gradual and

challenging over the next decades.[45] This becomes clear when looking at IMO objectives. The reduction of GHG from shipping should be reduced to 20 % - 30 % by 2030 and 70 % - 80 % by 2040 compared to 2008.[140] Despite that, no measures have been adopted to realize these objectives in order to fulfil the Paris Agreement.[41] Nowadays, MGO, compatible with diesel engines,[170] has become the predominant fuel in SECAs.[171] This shift has led to a reduction in PM emissions; however, it has not resulted in a substantial decrease in CO_2 emissions.[68,172,173] In order to satisfy IMO's regulation for ship emissions, forthcoming SECA-compliant mixture fuels are poised for market entry.[170,174] This will likely happen at a gradual pace as a result of technical, economic, and social considerations.[45]

1.5. New Possibilities for Source Apportionment in Modern Shipping

The expansion of the market for modern fuels is accompanied by a number of challenges, particularly in measurement technology. Unlike the initially dominant HFOs, compliant distillates differ not only in terms of FSC, VOCs, or particle mass.[175] They also cannot be identified by metallic markers such as nickel (Ni) or vanadium (V) that were commonly found in HFO-derived ship emissions.[176,177] As a consequence, the traditional metal markers are no longer the exclusive means of identifying ships. This poses challenges in light of the growing number of ECAs worldwide that are recently proposed for the benefit of human health.[145,146] Fuels are conventionally characterized based on their physical properties, whereas their chemical composition is typically analyzed using gas chromatography-mass spectrometry (GC-MS). Advanced chemical characterization is performed by comprehensive two-dimensional gas chromatography (GC × GC) or fourier-transform ion cyclotron resonance mass spectrometry (FTICR-MS).[104,178,179] However, these offline methods are disadvantageous for source apportionment. Offline methods require time and are therefore impractical for tracing immediately distinct markers to identify the source. This gives shipping companies the opportunity to take advantage on that. Specially, a method is required to identify ship emissions, particularly in urban contexts where diverse anthropogenic sources exist (e.g. domestic heating, biomass burning, power plants, and urban dust, among others). This is necessary in connection to global air pollution since coastal cities are inhabited by millions of people.[69] Modern analytical online methods are required that do not focus exclusively on metals and are able to identify the majority of ship emission sources in- and outside the ECAs by new chemical markers. It is not uncommon to use PAHs diagnostic ratios (DRs) to distinguish emission sources. Polycyclic aromatic hydrocarbons have previously been analyzed in both the gaseous and particulate phases using DRs to identify emission sources.[181] As illustrated in Fig. 1.7, emission sources can be distinguished by their gaseous PAHs via resonance-enhanced multiphoton ionization (REMPI). In 2017, Czech et al. found evidence for marker signatures in gas phase that could distinguish different

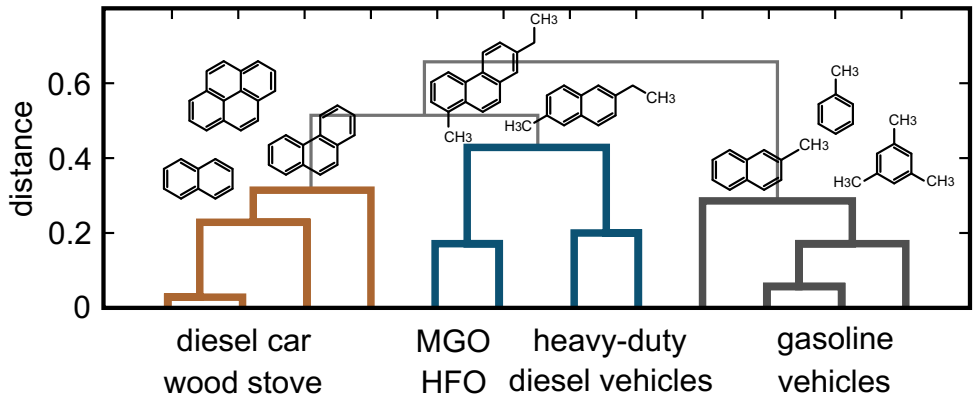

Figure 1.7.: Aromatic emission profiles emphasize the distinguishability of diverse combustion sources (modified after Ref. [180]).

fossil fuels by their polycyclic aromatic hydrocarbons[180] (see Fig. 1.7). However, it should be noted that REMPI-MS is typically insufficient for DRs. Diagnostic ratios are typically referring to isobaric substances that can be measured with GC-MS.[181] Consequently, one of the main motivations for this work was to test whether such emission sources could also be identified using an online method for individual particles. A method for discriminating marine fuels via single particles would offer several advantages for source apportionment. Single particles transport a bundle of chemical information from the exhaust of the ship to a distant analysing system nearly in real-time. Therefore, land-based online systems could be adapted to control and secure air quality in ECAs. In order to asses if there are discernible patterns in the PAH composition of different marine fuels, it is necessary to conduct both laboratory and field experiments. The laboratory experiment should investigate the impact of different combustion scenarios of a ship engine on its emissions, employing common marine fuels. A field study should be designed to verify the results of the laboratory experiment and provide further insights into the development of PAH patterns under real-world conditions. For these experiments, a single-particle mass spectrometer (SPMS) with a modern ionization technique is used as an online method, enabling the simultaneous investigation of both the inorganic and organic components of a particle.

1.6. Chemical Conversion of PAHs during and after Combustion Processes

As PAHs are considered a potential marker for marine fuels, it is essential to gain an understanding of their main characteristics and how they are formed in the combustion process of marine engines. In general, PAHs are defined as a class of organic compounds consisting of multiple fused aromatic rings composed entirely of carbon and hydrogen atoms. These rings can be arranged in a variety of ways, sharing one or more sites.[182] This ring structure is stable due to conjugated π-electrons. These electrons are delocalized over several rings.[183] Key characteristics of the PAHs are the aromaticity, the fused rings, hydrophobicity, and their environmental persistence.[182] That means, in more detail, that PAHs contain aromatic rings that adhere to Hückel's rule, which defines an aromatic compound as a planar, cyclically, through-conjugated molecule with $(4n+2)\,\pi$-electrons ($n \in \mathbb{N}$). However, it should be noted that there are exceptions for large annulenes.[184] An odd number of electron pairs leads to more stable aromatics, while an even number leads to more unstable aromatics, also known as antiaromatics with $(4n)\,\pi$-electrons.[184] The aromatic rings in PAHs are fused and share common carbon atoms, which distinguishes them from common aromatics with isolated rings.[185] PAHs are known to be hydrophobic, meaning that they do not dissolve in water, but in fats and organic solvents. This hydrophobicity allows them to persist in the environment due to their stable structure and can lead to accumulation in living organisms.[186]

PAHs are predominantly a product of incomplete combustion, encompassing biomass burning, domestic heating, industrial processes, and various fuel combustion processes, among others.[187] The growth and formation of PAHs in high-temperature combustion environments is described by the hydrogen abstraction carbon addition (HACA) process.[188,189] Firstly, Eq. 1.1 describes the 'Hydrogen Abstraction'. A hydrogen atom is removed from an existing aromatic hydrocarbon molecule. This could be facilitated for instance by reactive species, such as hydrogen atoms H• or hydroxyl radicals OH• in the environment.[190] The reaction of hydrogen results in the formation of a reactive radical site on the aromatic hydrocarbon.[191]

$$\mathrm{PAH} + \bullet\mathrm{OH} \longrightarrow [\mathrm{PAH}\text{ - H}]\bullet + \mathrm{H_2O} \tag{1.1}$$

The radical site on the aromatic hydrocarbon reacts with an acetylene molecule (C_2H_2). C_2H_2 is a common species in high-temperature environments due to its stability.[190–192]

$$\mathrm{PAH}\bullet + \mathrm{C_2H_2} \longrightarrow \mathrm{PAH{-}C_2H_2}\bullet \tag{1.2}$$

Finally, a new PAH ($PAH{-}C_2H_2\bullet$) is created. This process can be repeated several times to create new PAHs.[190] In the HACA framework, the formation of pyrene can be initiated by the reaction of a phenyl radical with acetylene, resulting in the generation of a phenylacetylene intermediate. The corresponding reaction mechanism is illustrated in Fig. 1.8. This phenylacetylene intermediate subsequently undergoes a series of transformations, leading to the formation of naphthalene, 1,2-ethynyl-naphthalene, and finally, phenanthrene. The final step in this process is the formation of pyrene.[192]

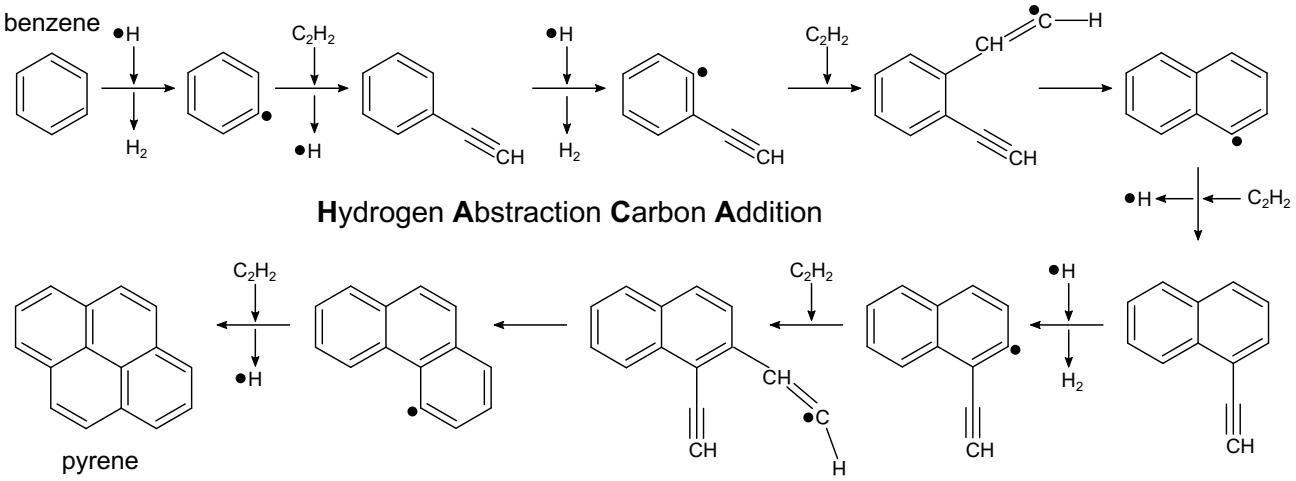

Figure 1.8.: Possible process for PAH growing. Reaction mechanism showing hydrogen abstraction carbon addition (HACA) from benzene to pyrene (modified after Ref. [193]).

Once in the atmosphere, after the combustion process, PAHs can undergo complex aging processes prior to their removal, mainly through dry deposition.[187] These transformations significantly influence their environmental fate and toxicity. The primary aging mechanisms can be categorized into photochemical, chemical, and physical processes.[187,194]
Photochemical aging predominantly occurs via UV radiation-induced reactions. In this process PAHs undergo photooxidation to form various oxygenated derivatives including quinones, ketones, and aldehydes.[195] The reaction kinetics depend on many parameters, including light intensity and thermodynamic conditions.[187,195] Keyte et al. (2013)[187] elucidated the atmospheric aging processes of PAHs, focusing on their reactions of key oxidants, including hydroxyl radicals •OH, ozone (O_3), nitrate radicals ($NO_3\bullet$), and nitrogen dioxide (NO_2). Additionally, it is imperative to acknowledge soot-initiated reactions. In those reactions soot light absorption results in the transfer of energy to an organic compound. This facilitates the formation of oxidants (e.g. for PAHs).[196]
These reactions of PAHs with oxidants lead to the formation of oxygen-containing functional groups,[197] ring-opening reactions, and oxygenated and nitrated PAH derivatives, which can alter their toxicity and environmental behavior. The rate of these reactions varies depending on the specific PAH structure and environmental conditions. Notably, the partitioning behavior of PAHs between the gas and particle phases influences their reactivity and long-range transport potential.[187,197,198]

To determine the origin of these PAHs, the concentration ratios of pairs of individual PAHs at receptor and source sites are examined. For this purpose, PAHs with analogous degradation properties in air are proposed, known as diagnostic ratios (DRs).[187,199] The formation and evolution of DRs during atmospheric aging processes provide crucial insights into PAH source apportionment. Initial DR values are determined by combustion conditions, including temperature and oxygen

availability. However, these ratios undergo systematic changes during atmospheric transport due to differences in reactivity among PAH species.[181] Common DR pairs, such as Pyrene/Fluoranthene and Anthracene/Phenanthrene, exhibit varying degrees of stability during atmospheric aging, influenced by species-specific vapor pressures and reactivity with atmospheric oxidants.[200] However, other DRs associated with aging exist, such as Benzo[a]pyrene/Benzo[e]pyrene (BaP/BeP).[181]
Notably, aging products can exhibit enhanced toxicity compared to their parent PAHs. This emphasizes the importance of understanding the underlying transformation processes for accurate environmental and health assessments.[195,201] The complexity of these aging mechanisms necessitates careful consideration when using PAHs and their distributions as source markers for monitoring ship emissions. Relevant PAHs are illustrated in Fig. 1.9.

a)

number of carbons in alkyl side chains	n = 0	n = 1	n = 2	n = 3	n = 4
PAHs	*m/z*				
phenanthrene, anthracene	178	192	206	220	234 (e.g. retene)
pyrene, fluoranthene	202	216	230		
benzanthracene(s), benzphenanthrene(s) (e.g. chrysene)	228	242			
benzpyrene(s), benzfluoranthene(s)	252	266			

b)

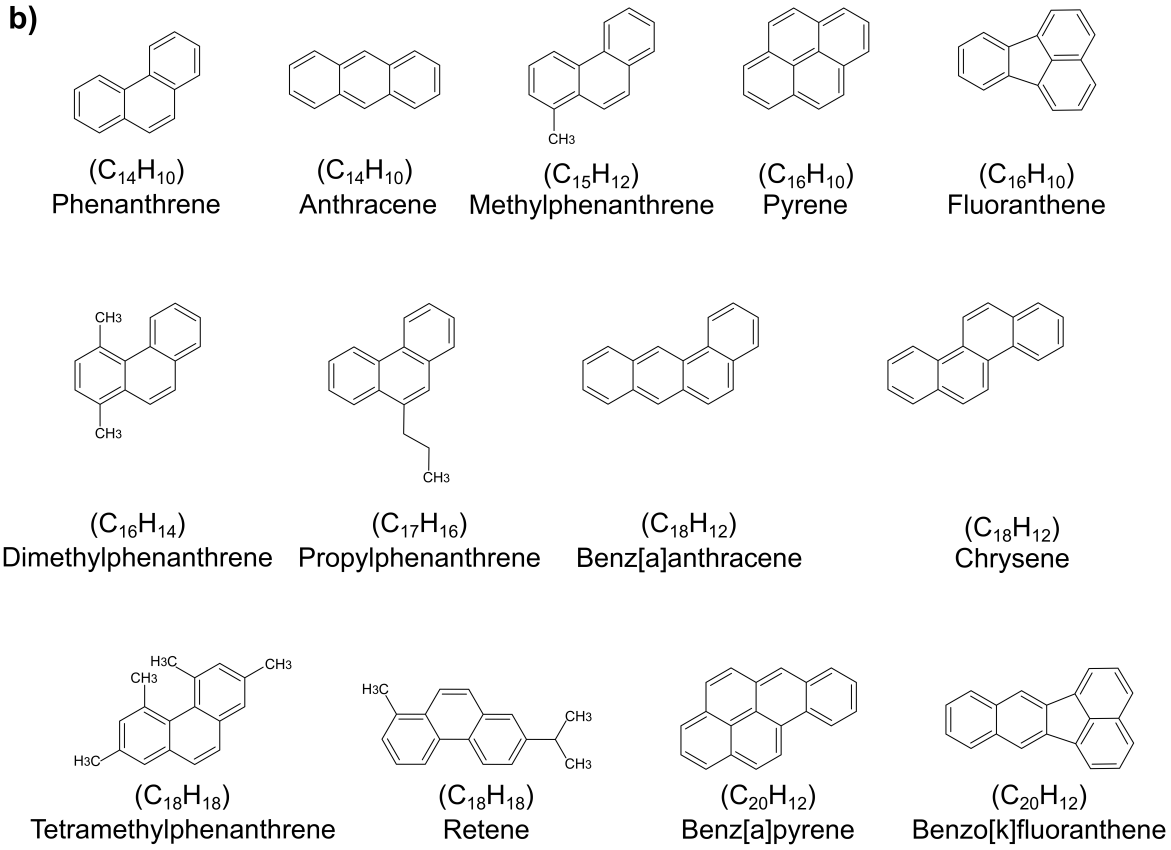

Figure 1.9.: PAHs that play a crucial role in the investigation of ship emissions. Table a) illustrates exemplary PAHs with corresponding numbers of aliphatic carbons and mass-to-charge ratios. These PAHs can be detected in individual particles of fuels[202,203] and are found in this work. b) Possible structural formulas of PAHs observed in the subsequent results.

Chapter 2.

Fundamentals of the Applied Techniques

This chapter elucidates the fundamental ionization mechanisms. Subsequently, the methodology employed in this work is discussed. The experimental setup, which was uniformly utilized for all experiments, is then described. The chapter closes with an evaluation method that was frequently utilized throughout this work. It is shown that the method is well-suited for the analysis of large datasets, such as those obtained from single-particle measurements, that are presented.

2.1. Laser Ionization Processes in Single-Particle Mass Spectrometry

In the domain of single-particle mass spectrometry, Morrical et al. (1998) introduced a method that became known as laser desorption-resonance-enhanced multiphoton ionization (LD-REMPI). This method enables the identification of PAHs at the single-particle level. However, soft ionization methods, such as REMPI, are often insufficient for ionizing the refractory components of a particle.[204] An ionization method developed in 2019 permits a combined interpretation of both PAHs and inorganics of the same particle by using spatially and temporally tailored laser pulses.[205] This method is essential for obtaining the desired chemical information from both single-particles in laboratory and field experiments. Prior to the detailed discussion of the method, its fundamental basis, the key ionization processes involving laser desorption/ionization (LDI) and resonance-enhanced multiphoton ionization (REMPI) are described.

2.1.1. Laser Desorption/Ionization

Laser desorption/ionization (LDI) represents the most common type of ionization in the field of single-particle mass spectrometry. This predominance can be attributed to its ability to analyze a wide range of substances, including refractory materials and metals. It produces a high ion yield, which is advantageous when dealing with limited sample material in ambient measurement contexts.[202,206–208] LDI is frequently generated with pulsed lasers, usually in the ultra-violet (UV) light spectrum. Nd:YAG lasers with fourth-harmonic generation (FHG) ($\lambda = 266\,\mathrm{nm}$) or various excimer lasers (KrF: $\lambda = 248\,\mathrm{nm}$ and ArF: $\lambda = 193\,\mathrm{nm}$) as well as N_2-lasers ($\lambda = 337\,\mathrm{nm}$) are suitable.[207,209,210] Although LDI is a well-established ionization method, the precise physical processes involved and the parameters that affect them remain poorly understood.[207]
In general, LDI in single-particle mass spectrometry is characterized by a complex interplay of physical and chemical processes that occur during laser-particle interaction.[211] When the laser photons interact with the particle surface, a cascade is triggered in which energy transfer processes lead to rapid heating rates of over $1000\,\mathrm{K\,s^{-1}}$. This results in near-instantaneous vaporization of the particle material.[51,212] The primary physical mechanisms encompass several distinct processes in which photothermal heating converts absorbed laser energy to thermal energy, and leads to explosive vaporization. Concurrently, photoelectronic processes facilitate direct ionization through multiphoton absorption.[51,213] In this work, a pulsed KrF-Excimer (248 nm) laser is used, delivering an appropriate pulse energy of 6 mJ.[203,214] The energy accumulation within excited molecules promotes desorption and ionization, enhancing the overall efficiency. Moreover, the rapid removal of electrons can result in particle disintegration via Coulomb explosion.[51,215] Within the expanding plume, multiple recombination processes occur simultaneously. This includes electron-ion recombination where free electrons can recombine with positive ions, reducing ion yield. Vaporized species can aggregate in the gas phase, forming cluster ions. Ion-molecule reactions in the plume lead to secondary ionization processes.[51,216] The processes evolve on different timescales, from femtoseconds for initial photon absorption to microseconds for

ion-molecule reactions.[212]
Matrix effects in single-particle analysis present particular complexity due to competitive ionization in which different species compete for available charge. Space charge effects in high ion density plumes have been shown to distort ion trajectories, while the chemical composition of particle surface layers has been demonstrated to strongly influence ionization probabilities.[217,218] Supression effects, where certain species can suppress the ionization of others, combine with phase and morphology influences. This affects energy coupling and creates a complex analytical environment.[219,220]
The optimization of instrumental parameters is highly dependent on laser parameters, including wavelength, pulse duration, fluence, spatial beam profile, and repetition rate. Particle properties such as the particle size and chemical composition, among others, also play a role.[51,216] Consequently, it is not yet feasible to make quantitative predictions concerning ion production or precise component quantifications.[205,207,221] However, LDI enables a fast investigation of the qualitative composition of a single particle. LDI of atmospheric particles leads to the generation of distinctive positive and negative ion signatures. While its anions often reveal organic fragments, electronegative elements such as Cl^-, carbon clusters, and complex ions (e.g. NO_2^-, NO_3^-), cations in positive mass spectra often include electropositive elements (eg. K^+, Ca^+ or Fe^+) and organic fragments (e.g. $C_xH_y^+$).[205,207]
In comparison to utilizing a solitary UV laser pulse for LDI, a two-step approach is used in this work. Initially, an IR laser pulse (10.6 µm) vaporizes the organic matter from the particle. Then, a second pulse from the excimer laser is directed towards the resulting plume, ionizing the molecules in the gas phase.[208] The separation of LD and ionization in this procedure is advantageous for multiple reasons. Firstly, the vaporization of molecules at high temperatures, which is a complex process in LD, can be avoided. Secondly, the laser intensities and photon energies can be reduced, thereby minimizing fragmentation.[222] Thirdly, since ionization takes place in the gas phase, matrix effects are decreased, which is advantageous for quantifying approaches.[223] However, it should be noted that the degree of fragmentation can increase with the intensity of the IR laser pulse that desorbs the molecule.[207]
LDI is applicable to the analysis of both organic and inorganic salts, as well as polycyclic aromatic hydrocarbons (PAHs) carried by single particles.[224,225] However, the efficacy of LDI is restricted for organics, leading to higher fragmentation. LDI is rather applicable for particles that are dominated by soot or parent PAHs.[208] Thus, LDI is an ideal tool for the investigation of emissions from the marine environment; however, for a good detection of the organics it is useful to add resonance-enhanced multiphoton ionization using UV wavelengths.[226]

2.1.2. Resonance-Enhanced Multiphoton Ionization

Resonance-enhanced multiphoton ionization (REMPI) is a soft ionization method, typically applied to molecules in gas phase. Consequently, a particle needs to be desorbed before using REMPI.[227] In this process a single photon is not sufficient to exceed the ionization potential of a molecule. Instead, $(n+m)$ photons ionize the molecule. The ionization probability P is proportional to the laser intensity. This allows the photon energy to be selected to minimize fragmentation.[205] In the majority of cases, UV- or vacuum UV photons are utilized.[228] This work employs a KrF*-laser with a wavelength of 248 nm and an energy density of 10^6 to $10^8\,\mathrm{W\,cm^{-2}}$, which shows a high selectivity for aromatic compounds. Thus, the laser is suitable for the study of PAHs.[203,226,229] REMPI exhibits high ionization efficiency for a number of compounds. The $(1+1)$ photon combination is sufficient to ionize a wide range of aromatics, with ionization potentials ranging from about 6 eV to 9.48 eV.[230] This renders it a suitable tool for use in analytical chemistry, investigating aromatic compounds in ship emissions and ambient air experiments.[229,231–234] A simplified scheme of a possible REMPI process is shown in Fig. 2.1. In REMPI, either monochromatic light or light of multiple wavelengths λ can be used. For instance, in $(1+1)$ REMPI, a first photon can excite a molecule and the second photon of the same wavelength causes its ionization. In the latter case, two different wavelengths are used for the excitation of the

molecule and its ionization. This method has the advantage over monochromatic REMPI that it allows for greater flexibility in its application.[232,235]

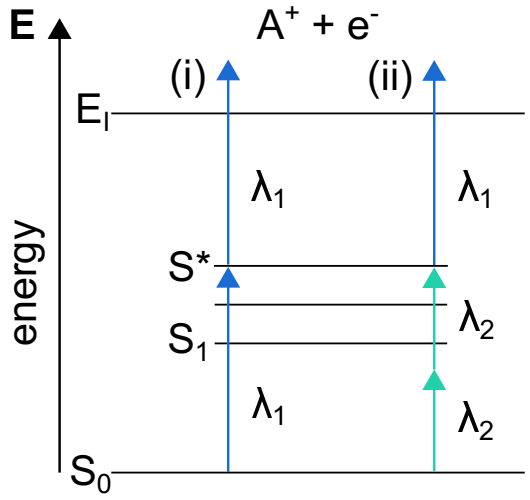

Figure 2.1: Scheme of resonance-enhanced multiphoton ionization ((n+m) REMPI) mechanisms: (i) monochromatic (1 + 1) REMPI uses two photons of the same wavelength (λ_1). The first photon excites the molecule from the ground state S_0 to an excited state S^*, while the second photon leads to an energy above the ionization potential E_I. In constrast, (ii) illustrates a (2 + 1) multi-colour REMPI, where two different wavelengths (λ_1 and λ_2) are used to exceed the ionization potential E_I of the molecule. REMPI is a soft ionization technique that exhibits high sensitivity towards organic molecules, including aromatic compounds.[231]

2.2. Improvement of Mass Resolution by Delayed Extraction

As previously indicated, LDI in SPMS is a complex ionization process in which the resulting ions can possess a range of kinetic energies distributed over many angles.[236] According to Li et al. (2018),[236] velocities can vary between 50 and 300 $\mathrm{m\,s^{-1}}$ in SPMS, depending on particle size.[236] The distribution of the kinetic energy of the ions depends on several parameters such as the properties of the matrix and the laser fluence.[237] This limits the precision of the mass resolution of the SPMS. It is restricted by two factors: spatial and energy dispersion.[236] The spatial dispersion is proportional to the particle size, which is negligible for the applications in this work.[236] However, the time-of-flight-mass analyzer is not able to compensate the total energy dispersion of all ions.[236] To address this challenge and enhance the mass resolution, the concept of delayed extraction is employed here.[216,236,238] This approach aims to mitigate the adverse impact of energy dispersion on the m/z resolution of ions. After the ions are formed in the ion source, they are not immediately extracted and accelerated by the electrodes. Instead the extraction process is delayed. The optimal delay time depends on the mass range of the ions of interest. However, it should be noted here that suboptimal choices of delay time can also degrade resolution. Ideally, the slower ions have sufficient kinetic energy during their drift to match the speed of the faster ions. Thus energy dispersion of the ion packet is reduced, resulting in a higher mass resolution of the SPMS.[236] In this study all ions are extracted with a delay time between 0.4 µs and 0.6 µs. Experiments have shown that this setting improves the resolution of the SPMS for the applications in this work.[205,238]

2.3. Time-of-Flight Mass Spectrometry

In the field of mass spectrometry, time-of-flight (ToF) systems represent a well-established technique. It facilitates the dispersion of ions with different m/z ratios over time during their flight in a field-free drift path of a known length. The system has two main advantages. Firstly, the m/z range of a ToF-system is nearly unlimited; secondly, the spectral mass acquisition rate is very high, potentially reaching rates of over 1000 Hz. Thus, a complete mass spectrum can be obtained from a single ionization event. The technique can be combined with other mass spectrometric techniques, making it ideal for both the investigation of samples in a laboratory setting and the analysis of ambient particles in real-time.[224] The principle of separating the individual m/z ratios of an ionized molecule is as follows. After

ionization, the positive ions reach a negative voltage and the negative ions reach a positive voltage (bipolar ToF-system). The ions with the charge $q = ze$ ($z \in \mathbb{N} \setminus \{0\}$) move towards the applied voltage U and thus carry the kinetic energy:

$$E_{\text{kin}} = \frac{mv^2}{2} = zeU = E_{\text{el}}. \tag{2.1}$$

If Eq. 2.1 is now converted according to the velocity v, the result is:

$$v = \sqrt{\frac{2zeU}{m}}. \tag{2.2}$$

Assuming that all ions start at the same time t_0, the applied voltage is $U = \text{const.}$ we obtain the time-of-flight t_{ToF} by inserting Eq. 2.2 into the ansatz $s = v \cdot t$:[224]

$$t_{\text{ToF}} = \frac{s}{\sqrt{2eU}} \cdot \sqrt{\frac{m}{z}}. \tag{2.3}$$

Incorporating of a reflectron (see Fig. 2.2) within the flight tube can enhance the resolution in a time-of-flight system. Reflectrons are typically comprised of ring electrodes angled in the direction of ion flight. The detector, typically a microchannel plate (MCP), is positioned on the opposite side, adjacent to the ion source. Ions of varying mass and, consequently, different E_{kin}, are initially accelerated by a voltage U_{a}.[224] Ions of higher E_{kin} traverse the field-free space at a higher velocity than ions with lower E_{kin}. Upon reaching the ring electrodes, which are subject to a counter voltage of approximately $1.05 - 1.1\,U_{\text{a}}$, the ions undergo a deceleration and acceleration process in the opposite direction. Ions of higher E_{kin} are drawn deeper into the electric field of the electrodes, resulting in a longer dwell time within the reflectron for larger E_{kin}. Consequently, a correction in the time-of-flight is achieved, thereby enhancing the resolution of the ToF-system. Although the ions must now traverse a greater distance to reach the MCP, the enhanced resolution achieved by the reflectron outweighs this disadvantage. As an alternative, the reflectron can be operated in linear mode by setting the reflectron voltage to zero, enabling the ions to be detected by the linear detector.[224] Reflectrons are standard in

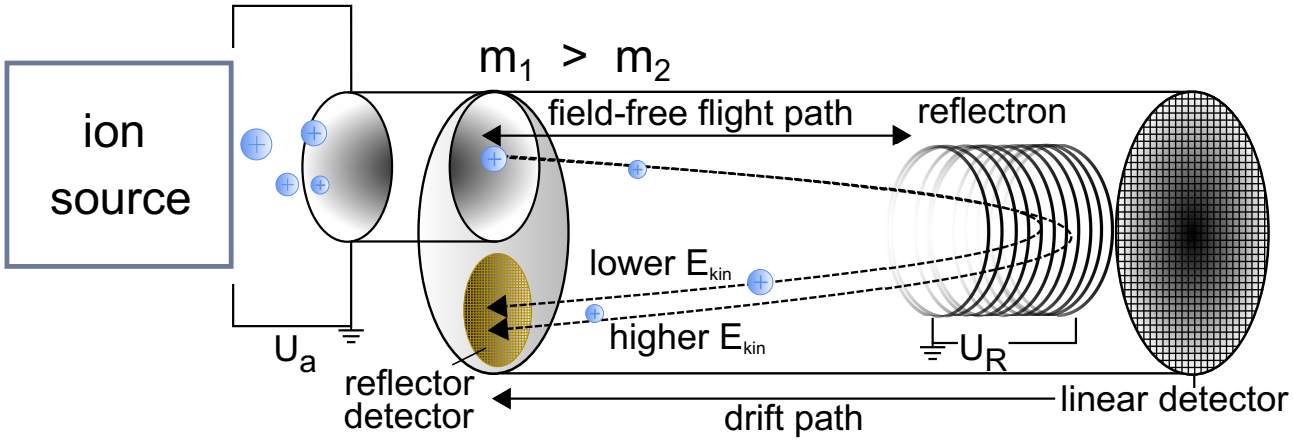

Figure 2.2.: Schematic structure of a reflectron: The reflectron employs a countervoltage to compensate for the differences in the kinetic energies of particles within the same mass range, enhancing the mass resolution (modified after Ref. [224]). Principle: Ions of different kinetic energy traverse the reflector to different extents before coming to rest and being ejected in the opposite direction. As a result, ions with higher kinetic energies are capable of traversing greater distances than those with lower kinetic energies, achieving a time focus at some point along the return trajectory. At this location, the detector receives ions of identical mass at approximately the same time. The placement of the detector beside the ion source is facilitated by a small angle between the axis of the flight path and the reflector.[224]

TOF-systems because of their ability to compensate for most of the spread energy of the ions.[239] This work uses reflectrons in SPMS.

2.3.1. Modern Ionization Technique for Single-Particle Mass Spectrometry

A single-particle mass spectrometer (SPMS) is suitable for detecting the chemical signature of individual particles.[205,207,240] This method enables the qualitative identification of the organic and inorganic nature of a free, isolated particle.[205,207,240] The use of SPMS is particularly advantageous for characterizing the aerosols mixing state.[207,241] The mixing state of aerosols refers to the distribution of chemical species across an ensemble of particles within an aerosol, thereby distinguishing internally and externally mixed states. In an internally mixed state, different aerosol components coexist within the same particle. This typically occurs due the aforementioned processes in the atmosphere. In contrast, an external mixture consists of compositionally distinct particles.[207,242]

The setup shown in Fig. 2.3 is the configuration of a bipolar single-particle mass spectrometer. Particles are transported to the instrument with a sample flow of $1\,\mathrm{L\,min^{-1}}$. Using an enrichment unit, the particles in this flow are concentrated into a flow of $0.1\,\mathrm{L\,min^{-1}}$ and enter the inlet system of the SPMS. Subsequently, particles are focused into a narrow beam using an aerodynamic lens, which concentrates the particle beam before it passes through a sizing unit.[243] In this unit, each particle is subjected to two pulses of Nd:YAG lasers with a wavelength of 532 nm. The scattered light emitted by the particle is detected by photomultipliers, which amplify the resulting electrical signal with each impact. The two electrical signals are used to calculate the speed of the particle and determine the trigger times of the subsequent laser systems. Initially, a pulsed CO_2-laser (25 mJ, 10.6 µm) desorbs the particles, creating an organic plume around the inorganic particle core. Both are then ionized by a KrF-excimer laser (6 mJ, 248.3 nm). Initially, the plume is ionized with a rectangular laser profile via REMPI. Almost simultaneously, the inorganics are ionized via LDI by focusing the beam on the particle core using a spherical mirror. Further information regarding the lasers utilized in this configuration is provided in the appendix.

The use of both resonance-enhanced multiphoton ionization (REMPI) and laser desorption/ionization (LDI) enables the simultaneous resolution of organic PAH signatures (REMPI) and the inorganics (LDI) of a particle. The excimer laser creates an unfocused beam profile with the advantage that the particle and its plume are hit in a precise manner, resulting in REMPI (see Fig. 2.1) without the occurrence of LDI. In a second step, the beam is focused with a spherical mirror to the refractory residue of the particle (LDI). The beam focus, described by the Rayleigh length, clearly shows a higher energy density than the unfocused beam profile. The energy density in the beam focus reaches values of over $2\,\mathrm{GW\,cm^{-2}}$, sufficient to ionize resistant particles.[205,214]
This process can be executed in two different modes: The initial mode is the sizing mode. The detectable particle size is constrained by the limitations of the scattering cross-section for Mie scattering.[207] The second mode is the so-called 'free-running mode'. The sizing lasers remain deactivated, and particles are hit at random by the CO_2- and the excimer laser, which are operated at a constant rate of 100 Hz. The advantage of the free-running mode is that it allows for the detection of smaller particles, although this comes with the loss of size information.

Once the particles have been ionized in a point ion source of high energy density, the extraction of all ions is executed with a delay ranging from 0.4 µs to 0.6 µs after the ionization pulse. This delay is implemented to enhance the quality of the mass spectra.[234,236,238] Subsequently, cations from LDI and PAHs from REMPI are recorded together in the positive flight tube of the SPMS, while anions are recorded in the negative flight tube. To ensure optimal resolution of the mass spectra, the SPMS utilizes reflectrons in both tubes. Additionally, the transmission of cations from the LDI process is attenuated by a factor of approximately 50 to ensure sufficient dynamic range for measuring both

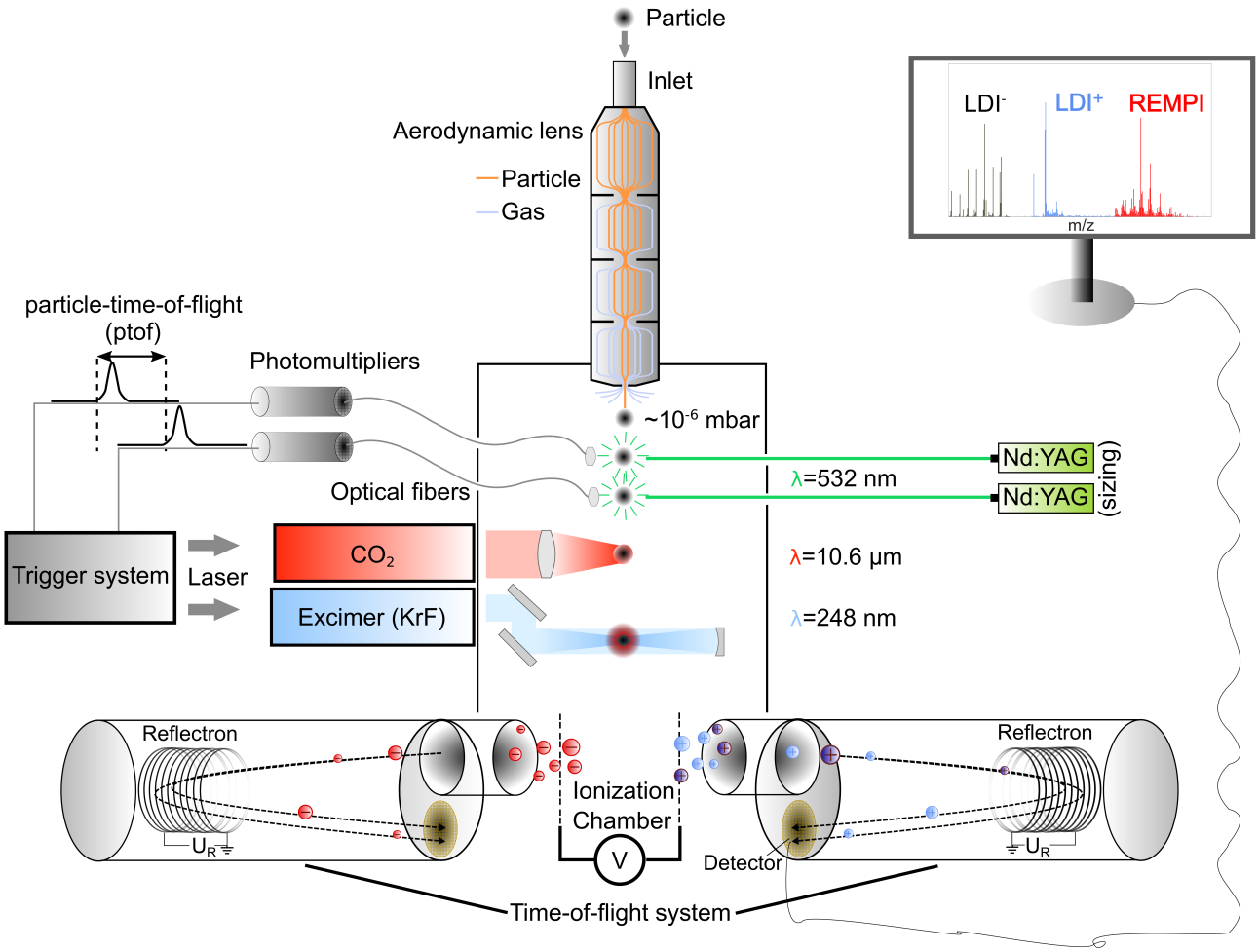

Figure 2.3.: The concept of the single-particle mass spectrometer utilizing a modern ionization technique. A single particle enters the instrument through the inlet. Subsequently, an aerodynamic lens converges the particle beam to a sizing unit, where the particle is hit twice by Nd:YAG lasers with a wavelength of 532 nm to determine its velocity. The scattered light of each hit particle is directed to a photomultiplier. The resulting electrical signal is used to trigger diverse laser systems with the appropriate timing. The initial laser system, a carbon dioxide laser (10.6 µm), strikes the particle, creating an organic plume by laser desorption (LD). Subsequently, this plume-covered particle is struck twice by an excimer laser (248 nm) with a flat-top profile. Therefore, the unfocused beam ionizes the plume (resonance-enhanced multiphoton ionization (REMPI)), although the energy density is insufficient to ionize the particle core. Consequently, the unfocused beam is reflected by a spherical mirror that focuses the beam on the inorganic core to ionize it (laser desorption/ionization (LDI). Following ionization, electrodes extract the ions with a delay of 0.6 µs. The ions then drift through reflectrons to enhance the resolution of the detected mass spectra. The mass-to-charge ratios of each particle are subsequently detected and computed with a customized LabVIEW program.

the strong ion flux from LDI and the weak ion flux from REMPI on the same detector (MCP).[238] The SPMS achieves a mass resolution R ≈ 800-1000 using these mechanisms.[238] Finally, utilizing these methods, the SPMS is capable of elucidating the distribution of important pollutants, including PAHs, soot and metals in single particles, providing insight into their mixing state.[202,205,229,244] An example for an accumulated mass spectrum of 88,000 single particles is illustrated in Fig. 2.4 showing ship emissions from MGO (more examples are found in the Appendix A.2). It is notable that the method using a wavelength of 248 nm for ionization is resonant to iron, which makes it sensitive to it and other metallic species such as nickel and vanadium.[234]

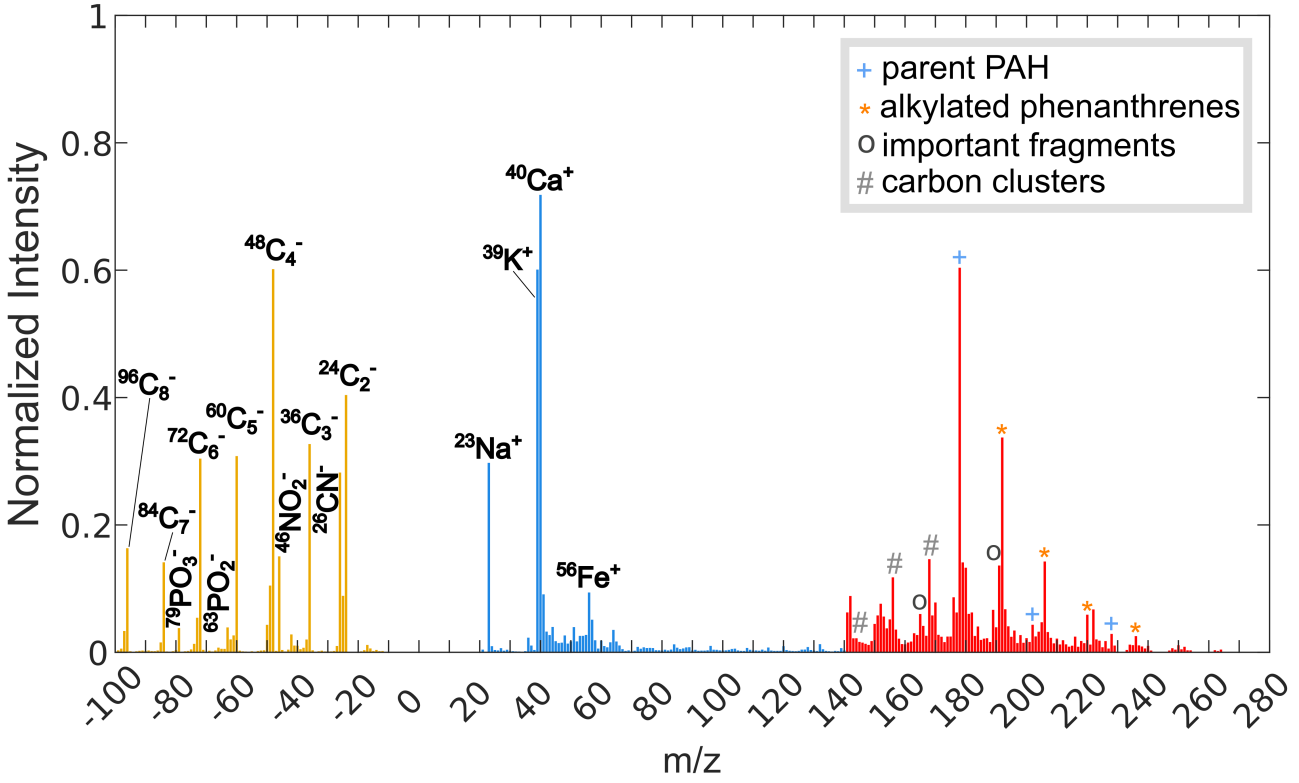

Figure 2.4.: Sum mass spectra of 88,000 single particles from ship emissions obtained via single-particle mass spectrometry (SPMS). The SPMS was employed to analyze particles emitted from a 1-cylinder, 4-stroke research ship engine operating on marine gas oil at a load of 60 kW. The resulting data reveal both m/z from anionic (yellow) and cationic (blue) species detected via laser desorption/ionization (LDI), as well as various polycyclic aromatic hydrocarbons (PAHs) identified via resonance-enhanced multiphoton ionization (REMPI) (red).

2.4. Clustering of Mass Spectral Signatures

The data for the mass spectra are recorded with a customized LabVIEW program. In this case, the typical hit rate (ratio of recorded single-particle mass spectra to optically detected and sized particles) is approximately 50 % as reported in similar studies.[205,214] The measured raw data are transformed into nominal data and subsequently evaluated using a series of Matlab programs. One such program employs a neural clustering algorithm designed for continuous-valued input data designated Adaptive Resonance Theory 2-A (ART 2-A), extracted from the open-source toolkit FATES (Flexible Analysis Toolkit for the Exploration of SPMS data).[245] It is commonly used for online clustering and pattern recognition tasks and has been demonstrated to be effective for the evaluation of extensive data pertaining to individual particles.[246] Key steps of the algorithm are shown in Fig. 2.5. At the outset, the input vectors (nominal data of all particles) are normalized. Subsequently, the cosine similarity between an input vector ($\text{particle}_{n>1}$) and the prototype (particle_1) of each cluster is calculated. In case the similarity exceeds the predefined resonance threshold ρ (which can be interpreted as the Euclidean distance) the input is assigned to the cluster in question. Otherwise, a new cluster center is created for the input. Upon assignment of an input to a cluster, the cluster prototype is adjusted incrementally through a weighted update. The strength of the adjustment depends on the predefined learning rate, denoted as η. This process can undergo various predefined iterations. Detailed information regarding the full algorithm can be found in Frank et al. (1998).[247] Finally, all particles are assigned to their respective clusters. This process can be repeated iteratively as required.[247,248] Consequently, this and other algorithms have been instrumental in analyzing the obtained SPMS data.

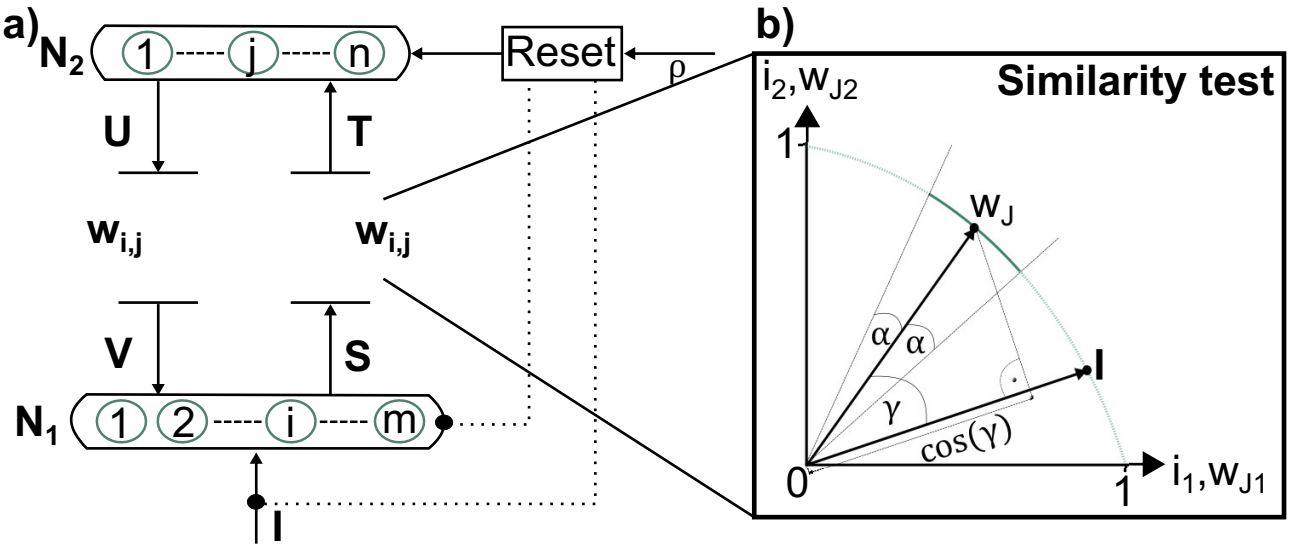

Figure 2.5.: a) Simplified ART-2-A algorithm showing the net activity between two neurons N_1 and N_2 with an input I and different bottom-up or top-down vectors (T,S,U,V) resulting from the comparison of input and the prototypes $W_{i,j}$. b) Similarity test between Input I and prototype $W_{i,j}$. If $\cos(\gamma) \geq \cos(\alpha) = \rho \longrightarrow$ assign input I to cluster (modified after Ref. [247]).

Chapter 3.

Results

This chapter presents the findings of investigations regarding the potential of SPMS for the detection of tracer elements in source apportionment. The research mainly focuses on PAHs as a possible marker for ship emissions. The experimental setup used to obtain these results can be found in the relevant publications and in the method section of this work.

3.1. Detection of Ship Emissions from Distillate Fuel Operation via Single-Particle Profiling of Polycyclic Aromatic Hydrocarbons

As previously motivated, shipping is a significant contributor to air pollution due to the combustion of both heavy fuel oils and distillate fuels. Released pollutants such as sulfur oxides (SO_x), nitrogen oxides (NO_x), particulate matter (PM), and PAHs[42] are of concern due to their well-documented carcinogenic and mutagenic properties.[97–100] While emissions from heavy fuel oils have been extensively studied, less attention has been given to those arising from the use of distillate fuels, which are often perceived as "cleaner" alternatives.[102,249] However, HFOs without supplementary technical support are no longer permitted in ECAs. The role of distillate fuels will become more important in the future.[137] In 2017, Czech et al. identified a distinct PAH pattern for different sources in the gas phase, prompting further investigation into its potential application in the particulate phase for ship emissions.[180] This study represents the first investigation of organic PAH patterns as novel ship markers utilizing a contemporary ionization technique for the analysis of fresh emissions at single-particle level.
Moreover, this study examines the potential of PAHs as a novel marker for ship emissions, given that established metals such as iron, vanadium, and nickel are ineffective markers for distillate fuels. Both a realistic ship engine in a laboratory setting and a field study in Sweden with passing ships were examined.
This publication[229] focuses on MGO because it is permitted in ECAs and is becoming increasingly prevalent in the maritime sector.[171] In the laboratory study, the particles emitted by a running one-cylinder four-stroke 80 kW research ship engine were measured under various load conditions (for further details see Streibel et al. (2017)[104]). The size distribution of the particles were recorded using a scanning mobility particle sizer. The objective was to measure the chemical signature of the PAHs and to investigate if it remains consistent in different load conditions and with varying particle sizes. Laboratory results were compared with those of the field measurements.

Fig. 3.1 presents the eight main clusters for around 50 % of all laboratory MGO particles, a common hit rate with this method.[214] The figure was produced using an ART 2-A cluster algorithm with manual post-processing. The results of recent studies demonstrate that unsupervised cluster algorithms (e.g. ART 2-A, K-means and their derivatives) are reliable and appropriate for the chemical apportionment of single particles.[246] Furthermore, Wang et al. (2024)[246] have demonstrated that these cluster algorithms can be used as a method to support real-time measurements, including single particles. Neural network-based methods are particularly effective for processing large amounts of data, such as complex SPMS spectra, at high speeds. Neural networks like ART 2-A and others will undoubtedly help by processing big data in the future rapidly, identifying complex patterns and enabling real-time measurements of single particles, even in the marine environment.[246]

The use of ART-2-A as a suitable tool clearly demonstrates the differences in the LDI spectra of Fig. 3.1. This provides qualitative features of the fuel particles. In combination with an ionization wavelength of 248 nm, resonant to iron and effective for other metal markers (e.g. vanadium) that commonly arise with HFO,[250] ART-2-A provides a clear advantage for interpreting the given spectra.

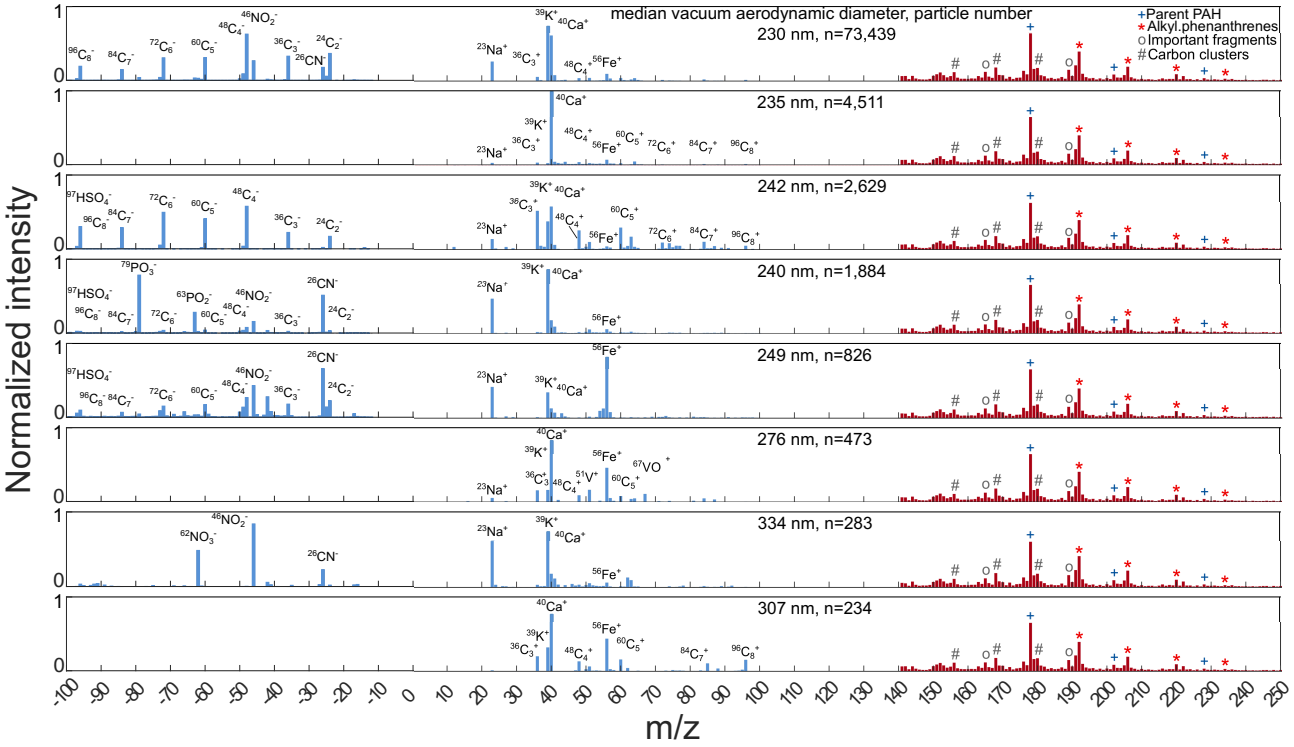

Figure 3.1.: Eight normalized mass spectra show the main clusters from the ART 2-A-clustering algorithm of bipolar LDI mass spectra (blue) for an engine load of 60 kW (75 %) of the research engine. Most clusters show distinct particle classes in the inorganics of the LDI signal, including soot classes represented by the carbon clusters C_n, which are present in both polarities. It is notable that the PAH pattern regarding the alkylated phenanthrenes in the REMPI signal (red) remains consistent. The most significant fragments in the PAH pattern are $m/z =$ 165 and $m/z = 189$ (modified after Ref. [229]).

LDI spectra of each cluster can be used as a counter sample to REMPI spectra, which present a nearly consistent PAH pattern over all clusters. Moreover, a comparison of the results presented in Fig. 2.4 and Fig. 3.1 reveals that this method is capable of discerning the mixing state of aerosols. While metals and salts can be distinguished from each other in the LDI (external mixture), the characteristic PAH pattern remains consistent across all clusters (internal mixture). This pattern is dominated by $m/z = 178$, which could be anthracene or phenantrene. The SPMS is unable to distinguish between these isobaric m/z values. The combustion pathways of anthracene are less well understood than those of phenanthrene. However, the higher thermal stability of phenanthrene,[251–253] along with recent predictions indicating a greater production of anthracene during the oxidation and pyrolysis of toluene[254] (common in commercial fuels) provides strong evidence that anthracene is the predominant product of the combustion process.[229,255,256]

Furthermore, the impact of particle size and engine load on the PAH pattern was investigated, in addition to the distinguishability and similarity between the clusters. Figure 3.2 compares spectra of 3,500 particles from the free-running mode and 3,500 particles from the sizing mode for each of the four distinct load conditions of the engine. The particle size distribution for 60 kW illustrates the range of particle sizes that can be obtained with the free-running and the sizing mode. It should be noted that the free-running mode is also capable of detecting significantly smaller particles than the sizing mode. However, the SPMS is unable to retain the particle size information due to the nature of this mode. The sizing mode is able to map the largest mass range of the particles, despite the smaller measuring range. This range includes $PM_{2.5}$, which is of particular importance from a health and environmental perspective.[8,257] From the comparison in Fig. 3.2 it becomes evident that more soot is observed in the free-running mode than in the corresponding sizing mode at 60 kW. This is to be expected. Soot

occurs more frequently as smaller particles[258,259] that are not fully detected in sizing mode. Compared to the sizing mode, the free-running mode exhibits a reduced contribution of parent PAHs, though the underlying causes of this phenomenon remain unclear. Moreover, there are no substantial disparities in the PAH pattern between the free-running and the sizing mode at 60 kW.[229] The individual load conditions (red areas) in the LDI and the REMPI also show a similar picture. Comparing the results for different load conditions reveals a slight shift to lighter PAHs as the load state increases. However, a consistent PAH pattern could be observed over the whole detectable size range as well as over all loads.

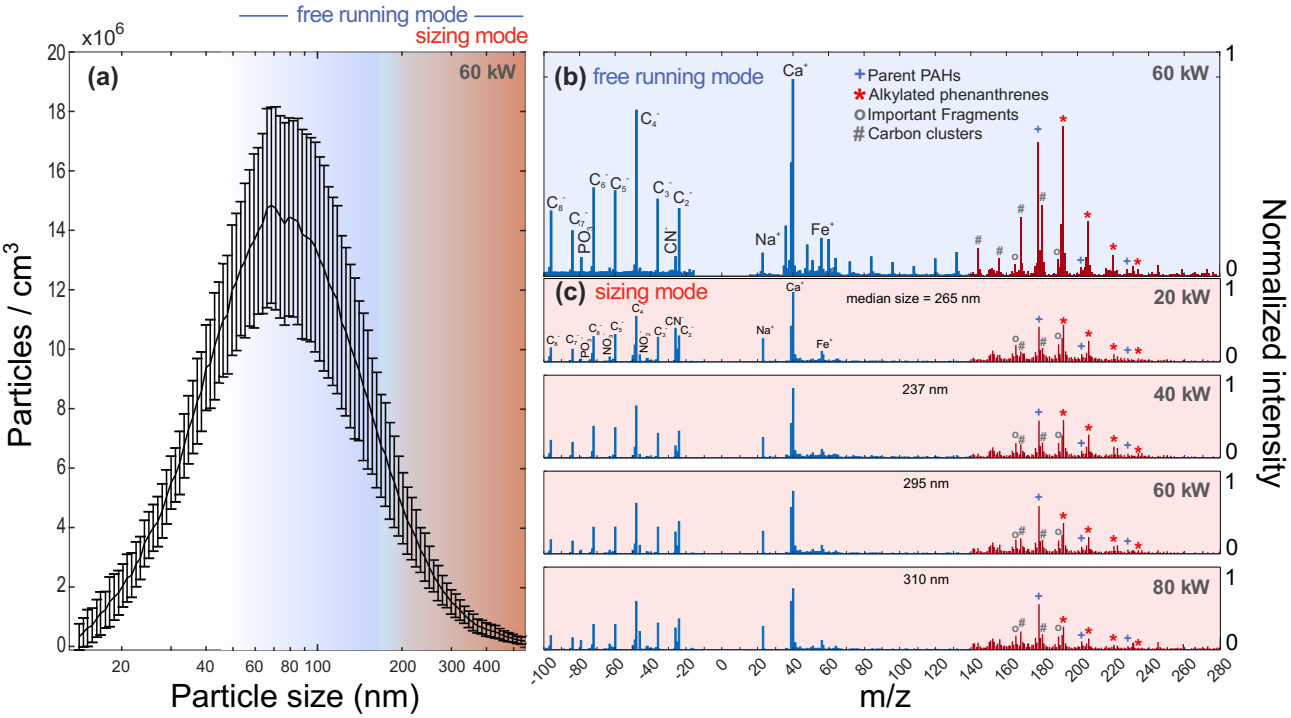

Figure 3.2.: (a) Particle size distribution of the research engine running on MGO at 60 kW load with representative size areas of the free-running mode (blue), where particles are detected at random without size information, and the sizing mode (red) of the SPMS. The size data was obtained using a scanning mobility particle sizer (model 3082, TSI, U.S.). A direct comparison of each $n = 3{,}500$ free-running data set (b) (which includes a greater proportion of smaller particles) with the common sizing data set (c) demonstrates that soot particles are dominant in free-running mode, while the sizing data set exhibits higher signals of phosphate and nitrate. However, the characteristic series of the alkylated phenanthrenes can be observed for all sizes. The analysis of n=3,500 for each of four different loads indicates that both the inorganic pattern and the characteristic PAH signature of the fuel exhibit minimal variation with increasing engine load. Only a subtle shift in the average PAH mass spectra towards lighter PAHs is visible (modified after Ref. [229]).

The violin diagram in Fig. 3.3 demonstrates a clear distinguishability between LDI and REMPI spectra underlining the potential of this work. It is likely that the distinctive PAH pattern in the REMPI signal originates from unburned fuel[180] and therefore primarily accounts for the dissimilarity between the two data sets. Under consideration of the aforementioned factors, the SPMS data obtained from the field study in Sweden[238] (see (i) in Fig. 3.4) underwent a comprehensive reanalysis. The measurement site is situated in close proximity to one of the primary maritime transportation routes leading to the Baltic Sea. A total of 292,242 particles were measured, of which 3,746 exhibited PAH signals.[229] The corresponding measurement results are presented in Fig. 3.4. Gray dots in Fig. 3.4 c) represent particles carrying PAHs, while red particles represent those carrying identified patterns of ship emissions, which are dominated by alkylated phenanthrenes. The latter are emphasized by a plume event (inside the black ellipse). By correlating these results with time and wind data, it is possible to deduce the origin of a particle. Hence it is possible to distinguish particles originating from land and particles originating

from the nearby ship track. The analysis demonstrates that the PAH pattern is predominantly present in low wind conditions and originates from the ship track. In contrast, these PAH patterns are rarely observed in particles originating from land. It is noteworthy that these particles are rarely observed at high wind speeds and distances exceeding 100 km.[229]
The data indicates a predominant contribution from maritime vessel emissions, with terrestrial sources playing a subordinate role in the observed particle composition. The experiment was conducted within a SECA, which requires ships to either run on distillate fuel or use a wet scrubber. The utilization of wind and cruising data facilitated the measurement of single particles carrying PAHs, which demonstrated that a ferry without scrubber technology was likely operating on MGO and crossing the measurement site 45 minutes before the plume event.[229]

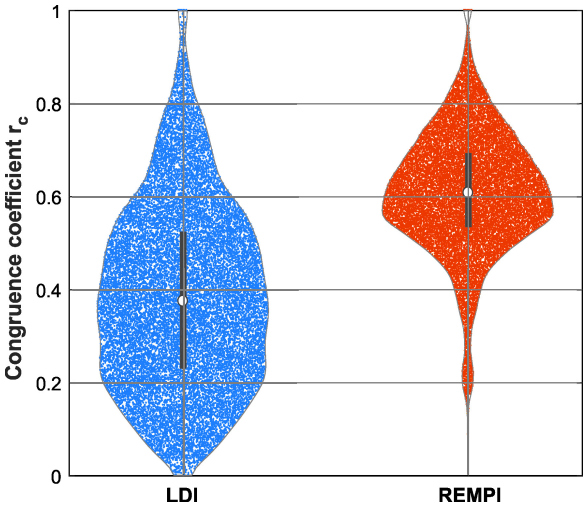

Figure 3.3: Distribution of congruence coefficients r_c between each $n = 25,000$ LDI- (blue) and REMPI data (red) of single particles. The median (white dot) of the REMPI data is higher, and the full distribution with a smaller interquartile range is more narrow compared to the LDI data of MGO, indicating a higher similarity of the REMPI data (modified after Ref. [229]).

The PAHs of this plume could be attributed to the pattern observed in the laboratory experiment, which reinforced the assumption that the plume originated from the ship. This underlines the potential of PAHs as a ship marker. However, despite the collection of measurements over the course of several days, Fig. 3.4 displays only a single, well-defined ship plume. The underlying cause can be attributed to the constrained detection and sizing capabilities of the method. These limitations complicate the detection of particles that fall below the sizing threshold[260] and those originating from vessels that have operated at a large distance over 20 km from the SPMS.[229] At such distances, particles can undergo diverse photochemical, chemical, and physical reactions that can lead to alterations in their chemical structure.[8–10]

The findings underline the possibility of tracing PAH patterns inside SECAs, even for ships operating on distillate fuels, which are often presumed to have a lower environmental impact. Remarkably, the majority of single particles from the laboratory experiment contained PAHs, whereas only a minority of PAHs are associated with ambient aerosols from the field study. This observation, combined with the comparison of Fig. 2.4 with the results presented in Fig. 3.1 and Fig. 3.4, underscores the capability of the SPMS to resolve the external mixing state of PAHs in ambient aerosols. This finding reinforces the potential of the employed method for source apportionment. Moreover, this study highlights the need for more comprehensive policies that address PAH emissions in addition to other regulated pollutants, such as SO_x and NO_x. However, a rapid switch to cleaner and healthier fuels is expensive and unrealistic in the near future.[155] Consequently, this study opens up the possibility of using PAHs as a new tracer for source apportionment, including distillate fuels that are established on the market, such as MGO.

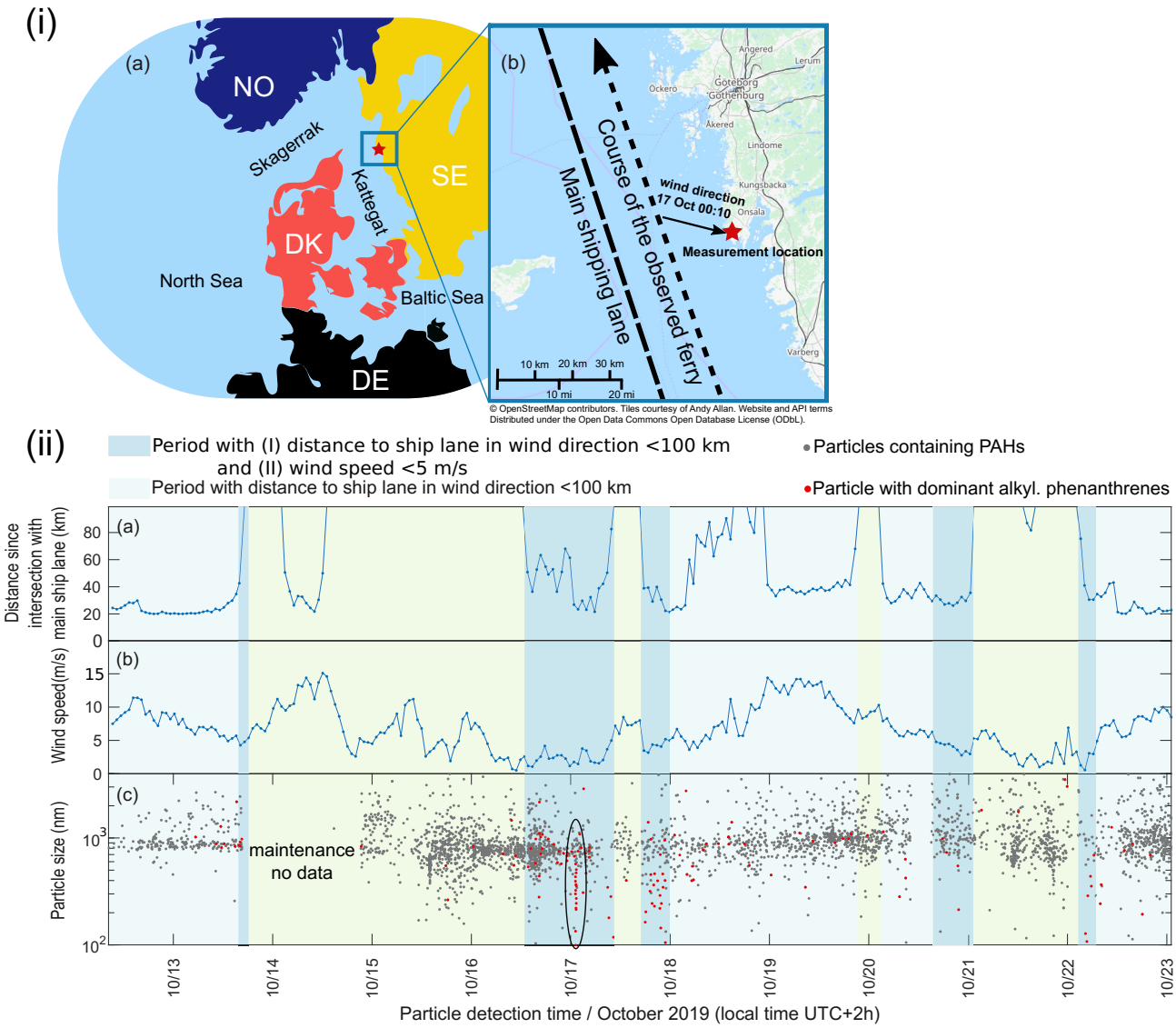

Figure 3.4.: (i) (a) Measurement site in Sweden near a main shipping lane within a SECA (map modified after Ref. [143]). (b) Shipping lane and location of the SPMS in Sweden measuring single particles from the ferry (map modified after Ref.[261]). (ii) Distance since intersection with main ship lane (a), wind speed data (b) and the particle size (c) of the measured events (gray, red dots) over the detection time (modified after Ref. [229]).

3.2. Polycyclic Aromatic Hydrocarbons as Fuel-Dependent Markers in Ship Engine Emissions using Single-Particle Mass Spectrometry

Following the discovery of a consistent PAH pattern in the initial study of MGO-powered ships on a single-particle basis, the objective of this study is to extend the knowledge gained to other marine fuels. Four different fuels were analyzed for the presence of PAH patterns in the REMPI, using the same methodology. In addition, the consistency and distinguishability of the patterns observed were evaluated. The fuels selected for this study are: MGO, HVO, and HFO 0.5 % (w/w) FSC, which are compliant with SECA's standard, and the non-compliant HFO 2.4 % (w/w) FSC, a fuel that is still widely used outside of ECAs.[154] Hence, this investigation covers the most common contemporary fuels and those that will account for a substantial proportion of maritime transport in the future.[45,154,155,171]

All fuels were tested in the laboratory setting with the single-cylinder, four-stroke, 80 kW research ship

engine, which allows for the analysis of the various fuels under different load conditions.[104] The results presented here focus on the load conditions of 20 kW and 60 kW. With this simulation we can study the chemical structure of emitted particles under conditions mimicking harbour entries and shallow water traverses (20 kW) and normal cruising speeds (60 kW).

Figure 3.5 illustrates the sum spectra of all fuels under a load of 60 kW. Each spectrum is the result of summing 10,000 individual particle measurements. Examination of the spectra exhibit discernible patterns in the REMPI spectrum. MGO exhibits the characteristic PAH pattern, with a predominant signal at $m/z = 178$, accompanied by a series of alkylated derivatives confirming the results of the first study. The mass spacing between the alkylated derivates remains constant at 14 Da.

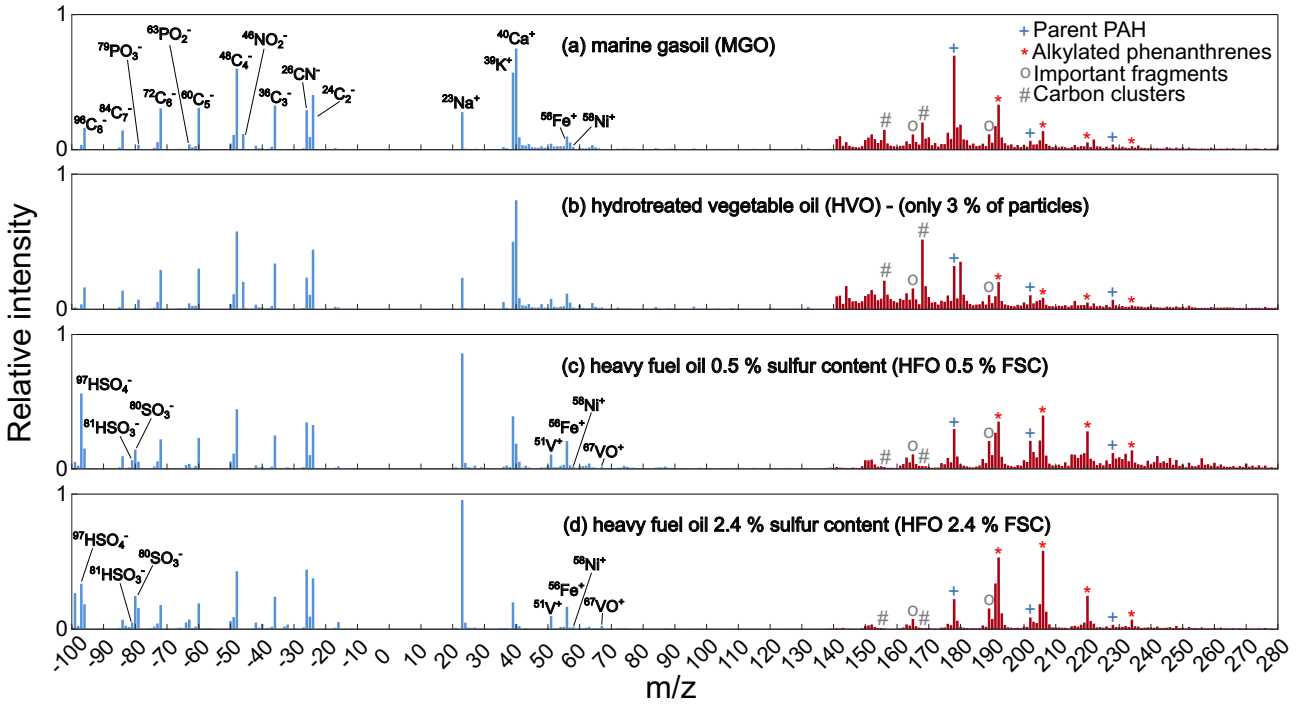

Figure 3.5.: Mass spectra ($n = 10{,}000$) obtained through dual-ionization techniques - laser desorption/ionization (LDI, blue) and resonance-enhanced multiphoton ionization (REMPI, red) - reveal distinct compositional profiles for four marine fuels at 75 % engine load. The inorganic fraction analysis of residual fuels demonstrates characteristic signatures of transition metals and sulfur. Marine gas oil (MGO) and hydrotreated vegetable oil (HVO) exhibit similar PAH distribution patterns, although HVO generates substantially lower absolute PAH signals (a normalization was made for comparison). Heavy fuel oils (HFO) display a distinctive profile characterized by higher molecular weight PAHs and enhanced alkylation, evidenced by a shift in signal maximum toward C_2-phenanthrene species (modified after Ref. [203]).

In the case of the remaining three fuels, a distinct and discernible progression is evident. Although minor differences are found between the two HFOs, a disparate pattern was observed in comparison to MGO. The pattern for HFO commences at higher masses, with a predominant C_2-phenanthrene peak at $m/z = 206$. Additionally, HVO exhibits a distinct PAH pattern that is different from other fuels. Given that HVO is a PAH-free fuel and that only 3 % of the particles in the sum spectra show any signals for PAHs, it can be assumed that these signals predominantly originate from lube oil and spillage of other particles rather than from the combustion process. Supplementary information regarding metal signals obtained from LDI is also beneficial in distinguishing between the fuels. However, the primary apportionment features can be attributed to the PAH pattern observed in the REMPI spectra.

To measure similarity between emission signatures of the four fuels, the congruence coefficient r_c is computed for 5,000 particles for each fuel.

$$r_c = \frac{\sum_{k,l} x_{k,l}^2 \, y_{k,l}^2}{\sqrt{(\sum_{k,l} x_{k,l}^2)(\sum_{k,l} y_{k,l}^2)}}. \tag{3.1}$$

The respective distribution of congruence coefficients from Eq.3.1 is presented in Fig. 3.6. The plot displays the similarity of the single REMPI data sets to each other. It shows a comparison to the LDI data set of MGO presenting a higher degree of similarity of the REMPI data compared to the LDI data. This high degree of similarity is evident when considering the narrow interquartile range of the REMPI data.

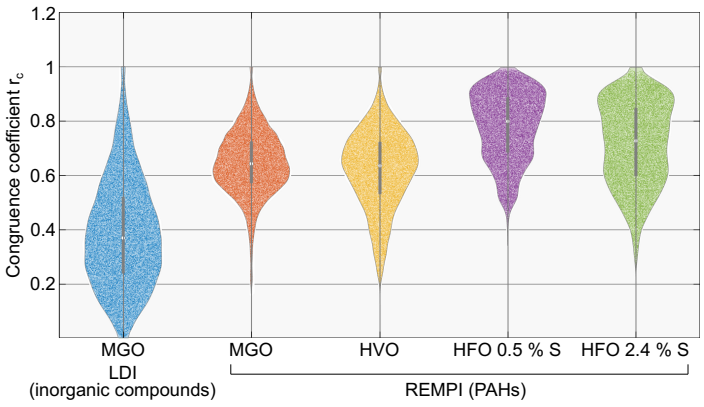

Figure 3.6: Distribution of congruence coefficients r_c for four marine fuels: MGO, HVO, HFO 0.5 % FSC, and HFO 2.4 % FSC (each $n = 5{,}000$). On the left hand, the first violin plot symbolizes the heterogeneity of the inorganic part. The adjacent violin plots demonstrate the higher homogeneity of the REMPI data dominated by PAHs, underlining the potential of PAHs as novel ship markers. The width of the plots depicts the number of particles within a bin, while the interquartile range provides the half of the particles as a grey bar with its median as a white dot (modified after Ref. [203]).

An essential goal of the work in this thesis is to determine the differentiability of PAH residues on particles as new ship emission markers. To assess the degree of distinguishability between the detectable particles, 1670 particles were analysed for each of the four fuels using a PCA method. Figure 3.7 shows the relationship between the load and fuel parameters in a PCA biplot and the relationship between these data and the particle size distribution. This provides definitive information about the variables responsible for the grouping of the loadings. The data covers over 57 % of the variance. The mass-to-charge ratio is represented by the plotted eigenvectors which have a strong influence on the distribution of the data. Each data set is enveloped by an ellipse representing a 95 % confidence interval.

The fuels can be visually separated due to the higher proportion of longer alkylated alkyl chains present in the homologue series of phenanthrene. This is the primary factor allowing fuel separation, as the proportion of unburned fuel exerts a dominant influence on the aromatic component of the single particles.[180] In this context, the prevalent peaks for HFO are the C_2- to C_4-alkylated phenanthrenes ($m/z = 206$, 220, and 234). Conversely, common fragments like $m/z = 189$ show a higher degree of alkylation. With the exception of MGO and HVO, the latter being regarded as the benchmark for the 'cleanest' hydrocarbon fuel, the 95 % confidence intervals of the remaining ellipses do not overlap. This suggests that the variances within fuel types is lower than among each other, reinforcing the potential of PAHs as ship markers.
With regard to the load effect (vertical direction) on the data, it is apparent that lower loads are more separated than higher loads. This is a result of higher contribution of unburned fuel. Nevertheless, the higher loads remain discernible, exhibiting a higher proportion of aromatics derived from high-temperature pyrosynthesis within the combustion chamber. Furthermore, the m/z ratios of 178 and 192 indicate a pulling effect of the fuels in the direction of PC2, particularly for MGO. These phenanthrenes exhibit minimal or no alkylation, which can be attributed to a pyrosynthesis process with reduced unburned fuel. Although the PCA biplot also indicates the contributions of the alkylized phenanthrenes ($m/z = 206$, 220, and 234) in the negative PC2 direction, it can be concluded that the variance of the

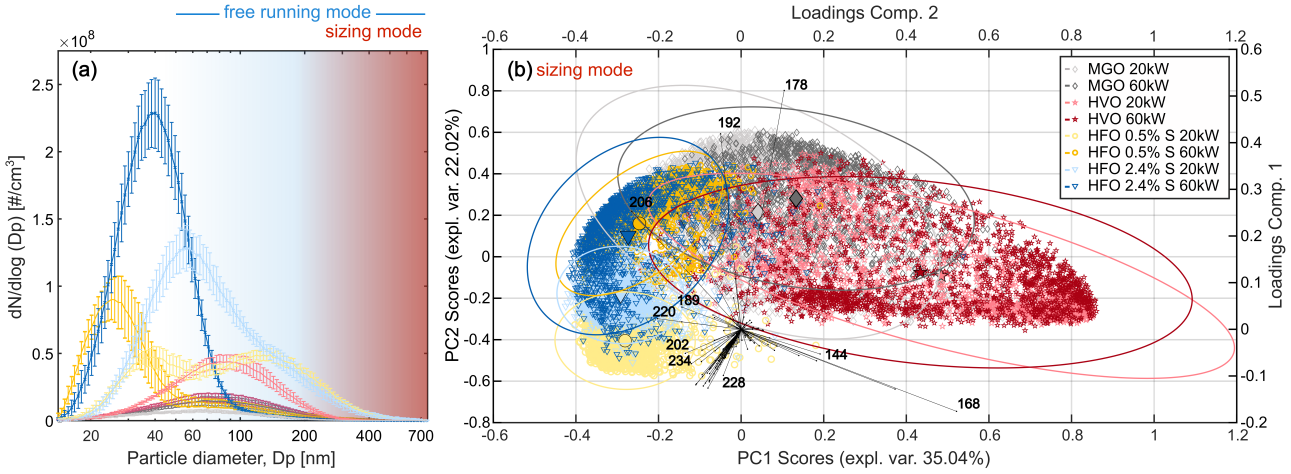

Figure 3.7.: (a) Size distribution of particles from different fuels: marine gas oil (MGO), hydrotreated vegetable oil (HVO), heavy fuel oil (HFO) (0.5 % FSC) and HFO (2.4 % FSC). The fuels are examined under two load conditions: 20 kW and 60 kW. Additionally, the blue and red areas represent the regions of free-running mode (in which size information from SPMS is absent) and sizing mode, respectively. (b) Corresponding principal component analysis of single particles from REMPI of all fuels that fall within the sizing mode area delineated in (a). The length of the eigenvectors represents the contribution of signals at different mass-to-charge ratios to the mass spectral differences. Ellipses depict the 95 % confidence interval for the principal component scores of each cluster. While the clusters are well separated for the low load conditions (light colours), the mass spectral signatures approach each other at higher load (dark colours), but remain distinguishable. The number of observations is $n = 1670$ for each of the fuels and loads (modified after Ref. [203]).

load effect is smaller than that of the fuel effect. Consequently, fuel particle emissions of 200 nm and larger can be differentiated via PCA despite a changing load.

In summary, the extension of the approach of using PAHs as marine fuel marker towards more fuel types has provided significant insight into the potential of the presented analysis method in differentiating marine fuel types. Commercially significant fuels (HFO, MGO)[155,262] were compared with one of the 'cleanest' hydrocarbon fuels currently available (HVO).[263] It was also demonstrated that the engine load and particle size have limited influence on the distinct PAH pattern. Distinguishable PAH patterns can be observed under different scenarios. The findings can also provide valuable insights for health assessments of ship emission exposure. Preliminary results of the first two studies have demonstrated the potential of PAHs as ship markers for relevant ship fuels in both a field study and a laboratory study. However, the increasing use of wet scrubbers in ECAs requires investigations to evaluate their impact on alkylated PAHs and improve PAH assessment as novel ship markers.

3.3. Limited Impact of Wet Scrubber Exhaust Treatment on the Chemical Composition of Individual Ship Emission Particles

Preliminary assessments suggest that PAHs may serve as novel markers for ship emissions. Nevertheless, a more accurate assessment requires consideration of the impact of scrubbers on fuels, particularly those not compliant with ECA regulations. The impact of scrubbers on the gas phase unequivocally demonstrates that wet exhaust systems are highly effective in reducing the sulfur content in the gas phase. In particular, the removal of SO_2 can be achieved with remarkable efficacy through this method.[264,265] However, there is a lack of knowledge regarding the impact of scrubbers on the particle phase. Preliminary findings suggest that the efficiency of scrubbers in removing $PM_{2.5}$ in the particle phase may be limited.[158] Therefore, it is evident that the health impacts of the emitted ship particles remain. Moreover, it has been demonstrated that the utilization of open-loop scrubbers has a profound

detrimental impact on the environment.[131,156,266] This motivates a study to assess whether the particles still exhibit the fuel-specific PAH patterns following the scrubber. The influence of an open-loop wet scrubber on the particle phase of the emitted HFO and the effect on potential PAH patterns is tested under varying load conditions. As in the two preceding studies, the experiments were conducted on an appropriate ship engine (for further details, see Streibel et al., 2017[104]). Furthermore, a downscaled open-loop wet scrubber (SAACKE, Germany) was installed downstream of the main apparatus, with water of a salinity of 10.5 ± 3.6 PSU at a pH value of approximately 8. Further details regarding the scrubber can be found in the work of Bendl et al. (2024).[267] The aerosol was measured at two temperatures: 200 °C before the scrubber (upstream) and 60 °C after (downstream). As in previous laboratory studies, the dilution factor was set to 1:25.

Figure 3.8 presents the accumulated sum spectra for upstream and downstream operation of the wet scrubber in open-loop mode at two different load conditions, 20 kW and 60 kW. Moreover, the signal contribution of PAHs at single-particle level is depicted on the right-hand side of Fig. 3.8. The

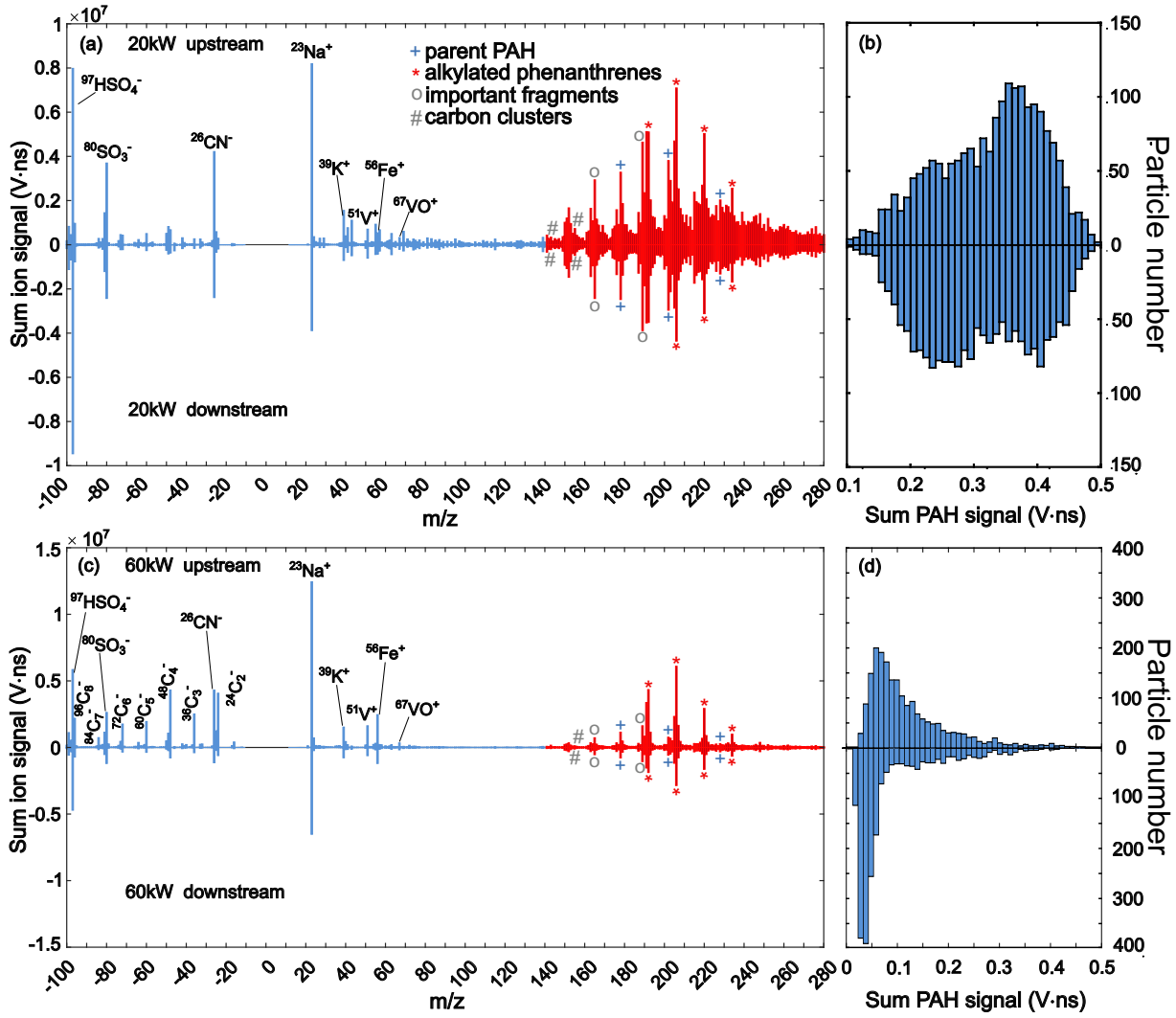

Figure 3.8.: Accumulated mass spectra of heavy fuel oil 2.4 % S (HFO) emissions with each $n = 2000$ particles for the upstream operation (top) and the downstream operation (bottom) of the scrubber at different load conditions — (a) 20 kW and (c) 60 kW. (b,d) Distinct particle distribution of the PAH signals before and after the scrubber, with minimal discernible variation. (c-d) At elevated load conditions, soot represents a significant proportion of the particles. The wet scrubber reduces the EC and PAH fraction of the particles. However, the typical PAH pattern of the fuel remains unaltered (modified after Ref. [159]).

accumulated mass spectra of HFO, the LDI (blue), demonstrate the presence of typical components, including metals, sulfur, soot, organic carbon fragments, and the classic ship markers vanadium and iron. They can be measured using the current method.[234] In addition to the typical metals, the REMPI (red) also displays the typical PAH patterns that have been linked to HFO previously in the second study of this work.[203] These are dominated by C_2-phenanthrene with $m/z = 206$. A comparison of the 20 kW and 60 kW data sets indicates that the proportion of OC and PAHs is higher under low load, while the accumulated mass spectra are dominated by soot due to the more efficient combustion of the fuel at higher load (higher temperatures).[268] Additionally, a slight increase in the sulfur content is observed in the form of HSO_4^- ($m/z = -97$), although this may be attributed to saturation effects at this channel. Therefore, SO_3^- at $m/z = -80$ is more representative of the sulfur reduction of the scrubber and is apparently reduced for both load conditions.
The experiment did not yield any evidence of the presence of water-soluble organic acids, which the SPMS is capable of monitoring in negative mode.[269] Conversely, the proportion of water-insoluble OC can be estimated through the PAHs, which are also insoluble in water.[182,186] The histogram on the right-hand side shows the PAH mixing state based on the distribution of the accumulated PAH signals across the particles. The distribution and PAH pattern for HFO remain largely unaffected by the scrubber, allowing for a clear recognition of the PAH pattern previously evaluated (see Section 3.2). The typical metallic markers (Fe, V, etc.) can be identified in the cation spectra of the LDI. It is noteworthy that the chemical signature within the particle phase remains largely unaltered downstream the scrubber, exhibiting only minor fluctuations, such as a reduction in EC content at high load conditions (60 kW). This finding was previously documented by Jeong et al. (2023)[157] in a separate study on the same scrubber, along with an increase in sulfate.[157] Elevated sulfate concentrations result from SO_2 dissolution in scrubber wash water, leading to sulfurous acid formation and subsequent secondary sulfate generation in the particulate phase.[244] The observed EC reduction stems from enhanced removal of smaller particles, particularly soot,[203,270,271] through diffusion-driven coagulation processes.[157,272] While the aggregated mass spectra suggest modest overall wet scrubber effects, a more detailed understanding of particle component alterations necessitated additional principal component analysis. The analysis examined compositional variance at the single-particle level for both LDI and REMPI and results are shown in Fig. 3.9.

Figure 3.9 accounts for nearly 70 % of the explained variance for HFO at 20 kW and 60 kW load condition (upstream and downstream). The study includes a comparison between MGO at 20 kW and 60 kW loads and a SECA-compliant fuel to emphasize the clear distinguishability between the fuels. Despite the operation of the wet scrubber, the principal component analysis (PCA) reveals a distinct separation between MGO and HFO across all conditions. The differentiation is a consequence of the disparate signatures of sulfate, iron, vanadium, calcium, and sodium. The effect of the scrubber is more pronounced than that of the load within the PCA. However, the typical PAH marker in the REMPI continues to exert a dominant influence on the fuel print, both with and without scrubber operation, and remains largely unaffected. The disparity primarily comes from the elevated sulfate signal at $m/z = -97$, which is attributed to the gas-to-particle conversion of SO_2. This underscores the capability of the method to analyze ship emissions utilizing a wavelength of 248 nm, as well as the potential of PAHs as a novel marker for modern ship emissions. Finally, the study demonstrates that the impact of wet scrubbers on the chemical composition of individual particles is minimal.[159] Due to the negligible chemical alterations in the particles induced by the scrubber, the correlation between emitted particles and removal efficiency can be utilised in future research to estimate environmental impacts. Furthermore, this finding can be employed to enhance the investigation of health implications associated with the utilisation of wet scrubbers.

Concluding the series of studies, PAHs are demonstrated to possess a tracer potential for source apportionment in the gas phase. PAHs also exhibited the potential to act as a novel marker for ship emissions at the single-particle level. This was achieved by taking advantage of well-resolved online data on single particles. The data leading to this conclusions was obtained using a modern

ionization method that is spatially flexible and can be deployed in a variety of settings. Multiple analytical methods were employed to examine a range of potential influencing factors on ship emissions. Despite the use of different fuels, loads, sizes, or technical devices (wet scrubber), the SPMS method was able to consistently measure PAH patterns for individual ship emissions and distinguish them. Furthermore, findings on the influence of wet scrubbers on the chemical composition of individual particles were collected, which could help investigate further health and environmental influences of scrubbers in the future.

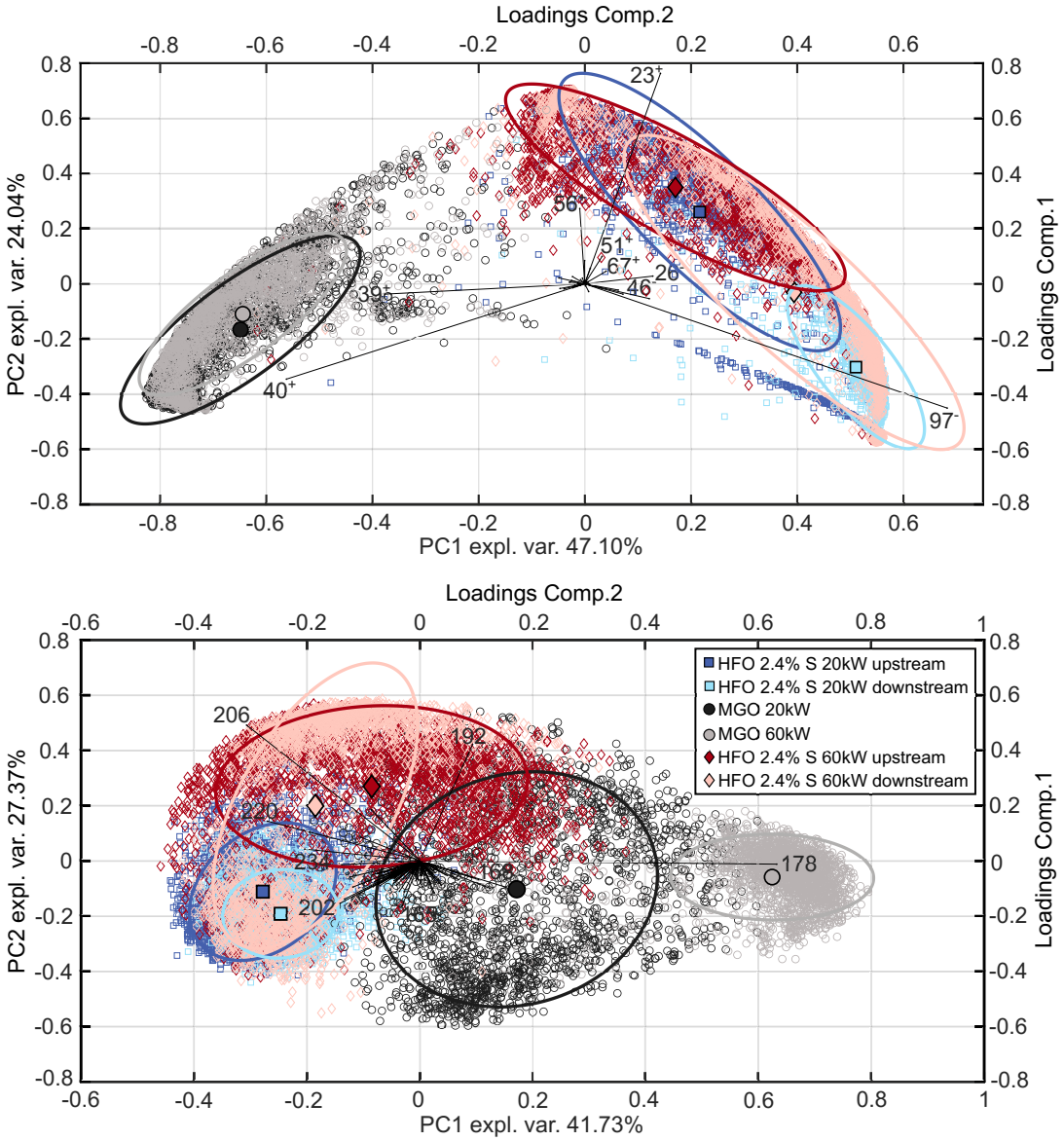

Figure 3.9.: The PCAs clearly show two different fuels: one heavy fuel oil (HFO) (blue, red) with an fuel sulfur content (FSC) of 2.4 %, and the SECA-compliant marine gas oil (MGO) (grey), each at a load of 20 kW and 60 kW, each with $n = 2000$. Furthermore, the PCA differentiates between the HFO in upstream (lighter blue/red) and downstream (darker blue/red) modes of an open-loop wet scrubber. The confidence interval for both PCAs is 68 %, with an explained variance of approximately 70 %. The upper PCA illustrates the LDI spectrum of individual particles. A clear distinction between the propellants can be observed, which is mainly evoked by the sulphur content ($m/z = -97$) of the HFO. A slight loading effect is discernible, but it is of no consequence for both fuels. Despite the influence of the scrubber being more pronounced than that of the fuel, all common HFO-derived metals remain. Similarly, in the second PCA, which presents the REMPI data for the same states, the load and scrubber effect do not impact the pattern of the important alkylated phenanthrenes. Here, too, the fuel effect, likely due to unburned fuel, is evidently higher (modified after Ref. [159]).

3.3.1. Potential of the Application Method

The preceding studies suggest the feasibility of PAHs as novel markers of ship emissions. Further investigations and field studies are recommended to investigate the respective PAH patterns under varying weather conditions and distances to the ships. This would facilitate a more robust determination of the signatures of PAHs, as these studies have not taken into account factors such as the complex aging processes of PAHs and other environmental influences. Even though a first field study on the Swedish coast measured individual particles at a shorter distance of $15-20\,\mathrm{km}$.[229] Long range capabilities have yet to be demonstrated. The present measurement method is still size-limited in sizing mode and does not yet detect ship emissions, which can often be smaller than 200 nm. However, the presented results show that field studies and laboratory measurements of PAH patterns are possible with the described methodology. It has been shown that certain PAH patterns can be consistently assigned to the respective fuels.[159,203,229] Consequently, it is recommended that more measurements are taken in the future to refine our understanding of PAHs as markers for ship emissions. This would enhance progress in source apportionment which is of particular importance in light of the expanding number of vessels using open-loop wet scrubbers,[38,59,161,162] and the gradual introduction of "cleaner" marine fuels.[45,155]

In the next section the method is extended to illustrate the broader potential of single-particle measurements as an online method. Its optimization and extension to other potential tracer elements is discussed.

3.4. Impact of Fuel Sulfur Regulations on Carbonaceous Particle Emission from a Marine Engine

In light of the growing body of evidence PAHs are suitable as novel ship markers, this recently published study explores the possibility of utilizing alternative tracers by utilizing emission factors (EF) of EC/OC. The relationship between fuel composition and the specific characteristics of soot in the microstructure was elucidated through multi-wavelength thermal-optical carbon analysis (MW-TOCA). This finding may be utilized in online monitoring by SPMS as an extension to transition metals and PAHs as markers of marine traffic.[273]

To evaluate the potential of EF of EC/OC ratios for source apportionment in the maritime sector, a series of filter samples of $PM_{2.5}$ from diverse shipping fuels were subjected to MW-TOCA analysis. To encompass a comprehensive range of commercial fuels currently available on the market, a variety of fuels with distinct FSC were analyzed. These include modern SECA-compliant fuels (HVO, MGO), globally compliant fuels (LS-HFO), and non-compliant fuels (HFO_{syn}, HFO) as of January 1st, 2020. It should be noted, however, that HFO_{syn} and HFO fuels are still in use in conjunction with exhaust-cleaning systems, such as scrubbers. The analysis of filter samples by MW-TOCA (combining established quantities of EC and OC with their optical properties[274]) was complemented by an investigation of changes in physicochemical properties of the particulate phase to compare the resulting emission factors (EFs). The same marine engine and scrubber were used as in the previous studies (for further details see Streibel et al. (2017)[104]).
It should be noted first that regulating the sulfur content of fuel alone does not significantly impact the EC/OC ratio. Instead, SECA-compliant fuels are produced through diverse production processes, resulting in varying EC/OC ratios. The study addresses the disparate behavior of the fuels during combustion at varying load conditions. It reveals that the emission factor of distillate fuels tends to remain constant with increasing engine load, whereas the EF of crude oil (HFO) decreases.[273] In general, the implementation of the upper sulfur limit of 0.5 % FSC (w/w) only has minor impact on

the carbonaceous emissions in case of the commonly used HFOs (LS-HFO and HS-HFO). The emission reduction in relation to the IMO engine test cycle E2 (see Fig. 3.10) when switching from HFO to distillate fuels can be explained by the lower emissions at 25 % engine load. The investigations in Fig. 3.10 demonstrate the applicability of MW-TOCA for the characterization of carbonaceous aerosol emissions from marine engines. In accordance with the approach proposed by Han et al. (2007),[275] EC and OC are separated into distinct fractions. EC is divided into char-EC (EC_1, and soot-EC (referring to the sum of EC_2 and EC_3)). OC is divided into four fractions (OC_1 - OC_4) as well as pyrolytic OC (OC_{pyro}), which accounts for differences in thermal refractiveness and, consequently, in soot microstructure.[275]

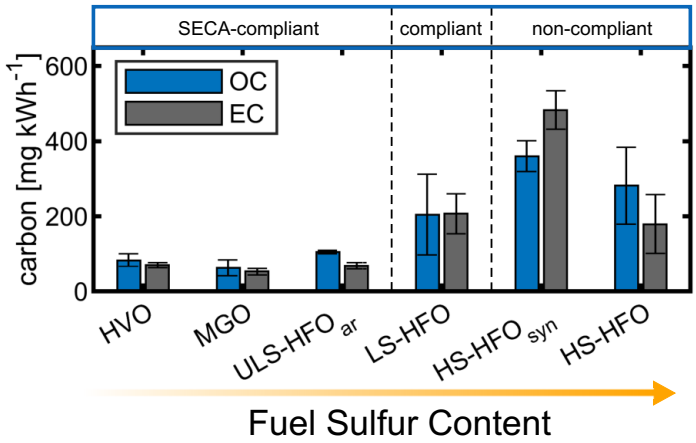

Figure 3.10: Emission factors of organic and elemental carbon (OC (blue), EC (grey)) are weighted according to the IMO engine test cycle E2. The data pertain to marine fuels of different fuel sulfur compliance levels. The standard deviation from $n = 5$ is indicated by error bars. (modified after Ref. [273]).

The differentiation of EC into char- and soot-EC provides insights into the distinct combustion pathways associated with various marine fuel types. The formation of char-EC is favoured by highly viscous, more dense fuels with low volatility. An example is HFO with a kinematic viscosity of 380 $mm^2 s^{-1}$ at 50 °C and a density of 0.990 $g cm^{-3}$ at 15 °C which undergoes pyrolysis of incompletely vaporized fuel droplets. In the *ImproveA* temperature protocol in TOCA, the addition of oxygen to a helium atmosphere results in the immediate oxidation of the graphite layers of EC_1, along with OC_{pyro}, due to the porous morphology and increased surface area of the EC_1.[273,276] Conversely, the formation of soot-EC is more dominant for the diesel-like fuels such as HVO or MGO, showing a kinematic viscosity of 2 $mm^2 s^{-1}$ and a density of 0.835 $g cm^{-3}$. Droplets of diesel-like fuels evaporate quickly. Consequently, the decomposition of hydrocarbons into radicals results in the generation of primarily soot-EC through radical-driven flame synthesis.[273]

Blends of SECA-compliant ULS-HFO exhibit properties that lie in between those of HFO and diesel-like fuels. These blends have a density that is comparable to that of HFO and a viscosity that is similar to that of diesel-like fuels. The resulting char- and soot-EC fractions lie between the HFOs and the diesel-like fuels. The intermediate behavior of hybrid fuels like ULS-HFO_{ar} demonstrate the impact of fuel properties, including aromatic content, viscosity and density, on the relative contribution of char- and soot-EC. Moreover, the impact of a wet scrubber operating on HS-HFO and HS-HFO_{syn} was tested.[157] However, the scrubber seems to have limited impact on the formation of the different EC-OC fractions as illustrated in Fig. 3.11.
In addition to the emission factors, the Simple Forcing Efficiency (SFE) study also addresses the optical properties of marine fuels, which gives insight into their impact on the climate. However, this topic will not be elaborated in depth here (for detailed information see Bauer et al. (2024)[273]). Furthermore, the findings demonstrate the influence of engine operation factors such as engine type or fuel switch protocols on the carbonaceous composition of ship emissions. Slow-speed, two-stroke engines predominantly emit char-EC, whereas medium-speed, four-stroke engines operating on distillate fuels exhibit higher soot-EC fractions. During transitional periods of fuel switching (e.g. when entering SECAs), residual metals and sulfur from HFOs modulate EC oxidation and soot formation.

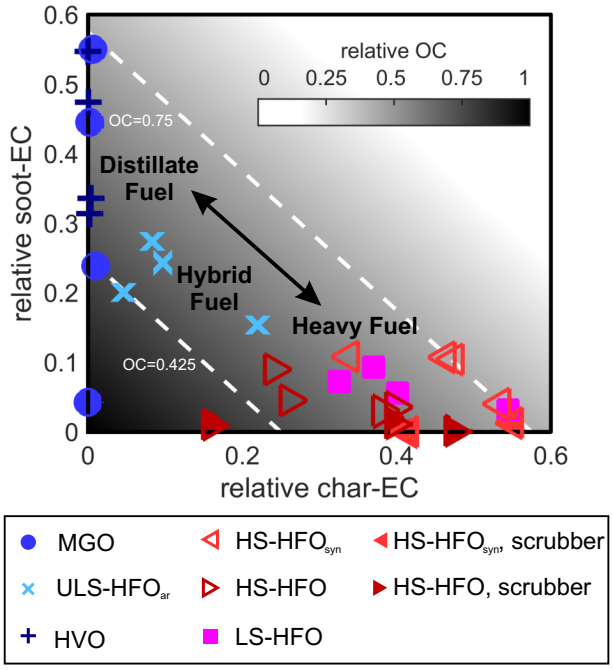

Figure 3.11: Distributions of OC, char-EC, and soot-EC. The fractions of OC, char-EC (EC1), and soot-EC (EC2 + EC3) for all 24 fuel/engine load combinations are as follows: Two distinct branches of diesel-like fuels are evident: HVO and MGO with a low char to EC ratio on one end and LS-HFO, HS-HFO$_{syn}$, and HS-HFO with a high char to EC ratio on the other. ULS-HFO$_{ar}$ occupies a unique position in between. The dashed lines show the relative OC range of 42.5 % to 75 %, which encompasses 90 % of the experiments. The filled red triangles represent HS-HFOsyn and HS-HFO emissions after open-loop wet scrubber treatment, as reported by Jeong et al. (2023)[157] (modified after Ref. [273]).

The analysis of the carbonaceous properties of different marine fuels with TOCA provides the motivation for further investigation of these species with SPMS. The observed differences in EC structure, influenced by fuel properties, were further linked to the distribution of carbon clusters. These clusters were generated by the ART-2-A algorithm produced by LDI in SPMS. As previously stated, a combined approach of LD-REMPI/LDI offers a promising pathway for identifying ship particulate emissions by distinct signatures of PAHs and transition metal traces.[203,229,277,278] Cluster analysis of carbon fragment ions revealed distinct patterns for compliant fuels, such as MGO, LS-HFO, and ULS-HFO$_{ar}$. Variations in the contributions of small, medium, and large carbon clusters are observed for different fuel types. The results from Fig. 3.12 suggest that char-EC particles from HFO emissions decompose into smaller carbon ions due to their porous morphology. More compact soot particles from diesel-like fuels such as MGO produce distinct cluster distributions. Notably, ULS-HFO$_{ar}$ emissions exhibit clusters dominated by large carbon fragments, likely reflecting enhanced soot inception due to higher soot precursor availability.

Overall, the cluster analysis confirms the assumption that different EC fractions on individual particles could be suitable for source apportionment of ship emissions. However, further laboratory studies on two-stroke ship engines and field studies inside SECAs are necessary for a better understanding and assessment of this approach.

To summarize, this study examines the effect of sulfur content in marine fuels on the emission of carbonaceous particles from ship engines employing a wet scrubber system. The analysis is centered on the transition to low-sulfur fuels, driven by international regulations from the IMO for a sulfur limit inside SECAs. The findings indicate that the change to different fuels with their specific fuel and combustion properties can influence other particle emissions, including the ratio of EC_1, EC_2, EC_3, and OC. This research elucidates the trade-offs associated with fuel sulfur regulations. It emphasizes the importance of understanding the interactions between fuel composition, combustion processes, and particle characteristics. It enhances the understanding of how fuel composition impacts PM, particularly in the maritime sector. It underscores the complex chemistry of carbonaceous particles, including their role in RF and air quality. Ultimately, the study demonstrates the potential of employing modern ionization techniques for single particles to qualitatively assess carbon with its different fractions of EC as a tracer element for marine traffic. Thus, in addition to transition metals and PAHs, another

possibility for source apportionment of ship emissions has been shown to be feasible using SPMS. Future investigations should focus on field studies under different weather circumstances. Additional laboratory experiments on larger and more prevalent two-stroke engines (employed in tankers and large vessels), which exhibit distinct combustion characteristics compared to four-stroke engines,[279,280] would complement the data obtained in this study and allow a better assessment of this marker approach.

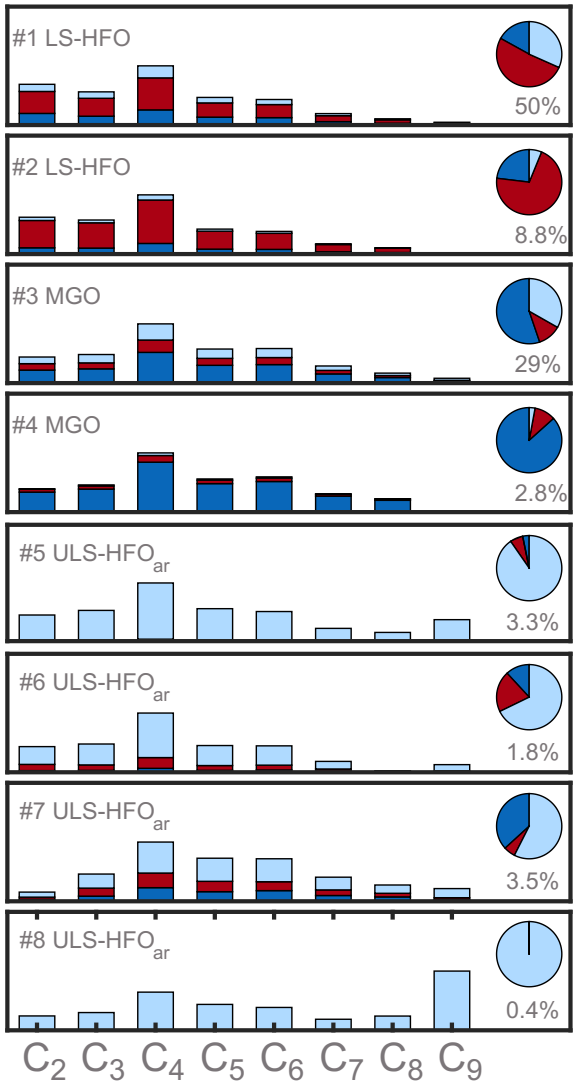

Figure 3.12.: Eight clusters from ART-2-A of C_n species with $n = 2, 3, \ldots, 9$ in negative LDI with the overall contribution of compliant or SECA-compliant fuels LS-HFO (dark red), MGO (dark blue), and ULS-HFO$_{ar}$ (light blue), presented in a pie chart. The cluster names are derived from the cluster-dominating fuel, and the percentages denote the contribution to the total cluster weights (modified after Ref. [273]).

3.5. A solid-state IR Laser for two-step Desorption/Ionization Processes in Single-Particle Mass Spectrometry

This study investigates the applicability of a prototype erbium solid-state laser (Er:YAG 1000 FQ, InnoLas Laser GmbH, Germany[208]) for laser desorption of particles in SPMS. The CO_2 laser, which has been used in all preceding studies of this work, has been demonstrated to be an effective method for the desorption of organics on individual particles. However, compared to ionization with Er:YAG lasers, the method is more cost-intensive and can result in a higher degree of fragmentation of the organics on single particles.[208, 281]
To ascertain whether a solid-state laser is also suitable for the desorption of organic material onto single particles (e.g. PAHs) and thus for the measurement of organic tracer elements, the study presents a detailed comparison between a 250 ns pulsed CO_2 laser and an erbium solid-state laser. The properties of these laser systems are listed in Tab. 3.1. The experimental setup is illustrated in Fig. 3.13.

	Laser	desorption	LDI	REMPI
Laser type, medium	Gas, CO_2	Solid-state, Er:YAG	Gas-Excimer, KrF	Gas-Excimer, KrF
λ (nm)	10600	2940	248	248
Beam diameter (mm)	1 x 1 (Gaussian)	5 x 5 (Flat top)	0.2 x 0.4 (Gaussian x Flat top)	5 x 10 (Gaussian x Flat top)
Pulse energy (mJ)	15	160	4	4
Pulse duration (ns)	250	200000	5	5
Peak irradiance ($W\,cm^{-2}$)	1.5 x 10^7	3.2 x 10^3	1.0 x 10^9	1.6 x 10^6

Table 3.1.: Overview of the laser properties (modified after Ref. [208]).

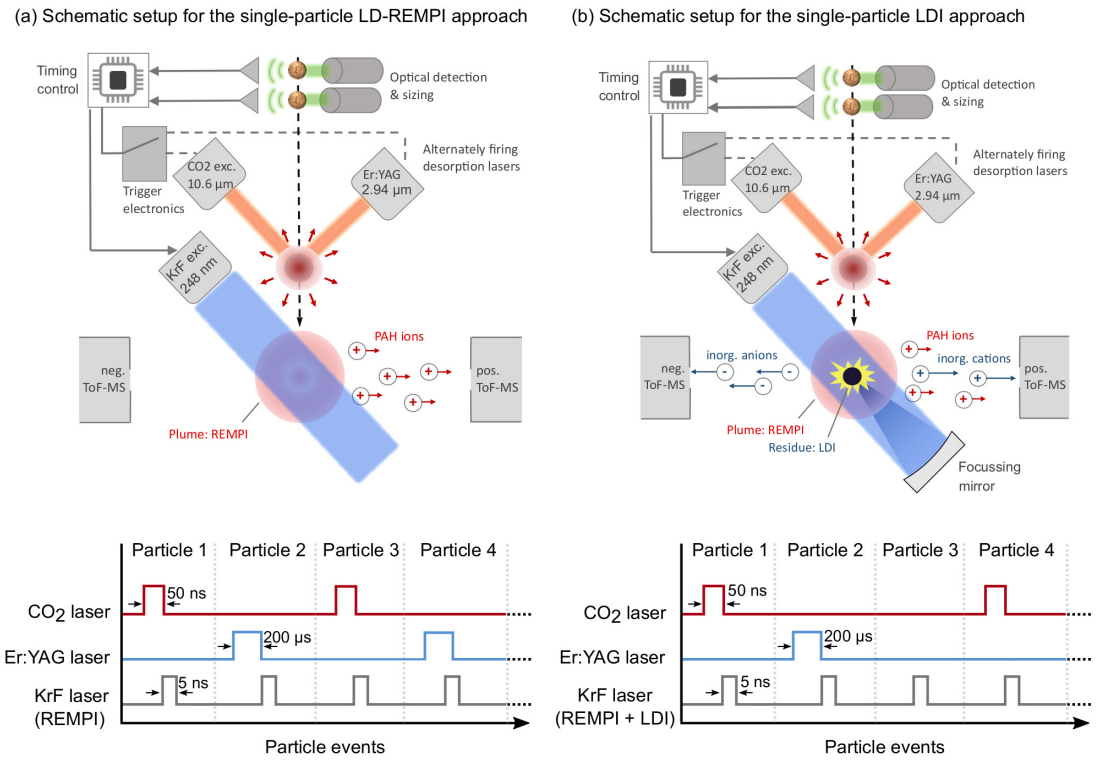

Figure 3.13.: The experimental setup for single-particle ionization employs two approaches: LD-REMPI and LDI. In the former, no backreflection occurs, while in the latter, a backreflected beam is directed towards the particle core. Additionally, to ensure a valid comparison, both the CO_2 laser and the Er:YAG laser are alternated on the single particles (modified after Ref. [208]).

As the two-step approach demonstrated efficacy in the context of ambient aerosols (see Section 3.1),[205,229] the configuration in Fig. 3.13 underwent a minor alteration. Rather than employing the CO_2 laser solely for desorption, the experiment compares the performance of the CO_2 laser with the Er:YAG laser. Particles entering the inlet are subjected to alternating irradiation by the CO_2 laser and the Er:YAG laser for LD before being subjected to excimer laser irradiation ionization. The experimental sequence is the following: The first particle is desorbed by the CO_2 laser, the second by the Er:YAG laser, and the third particle is not desorbed at all, but only hit by the excimer laser for LDI.[208]

In a series of experiments, a variety of samples, including wood ash, tar balls, and diesel, were examined. The results demonstrated that both the CO_2 laser and the Er:YAG laser yielded favorable outcomes when used with the REMPI. For additional classification, this study employs the neural network ART-2-A algorithm. Figure 3.14 shows the spectra obtained with both lasers. From the comparison of the results it becomes evident that the Er:YAG laser is well suited for the analysis of ambient particles.[208]

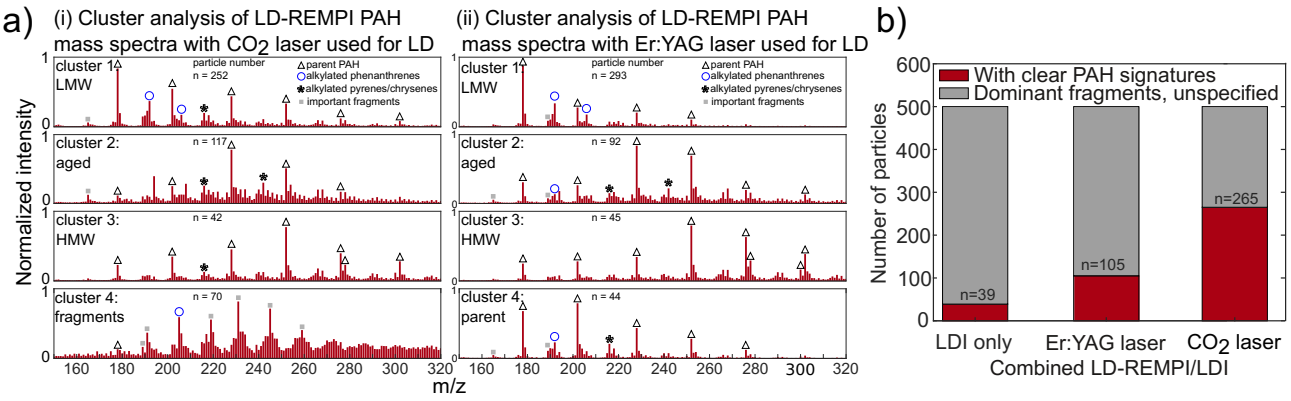

Figure 3.14.: a) ART-2-A clusters of the PAH mass spectra from ambient air particles with $n = 500$ particles were each exposed to two lasers: a CO_2 laser (i) and an Er:YAG laser (ii) for laser desorption (LD) before resonance-enhanced multiphoton ionization (REMPI). The mass spectral signatures and the number of particles in the upper three clusters are similar, comprising $> 80\,\%$ of the particles. In contrast, the fourth cluster, which constitutes less than $14\,\%$ of the particles, exhibited substantial disparities attributable to the enhanced fragmentation triggered by the CO_2 laser. These disparities can be attributed to the distinct characteristics of the laser beam profile and peak intensity. The findings demonstrate that the Er:YAG laser can substitute for the more prevalent CO_2 laser in single-particle LD, including in ambient air studies.
b) Direct comparison of LDI only, and with Er:YAG or CO_2 laser, shows the higher efficiency in the mass spectra of the LD-REMPI/LDI scheme compared to LDI only. The CO_2 laser shows lower fragmentation than the Er:YAG mass spectra. However, the Er:YAG is a prototype with intensity instabilities. The study expects a similar PAH detection efficiency with a more stable version of the Er:YAG laser (modified after Ref. [208]).

However, the prototype of the Er:YAG laser still exhibits intensity fluctuations during the measurements, indicating that further improvements can be made. Erbium:YAG lasers have the advantage of fragmenting organics less due to their wavelength and longer pulse duration.[208] Furthermore, solid-state lasers tend to operate more stably on average and are more readily commercially available, thus offering better maintenance reliability.[282,283] Despite the instabilities of the Er:YAG laser a comparison of the mass spectra of diesel particles and ambient aerosols subjected to both laser systems yielded comparable results in the mass spectra (see Fig. 3.15). This demonstrates that reliable results can be obtained with the Er:YAG laser. The LD-REMPI/LDI scheme, when used in conjunction with the Er:YAG laser, provides accurate and reliable PAH spectra, allowing the identification of important alkylated phenanthrenes, including the C_2 to C_4 phenanthrenes of higher mass-to-charge ratio. Consequently, this experiment successfully highlights the potential of the Er:YAG laser for the application in SPMS source apportionment of modern ship emission.

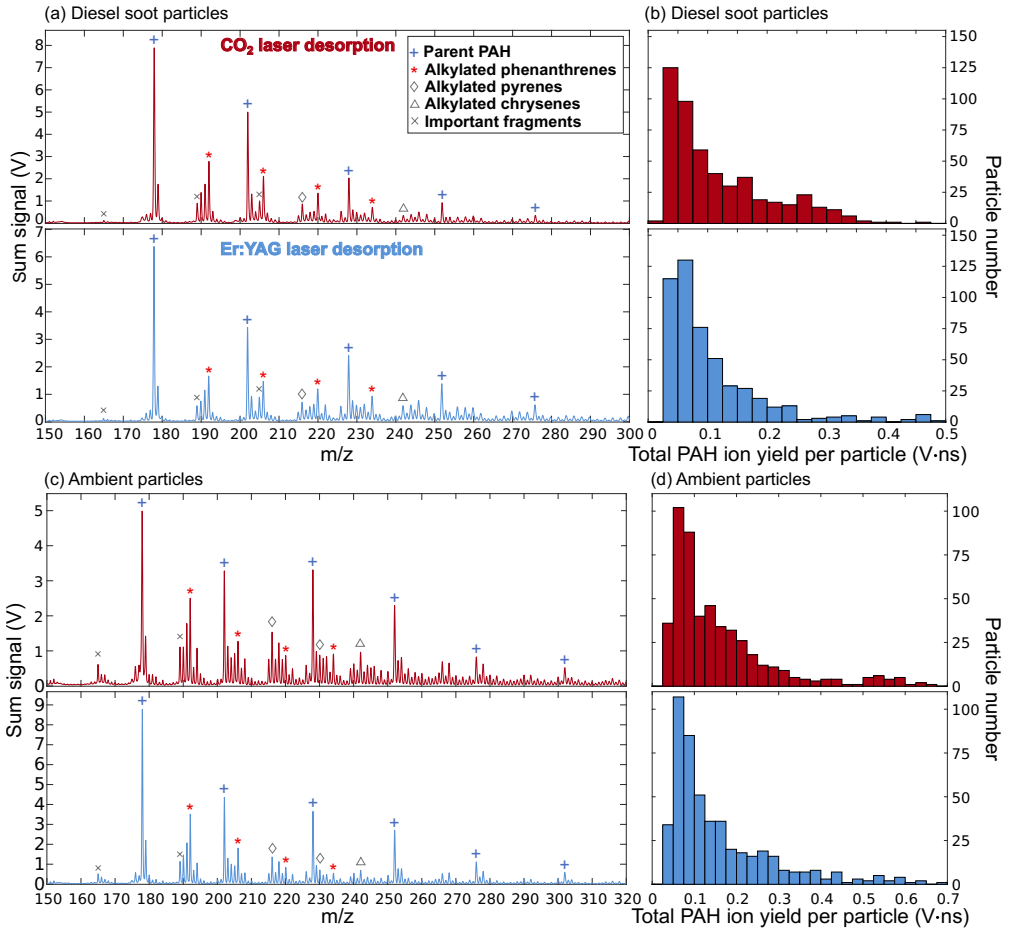

Figure 3.15.: (a,c) present sum spectra of diesel and ambient aerosols using both the CO_2 laser and the Er:YAG laser, respectively. Additionally, the sum spectra obtained with the CO2 laser and the Er:YAG exhibit sharp peaks of various PAHs, with comparable intensity. (b,d) show the associated particle number distribution to (a,c) over the intensity (V ns), respectively (modified after Ref. [208]).

The study's findings could lead to improved analytical capabilities in environmental monitoring. Fields like atmospheric science could profit as well, because understanding the composition of aerosols is crucial to estimate their impacts on air quality, climate change, and human health. Especially, the field of source apportionment for ship emissions could take advantage of this method using an Er:YAG laser system due to its stability and sensitivity to organic materials.[284] Finally, this two-step technique may be extended to other types of particulate analysis, providing a foundation for future developments in SPMS instrumentation and methodologies.

Chapter 4.

Summary and Outlook

The series of studies presented in this dissertation focus on organic markers, with a particular emphasis on polycyclic aromatic hydrocarbons, in ship engine emissions. This is critical as PAHs are recognized for their harmful effects on human health and the environment. The presented online single-particle mass spectrometry technique allows real-time analysis of single particles, which provides unparalleled insights into modern ship emissions and further sources.

The results demonstrate that single-particle mass spectrometry utilizing the combined ionization method of LD-REMPI/LDI represents a suitable pathway to measure and evaluate both inorganic and organic markers. It is conceivable that the technology could be enhanced for future field applications through the utilization of intensity-stable solid-state lasers. In particular, the potential of specific PAH patterns as novel markers for ship emissions can be explored, which is particularly interesting in the light of an anticipated growth of the market for new types of ship fuels. These markers could extend and complement existing metallic ship markers, such as vanadium, nickel, and iron. The PAH distributions were measured in a series of laboratory experiments and field measurements and analyzed for their consistency with regard to different parameters (e.g. particle size, load condition, similarity, supplement cleaning technique). This knowledge can serve as a basis for future measurements of organic markers in ship emissions. To consolidate and extend the findings presented here, further field measurements for ship emissions are recommended. While initial field measurements were successful in detecting ship plumes, further field measurements should be conducted in both ECAs and harbour cities with a diverse range of anthropogenic sources. Moreover, it is imperative to acknowledge the inherent limitations of the method, including its complexity, limited range, and constraints in the detection of ship particles smaller than the sizing limit of the SPMS. Additionally, the applicability of the method in diverse weather conditions must be considered to enhance its effectiveness for further investigations. The stability of the PAH markers must also be investigated under various weather conditions, including wind, sun, and rain, which affect the removal and aging mechanisms of PAHs. This will also enable a more comprehensive assessment of the potential of this measurement method and PAH patterns as ship markers. Moreover, the method can be employed to enhance understanding the complexity of PAH aging and their distribution. It can also assess the feasibility of utilizing PAH as a source marker for ship emissions in a complex environment characterized by diverse aerosol sources. Therefore, further laboratory experiments are proposed to enhance the evaluation and validation of the results obtained. These experiments could prioritize two-stroke ship engines and further shipping fuels, such as low-CO_2 shipping fuels (e.g. ammonia (NH_3)), where toxic amino-PAHs may also be produced. This engine type has a higher combustion efficiency and is the preferred choice for larger vessels, such as tankers, which are essential for global trade. Overall, the measurement technique used here for individual particles shows promising results. This is why it is suitable for the qualitative assessment of organic substances, with a focus on ship emissions. It could therefore be a useful addition for future source apportionment that is of growing concern due to the increasing number of modern ship fuels, which still impact the environment, the air quality, and therefore human health.

Appendix A.

Appendix

A.1. Laser Systems

The single-particle mass spectrometer utilized in this work employs a pair of distinct laser systems that are introduced in sequence. Prior to an examination of the individual laser systems, it is first necessary to present the fundamental principle of a laser. Firstly, the term 'laser' is an acronym that stands for 'light amplification by stimulated emission of radiation'. Lasers offer a number of advantages, including the generation of coherent monochromatic light with low divergence, the possibility of short pulses and high intensities.[284,285] The construction of a laser is based on four fundamental components: an energy source, an optical gain medium, a resonator and a structure for coupling out the light.[285,286] Fig. A.1 provides a simplified illustration of (a) key physical processes and (b) a typical resonator design (Fabry-Pérot cavity) commonly employed in laser systems.[287–290]
In general, in atoms and molecules electrons can be stimulated in order to attain discrete level.[284] Excitation from the ground state E_g can be achieved through the absorption of a photon (see Fig. A.1).

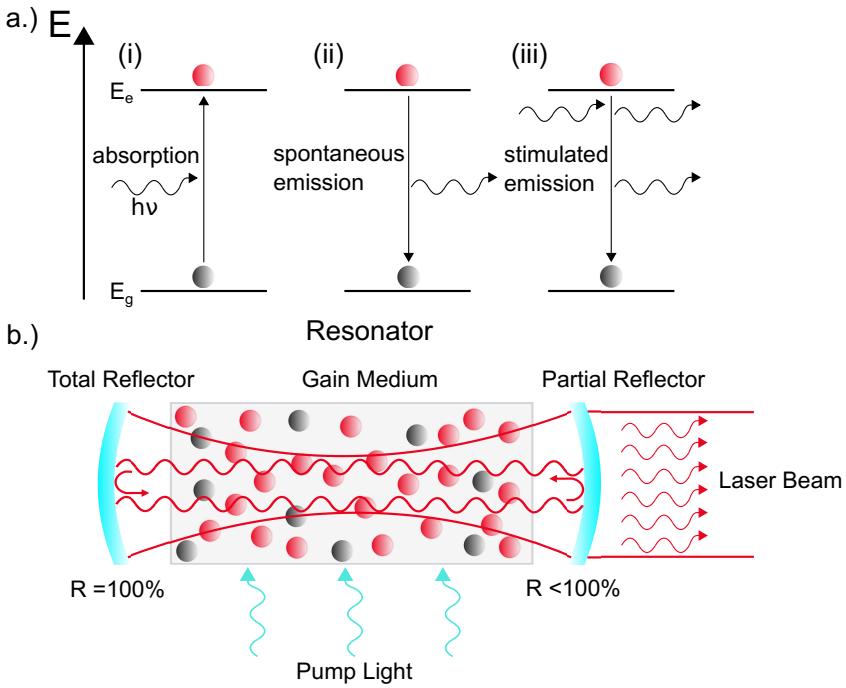

Figure A.1.: a.) (i) Absorption: A photon with the energy $E = h\nu$ is capable of transporting an electron to a higher energy level, provided that the photon energy is sufficient to overcome the energy difference between the ground and excited state. (ii) Spontaneous emission: An electron from an excited state transitions to a lower energy level by emitting a photon. (iii) Induced/stimulated emission: A photon induces an excited electron to transition to a lower energy level by emitting a second photon with the same physical properties as the first photon. Consequently, the incident light is amplified. b.) Simplified principle of a laser showing a Fabry-Pérot cavity as resonator: The gain medium must have a population inversion, where more atoms are in the excited state E_e than in the ground state E_g. The light is amplified within the resonator of length $l = n\lambda/2$ through the process of stimulated emission, which is induced by the photons that are reflected by the mirrors. A proportion of the photons is released at the site of the partial reflector, where the laser beam emerges.

The energy of the photon is equivalent to the energy difference between the ground state and the excited state $E_\mathrm{p} = \Delta E \equiv E_\mathrm{e} - E_\mathrm{g}$. Receiving this energy, the electron is excited, but the lifetime τ of the excited level is finite. In order to return to the energetically more favourable ground state E_g, the excited electron must emit a photon with the discrete energy $E = h \cdot \nu$, where h describes the Planck quantum of action and ν the frequency of the photon.[286]
The initiation of this process may be spontaneous or stimulated/induced. Spontaneous emission is the process whereby an atom or molecule emits a photon without the necessity of an external stimulus or excitation.[291] Conversely, induced emission needs an external stimulus. For instance, a photon of energy E_n ($n \in \mathbb{N} \setminus \{0\}$) encounters another excited electron, the latter also returns to the ground state E_g by emitting another photon. The emitted photon then exhibits the same properties (energy, phase, direction, polarization) as the photon that triggered the process.[284,285] This phenomenon is referred to as 'stimulated emission'. It can be repeated an unlimited number of times in an optical gain medium, provided that the number of atoms stimulated exceeds the number in the ground state. In contrast to spontaneous emission, the photons generated by stimulated emission amplify the emitted light wave.[284] This condition is also known as population inversion. In a state of thermal equilibrium, the distribution of atoms or molecules across multiple energy states adheres to a Boltzmann distribution, whereby they are more likely to occupy the ground state than an excited state.[285] Noteworthy in this context: A population inversion requires the use of an appropriate gain medium, which must provide at least a three-level system, as a two-level system is insufficient.[286] A critical factor to consider is that the atoms are incapable of being repopulated to the ground state via stimulated emission by the pump radiation, as their excitation energy is inadequate to facilitate this process. Consequently, with sufficiently intense pumping, it is feasible to achieve a population in the upper laser level that exceeds 50 %.[285,292] For simplification, in the context of a three-level system (e.g. rubidium laser (Cr^{3+}:Al_2O_3)[293]), the incoming photon would initially excite the atom from the ground state (level 1) to the upper level (level 3). Subsequently, the atom needs a high transition probability to relax to the metastable state (level 2) to prevent spotaneous or induced emission back to the ground state (level 1). Finally, the laser transition would occur from the metastable state (level 2) back to the ground state (level 1). In the context of a population inversion, it is advantageous for the metastable state (level 2) to possess a long lifetime τ. This allows for stimulated emission to occur with a higher probability.[294] However, pure three-level systems are rarely used.[292]

A.1.1. Nd:YAG Laser

Nd:YAG lasers represent a significant advancement in scientific and technological fields, with a multitude of applications spanning medicine, metrology, and spectroscopy.[295–298] It is a solid-state laser, whose radiation is generated by the presence of Nd^{3+} ions. Such ions are frequently found in yttrium-aluminium-garnet (YAG).[284] Figure A.2 illustrates the energy level where a wavelength of 1064 nm is emitted.

Given the suitability of different wavelengths and energies for different experiments, non-linear crystals (LBO, BBO, KDP, etc.) are frequently employed to alter the frequency of the laser.[299,300] The relationship between the electrical polarisation in the non-linear crystal and the inducing electric field

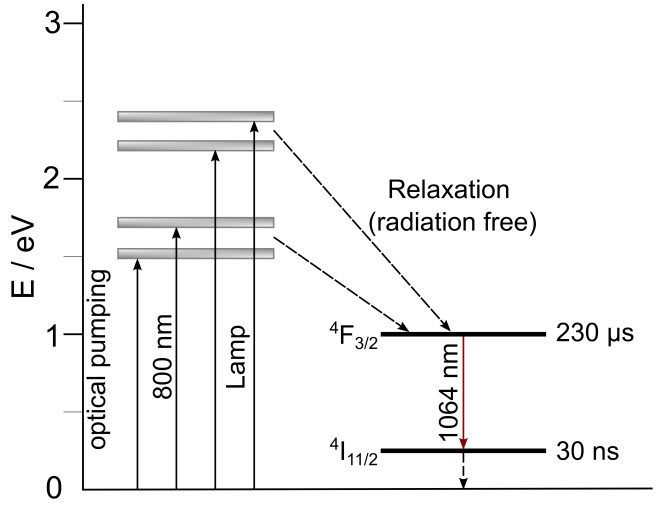

Figure A.2: Jablonski diagram illustrates a simplified scheme of the energy levels of a Nd:YAG laser (modified after Ref. [284]).

$\vec{E}(t) = \vec{E_0}\cos(\omega t)$ is utilized and general described by[291]

$$\vec{P} = \epsilon_0(\chi^{(1)}\vec{E} + \chi^{(2)}\vec{E}^2 + \chi^{(3)}\vec{E}^3 + ...). \tag{A.1}$$

In case of doubling the frequency ω to create the so called 'second harmonic generation' (SHG), it is useful to regard the relation $\vec{P}^{(2)}(t) \propto \vec{E}^2(t)$. Putting the term for the electric field into Eq. A.1 leads to:

$$\vec{P}^{(2)}(t) = \epsilon_0\chi^{(2)}\vec{E}^2(t) = \epsilon_0\chi^{(2)}\vec{E}_0^2\cos^2(\omega t). \tag{A.2}$$

At last using the trigonomic identity $\cos^2(\omega t) = \frac{1+\cos(2\omega t)}{2}$[301] finally gets the equation:

$$\vec{P}^{(2)}(t) = \frac{\epsilon_0\chi^{(2)}\vec{E}_0^2}{2}[1+\cos(2\omega t)]. \tag{A.3}$$

In Eq. A.3 the frequency ω is doubled to 2ω, which means that the SHG has a wavelength of $\lambda_{\mathrm{SHG}} = 532\,\mathrm{nm}$. The efficiency of this process is contingent upon two primary factors: the power of the incoming electric field, represented by the vector $\vec{E}(t)$, and the phase alignment of the fundamental frequency with the induced SHG. The use of nonlinear crystals can facilitate the generation of second-harmonic generation (SHG) or, subsequently, 'fourth-harmonic generation' (FHG) with a wavelength of 266 nm and a photon energy of $\approx 4.66\,\mathrm{eV}$, making it a suitable option for REMPI experiments.[232]

A.1.2. Erbium:YAG Laser

Similar to the Nd:YAG laser, the Erbium:YAG laser is utilized in medical and technical applications.[302,303] The laser utilizes erbium ions and yttrium aluminum garnet as the active medium. With a wavelength of 2.94 µm, it exhibits high absorption in water, making it highly effective for tissue ablation in medicine.[284,302] A corresponding Jablonski diagram is shown in Fig. A.3. Through continuous refinement since its development, the Erbium:YAG laser has become a stable solid-state laser, which is increasingly being applied in scientific and commercial sectors. The laser's wavelength and stability makes it suitable for use in spectroscopy, as evidenced by the results of study.[208]

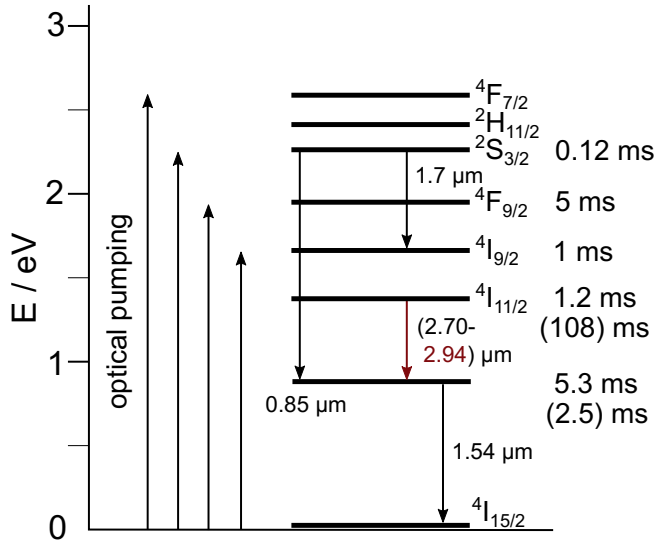

Figure A.3: Jablonski diagram illustrates a simplified scheme of the energy levels of a Er:YAG laser (modified after Ref. [284]). The utilized Er:YAG laser in study 3.5 provides a wavelength of 2.94 µm for desorption of divers samples associated with PAHs.[208]

A.1.3. Excimer Laser

An excimer laser is an effective tool for desorbing individual particles from ship emissions.[214] The term 'excimer' is derived from 'excited dimer' and refers to a diatomic molecule. In this context, a krypton fluoride laser is utilized. A simplified energy level diagram is illustrated in Fig. A.4. In summary, excimers are generated in gas discharges through collisions between excited krypton (Kr) atoms and fluorine (F_2) molecules. As the Kr atom approaches, an electron is transferred to the F_2 molecule, resulting in the formation of Kr^+ and F_2^- ions. When these ions collide, the excited dimer KrF* is formed through a harpoon reaction, accompanied by the emission of a fluorine atom.

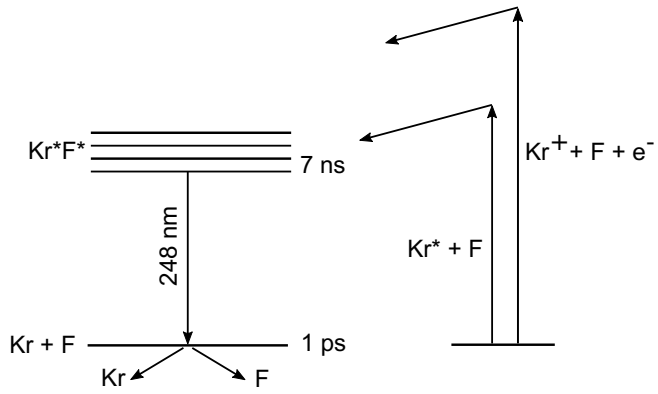

Figure A.4: Simplified Jablonski diagram of an KrF-laser that emits mostly the wavelength 248 nm (modified after Ref. [284]).

Additionally, there is a recombination process involving the ions produced during the gas discharge. For the conservation of momentum, another reaction partner would be required in this reaction scheme, but this has been omitted for reasons of simplicity.[284]

$$Kr^* + F_2 \longrightarrow KrF^* + F \tag{A.4}$$

The energy level diagram in Fig. A.4 illustrates the KrF laser. Radiation with a wavelength of 248 nm is emitted from a bound excited state. Subsequently, the molecule rapidly dissociates into Kr and F atoms in the ground state. The ground state of this laser type is significantly less stable (1 ps) compared to the excited state (9 ns), making it easier to achieve population inversion. This inherent instability of the ground state contributes to the suitability of this laser type for its applications.[284]

A.1.4. CO_2-Laser

The carbon dioxide laser is in general a useful tool in the research field due to its high potential power. Mostly, CO_2 laser systems are used as cw-laser. In this setup a pulsed CO_2 laser with a maximum trigger frequency of 100 Hz and a maximum energy of 25 mJ is used to evoke an organic plume around the particle through desorption. The carbon dioxide molecule is composed of two oxygen atoms and one carbon atom, which are cumulatively bonded to each other by a double bond. Therefore, three different vibrational states are possible. The molecule can be subjected to bending and stretching, both symmetrically and asymmetrically. These three vibrational states begin with 010, 100 and 001, whereby the laser emission comes from the 001 state, which emits radiation with a wavelength of mostly 9.6 µm, or predominantly in this setup with a wavelength of 10.6 µm (see Fig. A.5). The common gain medium for a carbon dioxide laser is a gaseous mixture of CO_2, N_2 and He.[284]

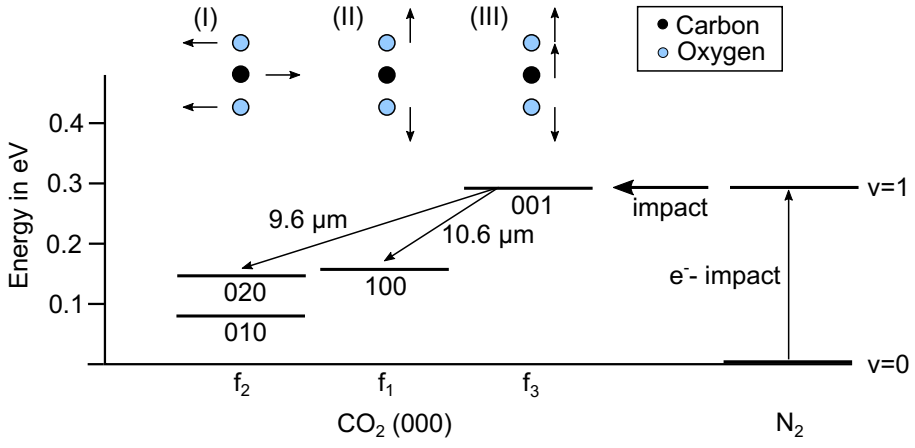

Figure A.5.: Simplified Jablonski diagram for carbon dioxide laser. Electrons and metastable N_2 molecules are formed by gas discharge. The more important N_2 molecules excite laser medium only to the highest state inducing population inversion that lead to stimulated emission. A variety of laser lines are generated. For this work, the transition from 001 to 100 with a wavelength of 10.6 µm is critical (modified after Ref. [284]).

A.2. Sum Mass Spectra of Heavy Fuel Oil

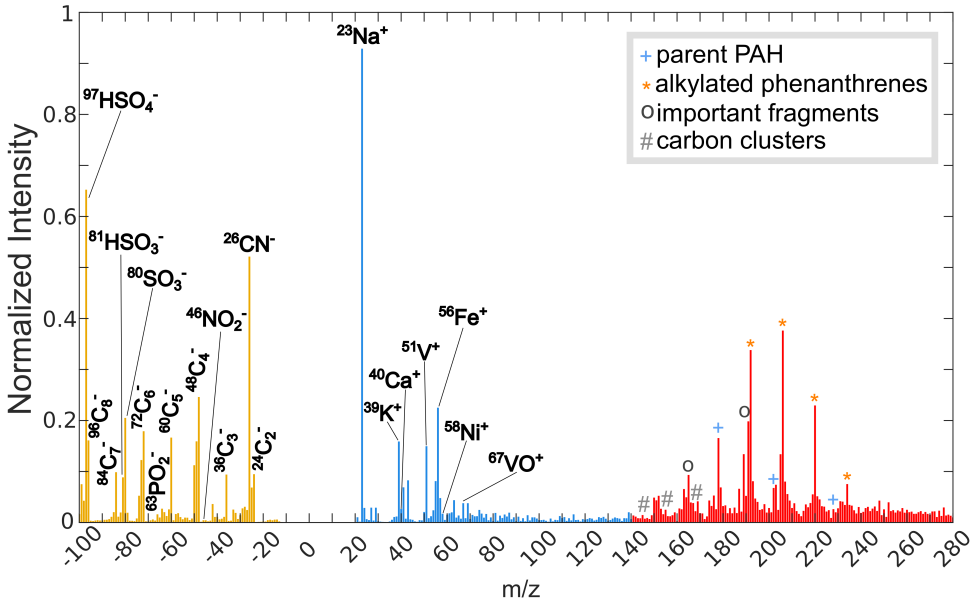

Figure A.6.: Sum mass spectra of $n = 135{,}000$ single particles from ship emissions obtained via single-particle mass spectrometry (SPMS). The SPMS was employed to analyze particles emitted from a 1-cylinder, 4-stroke research ship engine operating on heavy fuel oil with a sulfur content of 2.4 % at a load of 20 kW. The resulting data reveal both anionic (yellow) and cationic (blue) species detected via laser desorption/ionization (LDI), as well as various polycyclic aromatic hydrocarbons (PAHs) identified via resonance-enhanced multiphoton ionization (REMPI) (red).

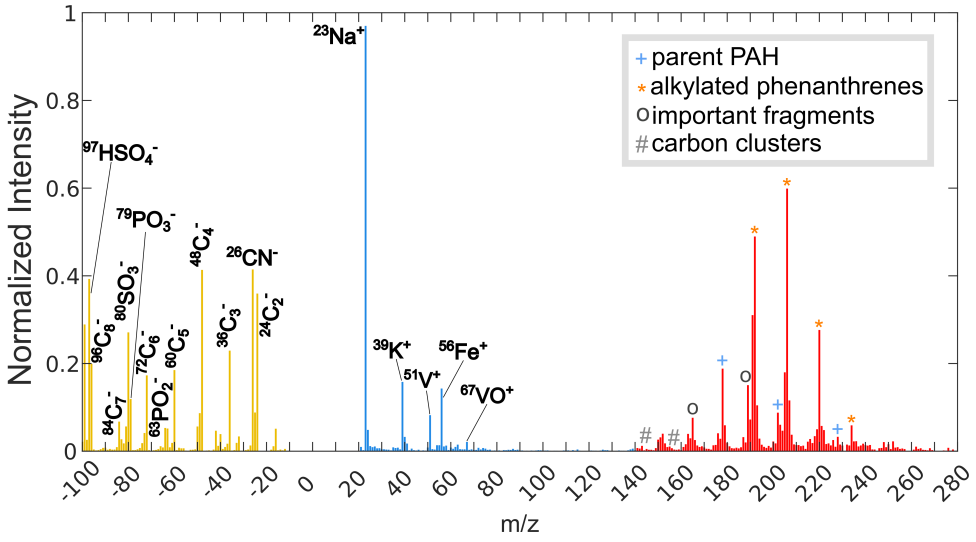

Figure A.7.: Sum mass spectra of $n = 50{,}000$ single particles from ship emissions obtained via single-particle mass spectrometry (SPMS). The SPMS was employed to analyze particles emitted from a 1-cylinder, 4-stroke research ship engine operating on heavy fuel oil with a sulfur content of 2.4 % at a load of 60 kW. The resulting data reveal both anionic (yellow) and cationic (blue) species detected via laser desorption/ionization (LDI), as well as various polycyclic aromatic hydrocarbons (PAHs) identified via resonance-enhanced multiphoton ionization (REMPI) (red).

Bibliography

[1] Aerosol Sampling: Science, Standards, Instrumentation and Applications. John Wiley & Sons Inc, 2007.

[2] Olivier Boucher. Atmospheric Aerosols: Properties and Climate Impacts. Springer Netherlands and Imprint: Springer, Dordrecht, 1st ed. 2015 edition, 2015.

[3] Spyros N. Pandis John H. Seinfeld, editor. Atmospheric Chemistry and Physics: From Air Pollution to Climate Change. Research and Perspectives in Neurosciences. John Wiley & Sons,Inc., Hoboken, New Jersey, 3rd ed. 2016 edition, 2016.

[4] Hyouk-Soo Kwon, Min Hyung Ryu, and Christopher Carlsten. Ultrafine particles: unique physicochemical properties relevant to health and disease. Experimental & molecular medicine, 52(3):318–328, 2020.

[5] Mian Chin, Thomas Diehl, Huisheng Bian, and Tom Kucsera. Aerosols in the atmosphere: sources, transport, and multi-decadal trends. In Air Pollution Modeling and its Application XXIV, pages 3–10. Springer, 2016.

[6] William C Hinds and Yifang Zhu. Aerosol technology: properties, behavior, and measurement of airborne particles. John Wiley & Sons, 2022.

[7] Barbara J Finlayson-Pitts and James N Pitts Jr. Chemistry of the upper and lower atmosphere: theory, experiments, and applications. Elsevier, 1999.

[8] Frank J Kelly and Julia C Fussell. Size, source and chemical composition as determinants of toxicity attributable to ambient particulate matter. Atmospheric environment, 60:504–526, 2012.

[9] Photoionization and Photo-Induced Processes in Mass Spectrometry: Fundamentals and Applications. Wiley-VCH Verlag GmbH & Co. KGaA, 2020.

[10] Neil M Donahue, AL Robinson, CO Stanier, and SN Pandis. Coupled partitioning, dilution, and chemical aging of semivolatile organics. Environmental science & technology, 40(8):2635–2643, 2006.

[11] Ulrich Pöschl and Manabu Shiraiwa. Multiphase chemistry at the atmosphere–biosphere interface influencing climate and public health in the anthropocene. Chemical reviews, 115(10):4440–4475, 2015.

[12] François Dulac, Stéphane Sauvage, and Eric Hamonou. Atmospheric Chemistry in the Mediterranean Region. Springer, 2023.

[13] Yan-Li Wang, Wei Song, Wen Yang, Xin-Chao Sun, Yin-Dong Tong, Xue-Mei Wang, Cong-Qiang Liu, Zhi-Peng Bai, and Xue-Yan Liu. Influences of atmospheric pollution on the contributions of major oxidation pathways to pm2. 5 nitrate formation in beijing. Journal of Geophysical Research: Atmospheres, 124(7):4174–4185, 2019.

[14] Tianyu Zhai, Keding Lu, Haichao Wang, Shengrong Lou, Xiaorui Chen, Renzhi Hu, and Yuanhang Zhang. Elucidate the formation mechanism of particulate nitrate based on direct

radical observations in the yangtze river delta summer 2019. Atmospheric Chemistry and Physics, 23(4):2379–2391, 2023.

[15] In-Sun Kang, Jinying Xi, and Hong-Ying Hu. Photolysis and photooxidation of typical gaseous vocs by uv irradiation: Removal performance and mechanisms. Frontiers of environmental science & engineering, 12:1–14, 2018.

[16] Kanglu Li, Hong Wang, Jianjun Li, and Fan Dong. Design and mechanism of photocatalytic oxidation for the removal of air pollutants: a review. Environmental Chemistry Letters, 20(4):2687–2708, 2022.

[17] Jeffrey K Bean and Lea Hildebrandt Ruiz. Gas–particle partitioning and hydrolysis of organic nitrates formed from the oxidation of α-pinene in environmental chamber experiments. Atmospheric Chemistry and Physics, 16(4):2175–2184, 2016.

[18] Jeongeun Ryu, Jeong Jae Kim, Hyeokjun Byeon, Taesik Go, and Sang Joon Lee. Removal of fine particulate matter (pm2. 5) via atmospheric humidity caused by evapotranspiration. Environmental pollution, 245:253–259, 2019.

[19] ML Wesely and BB Hicks. A review of the current status of knowledge on dry deposition. Atmospheric environment, 34(12-14):2261–2282, 2000.

[20] A.I. Calvo, V. Pont, F.J. Olmo, A. Castro, L. Alados-Arboledas, A.M. Vicente, M. Fernández-Raga, and R. Fraile. Air masses and weather types: A useful tool for characterizing precipitation chemistry and wet deposition. Aerosol and Air Quality Research, 12(5):856–878, 2012.

[21] Yanan Wu, Jiakai Liu, Jiexiu Zhai, Ling Cong, Yu Wang, Wenmei Ma, Zhenming Zhang, and Chunyi Li. Comparison of dry and wet deposition of particulate matter in near-surface waters during summer. PloS one, 13(6):e0199241, 2018.

[22] Hang Su, Yafang Cheng, and Ulrich Pöschl. New multiphase chemical processes influencing atmospheric aerosols, air quality, and climate in the anthropocene. Accounts of chemical research, 53(10):2034–2043, 2020.

[23] Jonathan PD Abbatt and Akkihebbal R Ravishankara. Opinion: Atmospheric multiphase chemistry–past, present, and future. Atmospheric Chemistry and Physics, 23(17):9765–9785, 2023.

[24] J. Arndt, J. Sciare, M. Mallet, G. C. Roberts, N. Marchand, K. Sartelet, K. Sellegri, F. Dulac, R. M. Healy, and J. C. Wenger. Sources and mixing state of summertime background aerosol in the north-western mediterranean basin. Atmospheric Chemistry and Physics.

[25] Mustafa Koçak, Nikos Mihalopoulos, and Nilgün Kubilay. Contributions of natural sources to high pm10 and pm2. 5 events in the eastern mediterranean. Atmospheric Environment, 41(18):3806–3818, 2007.

[26] Kimberly A Prather, Timothy H Bertram, Vicki H Grassian, Grant B Deane, M Dale Stokes, Paul J DeMott, Lihini I Aluwihare, Brian P Palenik, Farooq Azam, John H Seinfeld, et al.

Bringing the ocean into the laboratory to probe the chemical complexity of sea spray aerosol. Proceedings of the National Academy of Sciences, 110(19):7550–7555, 2013.

[27] Henrik Grythe, Johan Ström, Radovan Krejci, P Quinn, and Andreas Stohl. A review of sea-spray aerosol source functions using a large global set of sea salt aerosol concentration measurements. Atmospheric Chemistry and Physics, 14(3):1277–1297, 2014.

[28] S. Fuzzi, U. Baltensperger, K. Carslaw, S. Decesari, H. Denier van der Gon, M. C. Facchini, D. Fowler, I. Koren, B. Langford, U. Lohmann, E. Nemitz, S. Pandis, I. Riipinen, Y. Rudich, M. Schaap, J. G. Slowik, D. V. Spracklen, E. Vignati, M. Wild, M. Williams, and S. Gilardoni. Particulate matter, air quality and climate: lessons learned and future needs. Atmospheric Chemistry and Physics, 15(14):8217–8299, 2015.

[29] Jamie M Schiffer, Liora E Mael, Kimberly A Prather, Rommie E Amaro, and Vicki H Grassian. Sea spray aerosol: where marine biology meets atmospheric chemistry. ACS central science, 4(12):1617–1623, 2018.

[30] Fujiang Wang, Ying Chen, Xi Meng, Jiangping Fu, and Bo Wang. The contribution of anthropogenic sources to the aerosols over east china sea. Atmospheric Environment, 127:22–33, 2016.

[31] Frank Sommer, Volker Dietze, Anja Baum, Jan Sauer, Stefan Gilge, Christoph Maschowski, Reto Gieré, et al. Tire abrasion as a major source of microplastics in the environment. Aerosol and air quality research, 18(8):2014–2028, 2018.

[32] Adam E Thomas, Paulus S Bauer, Michelia Dam, Véronique Perraud, Lisa M Wingen, and James N Smith. Automotive braking is a source of highly charged aerosol particles. Proceedings of the National Academy of Sciences, 121(13):e2313897121, 2024.

[33] JoAnn Slama Lighty, John M Veranth, and Adel F Sarofim. Combustion aerosols: factors governing their size and composition and implications to human health. Journal of the Air & Waste Management Association, 50(9):1565–1618, 2000.

[34] Mahesh Tiwari, Sanjay Kumar Sahu, Rahul Chindhu Bhangare, Ajmal Yousaf, and Gauri Girish Pandit. Particle size distributions of ultrafine combustion aerosols generated from household fuels. Atmospheric Pollution Research, 5(1):145–150, 2014.

[35] United States Environmental Protection Agency. Overview of science processes in cmaq, 2023. `https://www.epa.gov/cmaq/overview-science-processes-cmaq` [Accessed: 13th February 2025].

[36] European Parliament. Emissions from planes and ships: facts and figures (infographic), 2019. `https://www.europarl.europa.eu/topics/en/article/20191129STO67756/emissions-from-planes-and-ships-facts-and-figures-infographic` [Accessed: 13th February 2025].

[37] Zhaofeng Lv, Huan Liu, Qi Ying, Mingliang Fu, Zhihang Meng, Yue Wang, Wei Wei, Huiming Gong, and Kebin He. Impacts of shipping emissions on pm 2.5 pollution in china. Atmospheric

Chemistry and Physics, 18(21):15811–15824, 2018.

[38] CE Delft. Study on methods and considerations for the determination of greenhouse gas emission reduction targets for international shipping. Publications Office of the European Union Luxembourg, 2019.

[39] Evert A Bouman, Elizabeth Lindstad, Agathe I Rialland, and Anders H Strømman. State-of-the-art technologies, measures, and potential for reducing ghg emissions from shipping–a review. Transportation Research Part D: Transport and Environment, 52:408–421, 2017.

[40] Jihong Chen, Yijie Fei, and Zheng Wan. The relationship between the development of global maritime fleets and ghg emission from shipping. Journal of environmental management, 242:31–39, 2019.

[41] Transport & Environment. Climate impact of shipping, 2024. `https://www.transportenvironment.org/challenges/ships/greenhouse-gases/` [Accessed: 13th February 2025].

[42] V. Eyring, H. W. Köhler, J. van Aardenne, and A. Lauer. Emissions from international shipping: 1. the last 50 years. Journal of Geophysical Research: Atmospheres, 110(D17), 2005.

[43] Annika K. Jägerbrand, Andreas Brutemark, Jennie Barthel Svedén, and Ing-Marie Gren. A review on the environmental impacts of shipping on aquatic and nearshore ecosystems. The Science of the total environment, 695:133637, 2019.

[44] Peng Geng, Erming Cao, Qinming Tan, and Lijiang Wei. Effects of alternative fuels on the combustion characteristics and emission products from diesel engines: A review. Renewable and Sustainable Energy Reviews, 71:523–534, 2017.

[45] Katharina Kohse-Höinghaus. Combustion in the future: The importance of chemistry. Proceedings of the Combustion Institute, 38(1):1–56, 2021.

[46] Jeffrey S Gaffney and Nancy A Marley. The impacts of combustion emissions on air quality and climate–from coal to biofuels and beyond. Atmospheric Environment, 43(1):23–36, 2009.

[47] Betty Croft, Randall V Martin, Richard H Moore, Luke D Ziemba, Ewan C Crosbie, Hongyu Liu, Lynn M Russell, Georges Saliba, Armin Wisthaler, Markus Müller, et al. Factors controlling marine aerosol size distributions and their climate effects over the northwest atlantic ocean region. Atmospheric Chemistry and Physics, 21(3):1889–1916, 2021.

[48] Jozef M Pacyna. Sources, particle size distribution and transport of aerosols. In Airborne particulate matter, pages 69–97. Springer, 1995.

[49] AI Calvo, C Alves, Amaya Castro, Véronique Pont, AM Vicente, and Roberto Fraile. Research on aerosol sources and chemical composition: Past, current and emerging issues. Atmospheric Research, 120:1–28, 2013.

[50] M Viana, J Pey, X Querol, A Alastuey, F De Leeuw, and Anke Lükewille. Natural sources of atmospheric aerosols influencing air quality across europe. Science of the total environment,

472:825–833, 2014.

[51] Ralf Zimmermann and Luke Hanley. Photoionization and photo-induced processes in mass spectrometry: Fundamentals and applications. John Wiley & Sons, 2021.

[52] Di Wu, Qing Li, Xiang Ding, Jianfeng Sun, Dan Li, Hongbo Fu, Monique Teich, Xingnan Ye, and Jianmin Chen. Primary particulate matter emitted from heavy fuel and diesel oil combustion in a typical container ship: characteristics and toxicity. Environmental science & technology, 52(21):12943–12951, 2018.

[53] Päivi T Aakko-Saksa, Kati Lehtoranta, Niina Kuittinen, Anssi Järvinen, Jukka-Pekka Jalkanen, Kent Johnson, Heejung Jung, Leonidas Ntziachristos, Stéphanie Gagné, Chiori Takahashi, et al. Reduction in greenhouse gas and other emissions from ship engines: Current trends and future options. Progress in Energy and Combustion Science, 94:101055, 2023.

[54] Marielle Christiansen, Erik Hellsten, David Pisinger, David Sacramento, and Charlotte Vilhelmsen. Liner shipping network design. European Journal of Operational Research, 286(1):1–20, 2020.

[55] Umwelt Bundesamt. Facts about maritime shipping and its environmental impact, 2022. `https://www.umweltbundesamt.de/en/topics/water/seas/maritime-shipping#facts-about-maritime-shipping-and-its-environmental-impact` [Accessed: 13th February 2025].

[56] Bill Karakostas and Takis Katsoulakos. State-of-the-Art Digital Twin Applications for Shipping Sector Decarbonization. IGI Global, 2024.

[57] Yevgeny Aksenov, Ekaterina E Popova, Andrew Yool, AJ George Nurser, Timothy D Williams, Laurent Bertino, and Jon Bergh. On the future navigability of arctic sea routes: High-resolution projections of the arctic ocean and sea ice. Marine Policy, 75:300–317, 2017.

[58] Jackie Dawson, Natalie Carter, Nicolien van Luijk, Colleen Parker, Melissa Weber, Alison Cook, Kayla Grey, and Jennifer Provencher. Infusing inuit and local knowledge into the low impact shipping corridors: An adaptation to increased shipping activity and climate change in arctic canada. Environmental Science & Policy, 105:19–36, 2020.

[59] Anthony Sardain, Erik Sardain, and Brian Leung. Global forecasts of shipping traffic and biological invasions to 2050. Nature Sustainability, 2(4):274–282, 2019.

[60] UNITED NATIONS. Paris agreement, 2015. `https://unfccc.int/sites/default/files/english_paris_agreement.pdf` [Accessed: 13th February 2025].

[61] Michael Traut, Alice Larkin, Kevin Anderson, Christophe McGlade, Maria Sharmina, and Tristan Smith. Co2 abatement goals for international shipping. Climate policy, 18(8):1066–1075, 2018.

[62] Veronika Eyring, Ivar SA Isaksen, Terje Berntsen, William J Collins, James J Corbett, Oyvind Endresen, Roy G Grainger, Jana Moldanova, Hans Schlager, and David S Stevenson. Transport impacts on atmosphere and climate: Shipping. Atmospheric Environment, 44(37):4735–4771, 2010.

[63] Huan Liu, Mingliang Fu, Xinxin Jin, Yi Shang, Drew Shindell, Greg Faluvegi, Cary Shindell, and Kebin He. Health and climate impacts of ocean-going vessels in east asia. Nature climate change, 6(11):1037–1041, 2016.

[64] Ulrike Lohmann and Johann Feichter. Global indirect aerosol effects: a review. Atmospheric Chemistry and Physics, 5(3):715–737, 2005.

[65] J. E. Jonson, M. Gauss, M. Schulz, J.-P. Jalkanen, and H. Fagerli. Effects of global ship emissions on european air pollution levels. Atmospheric Chemistry and Physics, 20(19):11399–11422, 2020.

[66] James J. Corbett, Paul S. Fischbeck, and Spyros N. Pandis. Global nitrogen and sulfur inventories for oceangoing ships. Journal of Geophysical Research: Atmospheres, 104(D3):3457–3470, 1999.

[67] James J. Corbett, James J. Winebrake, Erin H. Green, Prasad Kasibhatla, Veronika Eyring, and Axel Lauer. Mortality from ship emissions: a global assessment. Environmental science & technology, 41(24):8512–8518, 2007.

[68] Mikhail Sofiev, James J. Winebrake, Lasse Johansson, Edward W. Carr, Marje Prank, Joana Soares, Julius Vira, Rostislav Kouznetsov, Jukka-Pekka Jalkanen, and James J. Corbett. Cleaner fuels for ships provide public health benefits with climate tradeoffs. Nature communications, 9(1):406, 2018.

[69] United Nations Environment Programme. Coastal zone management. UNEP. Some 37 per cent of the world's population lives within 100 km of the coast, at a population density twice the global average., 2024. `https://www.unep.org/topics/ocean-seas-and-coasts/regional-seas-programme/coastal-zone-management` [Accessed: 13th February 2025].

[70] Jan Fuglestvedt, Terje Berntsen, Veronika Eyring, Ivar Isaksen, David S. Lee, and Robert Sausen. Shipping emissions: from cooling to warming of climate-and reducing impacts on health. Environmental science & technology, 43(24):9057–9062, 2009.

[71] V. Eyring, J. J. Corbett, D. S. Lee, and J. J. Winebrake. Brief summary of the impact of ship emissions on atmospheric composition, climate, and human health. 2007.

[72] Camilla Geels, Morten Winther, Camilla Andersson, Jukka-Pekka Jalkanen, Jørgen Brandt, Lise M. Frohn, Ulas Im, Wing Leung, and Jesper H. Christensen. Projections of shipping emissions and the related impact on air pollution and human health in the nordic region. Atmospheric Chemistry and Physics, 21(16):12495–12519, 2021.

[73] Lin Tang, Martin OP Ramacher, Jana Moldanová, Volker Matthias, Matthias Karl, Lasse Johansson, Jukka-Pekka Jalkanen, Katarina Yaramenka, Armin Aulinger, and Malin Gustafsson. The impact of ship emissions on air quality and human health in the gothenburg area–part 1: 2012 emissions. Atmospheric Chemistry and Physics, 20(12):7509–7530, 2020.

[74] World Health Organization. WHO global strategy on health, environment and climate change: the transformation needed to improve lives and well being sustainably through healthy environments. World Health Organization, 2020.

[75] Erin Scott. Darkening clouds after restrictions in maritime sulfur emissions. Nature Reviews Earth & Environment, 4(10):680–680, 2023.

[76] Ronald E Rasmussen. Effect of fuel properties on mutagenic activity in extracts of heavy-duty diesel exhaust particulate. Journal of the Air & Waste Management Association, 40(10):1391–1396, 1990.

[77] Michael Sjögren, Hang Li, Carol Banner, Joseph Rafter, Roger Westerholm, and Ulf Rannug. Influence of physical and chemical characteristics of diesel fuels and exhaust emissions on biological effects of particle extracts: a multivariate statistical analysis of ten diesel fuels. Chemical research in toxicology, 9(1):197–207, 1996.

[78] Jürgen Bünger, Jürgen Krahl, Hendrik Stein, and Michael Müller. Partikelemissionen und mutagenität von herkömmlichem dieselkraftstoff, schwedischem dieselkraftstoff mk1 und biodiesel. Landbauforschung Völkenrode, Sonderheft, 239:115–120, 2003.

[79] Robert Sturm. Modelling the deposition of fine particulate matter (pm 2.5) in the human respiratory tract. AME Medical Journal, 5(0), 2020.

[80] B Asgharian, Werner Hofmann, and Rudolf Bergmann. Particle deposition in a multiple-path model of the human lung. Aerosol Science & Technology, 34(4):332–339, 2001.

[81] Lidia Morawska and Junfeng Jim Zhang. Combustion sources of particles. 1. health relevance and source signatures. Chemosphere, 49(9):1045–1058, 2002.

[82] Athanasios Valavanidis, Konstantinos Fiotakis, and Thomais Vlachogianni. Airborne particulate matter and human health: toxicological assessment and importance of size and composition of particles for oxidative damage and carcinogenic mechanisms. Journal of Environmental Science and Health, Part C, 26(4):339–362, 2008.

[83] L Ferrari, M Carugno, and V Bollati. Particulate matter exposure shapes dna methylation through the lifespan. Clinical epigenetics, 11(1):129, 2019.

[84] Adam J Byrne, Sara A Mathie, Lisa G Gregory, and Clare M Lloyd. Pulmonary macrophages: key players in the innate defence of the airways. Thorax, 70(12):1189–1196, 2015.

[85] Giusy Daniela Albano, Angela Marina Montalbano, Rosalia Gagliardo, Giulia Anzalone, and Mirella Profita. Impact of air pollution in airway diseases: role of the epithelial cells (cell models and biomarkers). International Journal of Molecular Sciences, 23(5):2799, 2022.

[86] Svenja Offer, Elena Hartner, Sebastiano Di Bucchianico, Christoph Bisig, Stefanie Bauer, Jana Pantzke, Elias J Zimmermann, Xin Cao, Stefanie Binder, Evelyn Kuhn, et al. Effect of atmospheric aging on soot particle toxicity in lung cell models at the air–liquid interface: differential toxicological impacts of biogenic and anthropogenic secondary organic aerosols (soas). Environmental health perspectives, 130(2):027003, 2022.

[87] C. P. Yu and C. K. Diu. A comparative study of aerosol deposition in different lung models. American Industrial Hygiene Association journal, 43(1):54–65, 1982.

[88] Robert Sturm. Im fokus. Biologie in unserer Zeit, 41(4):256 – 261, 8 2011.

[89] Kunihiko Hiraiwa and Stephan F. van Eeden. Contribution of lung macrophages to the inflammatory responses induced by exposure to air pollutants. Mediators of inflammation, 2013:619523, 2013.

[90] Yves Christen, Henry Kennedy, and David C. van Essen, editors. Micro-, Meso- and Macro-Connectomics of the Brain. Research and Perspectives in Neurosciences. Springer International Publishing and Imprint: Springer, Cham, 1st ed. 2016 edition, 2016.

[91] Jie Yang, Yi Chen, Zhi Yu, Hui Ding, and Zhongfu Ma. The influence of pm2.5 on lung injury and cytokines in mice. Experimental and therapeutic medicine, 18(4):2503–2511, 2019.

[92] Ellen F Kirrane, Thomas J Luben, A Benson, Elizabeth Oesterling Owens, Jason D Sacks, Steven J Dutton, Meagan Madden, and Jennifer L Nichols. A systematic review of cardiovascular responses associated with ambient black carbon and fine particulate matter. Environment international, 127:305–316, 2019.

[93] Mahtab Tapak, Somaye Sadeghi, Tooba Ghazanfari, and Nariman Mosaffa. Chemical exposure and alveolar macrophages responses:'the role of pulmonary defense mechanism in inhalation injuries'. BMJ Open Respiratory Research, 10(1):e001589, 2023.

[94] Aurelia Magdalena Pisoschi and Aneta Pop. The role of antioxidants in the chemistry of oxidative stress: A review. European journal of medicinal chemistry, 97:55–74, 2015.

[95] Milad Ashrafizadeh, Zahra Ahmadi, Saeed Samarghandian, Reza Mohammadinejad, Habib Yaribeygi, Thozhukat Sathyapalan, and Amirhossein Sahebkar. Microrna-mediated regulation of nrf2 signaling pathway: Implications in disease therapy and protection against oxidative stress. Life Sciences, 244:117329, 2020.

[96] Xin Cao, Sara Padoan, Stephanie Binder, Stefanie Bauer, Jürgen Orasche, Corina-Marcela Rus, Ajit Mudan, Anja Huber, Evelyn Kuhn, Sebastian Oeder, et al. A comparative study of persistent dna oxidation and chromosomal instability induced in vitro by oxidizers and reference airborne particles. Mutation Research/Genetic Toxicology and Environmental Mutagenesis, 874:503446, 2022.

[97] Yu V Pashin and LM Bakhitova. Mutagenic and carcinogenic properties of polycyclic aromatic hydrocarbons. Environmental Health Perspectives, 30:185–189, 1979.

[98] Ki-Hyun Kim, Shamin Ara Jahan, Ehsanul Kabir, and Richard JC Brown. A review of airborne polycyclic aromatic hydrocarbons (pahs) and their human health effects. Environment international, 60:71–80, 2013.

[99] Hong Liu, David Weisman, Yuan-bei Ye, Bo Cui, Yan-he Huang, Adán Colón-Carmona, and Zong-hua Wang. An oxidative stress response to polycyclic aromatic hydrocarbon exposure is rapid and complex in arabidopsis thaliana. Plant Science, 176(3):375–382, 2009.

[100] Jørn A Holme, Jan Vondráček, Miroslav Machala, Dominique Lagadic-Gossmann, Christoph FA

Vogel, Eric Le Ferrec, Lydie Sparfel, and Johan Øvrevik. Lung cancer associated with combustion particles and fine particulate matter (pm2. 5)-the roles of polycyclic aromatic hydrocarbons (pahs) and the aryl hydrocarbon receptor (ahr). Biochemical pharmacology, page 115801, 2023.

[101] Ian M Kennedy. The health effects of combustion-generated aerosols. Proceedings of the Combustion Institute, 31(2):2757–2770, 2007.

[102] Sebastian Oeder, Tamara Kanashova, Olli Sippula, Sean C Sapcariu, Thorsten Streibel, Jose Manuel Arteaga-Salas, Johannes Passig, Marco Dilger, Hanns-Rudolf Paur, Christoph Schlager, et al. Particulate matter from both heavy fuel oil and diesel fuel shipping emissions show strong biological effects on human lung cells at realistic and comparable in vitro exposure conditions. PloS one, 10(6):e0126536, 2015.

[103] Giusy Daniela Albano, Rosalia Paola Gagliardo, Angela Marina Montalbano, and Mirella Profita. Overview of the mechanisms of oxidative stress: impact in inflammation of the airway diseases. Antioxidants, 11(11):2237, 2022.

[104] Thorsten Streibel, Jürgen Schnelle-Kreis, Hendryk Czech, Horst Harndorf, Gert Jakobi, Jorma Jokiniemi, Erwin Karg, Jutta Lintelmann, Georg Matuschek, Bernhard Michalke, et al. Aerosol emissions of a ship diesel engine operated with diesel fuel or heavy fuel oil. Environmental Science and Pollution Research, 24:10976–10991, 2017.

[105] Daniel Mueller, Stefanie Uibel, Masaya Takemura, Doris Klingelhoefer, and David A Groneberg. Ships, ports and particulate air pollution-an analysis of recent studies. Journal of Occupational Medicine and Toxicology, 6:1–6, 2011.

[106] James P Kehrer and Lars-Oliver Klotz. Free radicals and related reactive species as mediators of tissue injury and disease: implications for health. Critical reviews in toxicology, 45(9):765–798, 2015.

[107] Tomasz P Mikolajczyk, Piotr Szczepaniak, Francesca Vidler, Pasquale Maffia, Gerard J Graham, and Tomasz J Guzik. Role of inflammatory chemokines in hypertension. Pharmacology & therapeutics, 223:107799, 2021.

[108] Xu-Qin Jiang, Xiao-Dong Mei, and Di Feng. Air pollution and chronic airway diseases: what should people know and do? Journal of thoracic disease, 8(1):E31, 2016.

[109] Theo Vos, Stephen S Lim, Cristiana Abbafati, Kaja M Abbas, Mohammad Abbasi, Mitra Abbasifard, Mohsen Abbasi-Kangevari, Hedayat Abbastabar, Foad Abd-Allah, Ahmed Abdelalim, et al. Global burden of 369 diseases and injuries in 204 countries and territories, 1990–2019: a systematic analysis for the global burden of disease study 2019. The lancet, 396(10258):1204–1222, 2020.

[110] Natalie Mueller, Marie Westerby, and Mark Nieuwenhuijsen. Health impact assessments of shipping and port-sourced air pollution on a global scale: A scoping literature review. Environmental research, 216(Pt 1):114460, 2023.

[111] Frank J Kelly and Julia C Fussell. Air pollution and public health: emerging hazards and

improved understanding of risk. Environmental geochemistry and health, 37:631–649, 2015.

[112] Keith A Hunter, Peter S Liss, Vanisa Surapipith, Frank Dentener, Robert Duce, Maria Kanakidou, Nilgun Kubilay, Natalie Mahowald, Greg Okin, Manmohan Sarin, et al. Impacts of anthropogenic sox, nox and nh3 on acidification of coastal waters and shipping lanes. Geophysical Research Letters, 38(13), 2011.

[113] Urmas Raudsepp, Ilja Maljutenko, Mariliis Kõuts, Lena Granhag, Magda Wilewska-Bien, Ida-Maja Hassellöv, K Martin Eriksson, Lasse Johansson, Jukka-Pekka Jalkanen, Matthias Karl, et al. Shipborne nutrient dynamics and impact on the eutrophication in the baltic sea. Science of The Total Environment, 671:189–207, 2019.

[114] Graeme L Stephens, Denis O'Brien, Peter J Webster, Peter Pilewski, Seiji Kato, and Jui-lin Li. The albedo of earth. Reviews of geophysics, 53(1):141–163, 2015.

[115] Andrew S Ackerman, Owen B Toon, Jonathan P Taylor, Doug W Johnson, Peter V Hobbs, and Ronald J Ferek. Effects of aerosols on cloud albedo: Evaluation of twomey's parameterization of cloud susceptibility using measurements of ship tracks. Journal of the Atmospheric Sciences, 57(16):2684–2695, 2000.

[116] S Menon, VK Saxena, P Durkee, BN Wenny, and K Nielsen. Role of sulfate aerosols in modifying the cloud albedo: A closure experiment. Atmospheric research, 61(3):169–187, 2002.

[117] Johannes Quaas, Antti Arola, Brian Cairns, Matthew Christensen, Hartwig Deneke, Annica ML Ekman, Graham Feingold, Ann Fridlind, Edward Gryspeerdt, Otto Hasekamp, et al. Constraining the twomey effect from satellite observations: issues and perspectives. Atmospheric Chemistry and Physics, 20(23):15079–15099, 2020.

[118] Y-C Chen, MW Christensen, Lulin Xue, A Sorooshian, GL Stephens, RM Rasmussen, and JH Seinfeld. Occurrence of lower cloud albedo in ship tracks. Atmospheric Chemistry and Physics, 12(17):8223–8235, 2012.

[119] James Hansen and Larissa Nazarenko. Soot climate forcing via snow and ice albedos. Proceedings of the national academy of sciences, 101(2):423–428, 2004.

[120] Yun Qian, William I Gustafson Jr, L Ruby Leung, and Steven J Ghan. Effects of soot-induced snow albedo change on snowpack and hydrological cycle in western united states based on weather research and forecasting chemistry and regional climate simulations. Journal of Geophysical Research: Atmospheres, 114(D3), 2009.

[121] Ulrike Lohmann, Franz Friebel, Zamin A Kanji, Fabian Mahrt, Amewu A Mensah, and David Neubauer. Future warming exacerbated by aged-soot effect on cloud formation. Nature Geoscience, 13(10):674–680, 2020.

[122] A Wiedensohler, YF Cheng, A Nowak, B Wehner, P Achtert, M Berghof, W Birmili, ZJ Wu, M Hu, T Zhu, et al. Rapid aerosol particle growth and increase of cloud condensation nucleus activity by secondary aerosol formation and condensation: A case study for regional air pollution in northeastern china. Journal of Geophysical Research: Atmospheres, 114(D2), 2009.

[123] Delphine K Farmer, Christopher D Cappa, and Sonia M Kreidenweis. Atmospheric processes and their controlling influence on cloud condensation nuclei activity. Chemical Reviews, 115(10):4199–4217, 2015.

[124] Tianle Yuan, Hua Song, Lazaros Oreopoulos, Robert Wood, Huisheng Bian, Katherine Breen, Mian Chin, Hongbin Yu, Donifan Barahona, Kerry Meyer, et al. Abrupt reduction in shipping emission as an inadvertent geoengineering termination shock produces substantial radiative warming. Communications Earth & Environment, 5(1):281, 2024.

[125] AS Ackerman and OB Toon. Evaluation of the "twomey effect" with numerical cloud models and comparisons with observations. In Nucleation and Atmospheric Aerosols 1996, pages 788–791. Elsevier, 1996.

[126] Johannes Stapf, André Ehrlich, Evelyn Jäkel, Christof Lüpkes, and Manfred Wendisch. Reassessment of shortwave surface cloud radiative forcing in the arctic: consideration of surface-albedo–cloud interactions. Atmospheric Chemistry and Physics, 20(16):9895–9914, 2020.

[127] M Possanzini, P Buttini, and V Di Palo. Characterization of a rural area in terms of dry and wet deposition. Science of the Total Environment, 74:111–120, 1988.

[128] David R Turner, Moa Edman, Julián Alberto Gallego-Urrea, Björn Claremar, Ida-Maja Hassellöv, Anders Omstedt, and Anna Rutgersson. The potential future contribution of shipping to acidification of the baltic sea. Ambio, 47:368–378, 2018.

[129] Anita Singh and Madhoolika Agrawal. Acid rain and its ecological consequences. Journal of Environmental Biology, 29(1):15, 2007.

[130] Anders Omstedt, Moa Edman, Björn Claremar, and Anna Rutgersson. Modelling the contributions to marine acidification from deposited sox, nox, and nhx in the baltic sea: Past and present situations. Continental Shelf Research, 111:234–249, 2015.

[131] Anna Lunde Hermansson, Ida-Maja Hassellöv, Jana Moldanová, and Erik Ytreberg. Comparing emissions of polyaromatic hydrocarbons and metals from marine fuels and scrubbers. Transportation Research Part D: Transport and Environment, 97:102912, 2021.

[132] Sebnem Aksoyoglu, Urs Baltensperger, and André SH Prévôt. Contribution of ship emissions to the concentration and deposition of air pollutants in europe. Atmospheric Chemistry and Physics, 16(4):1895–1906, 2016.

[133] David R Turner, Ida-Maja Hassellöv, Erik Ytreberg, and Anna Rutgersson. Shipping and the environment: Smokestack emissions, scrubbers and unregulated oceanic consequences. Elem Sci Anth, 5:45, 2017.

[134] Aydin Tokuslu, Irsad Bayirhan, and Cem Gaziglu. Investigation the effect of sox emission reduction on transit ships emissions as of january 1, 2020. Thermal Science, 24(Suppl. 1):149–155, 2020.

[135] Transport & Environment. Regulation (eu) 2021/1119 of the european parliament and of the

council of 30 june 2021 establishing the framework for achieving climate neutrality and amending regulations (ec) no 401/2009 and (eu) 2018/1999 ('european climate law'), 2021. https://eur-lex.europa.eu/legal-content/EN/TXT/?uri=CELEX:32021R1119 [Accessed: 30th January 2025].

[136] Karin Bäckstrand. Towards a climate-neutral union by 2050? the european green deal, climate law, and green recovery. In Routes to a resilient European Union: interdisciplinary European studies, pages 39–61. Springer, 2022.

[137] Leo Čampara, Nermin Hasanspahić, and Srđan Vujičić. Overview of marpol annex vi regulations for prevention of air pollution from marine diesel engines. In SHS web of conferences, volume 58, page 01004. EDP Sciences, 2018.

[138] Zhanguang Wang, Song Zhou, Yongming Feng, and Yuanqing Zhu. Research of nox reduction on a low-speed two-stroke marine diesel engine by using egr (exhaust gas recirculation)–cb (cylinder bypass) and egb (exhaust gas bypass). International Journal of Hydrogen Energy, 42(30):19337–19345, 2017.

[139] Thuy Chu Van, Jerome Ramirez, Thomas Rainey, Zoran Ristovski, and Richard J Brown. Global impacts of recent imo regulations on marine fuel oil refining processes and ship emissions. Transportation Research Part D: Transport and Environment, 70:123–134, 2019.

[140] The Marine Environment Protection Committee. Annex 15, 2023 imo strategy on reduction of ghg emissions from ships, 2023. https://wwwcdn.imo.org/localresources/en/OurWork/Environment/Documents/annex/MEPC%2080/Annex%2015.pdf [Accessed: 30th January 2025].

[141] International Maritime Organization. Ships face lower sulphur fuel requirements in emission control areas from 1 january 2015, 2019. https://www.imo.org/en/MediaCentre/PressBriefings/Pages/44-ECA-sulphur.aspx [Accessed: 13th February 2025].

[142] Yuzhe Zhao, Yujun Fan, Kjetil Fagerholt, and Jingmiao Zhou. Reducing sulfur and nitrogen emissions in shipping economically. Transportation Research Part D: Transport and Environment, 90:102641, 2021.

[143] Fla-Shop.com. World svg map, 2024. https://www.fla-shop.com/svg/ [Accessed: 13th February 2025].

[144] Directorate-General for Mobility and Transport. New shipping fuel standards to reduce sulphur oxides in the mediterranean by 80 %, 2022. https://transport.ec.europa.eu/news-events/news/new-shipping-fuel-standards-reduce-sulphur-oxides-mediterranean-80-2022-12-16_en [Accessed: 13th February 2025].

[145] Sustainable Ships. Eca (emission control area), 2024. https://www.sustainable-ships.org/rules-regulations/eca [Accessed: 13th February 2025].

[146] The International Council On Clean Transportation. From concept to impact: Evaluating the potential for emissions reduction in the proposed north atlantic emission control area under different compliance scenarios, 2024. https://theicct.org/publication/evaluating-

the-potential-for-emissions-reduction-in-the-proposed-atleca-under-different-compliance-scenarios-june24/ [Accessed: 13th February 2025].

[147] Clean Arctic Alliance. Emission control areas- reducing air pollution from shipping, 2024. https://cleanarctic.org/2023/06/28/infographic-emission-control-areas-reducing-air-pollution-from-shipping/ [Accessed: 13th February 2025].

[148] Øyvind Endresen, Eirik Sørgård, Hanna Lee Behrens, Per Olaf Brett, and Ivar SA Isaksen. A historical reconstruction of ships' fuel consumption and emissions. Journal of Geophysical Research: Atmospheres, 112(D12), 2007.

[149] Hendryk Czech, Jürgen Schnelle-Kreis, Thorsten Streibel, and Ralf Zimmermann. New directions: Beyond sulphur, vanadium and nickel–about source apportionment of ship emissions in emission control areas. Atmospheric Environment, 163:190–191, 2017.

[150] The Marine Environment Protection Committee. Amendments to the annex of the protocol of 1997 to amend the international convention for the prevention of pollution from ships, 1973, as modified by the protocol of 1978 relating thereto (revised marpol annex vi), 2008. https://www.lemoci.com/media/omi-2008-marpol-annexe-6.pdf [Accessed: 30th January 2025].

[151] Kati Lehtoranta, Päivi Aakko-Saksa, Timo Murtonen, Hannu Vesala, Leonidas Ntziachristos, Topi Rönkkö, Panu Karjalainen, Niina Kuittinen, and Hilkka Timonen. Particulate mass and nonvolatile particle number emissions from marine engines using low-sulfur fuels, natural gas, or scrubbers. Environmental science & technology, 53(6):3315–3322, 2019.

[152] Paul Gilbert, Conor Walsh, Michael Traut, Uchenna Kesieme, Kayvan Pazouki, and Alan Murphy. Assessment of full life-cycle air emissions of alternative shipping fuels. Journal of cleaner production, 172:855–866, 2018.

[153] Alexandros M Goulielmos. The decarbonization of the shipping industry and the new fuel issue. Modern Economy, 12(12):1999–2022, 2021.

[154] IMO; Statista estimates. Annual fuel consumption by ships worldwide from 2019 to 2020, by fuel type, 2023. https://www.statista.com/statistics/1266963/amount-of-fuel-consumed-by-ships-worldwide-by-fuel-type/ [Accessed: 13th February 2025].

[155] A Kersing and M Stone. The shipping industry's fuel choices on the path to net zero. McKinsey & Company: New York, NY, USA, 2023.

[156] Hulda Winnes, Erik Fridell, and Jana Moldanová. Effects of marine exhaust gas scrubbers on gas and particle emissions. Journal of marine science and engineering, 8(4):299, 2020.

[157] Seongho Jeong, Jan Bendl, Mohammad Saraji-Bozorgzad, Uwe Käfer, Uwe Etzien, Julian Schade, Martin Bauer, Gert Jakobi, Jürgen Orasche, Kathrin Fisch, et al. Aerosol emissions from a marine diesel engine running on different fuels and effects of exhaust gas cleaning measures. Environmental Pollution, 316:120526, 2023.

[158] Jiacheng Yang, Tianbo Tang, Yu Jiang, Georgios Karavalakis, Thomas D Durbin, J Wayne Miller, David R Cocker III, and Kent C Johnson. Controlling emissions from an ocean-going container vessel with a wet scrubber system. Fuel, 304:121323, 2021.

[159] Lukas Anders, Martin Bauer, Seongho Jeong, Marco Schmidt, Haseeb Hakkim, Aleksandrs Kalamašņikovs, Ellen Iva Rosewig, Julian Schade, Robert Irsig, Sven Ehlert, Jan Bendl, Mohammad Reza Saraji-Bozorgzad, Barbara Giocastro, Uwe Käfer, Uwe Etzien, Bert Buchholz, Thomas Adam, Hendryk Sklorz, Martin andCzech, Johannes Passig, and Ralf Zimmermann. Limited impact of wet scrubber exhaust treatment on the chemical composition of individual ship emission particles. submitted in Environmental Chemistry Letters, submitted in Nov. 2024.

[160] Alba Martínez-López, África Marrero, Yumara Martín-Cruz, and Marcos Míguez González. Environmental assessment model for scrubbers versus alternative mitigation systems for feeder vessels in liner shipping. Journal of environmental management, 321:115954, 2022.

[161] Hayoung Jang, Byongug Jeong, Peilin Zhou, Seungman Ha, Dong Nam, Joongwon Kim, and Jae-ung Lee. Development of parametric trend life cycle assessment for marine sox reduction scrubber systems. Journal of cleaner production, 272:122821, 2020.

[162] Klara Andersson, Byongug Jeong, and Hayoung Jang. Life cycle and cost assessment of a marine scrubber installation. Journal of International Maritime Safety, Environmental Affairs, and Shipping, 4(4):162–176, 2020.

[163] The International Council On Clean Transportation. Scrubbers on ships: Time to close the open loop(hole), 2020. `https://theicct.org/scrubbers-on-ships-time-to-close-the-open-loophole/` [Accessed: 13th February 2025].

[164] Ida-Maja Hassellöv. Scrubber technology: Bad news for the marine environment. In Regulation of Risk, pages 353–368. Brill Nijhoff, 2022.

[165] Johannes Teuchies, Tom JS Cox, Katrien Van Itterbeeck, Filip JR Meysman, and Ronny Blust. The impact of scrubber discharge on the water quality in estuaries and ports. Environmental Sciences Europe, 32:1–11, 2020.

[166] O Marin-Enriquez, A Krutwa, and K Ewert. Environmental impacts of exhaust gas cleaning systems for reduction of sox on ships-analysis of status quo. Report complied within the framework of the project ImpEx; German Environment Agency: Dessau-Roßlau, Germany, 2021.

[167] Ship & Bunker. Benchmark bunker prices, 2025. `https://shipandbunker.com/about/about-sb-prices` [Accessed: 30th January 2025].

[168] Nathan Gray, Shane McDonagh, Richard O'Shea, Beatrice Smyth, and Jerry D Murphy. Decarbonising ships, planes and trucks: An analysis of suitable low-carbon fuels for the maritime, aviation and haulage sectors. Advances in Applied Energy, 1:100008, 2021.

[169] Statista. Anzahl der schiffe in der welthandelsflotte im jahr 2023 nach schiffstypen, 2023. `https://de.statista.com/statistik/daten/studie/29147/umfrage/anzahl-der-handelsschiffe-in-der-welthandelsflotte/` [Accessed: 13th February 2025].

[170] Gang Nam Lee, Jong Mu Kim, Kwang Hyo Jung, Hyun Park, Hag Soo Jang, Chung Seong Lee, and Ji Won Lee. Environmental life-cycle assessment of eco-friendly alternative ship fuels (mgo, lng, and hydrogen) for 170 gt nearshore ferry. Journal of Marine Science and Engineering, 10(6):755, 2022.

[171] Anu Lähteenmäki-Uutela, Johanna Yliskylä-Peuralahti, Sari Repka, and Johan Mellqvist. What explains seca compliance: rational calculation or moral judgment? WMU Journal of Maritime Affairs, 18:61–78, 2019.

[172] Ling Sun, Xinghe Wang, Zijiang Hu, Wei Liu, and Zhong Ning. Carbon reduction and cost control of container shipping in response to the european union emission trading system. Environmental Science and Pollution Research, 31(14):21172–21188, 2024.

[173] P. Lauer, B. Behrends, M. Hinz, and S. Eylmann. Luftschadstoffe in der seeschifffahrt – erstellung einer maßnahmenmatrix der minderungsoptionen sowie durchführung und analyse einer black carbon- messkampagne in abhängigkeit von der kraftstoffqualität, 2024. `https://www.umweltbundesamt.de/sites/default/files/medien/11850/publikationen/66_2024_texte_luftschadstoffe_seeschifffahrt.pdf` [Accessed: 12th January 2025].

[174] JE Buckingham. Future fuels for commercial shipping. LNG/LPG and alternative fuels, London, 2020.

[175] Maria Zetterdahl, Jana Moldanova, Xiangyu Pei, Ravi Kant Pathak, and Benjamin Demirdjian. Impact of the 0.1% fuel sulfur content limit in seca on particle and gaseous emissions from marine vessels. Atmospheric Environment, 145:338–345, 2016.

[176] J Isakson, TA Persson, and E Selin Lindgren. Identification and assessment of ship emissions and their effects in the harbour of göteborg, sweden. Atmospheric Environment, 35(21):3659–3666, 2001.

[177] Mar Viana, Fulvio Amato, Andrés Alastuey, Xavier Querol, Teresa Moreno, Saul Garcia Dos Santos, María Dolores Herce, and Rosalía Fernández-Patier. Chemical tracers of particulate emissions from commercial shipping. Environmental science & technology, 43(19):7472–7477, 2009.

[178] Theo Schwemer, Christopher P Rüger, Martin Sklorz, and Ralf Zimmermann. Gas chromatography coupled to atmospheric pressure chemical ionization ft-icr mass spectrometry for improvement of data reliability. Analytical chemistry, 87(24):11957–11961, 2015.

[179] Maxime Sueur, Christopher P Rüger, Julien F Maillard, Hélène Lavanant, Ralf Zimmermann, and Carlos Afonso. Selective characterization of petroporphyrins in shipping fuels and their corresponding emissions using electron-transfer matrix-assisted laser desorption/ionization fourier transform ion cyclotron resonance mass spectrometry. Fuel, 332:126283, 2023.

[180] Hendryk Czech, Benjamin Stengel, Thomas Adam, Martin Sklorz, Thorsten Streibel, and Ralf Zimmermann. A chemometric investigation of aromatic emission profiles from a marine engine in comparison with residential wood combustion and road traffic: Implications for source

apportionment inside and outside sulphur emission control areas. Atmospheric environment, 167:212–222, 2017.

[181] Marek Tobiszewski and Jacek Namieśnik. Pah diagnostic ratios for the identification of pollution emission sources. Environmental pollution, 162:110–119, 2012.

[182] Paul D Boehm. Polycyclic aromatic hydrocarbons (pahs). In Environmental forensics, pages 313–337. Elsevier, 1964.

[183] Oleksandr Kysliak, Simon HF Schreiner, Niklas Grabicki, Phil Liebing, Florian Weigend, Oliver Dumele, and Robert Kretschmer. A planar five-membered aromatic ring stabilized by only two π-electrons. Angewandte Chemie International Edition, 61(31):e202206963, 2022.

[184] Miquel Sola. Aromaticity rules. Nature Chemistry, 14(6):585–590, 2022.

[185] Harold Rabinowitz and Suzanne Vogel. The Manual of Scientific Style: a guide for authors, editors, and researchers. Elsevier, 2009.

[186] Shanti Lamichhane, KC Bal Krishna, and Ranjan Sarukkalige. Polycyclic aromatic hydrocarbons (pahs) removal by sorption: a review. Chemosphere, 148:336–353, 2016.

[187] Ian J Keyte, Roy M Harrison, and Gerhard Lammel. Chemical reactivity and long-range transport potential of polycyclic aromatic hydrocarbons–a review. Chemical Society Reviews, 42(24):9333–9391, 2013.

[188] Michael Frenklach, David W Clary, William C Gardiner Jr, and Stephen E Stein. Detailed kinetic modeling of soot formation in shock-tube pyrolysis of acetylene. In Symposium (International) on Combustion, volume 20, pages 887–901. Elsevier, 1985.

[189] Michael Frenklach, Ravi I Singh, and Alexander M Mebel. On the low-temperature limit of haca. Proceedings of the Combustion Institute, 37(1):969–976, 2019.

[190] Bikau Shukla and Mitsuo Koshi. A novel route for pah growth in haca based mechanisms. Combustion and flame, 159(12):3589–3596, 2012.

[191] Xiaoqing You, Russell Whitesides, Dmitry Zubarev, William A Lester Jr, and Michael Frenklach. Bay-capping reactions: Kinetics and influence on graphene-edge growth. Proceedings of the Combustion Institute, 33(1):685–692, 2011.

[192] Peng Liu, Zepeng Li, Anthony Bennett, He Lin, S Mani Sarathy, and William L Roberts. The site effect on pahs formation in haca-based mass growth process. Combustion and Flame, 199:54–68, 2019.

[193] Edina Reizer, Béla Viskolcz, and Béla Fiser. Formation and growth mechanisms of polycyclic aromatic hydrocarbons: A mini-review. Chemosphere, 291:132793, 2022.

[194] Ana Lúcia C Lima, John W Farrington, and Christopher M Reddy. Combustion-derived polycyclic aromatic hydrocarbons in the environment—a review. Environmental forensics, 6(2):109–131, 2005.

[195] Agnieszka Krzyszczak and Bożena Czech. Occurrence and toxicity of polycyclic aromatic hydrocarbons derivatives in environmental matrices. Science of the Total Environment, 788:147738, 2021.

[196] Meng Li, Fengxia Bao, Yue Zhang, Wenjing Song, Chuncheng Chen, and Jincai Zhao. Role of elemental carbon in the photochemical aging of soot. Proceedings of the National Academy of Sciences, 115(30):7717–7722, 2018.

[197] Agnieszka Krzyszczak, Michał P Dybowski, Robert Zarzycki, Rafał Kobyłecki, Patryk Oleszczuk, and Bożena Czech. Long-term physical and chemical aging of biochar affected the amount and bioavailability of pahs and their derivatives. Journal of Hazardous Materials, 440:129795, 2022.

[198] Daekyun Kim, Benjamin M Kumfer, Cort Anastasio, Ian M Kennedy, and Thomas M Young. Environmental aging of polycyclic aromatic hydrocarbons on soot and its effect on source identification. Chemosphere, 76(8):1075–1081, 2009.

[199] Bernd RT Simoneit. Application of molecular marker analysis to vehicular exhaust for source reconciliations. International Journal of Environmental Analytical Chemistry, 22(3-4):203–232, 1985.

[200] Johany Ringuet, Alexandre Albinet, Eva Leoz-Garziandia, Hélène Budzinski, and Eric Villenave. Reactivity of polycyclic aromatic compounds (pahs, npahs and opahs) adsorbed on natural aerosol particles exposed to atmospheric oxidants. Atmospheric Environment, 61:15–22, 2012.

[201] Amy IH Hrdina, Ishwar N Kohale, Simran Kaushal, Jamie Kelly, Noelle E Selin, Bevin P Engelward, and Jesse H Kroll. The parallel transformations of polycyclic aromatic hydrocarbons in the body and in the atmosphere. Environmental Health Perspectives, 130(2):025004, 2022.

[202] Johannes Passig, Julian Schade, Markus Oster, Matthias Fuchs, Sven Ehlert, Cornelia Jäger, Martin Sklorz, and Ralf Zimmermann. Aerosol mass spectrometer for simultaneous detection of polyaromatic hydrocarbons and inorganic components from individual particles. Analytical Chemistry, 89(12):6341–6345, 2017.

[203] Lukas Anders, Julian Schade, Ellen Iva Rosewig, Marco Schmidt, Robert Irsig, Seongho Jeong, Uwe Käfer, Thomas Gröger, Jan Bendl, Mohammad Reza Saraji-Bozorgzad, et al. Polycyclic aromatic hydrocarbons as fuel-dependent markers in ship engine emissions using single-particle mass spectrometry. Environmental Science: Atmospheres, 2024.

[204] BD Morrical, DP Fergenson, and KA Prather. Coupling two-step laser desorption/ionization with aerosol time-of-flight mass spectrometry for the analysis of individual organic particles. Journal of the American Society for Mass Spectrometry, 9(10):1068–1073, 1998.

[205] Julian Schade, Johannes Passig, Robert Irsig, Sven Ehlert, Martin Sklorz, Thomas Adam, Chunlin Li, Yinon Rudich, and Ralf Zimmermann. Spatially shaped laser pulses for the simultaneous detection of polycyclic aromatic hydrocarbons as well as positive and negative inorganic ions in single particle mass spectrometry. Analytical chemistry, 91(15):10282–10288, 2019.

[206] Jürgen H Gross and Jürgen H Gross. Ambient mass spectrometry. Mass Spectrometry: A

Textbook, pages 621–649, 2011.

[207] Johannes Passig and Ralf Zimmermann. Laser ionization in single-particle mass spectrometry. Photoionization and Photo-Induced Processes in Mass Spectrometry: Fundamentals and Applications, pages 359–411, 2021.

[208] Marco Schmidt, Haseeb Hakkim, Lukas Anders, Aleksandrs Kalamašņikovs, Thomas Kröger-Badge, Robert Irsig, Norbert Graf, Reinhard Kelnberger, Johannes Passig, and Ralf Zimmermann. A solid-state ir laser for two-step desorption/ionization processes in single-particle mass spectrometry. submitted in EGUsphere, 2024:1–23, submitted in Aug. 2024.

[209] Scott C Russell. Microorganism characterization by single particle mass spectrometry. Mass spectrometry reviews, 28(2):376–387, 2009.

[210] R Zimmermann, T Ferge, M Gälli, and R Karlsson. Application of single-particle laser desorption/ionization time-of-flight mass spectrometry for detection of polycyclic aromatic hydrocarbons from soot particles originating from an industrial combustion process. Rapid communications in mass spectrometry, 17(8):851–859, 2003.

[211] Renato Zenobi and Richard Knochenmuss. Ion formation in maldi mass spectrometry. Mass spectrometry reviews, 17(5):337–366, 1998.

[212] Richard Knochenmuss and Leonid V Zhigilei. Molecular dynamics simulations of maldi: laser fluence and pulse width dependence of plume characteristics and consequences for matrix and analyte ionization. Journal of mass spectrometry, 45(4):333–346, 2010.

[213] Klaus Dreisewerd. The desorption process in maldi. Chemical reviews, 103(2):395–426, 2003.

[214] Johannes Passig, Julian Schade, Robert Irsig, Lei Li, Xue Li, Zhen Zhou, Thomas Adam, and Ralf Zimmermann. Detection of ship plumes from residual fuel operation in emission control areas using single-particle mass spectrometry. Atmospheric Measurement Techniques, 14(6):4171–4185, 2021.

[215] Richard Knochenmuss. Ion formation mechanisms in uv-maldi. Analyst, 131(9):966–986, 2006.

[216] Michael Karas and Ralf Krüger. Ion formation in maldi: the cluster ionization mechanism. Chemical reviews, 103(2):427–440, 2003.

[217] Melissa S Reinard and Murray V Johnston. Ion formation mechanism in laser desorption ionization of individual nanoparticles. Journal of the American Society for Mass Spectrometry, 19:389–399, 2008.

[218] Bochao Zhang, Miaohong He, Wei Hang, and Benli Huang. Minimizing matrix effect by femtosecond laser ablation and ionization in elemental determination. Analytical chemistry, 85(9):4507–4511, 2013.

[219] Richard Knochenmuss, Frédéric Dubois, Michael J Dale, and Renato Zenobi. The matrix suppression effect and ionization mechanisms in matrix-assisted laser desorption/ionization. Rapid Communications in Mass Spectrometry, 10(8):871–877, 1996.

[220] R Knochenmuss, A Stortelder, K Breuker, and R Zenobi. Secondary ion–molecule reactions in matrix-assisted laser desorption/ionization. Journal of mass spectrometry, 35(11):1237–1245, 2000.

[221] Deborah S Gross, Markus E Gälli, Philip J Silva, and Kimberly A Prather. Relative sensitivity factors for alkali metal and ammonium cations in single-particle aerosol time-of-flight mass spectra. Analytical Chemistry, 72(2):416–422, 2000.

[222] Marco Schmidt, Robert Irsig, Dumitru Duca, Christian Peltz, Johannes Passig, and Ralf Zimmermann. Laser-pulse-length effects in ultrafast laser desorption. Analytical Chemistry, 95(51):18776–18782, 2023.

[223] Ephraim Woods, Geoffrey D Smith, Yury Dessiaterik, Tomas Baer, and Roger E Miller. Quantitative detection of aromatic compounds in single aerosol particle mass spectrometry. Analytical chemistry, 73(10):2317–2322, 2001.

[224] Jürgen H Gross. Mass spectrometry: a textbook. Springer Science & Business Media, 2006.

[225] F Gaie-Levrel, S Perrier, E Perraudin, C Stoll, N Grand, and M Schwell. Development and characterization of a single particle laser ablation mass spectrometer (splam) for organic aerosol studies. Atmospheric Measurement Techniques, 5(1):225–241, 2012.

[226] Luke Hanley and Ralf Zimmermann. Light and molecular ions: the emergence of vacuum uv single-photon ionization in ms, 2009.

[227] Gert von Helden, Deniz van Heijnsbergen, and Gerard Meijer. Resonant ionization using ir light: A new tool to study the spectroscopy and dynamics of gas-phase molecules and clusters. The Journal of Physical Chemistry A, 107(11):1671–1688, 2003.

[228] Thorsten Streibel and Ralf Zimmermann. Resonance-enhanced multiphoton ionization mass spectrometry (REMPI-ms): applications for process analysis. Annual review of analytical chemistry. Palo Alto, Calif. : Annual Reviews, 2008, 2014. Thorsten Streibel; Ralf Zimmermann.

[229] Lukas Anders, Julian Schade, Ellen Iva Rosewig, Thomas Kröger-Badge, Robert Irsig, Seongho Jeong, Jan Bendl, Mohammad Reza Saraji-Bozorgzad, Jhih-Hong Huang, Fu-Yi Zhang, et al. Detection of ship emissions from distillate fuel operation via single-particle profiling of polycyclic aromatic hydrocarbons. Environmental Science: Atmospheres, 3(8):1134–1144, 2023.

[230] Haruo Kuroda. Ionization potentials of polycyclic aromatic hydrocarbons. Nature, 201(4925):1214–1215, 1964.

[231] David M Lubman and Mel N Kronick. Mass spectrometry of aromatic molecules with resonance-enhanced multiphoton ionization. Analytical Chemistry, 54(4):660–665, 1982.

[232] Thorsten Streibel and Ralf Zimmermann. Resonance-enhanced multiphoton ionization mass spectrometry (rempi-ms): applications for process analysis. Annual Review of Analytical Chemistry, 7(1):361–381, 2014.

[233] Mengna Yuan and Junji Cao. Development and application of photoionization technology for

organic analysis of particulate matter. Aerosol Science and Engineering, 6(2):127–134, 2022.

[234] Johannes Passig, Julian Schade, Ellen Iva Rosewig, Robert Irsig, Thomas Kröger-Badge, Hendryk Czech, Martin Sklorz, Thorsten Streibel, Lei Li, Xue Li, et al. Resonance-enhanced detection of metals in aerosols using single-particle mass spectrometry. Atmospheric Chemistry and Physics, 20(12):7139–7152, 2020.

[235] John C Lindon, George E Tranter, and David Koppenaal. Encyclopedia of spectroscopy and spectrometry. Academic Press, 2016.

[236] Lei Li, Liu Liu, Li Xu, Mei Li, Xue Li, Wei Gao, Zhengxu Huang, and Ping Cheng. Improvement in the mass resolution of single particle mass spectrometry using delayed ion extraction. Journal of The American Society for Mass Spectrometry, 29(10):2105–2109, 2018.

[237] Marvin L Vestal. Modern maldi time-of-flight mass spectrometry. Journal of mass spectrometry, 44(3):303–317, 2009.

[238] Johannes Passig, Julian Schade, Robert Irsig, Thomas Kröger-Badge, Hendryk Czech, Thomas Adam, Henrik Fallgren, Jana Moldanova, Martin Sklorz, Thorsten Streibel, et al. Single-particle characterization of polycyclic aromatic hydrocarbons in background air in northern europe. Atmospheric Chemistry and Physics Discussions, 2021:1–31, 2021.

[239] BA Mamyrin, VI Karataev, DV Shmikk, and VA Zagulin. The mass-reflectron, a new nonmagnetic time-of-flight mass spectrometer with high resolution. Zh. Eksp. Teor. Fiz, 64(1):82–89, 1973.

[240] Kimberly A Prather, Trent Nordmeyer, and Kimberly Salt. Real-time characterization of individual aerosol particles using time-of-flight mass spectrometry. Analytical Chemistry, 66(9):1403–1407, 1994.

[241] Camille M Sultana, Douglas B Collins, and Kimberly A Prather. Effect of structural heterogeneity in chemical composition on online single-particle mass spectrometry analysis of sea spray aerosol particles. Environmental Science & Technology, 51(7):3660–3668, 2017.

[242] N Riemer, AP Ault, M West, RL Craig, and JH Curtis. Aerosol mixing state: Measurements, modeling, and impacts. Reviews of Geophysics, 57(2):187–249, 2019.

[243] Yongxuan Su, Michele F Sipin, Hiroshi Furutani, and Kimberly A Prather. Development and characterization of an aerosol time-of-flight mass spectrometer with increased detection efficiency. Analytical Chemistry, 76(3):712–719, 2004.

[244] Andrew P Ault, Cassandra J Gaston, Ying Wang, Gerardo Dominguez, Mark H Thiemens, and Kimberly A Prather. Characterization of the single particle mixing state of individual ship plume events measured at the port of los angeles. Environmental science & technology, 44(6):1954–1961, 2010.

[245] Camille M Sultana, Gavin C Cornwell, Paul Rodriguez, and Kimberly A Prather. Fates: a flexible analysis toolkit for the exploration of single-particle mass spectrometer data. Atmospheric Measurement Techniques, 10(4):1323–1334, 2017.

[246] Guanzhong Wang, Heinrich Ruser, Julian Schade, Johannes Passig, Thomas Adam, Günther Dollinger, and Ralf Zimmermann. Machine learning approaches for automatic classification of single-particle mass spectrometry data. Atmospheric Measurement Techniques, 17(1):299–313, 2024.

[247] Thomas Frank, K-F Kraiss, and Torsten Kuhlen. Comparative analysis of fuzzy art and art-2a network clustering performance. IEEE Transactions on Neural networks, 9(3):544–559, 1998.

[248] Gail A Carpenter, Stephen Grossberg, and David B Rosen. Art 2-a: An adaptive resonance algorithm for rapid category learning and recognition. Neural networks, 4(4):493–504, 1991.

[249] Ahad Al-Enazi, Eric C Okonkwo, Yusuf Bicer, and Tareq Al-Ansari. A review of cleaner alternative fuels for maritime transportation. Energy Reports, 7:1962–1985, 2021.

[250] Allen D Uhler, Scott A Stout, Gregory S Douglas, Edward M Healey, and Stephen D Emsbo-Mattingly. Chemical character of marine heavy fuel oils and lubricants. In Standard handbook oil spill environmental forensics, pages 641–683. Elsevier, 2016.

[251] Shanti A Kudchadker, Arvind P Kudchadker, and Bruno J Zwolinski. Chemical thermodynamic properties of anthracene and phenanthrene. The Journal of Chemical Thermodynamics, 11(11):1051–1059, 1979.

[252] María Victoria Roux, Manuel Temprado, James S Chickos, and Yatsuhisa Nagano. Critically evaluated thermochemical properties of polycyclic aromatic hydrocarbons. Journal of Physical and Chemical Reference Data, 37(4):1855–1996, 2008.

[253] Branko Ruscic and David Bross. Active thermochemical tables (atct) thermochemical values ver. 1.128, 2023. `https://www.anl.gov/argonne-scientific-publications/pub/184353` [Accessed: 13th February 2025].

[254] Akira Matsugi and Shunsuke Suzuki. Anthracene formation pathways in toluene combustion: Reactions of benzyl and 2-methylphenyl radicals. Combustion and Flame, 267:113603, 2024.

[255] Jan T Andersson and Christine Achten. Time to say goodbye to the 16 epa pahs? toward an up-to-date use of pacs for environmental purposes. Polycyclic aromatic compounds, 35(2-4):330–354, 2015.

[256] Wenyu Sun, Alaa Hamadi, Said Abid, Nabiha Chaumeix, and Andrea Comandini. Detailed experimental and kinetic modeling study of toluene/c2 pyrolysis in a single-pulse shock tube. Combustion and Flame, 226:129–142, 2021.

[257] Alan C Lloyd and Thomas A Cackette. Diesel engines: environmental impact and control. Journal of the Air & Waste Management Association, 51(6):809–847, 2001.

[258] S Chippett and WA Gray. The size and optical properties of soot particles. Combustion and Flame, 31:149–159, 1978.

[259] RJ Santoro, HG Semerjian, and Richard A Dobbins. Soot particle measurements in diffusion flames. Combustion and Flame, 51:203–218, 1983.

[260] Daniel M Murphy. The design of single particle laser mass spectrometers. Mass Spectrometry Reviews, 26(2):150–165, 2007.

[261] Openstreetmap contributors. Kattegat, 2025. https://www.openstreetmap.org/export#map=9/57.553/12.269&layers=T [Accessed: 11th February 2025].

[262] Branwen Ap Dafydd Tomos, Laurence Stamford, Andrew Welfle, and Alice Larkin. Decarbonising international shipping–a life cycle perspective on alternative fuel options. Energy Conversion and Management, 299:117848, 2024.

[263] MA Ershov, VD Savelenko, UA Makhova, AE Makhmudova, AV Zuikov, VM Kapustin, TMM Abdellatief, NO Burov, T Geng, MA Abdelkareem, et al. Current challenge and innovative progress for producing hvo and fame biodiesel fuels and their applications, waste biomass valorization (2022).

[264] Shaolong Yang, Xinxiang Pan, Zhitao Han, Dongsheng Zhao, Bojun Liu, Dekang Zheng, and Zhijun Yan. Removal of nox and so2 from simulated ship emissions using wet scrubbing based on seawater electrolysis technology. Chemical Engineering Journal, 331:8–15, 2018.

[265] Terence Chin, Ivan Tam, and Chun-Yang Yin. Wet scrubbing process with oxidation and reduction in series for removal of so2 and no from marine diesel engine exhaust. Chemical Engineering Journal, 464:142299, 2023.

[266] Peter Thor, Maria E Granberg, Hulda Winnes, and Kerstin Magnusson. Severe toxic effects on pelagic copepods from maritime exhaust gas scrubber effluents. Environmental science & technology, 55(9):5826–5835, 2021.

[267] Jan Bendl, Mohammad Reza Saraji-Bozorgzad, Uwe Käfer, Sara Padoan, Ajit Mudan, Uwe Etzien, Barbara Giocastro, Julian Schade, Seongho Jeong, Evelyn Kuhn, et al. How do different marine engine fuels and wet scrubbing affect gaseous air pollutants and ozone formation potential from ship emissions? Environmental Research, 260:119609, 2024.

[268] DA Lack and JJ Corbett. Black carbon from ships: a review of the effects of ship speed, fuel quality and exhaust gas scrubbing. Atmospheric Chemistry and Physics, 12(9):3985–4000, 2012.

[269] Kerri A Denkenberger, Ryan C Moffet, John C Holecek, Thomas P Rebotier, and Kimberly A Prather. Real-time, single-particle measurements of oligomers in aged ambient aerosol particles. Environmental Science & Technology, 41(15):5439–5446, 2007.

[270] B Mewes and JM Seitzman. Soot volume fraction and particle size measurements with laser-induced incandescence. Applied optics, 36(3):709–717, 1997.

[271] Liji Xiao, Weiguo Zeng, Guangfu Liao, Changfeng Yi, and Zushun Xu. Thermally and chemically stable candle soot superhydrophobic surface with excellent self-cleaning properties in air and oil. ACS Applied Nano Materials, 1(3):1204–1211, 2018.

[272] Sotiris E Pratsinis and Kyo-Seon Kim. Particle coagulation, diffusion and thermophoresis in laminar tube flows. Journal of Aerosol Science, 20(1):101–111, 1989.

[273] Martin Bauer, Hendryk Czech, Lukas Anders, Johannes Passig, Uwe Etzien, Jan Bendl, Thorsten Streibel, Thomas W Adam, Bert Buchholz, and Ralf Zimmermann. Impact of fuel sulfur regulations on carbonaceous particle emission from a marine engine. npj Climate and Atmospheric Science, 7(1):288, 2024.

[274] L-WA Chen, JC Chow, XL Wang, JA Robles, BJ Sumlin, DH Lowenthal, R Zimmermann, and JG Watson. Multi-wavelength optical measurement to enhance thermal/optical analysis for carbonaceous aerosol. Atmospheric Measurement Techniques, 8(1):451–461, 2015.

[275] Yongming Han, Junji Cao, Judith C Chow, John G Watson, Zhisheng An, Zhangdong Jin, Kochy Fung, and Suixin Liu. Evaluation of the thermal/optical reflectance method for discrimination between char-and soot-ec. Chemosphere, 69(4):569–574, 2007.

[276] Marie Elmquist, Gerard Cornelissen, Zofia Kukulska, and Örjan Gustafsson. Distinct oxidative stabilities of char versus soot black carbon: Implications for quantification and environmental recalcitrance. Global biogeochemical cycles, 20(2), 2006.

[277] Ellen Iva Rosewig, Julian Schade, Johannes Passig, Helena Osterholz, Robert Irsig, Dominik Smok, Nadine Gawlitta, Jürgen Schnelle-Kreis, Jan Hovorka, Detlef Schulz-Bull, et al. Remote detection of different marine fuels in exhaust plumes by onboard measurements in the baltic sea using single-particle mass spectrometry. Atmosphere, 14(5):849, 2023.

[278] Ellen Iva Rosewig, Julian Schade, Heinrich Ruser, Johannes Passig, Ralf Zimmermann, and Thomas W Adam. Detection and analysis of ship emissions using single-particle mass spectrometry: A land-based field study in the port of rostock, germany. Atmospheric Environment: X, 24:100302, 2024.

[279] W Alturki. Four-stroke and two-stroke marine engines comparison and application. International Journal of Engineering Research and Applications, 7(4 Part 3):49–56, 2017.

[280] Bulut Ozan Ceylan. Investigation of seasonal effects on two-stroke marine diesel engine performance parameters and emissions. Journal of Marine Science and Application, 22(4):795–808, 2023.

[281] Matthias Bente, Martin Sklorz, Thorsten Streibel, and Ralf Zimmermann. Online laser desorption-multiphoton postionization mass spectrometry of individual aerosol particles: molecular source indicators for particles emitted from different traffic-related and wood combustion sources. Analytical Chemistry, 80(23):8991–9004, 2008.

[282] Evgeni Sorokin, Sergey Naumov, and Irina T Sorokina. Ultrabroadband infrared solid-state lasers. IEEE Journal of Selected Topics in Quantum Electronics, 11(3):690–712, 2005.

[283] Alphan Sennaroglu. Solid-state lasers and applications. CRC press, 2017.

[284] Hans Joachim Eichler and Jürgen Eichler. Laser: Bauformen, Strahlführung, Anwendungen. Springer-Verlag, 2015.

[285] Hans-Jörg Kull. Laserphysik: physikalische Grundlagen des Laserlichts und seine

Wechselwirkung mit Materie. Oldenbourg Verlag, 2010.

[286] Max Diem. Quantenmechanische Grundlagen der Molekülspektroskopie. John Wiley & Sons, 2021.

[287] Yoshihisa Yamamoto. Characteristics of algaas fabry-perot cavity type laser amplifiers. IEEE Journal of Quantum Electronics, 16(10):1047–1052, 1980.

[288] David Hunger, Tilo Steinmetz, Yves Colombe, Christian Deutsch, Theodor W Hänsch, and Jakob Reichel. A fiber fabry–perot cavity with high finesse. New Journal of Physics, 12(6):065038, 2010.

[289] Michel JF Digonnet. Rare-earth-doped fiber lasers and amplifiers, revised and expanded. CRC press, 2001.

[290] Orazio Svelto, David C Hanna, et al. Principles of lasers, volume 1. Springer, 2010.

[291] Wolfgang Demtröder. Laserspektroskopie: Grundlagen und Techniken. Springer-Verlag, 2007.

[292] Rüdiger Paschotta. Four-level and three-level laser gain media.

[293] P Davidovits and R Novick. The optically pumped rubidium maser. Proceedings of the IEEE, 54(2):155–170, 1966.

[294] William F Krupke, Raymond J Beach, V Keith Kanz, and Stephen A Payne. Resonance transition 795-nm rubidium laser. Optics letters, 28(23):2336–2338, 2003.

[295] W Krichbaumer, H Herrmann, E Nagel, R Häring, J Streicher, Ch Werner, A Mehnert, Th Halldorsson, S Heinemann, P Peuser, et al. A diode-pumped nd: Yag lidar for airborne cloud measurements. Optics & Laser Technology, 25(5):283–287, 1993.

[296] JA Werner, BM Lippert, UW Geisthoff, and H Rudert. Nd: Yag-lasertherapie der rezidivierenden epistaxis bei hereditärer hämorrhagischer teleangiektasie. Laryngo-Rhino-Otologie, 76(08):495–501, 1997.

[297] Louis St-Onge, V Detalle, and Mohamad Sabsabi. Enhanced laser-induced breakdown spectroscopy using the combination of fourth-harmonic and fundamental nd: Yag laser pulses. Spectrochimica Acta Part B: Atomic Spectroscopy, 57(1):121–135, 2002.

[298] Carlos Jacinto, AA Andrade, Tomaz Catunda, SM Lima, and Mauro Luciano Baesso. Thermal lens spectroscopy of nd: Yag. Applied Physics Letters, 86(3), 2005.

[299] Ch Chen, Z Lin, and ZDAJDODOI s Wang. The development of new borate-based uv nonlinear optical crystals. Applied Physics B, 80:1–25, 2005.

[300] David N Nikogosyan. Nonlinear optical crystals: a complete survey. Springer Science & Business Media, 2006.

[301] Peter Furlan. Das gelbe Rechenbuch: für Ingenieure, Naturwissenschaftler und Mathematiker; Rechenverfahren der Höheren Mathematik in Einzelschritten erklärt. 1. Lineare Algebra,

Differentialrechnung. Verlag Furlan, 2004.

[302] Gabriele Teikemeier and David J Goldberg. Skin resurfacing with the erbium: Yag laser. Dermatologic surgery, 23(8):685–687, 1997.

[303] Isao Ishikawa, Akira Aoki, and Aristeo Atsushi Takasaki. Potential applications of erbium: Yag laser in periodontics. Journal of periodontal research, 39(4):275–285, 2004.

Volume 3
Number 8
August 2023
Pages 1127–1244

Environmental Science Atmospheres

rsc.li/esatmospheres

ISSN 2634-3606

ROYAL SOCIETY OF CHEMISTRY

PAPER
Johannes Passig *et al.*
Detection of ship emissions from distillate fuel operation *via* single-particle profiling of polycyclic aromatic hydrocarbons

Environmental Science: Atmospheres

ROYAL SOCIETY OF CHEMISTRY

PAPER

View Article Online
View Journal | View Issue

Cite this: *Environ. Sci.: Atmos.*, 2023, **3**, 1134

Detection of ship emissions from distillate fuel operation *via* single-particle profiling of polycyclic aromatic hydrocarbons†

Lukas Anders,[abc] Julian Schade,[abce] Ellen Iva Rosewig,[abc] Thomas Kröger-Badge,[ab] Robert Irsig,[cd] Seongho Jeong,[abc] Jan Bendl,[e] Mohammad Reza Saraji-Bozorgzad,[abde] Jhih-Hong Huang,[f] Fu-Yi Zhang,[f] Chia C. Wang,[f] Thomas Adam,[abe] Martin Sklorz,[ab] Uwe Etzien,[g] Bert Buchholz,[g] Hendryk Czech,[ab] Thorsten Streibel,[abc] Johannes Passig *[abc] and Ralf Zimmermann[abc]

Received 17th April 2023
Accepted 12th July 2023

DOI: 10.1039/d3ea00056g

rsc.li/esatmospheres

Using novel ionization technologies in single-particle mass spectrometry (SPMS), we analyzed the polycyclic aromatic hydrocarbons (PAHs) on individual particles from a research ship engine running on marine gasoil (MGO). We found a rather uniform PAH signature on the majority of particles. The PAH pattern is stable for all engine loads and particle sizes and differs from typical signatures of other pyrogenic and petrogenic PAH sources. Based on this observation, we conducted a field experiment and observed that the appearance of this PAH signature is associated with marine air masses. Moreover, we could detect the plume of a single ship passage at 15–20 km distance by the transient appearance of particles with the same distinct PAH profile. Consequently, we suggest the use of the specific PAH pattern as a new marker to detect and monitor ship emissions, independent of the conventional metal signatures that are not applicable for compliant fuels in emission control areas and coastal waters.

Environmental significance

Air pollution from ships affects the atmospheric environment, with substantial impact on public health and climate. Emission control areas (ECAs) were installed worldwide to protect coastal regions against ship emissions by limiting the fuel's sulfur content. In ECAs, the traditional bunker fuels are replaced by *e.g.* marine gasoil, which also produces aerosols with severe health effects. Such distillate fuels do not contain metals from the refinery process. Thus, the traditional marker concept for ship emissions becomes obsolete because it is based on these metals. Ship emission detection, source apportionment and risk assessment therefore require novel marker concepts. Here we target this gap by introducing a new method to detect ship emission particles by using their content of polycyclic aromatic hydrocarbons.

Introduction

The marine transport sector is a major contributor to the global burden of air pollution. While nearly all air pollutants in Europe and the U.S. have decreased within the last few decades, ship emissions have changed less and currently contribute substantially to the total emissions of PM 2.5.[1–7] Regulations target the fuel sulfur content by a global 0.5% sulfur cap since 2020 and a maximum of 0.1% S in sulfur emission control areas (SECAs), *e.g.* along the U.S. coast, the entire North Sea and Baltic Sea as well as in many harbors and coastal regions worldwide.[8] Shipowners can either switch to compliant low-sulfur fuels (*e.g.* marine gasoil and MGO) or install an exhaust cleaning device ('scrubber'), allowing them to use the cheaper high-sulfur heavy fuel oils also in SECAs.[9,10] While the sulfur regulations and the resulting changes to cleaner fuels reduced total particulate matter emissions with benefits for ecosystems and human health,[11–13] the use of scrubbers can have collateral effects on the environment.[10,14–16] Beyond the sulfur aspect, the fuel type strongly affects the physical and chemical properties of the emissions[17–19] and their health effects.[20,21] Most ships in SECAs currently operate with MGO;[9]

[a]*Joint Mass Spectrometry Centre, Department of Analytical and Technical Chemistry, University of Rostock, 18051 Rostock, Germany. E-mail: johannes.passig@uni-rostock.de*

[b]*Comprehensive Molecular Analytics, Helmholtz Centre Munich, 85764 Neuherberg, Germany*

[c]*Department Life, Light & Matter, University of Rostock, 18051 Rostock, Germany*

[d]*Photonion GmbH, 19061 Schwerin, Germany*

[e]*Faculty for Mechanical Engineering, Institute of Chemistry and Environmental Engineering, University of the Bundeswehr Munich, 85577 Neubiberg, Germany*

[f]*Department of Chemistry and Aerosol Science Research Center, National Sun Yat-sen University, Kaohsiung, Taiwan 804, Republic of China*

[g]*Chair of Piston Machines and Internal Combustion Engines, University of Rostock, Germany*

† Electronic supplementary information (ESI) available. See DOI: https://doi.org/10.1039/d3ea00056g

however, the use of these cleaner fuels without filter technologies also produces severe health effects.[21]

Estimates of the burden of air pollution from ships are mainly based on laboratory/on-ship studies[18,22,23] and transport modelling.[24] Monitoring of ship plumes under clean air conditions is possible through gas phase measurements[25–27] and transient increases in particle number concentrations, black carbon or SO_x.[28,29] However, in populated coastal regions with complex aerosols, source apportionment relies on chemical markers for shipping, usually combinations of the transition metals vanadium(V), nickel (Ni) and iron (Fe).[30–32]

Single-particle mass spectrometry (SPMS) detects these particle-bound metals in real time,[33–36] and hence, it is applicable for monitoring ship emissions and source apportionment in complex environments.[37–40] Recently, the sensitivity of SPMS to metals has been increased by exploiting laser-atom resonances.[41] With this approach, individual ship plumes have been detected in an urban background from >10 km distance, and also from ships with scrubbers installed.[42]

Of note, source apportionment based on transition metals is only applicable if the ships run on residual fuels or on partly residual fuels such as marine diesel oil. For the distillate fuels that dominate in SECAs and gain importance in the course of the new global regulations, novel marker approaches based on polycyclic aromatic hydrocarbons (PAHs) have been suggested.[43,44] In parallel, new ionization methods for SPMS were introduced, yielding detailed mass spectra of PAHs in addition to the particle's inorganic composition.[45,46] Consequently, the combination of the novel single-particle PAH analyses with PAH marker concepts opens new avenues for source apportionment.

Here we present the first study applying single-particle mass spectrometry to investigate the fresh emissions of a ship engine. We used the recently developed SPMS techniques that reveal signatures of PAHs on a single-particle basis.[46] Thus, we were able to evaluate and establish the predicted PAH markers for MGO combustion on ships. To prove this new concept for source apportionment of ship emissions under real-world conditions, we present the first detection of a ship plume by using PAH emissions.

Methods

Ship engine and sampling

The laboratory experiments were conducted using a one-cylinder four-stroke 80 kW research ship engine with common rail injection. The engine is a well-documented model for ship propulsion systems,[47] capable of operating with all common ship fuels; for details see Streibel *et al.*[18] Four different operating points were investigated: 100, 75, 50 and 25% load, each for one hour and with a run-in time of 25 min for stabilization. The aerosol was sampled, and transported through a cyclone separator (cutoff diameter 10 μm) at a temperature of 200 °C. Using a two-stage ejector dilution system (eDiluter, Dekati Ltd., Finland), the aerosol was cooled to room temperature and diluted by a factor of 1 : 25 with clean, dried and particle-free air. From 1 L min^{-1} aerosol transported to the SPMS system, 0.1 L min^{-1} was guided into the instrument. Further details of the sampling setup were given by Jeong *et al.*[7]

SPMS instrumentation

The new laser ionization scheme for combined measurements of inorganic composition and PAHs has been described in detail in another publication.[46] The instrument and parameters were not changed. In brief, the particles are accelerated and focused by an aerodynamic lens system before optical detection and sizing. When entering the ion source of the mass spectrometer, each detected particle is exposed to an IR pulse for laser desorption (LD) of the organic material. An unfocused UV beam (λ = 248 nm) from a KrF excimer laser intersects the expanding gaseous plume, inducing resonance-enhanced multiphoton ionization (REMPI) of PAHs in the plume. The laser beam is back-reflected and focused into the center of the plume, where it hits the particle residue for laser desorption/ionization (LDI) of inorganic and refractory particle compounds at high laser intensities (~2 GW cm^{-2}). The positive flight tube of the mass analyzer detects the PAHs together with cations from LDI, while the opposite negative flight tube measures anions from LDI. Ion signals were recorded with a 14-bit digitizer (ADQ14, Teledyne SP Devices AB, Sweden) and custom LabView software. Note that in SPMS, the peak height is not directly convertible to the mass concentration of a specific substance. The new method applied here yields PAH mass spectra from individual particles; however, it cannot distinguish between isobar substances, *e.g.* phenanthrene *vs.* anthracene or benzo[*a*]pyrene *vs.* perylene.

Analysis of single-particle mass spectra

For the clustering of mass spectral signatures, we used the adaptive resonance theory neural network algorithm, ART-2a.[48] The program code was taken from the open-source toolkit FATES[49] and embedded in custom Matlab software (MathWorks Inc.). With regard to the different ionization processes, LDI and REMPI mass spectra were separately normalized and independently clustered using a vigilance factor of 0.8, a learning rate of 0.05, and 20 iterations.[50] In order to identify the main particle classes, we applied a regrouping algorithm, where clusters from the initial clustering are merged in a second ART-2a run.[51] The results were regularly cross-checked against those of manual merging.

Ambient air sampling

The field experiments shown here were part of a measurement campaign at the Swedish West coast.[50] The clean air conditions there required aerosol preconcentration (Model 4240, MSP corp., USA)[52] and drying (Model MD-700-12S-1, Perma Pure LLC, U.S.). Wind data were acquired from the local station Nidingen, 8 km south of the sampling site.[53]

Results and discussion

Particle types emitted by the laboratory ship engine

First, we investigated the ship engine's exhaust aerosol with respect to the single-particle chemical composition of inorganic

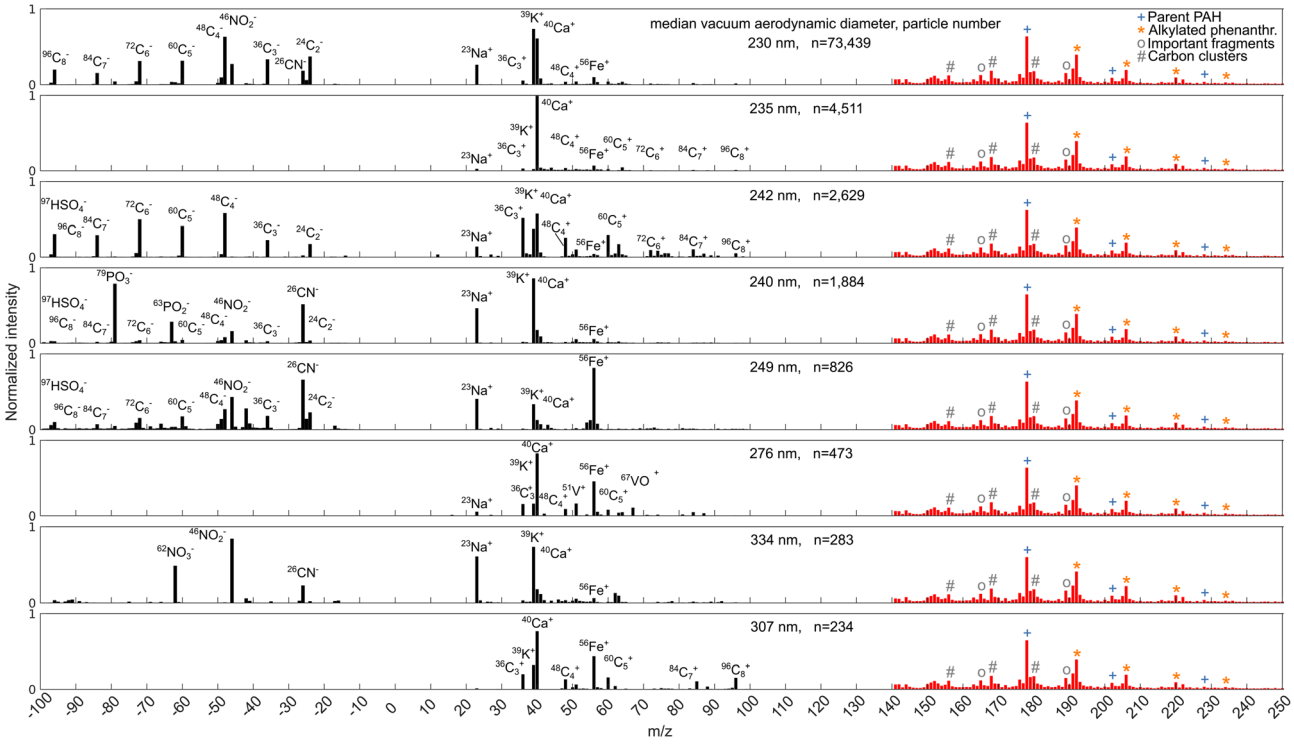

Fig. 1 Mass spectra of the eight main particle classes from ART2a-clustering of bipolar LDI mass spectra (black) for 60 kW (75%) load of the research ship engine. The inorganic particle composition *via* LDI reveals distinct particle classes, *e.g.* soot particles indicated by carbon clusters C_n of both polarities. Of note, the PAH pattern from REMPI (red) is very similar for these particle groups, showing strong signals from alkylated phenanthrenes. Important PAH fragments appear at $m/z = 165$ and $m/z = 189$.

substances from laser desorption/ionization (LDI), similar to previous studies on light duty[54,55] and heavy-duty vehicles.[56] Fig. 1 shows the weight matrices (mass spectra of cluster centers) of the ART2a-clustering and regrouping of LDI mass spectra from 84 143 individual particles measured during engine operation with 60 kW (75%) load. The inorganic composition of the main particle types resembles previous experiments on truck engines,[56] with the majority of soot-dominated particles and peaks from organic fragments. Strong signals from Ca^+ and phosphate signatures can be attributed to lube oil residues.[56,57] Particle-bound Fe is resonantly ionized in our SPMS, leading to substantial signal enhancement.[41]

PAH signatures and their distribution over the particle ensemble

The new ionization method used here yields PAH mass spectra from about 50% of all ship emission particles in the current measurement. This equals the typical hit rate for PAHs with this technology[46] and thus suggests that the majority of detected particles contain PAHs. This is not surprising because a large fraction of the PAHs is in the gas phase after combustion and condenses on the particles when the temperature drops in the exhaust system. The average PAH mass spectra of the LDI-derived particle types are shown as red bars in Fig. 1. Independent of the particle type, the PAH mass spectra are dominated by a signal series in m/z sequences of 14 Da beginning at $m/z = 178$ – a profile that has previously been associated with ship engine emissions from distillate fuel operation, both in on-line measurements of the hot flue gas as well as in filter samples.[18,44,58] The peak at $m/z = 178$ can stem from both phenanthrene and anthracene; however, anthracene is nearly exclusively produced in the combustion process and has a lower degree of substitution.[60] The pronounced alkylation pattern in our experiments indicates the dominance of phenanthrene and its alkylated derivatives over anthracene. In piston engines, the combustion temperature determines the number of rings as well as the degree of substitution, *e.g.* alkylation,[59] and large diesel engines show higher alkylation degrees resulting from higher amounts of unburnt fuel.[23,44]

Of note, the average PAH signatures of all particle types are nearly identical, as apparent from the average PAH mass spectra in the respective groups (red bars in Fig. 1). In order to prove the stability of this signature among the individual particles – and therefore its suitability as a marker profile – we performed a statistical analysis of their homogeneity in the particle ensemble. The violin plots in Fig. 2 show the distribution of the congruence coefficients r_C for each 25 000 particle LDI mass spectra (blue) and the respective PAH mass spectra (red) according to

$$r_C = \frac{\sum_{i,j} x_{i,j} y_{i,j}}{\sqrt{\left(\sum_{i,j} {x_{i,j}}^2\right)\left(\sum_{i,j} {y_{i,j}}^2\right)}}$$

with x and y representing the individual mass spectra. The distribution of r_C as a measure of the similarity between mass

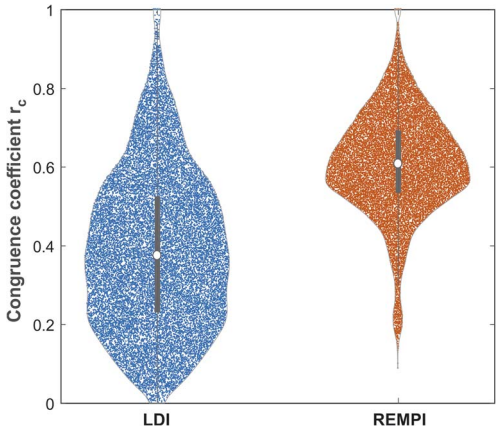

Fig. 2 Distribution of the congruence coefficients r_C between the single-particle mass spectra. The median r_C from the PAH mass spectra (white circle in the red probability density plot) is higher and its distribution is narrower compared to that from the LDI mass spectra of the same particles. The high similarity between PAH mass spectra supports their capability as a marker signature. Grey bars: interquartile range, $n = 25\,000$.

spectra shows that the individual PAH signatures are much more uniform than the signatures of the particle's inorganic composition from LDI. The higher similarity of PAH spectra is likely a result of incomplete combustion and imprints of the fuel signature, emphasizing the suitability of single-particle PAH spectra as fuel markers.

The effect of the particle size

SPMS yields the individual particle size; however, the optical detection efficiency drops rapidly for particles smaller than 200 nm, and thus, the instrument probes the fraction of the largest emitted particles. Of note, this size mode includes many particles of aged ship plumes in field applications[4] and coincides with the size of long-range transported particles.[61] Because of the instrument's bias towards large particles in conventional SPMS sizing mode, we performed additional experiments in the so-called free running mode that includes ultrafine particles. In this operation mode, the instrument's optical detection- and sizing unit is inactive and the desorption- and ionization lasers fire with a 100 Hz repetition rate into the particle beam, hitting particles on a random basis. Thus, the limits of optical particle detection can be overcome, however, at the cost of lost size information. Fig. 3(a) shows that the particle size distribution measured *via* a scanning mobility particle sizer (SMPS) peaks at around 80 nm. The SMPS-derived size distribution combined with the lower limit of SPMS spectrum generation at around 50 nm (ref. 62) suggests that particles between 50 and 150 nm size are dominant in the mass spectra measured in free running mode. Fig. 3(b) shows the average mass spectra of 5000 particles measured in free running mode in comparison to Fig. 3(c) where the average mass spectra of the same number of particles measured in conventional sizing mode are shown. The smaller particles measured in free running mode are soot-dominated and the larger particles show stronger phosphate and nitrate signals and more fragment peaks from organic carbon, *e.g.* in the PAH spectrum. This behavior can be attributed to a larger fraction of soot particles in the ultrafine mode and stronger contributions from lube oil and cold zones near the cylinder walls for the larger particles; see Toner *et al.*[56] The PAH mass spectra in free running mode show a slightly lower contribution from parent PAHs and fragments; the reason is not known. However, the PAH signature is still characterized by the intense homologue series of alkylated phenanthrenes. A cluster analysis of particle spectra in free running mode is provided in ESI, Fig. S1.†

The effect of the engine load

The third investigated key parameter with potential influence on the PAH signatures is the engine load, as shown by a direct

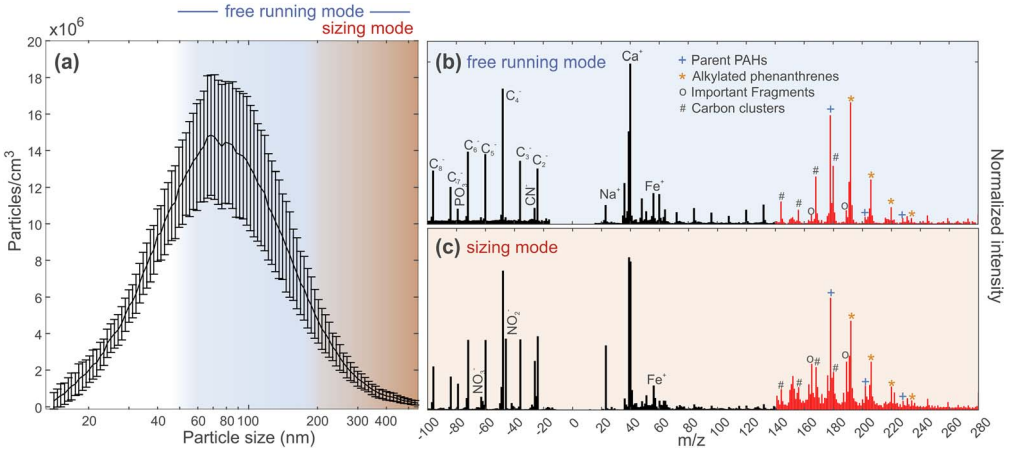

Fig. 3 (a) Particle size distribution of the research ship engine running on MGO at 60 kW load, measured by using a scanning mobility particle sizer (model 3082, TSI, U.S.). The blue shaded area illustrates the particle detection range of the SPMS in free running mode where particles of all sizes are hit at random, but size information from this instrument is not available. The red area indicates the coverage in normal sizing mode. The comparison of average mass spectra obtained in (b) free running mode (more smaller particles) and (c) in sizing mode (more larger particles) reveals that the characteristic series of alkylated phenanthrenes appears at all sizes. The additional series ($m/z = 231 + n \times 14$) is formed by fragments.[64]

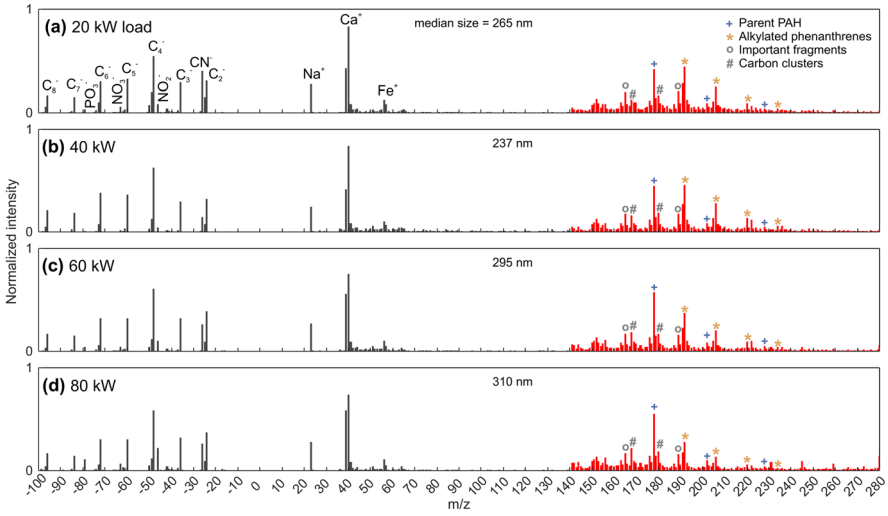

Fig. 4 With increasing engine load, the only noticeable change in the average PAH mass spectra (each $n = 3500$) is a subtle shift towards lighter PAHs. The pronounced alkylated phenanthrenes as the key feature indicating ship emissions from distillate fuels are hardly affected as well as the inorganic particle composition from LDI.

comparison of average mass spectra in Fig. 4. While the particle's organic content is highest at low load[18] and total PAH signals are slightly decreasing with increasing load (compensated by signal normalization as shown in Fig. 4), the general profile with strong alkylated phenanthrenes remains clearly visible. The inorganic composition reveals an increase in the nitrate signals with higher engine load and combustion temperature. The particle size distribution for all loads is given in ESI, Fig. S2.†

In summary, the vast majority of PAH-containing particles from MGO operation show a characteristic PAH pattern whose key feature, a dominant row from phenanthrene and its alkylated derivatives, is nearly unaffected by the particle type, size and engine load. The measured PAHs are a mixture of combustion products and residues of unburnt fuel and lube oil.[23,44] Spencer *et al.* found comparable PAH signatures in the majority of the droplets of sprayed diesel fuel using LDI-based SPMS.[63] Of note, the parent PAHs (*e.g.* $m/z = 178$) were nearly absent in this study as they originate from reactions between hydrocarbon radicals during combustion[59] while the alkylated species appear to be mainly fuel residues.[23] A further key difference between the droplet studies and our emission experiments is the much higher concentration of PAHs in the diesel fuel droplets,[10,18,63,64] and thus, they were detectable *via* LDI even in negative mode.[63]

We also investigated the diversity of PAH signatures by ART2a-clustering of single-particle REMPI mass spectra and analyzed the corresponding inorganic particle composition. Only a minority of particles produce substantially different PAH mass spectra, as shown in ESI, Fig. S3.†

Ship plume detection via PAHs in the field

To demonstrate the field applicability of our PAH-marker approach, we re-analyze subsets of the data from a field study at the Swedish coast in autumn 2019, see Passig *et al.*[50] for details. Briefly, we used the same SPMS system and the same configuration as in the laboratory but with additional particle concentration (see the "Methods" section above) to account for the general clean air conditions with less than 10 μg m^{-3} PM2.5. In the timeframe considered, circulating winds transported both terrestrial as well as marine aerosols to the sampling site (Fig. 5). From 292 242 chemically characterized particles in the period, 3746 particles showed PAH signals. Fig. S4 in the ESI† shows one of the resulting clusters exhibiting a PAH spectrum with dominant alkylated phenanthrenes, similar to the experimental results with the research ship engine. The corresponding inorganic composition from LDI reveals soot with Ca and Fe contributions, organic carbon (OC) peaks and some ageing signatures (*e.g.* $^{43}C_2H_3O^+$ contribution at $m/z = 43$). In order to investigate the sources of these particles, we correlated their appearance time with local wind data. Fig. 6(a) shows the distance from the intersection point of the wind trajectory with the main shipping lane to the measurement site as a function of time.

The wind speed is plotted in Fig. 6(b). The detection time and the size of all PAH-containing particles are depicted in Fig. 6(c) as grey dots, and the red dots represent the particles with dominant alkylated phenanthrenes. Obviously, these

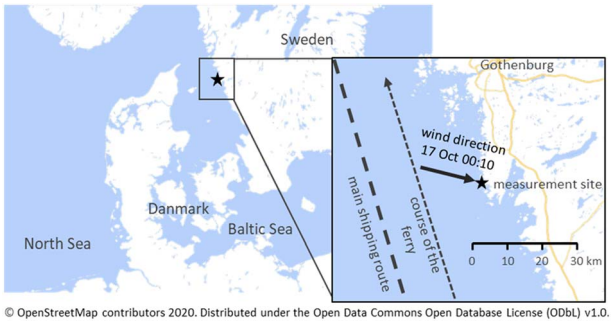

Fig. 5 Overview map of the region and the sampling site.

particles were mainly detected during periods of short distance travel to the ship lane and at low wind speeds, while at high wind speeds and especially during wind from land (distance > 100 km as shown in in Fig. 6(a)) they were only rarely detected. This behavior points to ship traffic as a probable source and indicates that land-based sources are of minor importance for this PAH signature.

Fig. 6(c) also shows a transient event of rather small particles (circled) indicating a single, less distant source. These particles also show the mentioned PAH profile but smaller peaks from OC, see ESI, Fig. S4(b)† for an average spectrum. Ship transponder data (AIS) revealed a ferry heading north at about 15–20 km distance to the sampling site 45 min before the event, see the inset of Fig. 5. The ferry traveled closer to the coastline than most other ships, and its lights were visible in the night. The ship was not equipped with a scrubber, so it is mandatory for it to use distillate fuel (*i.e.* MGO).

Complementarity with previous concepts

Our findings emphasize the potential of single-particle PAH measurements for ship plume detection and source apportionment of ship emissions. Previous SPMS approaches without PAH evaluation were based on a unique combination of transition metals from bunker fuel residues; however, the global change to cleaner fuels requires novel strategies.[65] Apart from transition metals, conventional SPMS can identify soot particles from many sources. However, it can hardly differentiate between the emissions from different engine types, although rather subtle changes in the SPMS mass spectra have been described.[54,56,63,66] The approach presented here focuses on organic fuel residues and combustion products, harnessing the high sensitivity for PAHs based on the resonant ionization process. Consequently, it reveals fuel and combustion characteristics beyond metals or lube oil additives. PAHs can also be detected with conventional SPMS, however, with less sensitivity and strong fragmentation that affects the reproducibility of mass spectra.[46,67–69]

Potential ambiguities and interferences with land-based diesel emissions

An important limitation could arise from interferences with other sources with potentially similar PAH emission profiles. Czech *et al.* performed gas phase analyses of PAHs from different sources emphasizing a unique profile of large (ship) diesel engines.[44] However, this study included the signatures of the lighter two-ring PAHs which are limited to the gas phase and not available here to differentiate between ship engines running on MGO and smaller diesel engines. Spencer *et al.* found comparable PAH signatures in lube oil and diesel droplets[63] where they have high concentrations,[64] but not in the exhaust emissions, probably because of lower sensitivity to PAHs in the LDI ionization used by their SPMS instrument.[68,70] A minor class of PAH-containing particles was determined in a study on heavy-duty vehicle emissions using the same instrument.[71] The

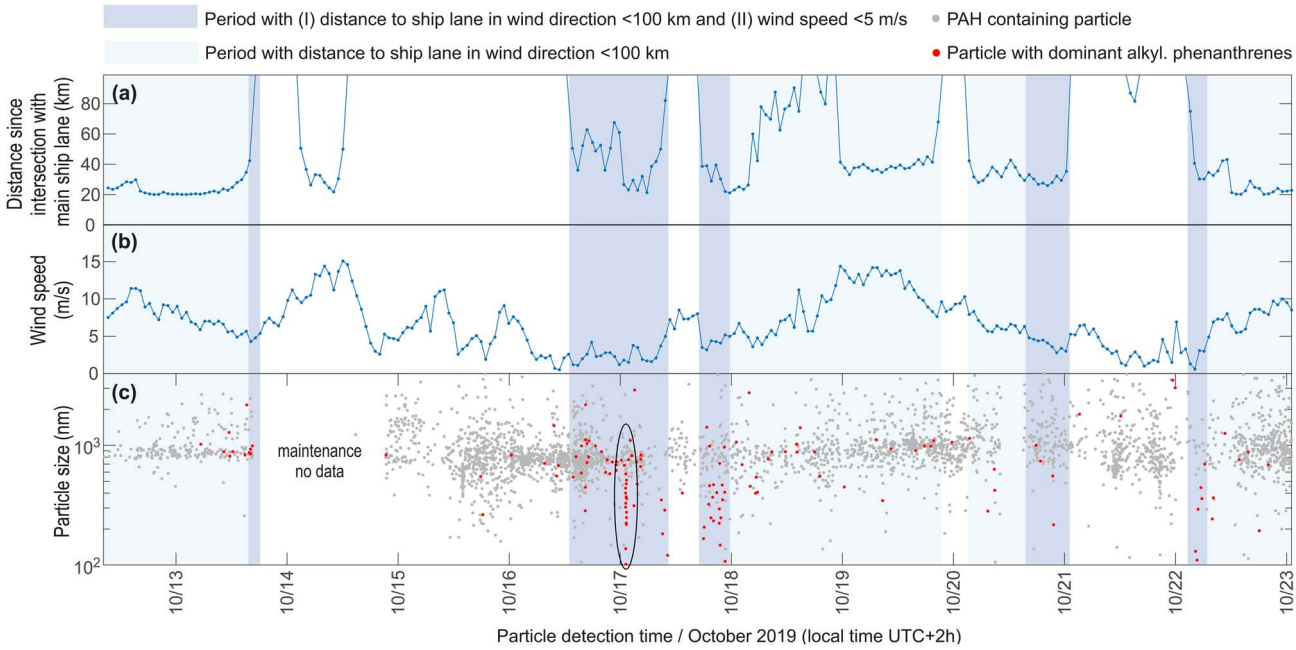

Fig. 6 Time course of wind data and particle detection events. (a) Distance from the measurement site to the main ship lane in the wind direction as derived from data of the local meteorological station. (b) Local wind speed from the same data. (c) Particle sizes and detection times for all PAH-containing particles (grey dots). The red dots represent PAH-containing particles with strong signals of alkylated phenanthrenes, belonging to the cluster shown in the ESI, Fig. S4(a).† Of note, the appearance of such particles is associated with light onshore winds and rather small distances to the ship lane in the wind direction (dark blue shaded periods). Only few particles of this type were detected in winds from the land, despite a motorway (20 km distance), the city of Gothenburg and active farming in the region. A transient signal of small particles from this type can even be attributed to an individual ship passage (circled).

PAHs in these experiments were dominated by the four-ring parent PAHs at $m/z = 202$ in contrast to the strong alkylated phenanthrenes observed here for ship emissions.

We have conducted unpublished experiments with different kinds of logwood, biomass burning and brown coal so far; all of them have not produced similar PAH signatures, as shown in ESI, Fig. S5(a) and (b).† Using gas chromatography MS, Martens *et al.* found a ratio between phenanthrene and the sum of its alkylated derivatives of 2–6 for logwood and 0.4–4 for brown coal combustion,[72] while this factor is 0.4–1 in the experiments shown here, dependent on the engine load. However, in a preliminary experiment with a 5.7 kW diesel power generator, we observed PAH profiles comparable to that of the ship engine with MGO described here, see ESI, Fig. S5(c)† for a mass spectrum. We therefore assume that particles from diesel engines without exhaust cleaning devices bear the highest potential for interferences with the proposed ship emission markers. We expect that these interferences are of minor importance for two reasons: firstly, since most road traffic vehicles are nowadays equipped with particle filters, the quantity of land-based diesel particle emissions from such old cars, tractors, stationary engines, *etc.* is much lower compared to ship traffic emissions.[3] Secondly, if the measurements are performed close to the coastline during on-shore winds, *e.g.* for ship plume detection, particles of terrestrial origin reveal ageing markers in the SPMS. Actually, during our ambient air campaign with several thousand PAH-containing particles, the described pattern with dominant alkylated phenanthrenes was predominantly observed in soot particles during on-shore winds, as shown in Fig. 6.

Additional ambiguity arises from the different degradation dynamics of individual PAH compounds which have been discussed as a key limitation for the diagnostic ratio approach in source apportionment of PAHs.[73–75] However, the atmospheric residence time for the particles is in the range of minutes to a few hours before individual ship plumes disintegrate by dispersion and mixing.[76] We expect therefore, a limited effect of aging on the characteristic pattern of PAHs. Note that heterogeneous PAH degradation in the atmosphere is often much slower than in lab experiments,[77] for example, from shielding effects.[78,79]

Both the plume travel distance and wind speed are comparable to those of former experiments where resonant ionization of metals has been applied for sensitivity enhancement to Fe, Ni and V,[42,80] so it is a realistic scenario and detection range for optimized SPMS methods.

Conclusions

Our study showed the application of a new ionization method in SPMS to identify ship emission particles based on their PAH composition. The laboratory experiments indicate a high stability of the proposed marker signature throughout different particle types, engine loads and particle sizes. The respective particles can be found in ambient air and are associated with a marine background. Moreover, under appropriate wind conditions, individual plumes from ships running on MGO can be detected over a distance of several kilometers. A major ambiguity of this approach results from interferences with diesel-powered engines that not equipped with exhaust treatment. However, considering the local geography and weather conditions, these inaccuracies in source apportionment can easily be minimized.

To further emphasize the real-world application of the new PAH-based concept, future experiments will focus on many ship plumes in contrast to the occasional event presented here. Therefore, the optical particle detection of the instrument will be improved towards higher sensitivity and the measurement site will be closer to the shipping lane. This method is currently under evaluation for the identification of different types of distillate and residual fuels that gain importance with new regulations.[10,81] In combination with the resonant ionization of metals that substantially improves the detection of the traditional metal markers,[41,42] the approach could be generalized for the coverage and identification of all relevant ship fuels currently on the market. Further interesting applications will be the real-time measurement of ship plume ageing effects and PAH deposition in the surface water.

Author contributions

L. A., J. S., I. E. R., J. H. H and F. Y. Z. performed the SPMS experiments. L. A., J. S. and J. P. analyzed the data. T. K. B. and R. I. provided technical assistance. S. J., J. B., U. E., M. S. and M. R. S performed the aerosol characterization experiments at the engine. U. E. and B. B. provided the research ship engine and operated it. T. S., B. B. and R. Z. developed and managed the project and raised funding. J. S., C. W. H. C. and R. Z. participated in scientific discussions and provided expert advice. J. P. conceived the study, assisted with the experiments and wrote the manuscript.

Conflicts of interest

There are no conflicts to declare.

Acknowledgements

This research was supported by the German Federal Ministry for Economic Affairs and Climate Action (SAARUS project, grant no. 03SX483D), and by the Helmholtz Association (International Laboratory aeroHEALTH – Interlabs-0005). This research was funded by dtec.bw - Digitilization and Technology Research Center of the Bundeswehr (projects "LUKAS" and "MORE"). dtec.bw is funded by the European Union – NextGenerationEU. The authors want to thank Felix Lange (Langefreunde® Design Studio, Germany) for creating the Table of Contents Graphic.

References

1 EEA, *National emissions reported to the convention on long-range transboundary air pollution (LRTAP convention)*, **https://www.eea.europa.eu/data-and-maps/data/national-emissions-reported-to-the-convention-on-long-range-**

transboundary-air-pollution-lrtap-convention-13, accessed 22 August 2021.
2 International Transport Forum, *Reducing Sulphur Emissions from Ships: the Impact of International Regulation*, https://www.itf-oecd.org/reducing-sulphur-emissions-ships-impact-international-regulation-ships_5jlwvz8mqq9s-en, accessed 30 November 2020.
3 J. E. Jonson, M. Gauss, M. Schulz, J. P. Jalkanen and H. Fagerli, Effects of global ship emissions on European air pollution levels, *Atmos. Chem. Phys.*, 2020, **20**, 11399–11422.
4 S. Ausmeel, A. Eriksson, E. Ahlberg, M. K. Sporre, M. Spanne and A. Kristensson, Ship plumes in the Baltic Sea Sulfur Emission Control Area: chemical characterization and contribution to coastal aerosol concentrations, *Atmos. Chem. Phys.*, 2020, **20**, 9135–9151.
5 EPA, *Our Nation's Air*, https://gispub.epa.gov/air/trendsreport/2020/#home, accessed 22 August 2021.
6 N. Kuittinen, J. P. Jalkanen, J. Alanen, L. Ntziachristos, H. Hannuniemi, L. Johansson, P. Karjalainen, E. Saukko, M. Isotalo, P. Aakko-Saksa, K. Lehtoranta, J. Keskinen, P. Simonen, S. Saarikoski, E. Asmi, T. Laurila, R. Hillamo, F. Mylläri, H. Lihavainen, H. Timonen and T. Rönkkö, Shipping Remains a Globally Significant Source of Anthropogenic PN Emissions Even after 2020 Sulfur Regulation, *Environ. Sci. Technol.*, 2021, **55**, 129–138.
7 S. Jeong, J. Bendl, M. Saraji-Bozorgzad, U. Käfer, U. Etzien, J. Schade, M. Bauer, G. Jakobi, J. Orasche, K. Fisch, P. P. Cwierz, C. P. Rüger, H. Czech, E. Karg, G. Heyen, M. Krausnick, A. Geissler, C. Geipel, T. Streibel, J. Schnelle-Kreis, M. Sklorz, D. E. Schulz-Bull, B. Buchholz, T. Adam and R. Zimmermann, Aerosol emissions from a marine diesel engine running on different fuels and effects of exhaust gas cleaning measures, *Environ. Pollut.*, 2022, **316**, 120526.
8 IMO, *Annex VI of MARPOL 73/78, Regulations for the Prevention of Air Pollution from Ships Reg. 14*, https://www.imo.org/en/OurWork/Environment/Pages/Air-Pollution.aspx, accessed 30 August 2021.
9 A. Lähteenmäki-Uutela, J. Yliskylä-Peuralahti, S. Repka and J. Mellqvist, What explains SECA compliance: rational calculation or moral judgment?, *WMU Journal of Maritime Affairs*, 2019, **18**, 61–78.
10 A. Lunde Hermansson, I.-M. Hassellöv, J. Moldanová and E. Ytreberg, Comparing emissions of polyaromatic hydrocarbons and metals from marine fuels and scrubbers, *Transportation Research Part D: Transport and Environment*, 2021, **97**, 102912.
11 M. Sofiev, J. J. Winebrake, L. Johansson, E. W. Carr, M. Prank, J. Soares, J. Vira, R. Kouznetsov, J. P. Jalkanen and J. J. Corbett, Cleaner fuels for ships provide public health benefits with climate tradeoffs, *Nat. Commun.*, 2018, **9**, 406.
12 J. E. Jonson, M. Gauss, J. P. Jalkanen and L. Johansson, Effects of strengthening the Baltic Sea ECA regulations, *Atmos. Chem. Phys.*, 2019, **19**, 13469–13487.
13 C. Yu, D. Pasternak, J. Lee, M. Yang, T. Bell, K. Bower, H. Wu, D. Liu, C. Reed, S. Bauguitte, S. Cliff, J. Trembath, H. Coe and J. D. Allan, Characterizing the Particle Composition and Cloud Condensation Nuclei from Shipping Emission in Western Europe, *Environ. Sci. Technol.*, 2020, **54**, 15604–15612.
14 H. Winnes, E. Fridell and J. Moldanová, Effects of Marine Exhaust Gas Scrubbers on Gas and Particle Emissions, *J. Mar. Sci. Eng.*, 2020, **8**(4), 299.
15 P. Thor, M. E. Granberg, H. Winnes and K. Magnusson, Severe Toxic Effects on Pelagic Copepods from Maritime Exhaust Gas Scrubber Effluents, *Environ. Sci. Technol.*, 2021, **55**, 5826–5835.
16 D. R. Turner, I. M. Hassellöv, E. Ytreberg and A. Rutgersson, Shipping and the environment: Smokestack emissions, scrubbers and unregulated oceanic consequences, *Elementa - Sci. Anthrop.*, 2017, **5**(45), DOI: 10.1525/elementa.167.
17 J. Moldanová, E. Fridell, H. Winnes, S. Holmin-Fridell, J. Boman, A. Jedynska, V. Tishkova, B. Demirdjian, S. Joulie, H. Bladt, N. P. Ivleva and R. Niessner, Physical and chemical characterisation of PM emissions from two ships operating in European Emission Control Areas, *Atmos. Meas. Tech.*, 2013, **6**, 3577–3596.
18 T. Streibel, J. Schnelle-Kreis, H. Czech, H. Harndorf, G. Jakobi, J. Jokiniemi, E. Karg, J. Lintelmann, G. Matuschek, B. Michalke, L. Müller, J. Orasche, J. Passig, C. Radischat, R. Rabe, A. Reda, C. Rüger, T. Schwemer, O. Sippula, B. Stengel, M. Sklorz, T. Torvela, B. Weggler and R. Zimmermann, Aerosol emissions of a ship diesel engine operated with diesel fuel or heavy fuel oil, *Environ. Sci. Pollut. Res.*, 2017, **24**, 10976–10991.
19 Di Wu, Q. Li, X. Ding, J. Sun, D. Li, H. Fu, M. Teich, X. Ye and J. Chen, Primary Particulate Matter Emitted from Heavy Fuel and Diesel Oil Combustion in a Typical Container Ship: Characteristics and Toxicity, *Environ. Sci. Technol.*, 2018, **52**, 12943–12951.
20 J. J. Winebrake, J. J. Corbett, E. H. Green, A. Lauer and V. Eyring, Mitigating the Health Impacts of Pollution from Oceangoing Shipping: An Assessment of Low-Sulfur Fuel Mandates, *Environ. Sci. Technol.*, 2009, **43**, 4776–4782.
21 S. Oeder, T. Kanashova, O. Sippula, S. C. Sapcariu, T. Streibel, J. M. Arteaga-Salas, J. Passig, M. Dilger, H. R. Paur, C. Schlager, S. Mülhopt, S. Diabaté, C. Weiss, B. Stengel, R. Rabe, H. Harndorf, T. Torvela, J. K. Jokiniemi, M. R. Hirvonen, C. Schmidt-Weber, C. Traidl-Hoffmann, K. A. BéruBé, A. J. Wlodarczyk, Z. Prytherch, B. Michalke, T. Krebs, A. S. H. Prévôt, M. Kelbg, J. Tiggesbäumker, E. Karg, G. Jakobi, S. Scholtes, J. Schnelle-Kreis, J. Lintelmann, G. Matuschek, M. Sklorz, S. Klingbeil, J. Orasche, P. Richthammer, L. Müller, M. Elsasser, A. Reda, T. Gröger, B. Weggler, T. Schwemer, H. Czech, C. P. Rüger, G. Abbaszade, C. Radischat, K. Hiller, J. T. M. Buters, G. Dittmar and R. Zimmermann, Particulate matter from both heavy fuel oil and diesel fuel shipping emissions show strong biological effects on

human lung cells at realistic and comparable in vitro exposure conditions, *PLoS One*, 2015, **10**, e0126536.

22 F. Zhang, Y. Chen, C. Tian, D. Lou, J. Li, G. Zhang and V. Matthias, Emission factors for gaseous and particulate pollutants from offshore diesel engine vessels in China, *Atmos. Chem. Phys.*, 2016, **16**, 6319–6334.

23 O. Sippula, B. Stengel, M. Sklorz, T. Streibel, R. Rabe, J. Orasche, J. Lintelmann, B. Michalke, G. Abbaszade, C. Radischat, T. Gröger, J. Schnelle-Kreis, H. Harndorf and R. Zimmermann, Particle Emissions from a Marine Engine: Chemical Composition and Aromatic Emission Profiles under Various Operating Conditions, *Environ. Sci. Technol.*, 2014, **48**, 11721–11729.

24 M. Karl, J. E. Jonson, A. Uppstu, A. Aulinger, M. Prank, M. Sofiev, J. P. Jalkanen, L. Johansson, M. Quante and V. Matthias, Effects of ship emissions on air quality in the Baltic Sea region simulated with three different chemistry transport models, *Atmos. Chem. Phys.*, 2019, **19**, 7019–7053.

25 A. Seyler, F. Wittrock, L. Kattner, B. Mathieu-Üffing, E. Peters, A. Richter, S. Schmolke and J. P. Burrows, Monitoring shipping emissions in the German Bight using MAX-DOAS measurements, *Atmos. Chem. Phys.*, 2017, **17**, 10997–11023.

26 J. Mellqvist, J. Beecken, V. Conde and J. Ekholm, Surveillance of sulphur emissions from ships in Danish waters. *Report to the Danish Environmental Protection Agency*., **https://research.chalmers.se/publication/500251**, accessed 24 November 2020.

27 Y. Zhang, F. Deng, H. Man, M. Fu, Z. Lv, Q. Xiao, X. Jin, S. Liu, K. He and H. Liu, Compliance and port air quality features with respect to ship fuel switching regulation: a field observation campaign, SEISO-Bohai, *Atmos. Chem. Phys.*, 2019, **19**, 4899–4916.

28 S. Ausmeel, A. Eriksson, E. Ahlberg and A. Kristensson, Methods for identifying aged ship plumes and estimating contribution to aerosol exposure downwind of shipping lanes, *Atmos. Meas. Tech.*, 2019, **12**, 4479–4493.

29 S. Celik, F. Drewnick, F. Fachinger, J. Brooks, E. Darbyshire, H. Coe, J. D. Paris, P. G. Eger, J. Schuladen, I. Tadic, N. Friedrich, D. Dienhart, B. Hottmann, H. Fischer, J. N. Crowley, H. Harder and S. Borrmann, Influence of vessel characteristics and atmospheric processes on the gas and particle phase of ship emission plumes: in situ measurements in the Mediterranean Sea and around the Arabian Peninsula, *Atmos. Chem. Phys.*, 2020, **20**, 4713–4734.

30 F. Zhang, Y. Chen, C. Tian, X. Wang, G. Huang, Y. Fang and Z. Zong, Identification and quantification of shipping emissions in Bohai Rim, China, *Sci. Total Environ.*, 2014, **497–498**, 570–577.

31 V. Celo, E. Dabek-Zlotorzynska and M. McCurdy, Chemical Characterization of Exhaust Emissions from Selected Canadian Marine Vessels: The Case of Trace Metals and Lanthanoids, *Environ. Sci. Technol.*, 2015, **49**, 5220–5226.

32 X. Wang, Y. Shen, Y. Lin, J. Pan, Y. Zhang, P. K. K. Louie, M. Li and Q. Fu, Atmospheric pollution from ships and its impact on local air quality at a port site in Shanghai, *Atmos. Chem. Phys.*, 2019, **19**, 6315–6330.

33 K.-P. Hinz and B. Spengler, Instrumentation, data evaluation and quantification in on-line aerosol mass spectrometry, *J. Mass Spectrom.*, 2007, **42**, 843–860.

34 D. M. Murphy, The design of single particle laser mass spectrometers, *Mass Spectrom. Rev.*, 2007, **26**, 150–165.

35 K. A. Pratt and K. A. Prather, Mass spectrometry of atmospheric aerosols-recent developments and applications. Part II: on-line mass spectrometry techniques, *Mass Spectrom. Rev.*, 2012, **31**, 17–48.

36 J. Passig and R. Zimmermann, in *Photoionization and Photo-Induced Processes in Mass Spectrometry*, ed. R. Zimmermann and L. Hanley, Wiley-VCH, Weinheim, 2020.

37 R. M. Healy, I. P. O'Connor, S. Hellebust, A. Allanic, J. R. Sodeau and J. C. Wenger, Characterisation of single particles from in-port ship emissions, *Atmos. Environ.*, 2009, **43**, 6408–6414.

38 A. P. Ault, C. I. Gaston, Y. Wang, G. Dominguez, M. H. Thiemens and K. A. Prather, Characterization of the single particle mixing state of individual ship plume events measured at the Port of Los Angeles, *Environ. Sci. Technol.*, 2010, **44**, 1954–1961.

39 Z. Liu, X. Lu, J. Feng, Q. Fan, Y. Zhang and X. Yang, Influence of Ship Emissions on Urban Air Quality: A Comprehensive Study Using Highly Time-Resolved Online Measurements and Numerical Simulation in Shanghai, *Environ. Sci. Technol.*, 2017, **51**, 202–211.

40 Q. Xiao, M. Li, H. Liu, M. Fu, F. Deng, Z. Lv, H. Man, X. Jin, S. Liu and K. He, Characteristics of marine shipping emissions at berth: profiles for particulate matter and volatile organic compounds, *Atmos. Chem. Phys.*, 2018, **18**, 9527–9545.

41 J. Passig, J. Schade, E. I. Rosewig, R. Irsig, T. Kröger-Badge, H. Czech, M. Sklorz, T. Streibel, L. Li, X. Li, Z. Zhou, H. Fallgren, J. Moldanova and R. Zimmermann, Resonance-enhanced detection of metals in aerosols using single-particle mass spectrometry, *Atmos. Chem. Phys.*, 2020, **20**, 7139–7152.

42 J. Passig, J. Schade, R. Irsig, L. Li, X. Li, Z. Zhou, T. Adam and R. Zimmermann, Detection of Ship Plumes from Residual Fuel Operation in Emission Control Areas using Single-Particle Mass Spectrometry, *Atmos. Meas. Tech.*, 2021, **2021**, 4171–4185.

43 H. Czech, J. Schnelle-Kreis, T. Streibel and R. Zimmermann, New directions: Beyond sulphur, vanadium and nickel – about source apportionment of ship emissions in emission control areas, *Atmos. Environ.*, 2017, **163**, 190–191.

44 H. Czech, B. Stengel, T. Adam, M. Sklorz, T. Streibel and R. Zimmermann, A chemometric investigation of aromatic emission profiles from a marine engine in comparison with residential wood combustion and road traffic: implications for source apportionment inside and outside sulphur emission control areas, *Atmos. Environ.*, 2017, **167**, 212–222.

45 J. Passig, J. Schade, M. Oster, M. Fuchs, S. Ehlert, C. Jäger, M. Sklorz and R. Zimmermann, Aerosol Mass Spectrometer for Simultaneous Detection of Polyaromatic Hydrocarbons

and Inorganic Components from Individual Particles, *Anal. Chem.*, 2017, **89**, 6341–6345.

46 J. Schade, J. Passig, R. Irsig, S. Ehlert, M. Sklorz, T. Adam, C. Li, Y. Rudich and R. Zimmermann, Spatially Shaped Laser Pulses for the Simultaneous Detection of Polycyclic Aromatic Hydrocarbons as well as Positive and Negative Inorganic Ions in Single Particle Mass Spectrometry, *Anal. Chem.*, 2019, **91**, 10282–10288.

47 L. Mueller, G. Jakobi, H. Czech, B. Stengel, J. Orasche, J. M. Arteaga-Salas, E. Karg, M. Elsasser, O. Sippula, T. Streibel, J. G. Slowik, A. S. Prevot, J. Jokiniemi, R. Rabe, H. Harndorf, B. Michalke, J. Schnelle-Kreis and R. Zimmermann, Characteristics and temporal evolution of particulate emissions from a ship diesel engine, *Appl. Energy*, 2015, **155**, 204–217.

48 X. H. Song, P. K. Hopke, D. P. Fergenson and K. A. Prather, Classification of Single Particles Analyzed by ATOFMS Using an Artificial Neural Network, ART-2A, *Anal. Chem.*, 1999, **71**, 860–865.

49 C. M. Sultana, G. C. Cornwell, P. Rodriguez and K. A. Prather, FATES: a flexible analysis toolkit for the exploration of single-particle mass spectrometer data, *Atmos. Meas. Tech.*, 2017, **10**, 1323–1334.

50 J. Passig, J. Schade, R. Irsig, T. Kröger-Badge, H. Czech, T. Adam, H. Fallgren, J. Moldanova, M. Sklorz, T. Streibel and R. Zimmermann, Single-particle characterization of polycyclic aromatic hydrocarbons in background air in northern Europe, *Atmos. Chem. Phys.*, 2022, **22**, 1495–1514.

51 W. Zhao, P. K. Hopke and K. A. Prather, Comparison of two cluster analysis methods using single particle mass spectra, *Atmos. Environ.*, 2008, **42**, 881–892.

52 F. J. Romay, D. L. Roberts, V. A. Marple, B. Y. H. Liu and B. A. Olson, A High-Performance Aerosol Concentrator for Biological Agent Detection, *Aerosol Sci. Technol.*, 2002, **36**, 217–226.

53 SMHI, *Sveriges meteorologiska och hydrologiska institut*, **https://www.smhi.se/data/meteorologi/ladda-ner-meteorologiska-observationer#param=airtemperature Instant**,stations=all,stationid=71190, accessed 2 September 2021.

54 D. A. Sodeman, S. M. Toner and K. A. Prather, Determination of Single Particle Mass Spectral Signatures from Light-Duty Vehicle Emissions, *Environ. Sci. Technol.*, 2005, **39**, 4569–4580.

55 J. Yang, S. Ma, B. Gao, X. Li, Y. Zhang, J. Cai, M. Li, L. Yao, B. Huang and M. Zheng, Single particle mass spectral signatures from vehicle exhaust particles and the source apportionment of on-line PM2.5 by single particle aerosol mass spectrometry, *Sci. Total Environ.*, 2017, **593–594**, 310–318.

56 S. M. Toner, D. A. Sodeman and K. A. Prather, Single Particle Characterization of Ultrafine and Accumulation Mode Particles from Heavy Duty Diesel Vehicles Using Aerosol Time-of-Flight Mass Spectrometry, *Environ. Sci. Technol.*, 2006, **40**, 3912–3921.

57 J. Lyyränen, J. Jokiniemi, E. I. Kauppinen and J. Joutsensaari, Aerosol characterisation in medium-speed diesel engines operating with heavy fuel oils, *J. Aerosol Sci.*, 1999, **30**, 771–784.

58 C. Radischat, O. Sippula, B. Stengel, S. Klingbeil, M. Sklorz, R. Rabe, T. Streibel, H. Harndorf and R. Zimmermann, Real-time analysis of organic compounds in ship engine aerosol emissions using resonance-enhanced multiphoton ionisation and proton transfer mass spectrometry, *Anal. Bioanal. Chem.*, 2015, **407**, 5939–5951.

59 M. Frenklach, Reaction mechanism of soot formation in flames, *Phys. Chem. Chem. Phys.*, 2002, **4**, 2028–2037.

60 J. T. Andersson and C. Achten, Time to Say Goodbye to the 16 EPA PAHs? Toward an Up-to-Date Use of PACs for Environmental Purposes, *Polycyclic Aromat. Compd.*, 2015, **35**, 330–354.

61 J. H. Seinfeld and S. N. Pandis, *Atmospheric Chemistry and Physics: from Air Pollution to Climate Change*, Wiley, 2016.

62 D. B. Kane and M. V. Johnston, Size and Composition Biases on the Detection of Individual Ultrafine Particles by Aerosol Mass Spectrometry, *Environ. Sci. Technol.*, 2000, **34**, 4887–4893.

63 M. T. Spencer, L. G. Shields, D. A. Sodeman, S. M. Toner and K. A. Prather, Comparison of oil and fuel particle chemical signatures with particle emissions from heavy and light duty vehicles, *Atmos. Environ.*, 2006, **40**, 5224–5235.

64 P. T. Williams, K. D. Bartle and G. E. Andrews, The relation between polycyclic aromatic compounds in diesel fuels and exhaust particulates, *Fuel*, 1986, **65**, 1150–1158.

65 G. Yu, Y. Zhang, F. Yang, B. He, C. Zhang, Z. Zou, X. Yang, N. Li and J. Chen, Dynamic Ni/V Ratio in the Ship-Emitted Particles Driven by Multiphase Fuel Oil Regulations in Coastal China, *Environ. Sci. Technol.*, 2021, **55**, 15031–15039.

66 S. M. Toner, L. G. Shields, D. A. Sodeman and K. A. Prather, Using mass spectral source signatures to apportion exhaust particles from gasoline and diesel powered vehicles in a freeway study using UF-ATOFMS, *Atmos. Environ.*, 2008, **42**, 568–581.

67 M. Bente, M. Sklorz, T. Streibel and R. Zimmermann, Online laser desorption-multiphoton postionization mass spectrometry of individual aerosol particles: molecular source indicators for particles emitted from different traffic-related and wood combustion sources, *Anal. Chem.*, 2008, **80**, 8991–9004.

68 R. Zimmermann, T. Ferge, M. Gälli and R. Karlsson, Application of single-particle laser desorption/ionization time-of-flight mass spectrometry for detection of polycyclic aromatic hydrocarbons from soot particles originating from an industrial combustion process, *Rapid Commun. Mass Spectrom.*, 2003, **17**, 851–859.

69 B. D. Morrical, D. P. Fergenson and K. A. Prather, Coupling two-step laser desorption/ionization with aerosol time-of-flight mass spectrometry for the analysis of individual organic particles, *J. Am. Soc. Mass Spectrom.*, 1998, **9**, 1068–1073.

70 F. Gunzer, S. Krüger and J. Grotemeyer, Photoionization and photofragmentation in mass spectrometry with visible and UV lasers, *Mass Spectrom. Rev.*, 2019, **38**, 202–217.

71 L. G. Shields, D. T. Suess and K. A. Prather, Determination of single particle mass spectral signatures from heavy-duty diesel vehicle emissions for PM2.5 source apportionment, *Atmos. Environ.*, 2007, **41**, 3841–3852.

72 P. Martens, H. Czech, J. Orasche, G. Abbaszade, M. Sklorz, B. Michalke, J. Tissari, T. Bizjak, M. Ihalainen, H. Suhonen, P. Yli-Pirilä, J. Jokiniemi, O. Sippula and R. Zimmermann, Brown Coal and Logwood Combustion in a Modern Heating Appliance: The Impact of Combustion Quality and Fuel on Organic Aerosol Composition, *Environ. Sci. Technol.*, 2023, **57**, 5532–5543.

73 K. Ravindra, R. Sokhi and R. van Grieken, Atmospheric polycyclic aromatic hydrocarbons: Source attribution, emission factors and regulation, *Atmos. Environ.*, 2008, **42**, 2895–2921.

74 M. Tobiszewski and J. Namieśnik, PAH diagnostic ratios for the identification of pollution emission sources, *Environ. Pollut.*, 2012, **162**, 110–119.

75 T. Miersch, H. Czech, A. Hartikainen, M. Ihalainen, J. Orasche, G. Abbaszade, J. Tissari, T. Streibel, J. Jokiniemi, O. Sippula and R. Zimmermann, Impact of photochemical ageing on Polycyclic Aromatic Hydrocarbons (PAH) and oxygenated PAH (Oxy-PAH/OH-PAH) in logwood stove emissions, *Sci. Total Environ.*, 2019, **686**, 382–392.

76 A. Petzold, J. Hasselbach, P. Lauer, R. Baumann, K. Franke, C. Gurk, H. Schlager and E. Weingartner, Experimental studies on particle emissions from cruising ship, their characteristic properties, transformation and atmospheric lifetime in the marine boundary layer, *Atmos. Chem. Phys.*, 2008, **8**, 2387–2403.

77 I. J. Keyte, R. M. Harrison and G. Lammel, Chemical reactivity and long-range transport potential of polycyclic aromatic hydrocarbons – a review, *Chem. Soc. Rev.*, 2013, **42**, 9333–9391.

78 M. Shrivastava, S. Lou, A. Zelenyuk, R. C. Easter, R. A. Corley, B. D. Thrall, P. J. Rasch, J. D. Fast, S. L. M. Simonich, H. Shen and S. Tao, Global long-range transport and lung cancer risk from polycyclic aromatic hydrocarbons shielded by coatings of organic aerosol, *Proc. Natl. Acad. Sci.*, 2017, **114**, 1246–1251.

79 P. A. Alpert, J. Dou, P. Corral Arroyo, F. Schneider, J. Xto, B. Luo, T. Peter, T. Huthwelker, C. N. Borca, K. D. Henzler, T. Schaefer, H. Herrmann, J. Raabe, B. Watts, U. K. Krieger and M. Ammann, Photolytic radical persistence due to anoxia in viscous aerosol particles, *Nat. Commun.*, 2021, **12**, 1769.

80 E. I. Rosewig, J. Schade, J. Passig, H. Osterholz, R. Irsig, D. Smok, N. Gawlitta, J. Schnelle-Kreis, J. Hovorka, D. Schulz-Bull, R. Zimmermann and T. Adam, Remote Detection of Different Marine Fuels in Exhaust Plumes by Onboard Measurements in the Baltic Sea Using Single-Particle Mass Spectrometry, *Atmosphere*, 2023, **14**(5), 849.

81 K. Lehtoranta, P. Aakko-Saksa, T. Murtonen, H. Vesala, L. Ntziachristos, T. Rönkkö, P. Karjalainen, N. Kuittinen and H. Timonen, Particulate Mass and Nonvolatile Particle Number Emissions from Marine Engines Using Low-Sulfur Fuels, Natural Gas, or Scrubbers, *Environ. Sci. Technol.*, 2019, **53**, 3315–3322.

Volume 4
Number 7
July 2024
Pages 701–832

Environmental Science
Atmospheres

rsc.li/esatmospheres

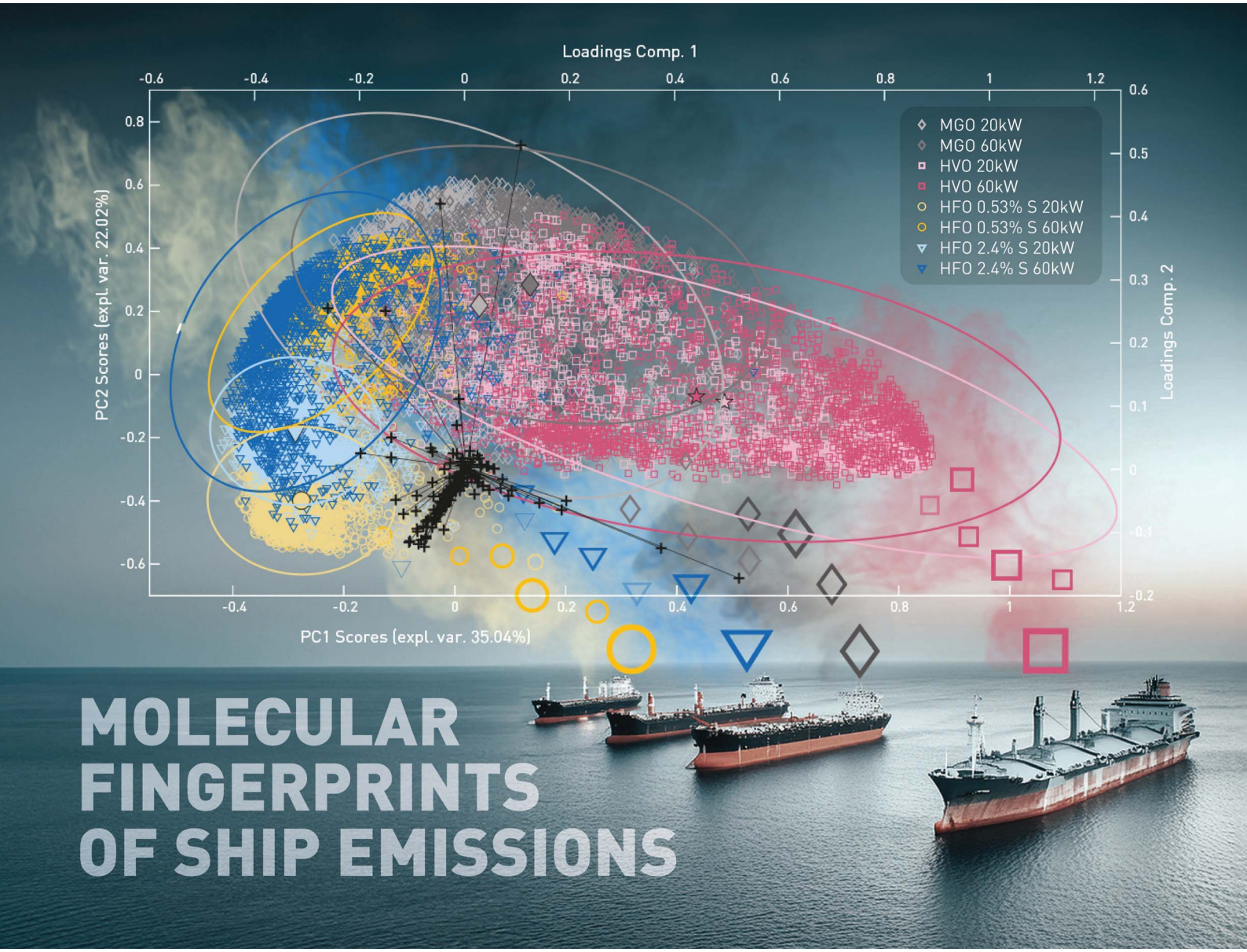

MOLECULAR FINGERPRINTS OF SHIP EMISSIONS

ISSN 2634-3606

ROYAL SOCIETY OF CHEMISTRY

PAPER
Johannes Passig *et al.*
Polycyclic aromatic hydrocarbons as fuel-dependent markers in ship engine emissions using single-particle mass spectrometry

Environmental Science: Atmospheres

ROYAL SOCIETY OF CHEMISTRY

PAPER

View Article Online
View Journal | View Issue

Cite this: *Environ. Sci.: Atmos.*, 2024, **4**, 708

Polycyclic aromatic hydrocarbons as fuel-dependent markers in ship engine emissions using single-particle mass spectrometry†

Lukas Anders,[ab] Julian Schade,[abc] Ellen Iva Rosewig,[ab] Marco Schmidt,[ab] Robert Irsig,[d] Seongho Jeong,[abc] Uwe Käfer,‡[a] Thomas Gröger,[a] Jan Bendl,[ac] Mohammad Reza Saraji-Bozorgzad,[acd] Thomas Adam,[ac] Uwe Etzien,[e] Hendryk Czech,[a] Bert Buchholz,[e] Thorsten Streibel,[ab] Johannes Passig *[ab] and Ralf Zimmermann[ab]

We investigated the fuel-dependent single-particle mass spectrometric signatures of polycyclic aromatic hydrocarbons (PAHs) from the emissions of a research ship engine operating on marine gas oil (MGO), hydrotreated vegetable oil (HVO) and two heavy fuel oils (HFO), one with compliant and one with non-compliant fuel sulfur content. The PAH patterns are only slightly affected by the engine load and particle size, and contain sufficient dissimilarity to discriminate between the marine fuels used in our laboratory study. Hydrotreated vegetable oil (HVO) produced only weak PAH signals, supporting that fuel residues, rather than combustion conditions, determine the PAH emissions. The imprint of the fuel in the resulting PAH signatures, combined with novel single-particle characterization capabilities for inorganic and organic components, opens up new opportunities for source apportionment and air pollution monitoring. The approach is independent of metals, the traditional markers of ship emissions, which are becoming less important as new emission control policies are implemented and fuels become more diverse.

Received 24th March 2024
Accepted 18th May 2024

DOI: 10.1039/d4ea00035h

rsc.li/esatmospheres

Environmental significance

Ship emissions are a major source of air pollution, causing serious impacts on human health, environment and climate. Various sulfur emission regulations have come into force in recent years, leading to a diversification of marine fuels. As a result, there is a need for alternatives to the traditional markers of ship emissions, taking into account the new fuel types. Here we show how the characteristic signatures of polyaromatic hydrocarbons can be used to identify the fuel for the purposes of monitoring and surveillance.

Introduction

Global shipping has a significant impact on human health, ecosystem quality and climate change through the release of anthropogenic emissions such as carbon dioxide (CO_2), sulfur oxides (SO_X), nitrogen oxides (NO_X) and particulate matter (PM) into the atmosphere.[1–6] Maritime transport facilitates over 90% of global trade volume,[7] and trends indicate that demand for shipping will increase by up to 50% by 2030 compared to 2016 levels.[8] To reduce the environmental and health burden, sulfur emission control areas (SECAs) have been established in many coastal regions (*e.g.* North America, North Sea, Baltic Sea, United States Caribbean Sea[9]), limiting the fuel sulfur content (FSC). The current EU sulfur directives require ships to use fuels with a maximum FSC of 0.1% m m^{-1} inside SECAs since 2015.[9] A global sulfur cap of 0.5% m m^{-1} outside SECA zones was put in place in 2020.[10] As a result, the range of fuels available has diversified, including bunker fuels ("Heavy Fuel Oils", HFOs) with varying sulfur contents. The majority of ships operating in SECAs have transitioned to use distillate fuels such as marine gas oil (MGO).[11] This has resulted in a significant reduction in particulate matter (PM) emissions.[12,13] However, it is important to recognize that the use of low sulfur containing fuels without filter technology may still have a substantial impact on human health.[14]

[a]*Joint Mass Spectrometry Centre, Analytical Chemistry, University of Rostock, Helmholtz Centre Munich, Comprehensive Molecular Analytics, 85764 Neuherberg, 18059 Rostock, Germany. E-mail: lukas.anders2@uni-rostock.de; johannes.passig@uni-rostock.de*

[b]*Department Life, Light & Matter, University of Rostock, 18059 Rostock, Germany*

[c]*Faculty of Mechanical Engineering, Institute of Chemistry and Environmental Engineering, University of the Bundeswehr Munich, 85577 Neubiberg, Germany*

[d]*Photonion GmbH, 19061 Schwerin, Germany*

[e]*Chair of Piston Machines and Internal Combustion Engines, University of Rostock, 18059 Rostock, Germany*

† Electronic supplementary information (ESI) available: Fig. S1: sum mass spectra without normalization. Fig. S2: sum mass spectra for 25% engine load. See DOI: https://doi.org/10.1039/d4ea00035h

‡ Currently at: Atmospheric Chemistry, Leibniz Institute for Tropospheric Research, Leipzig, Germany

Ships are powered by large diesel engines that do not have the aftertreatment of exhaust gases that is common in road vehicles. Ship emissions aerosols are therefore part of diesel exhaust particles (DEP), which are classified by the International Agency for Research on Cancer (IARC) as a group 1 carcinogen with an increased risk of lung cancer. The particles (*e.g.* soot) also carry carcinogenic PAHs,[15–17] can cause oxidative stress and are cytotoxic.[18]

Even high-sulfur containing fuels can be legally used on ships if exhaust gas cleaning systems such as scrubbers reduce the sulfur emissions to levels similar to those of compliant fuels.[19] While ship emissions from fuels that comply with current regulations are reported to be reduced,[20–22] the use of wet scrubbers can still have a devastating impact on the environment.[23,24] One possible way to reduce both greenhouse gas and PM emissions from shipping is to use alternative fuels such as hydrotreated vegetable oil (HVO).[25] However, such fuels are costly and available only in limited quantities.[26,27]

The increased diversity of fuel types and the growing use of distillate fuels pose new challenges for air pollution monitoring, surveillance and source apportionment. The traditional markers of ship emissions are the transition metals V, Ni or Fe – *i.e.* residues from bunker fuels.[28] Based on these metals, single-particle mass spectrometry (SPMS) is capable to detect ship emissions in real time,[29–34] including complex atmospheric environments[33] even if scrubbers are used in SECAs.[31] However, the metals are not emitted during operation on distillate fuels and therefore new markers beyond the transition metals are needed.[28]

Characteristic patterns of volatile and semi-volatile aromatic hydrocarbons from ship emissions have been reported.[35] Recently, it was shown that ship emission particles from MGO combustion can be identified by their profile of PAHs,[36] using a new technology in single-particle mass spectrometry (SPMS).[37] Anders *et al.*[36] studied emissions from a research ship engine running on MGO and described a consistent PAH pattern with high homogeneity that was also found in marine ambient air. A transient appearance of this pattern could also be attributed to a distant ship passage, emphasizing the potential of single-particle PAH profiling as a novel marker concept for ship emissions from distillate fuels. The novel capability to characterize PAHs along with the inorganic composition of individual particles has sparked new applications and source apportionment capabilities.[38] Here we extend the new approach to currently relevant marine fuels and describe the single-particle PAH emissions from a research ship engine running on two HFOs with different sulfur contents, MGO and HVO. Complementary to the particle's inorganic composition, the PAH patterns we observed for our multi-fuel research engine provide the basis for a sophisticated approach to ship emission monitoring and control, covering and discriminating between different compliant and non-compliant fuels in real-time scenarios.[36,38]

Methods

Research ship engine, fuels and sampling

The experiments were carried out on a 1-cylinder, 4-stroke, 80 kW research marine engine with common rail injection, installed at the "Institute of Piston Machines and Internal Combustion Engines" in Rostock, Germany. This engine is a well-characterized model for ship emission studies and is suitable for all types of marine fuels.[39] The investigated fuels include (I) the SECA-compliant fuels MGO and HVO, (II) HFO with 0.5% FSC as a compliant fuel for waters outside SECAs, and (III) HFO with 2.4% FSC, which can only be used legally with sulfur scrubber technology. Further details on the fuel can be found elsewhere.[40] In addition, to show an appropriate range of engine operations, four different loads of 80 kW, 60 kW, 40 kW and 20 kW were investigated, corresponding to the relative engine loads of 100%, 75%, 50%, and 25%, respectively. All levels were operated for at least one hour, with a running-in period of 25 minutes for stabilization. The emitted aerosol was sampled and passed at a temperature of 200 °C through a cyclone with a cut-off size of 10 μm. The aerosol was diluted with dried and particle-free air in a two-stage ejector dilution system (eDiluter, Dekati Ltd, Finland). The dilution ratio was 1 : 50 for the experiments with the heavy fuel oils, while a dilution ratio of 1 : 25 was used for the MGO and HVO fuels, respectively. Finally, from a total flow of 1 L min^{-1} that was transported to the SPMS, 0.1 L min^{-1} was directed into the system. In addition to the SPMS' optical sizing unit, particle size distributions were also measured using a scanning mobility particle sizer (TSI; model 3082) downstream of the SPMS after further dilution by a factor of 100. Further detailed information on the sampling setup can be found in Jeong *et al.*[40]

Single-particle mass spectrometer with PAH characterization

The ability to measure chemical profiles of individual particles makes single-particle mass spectrometry (SPMS) a unique tool for source identification in complex atmospheric environments. Here, a novel ionization setup was applied, using spatially and temporally tailored laser pulses to simultaneously induce laser desorption/ionization (LDI) and resonance-enhanced multi-photon ionization (REMPI) of particle components. The technique provides single-particle information on the inorganic composition (*via* LDI) and particle-bound PAHs (*via* REMPI).[37] In brief, a narrow particle beam is formed by an aerodynamic lens at the inlet of the instrument. Individual particles in the beam are then optically detected and sized. Subsequently, each particle is exposed to an IR pulse from a CO_2 laser (10.6 μm, 20 mJ pulse energy), which desorbs organic matter and creates a gaseous plume surrounding the refractory particle residue. In the ionization step, an unfocused UV pulse from a KrF excimer laser (248 nm wavelength, 6 mJ pulse energy) ionizes the desorbed PAHs in the plume *via* REMPI.[41] The laser light is then backreflected and focused into the ion source, ionizing the refractory residue of the same particle *via* LDI at much higher laser intensity. PAH ions are measured in the positive arm of the bipolar Time-Of-Flight (TOF) mass spectrometer, while inorganic compounds from LDI are detected in both the positive and negative flight tubes. All ion signals are recorded by a 14 bit digitizer (ADQ14, Teledyne SP Devices AB, Sweden) and a customized software based on LabVIEW (National Instruments Inc.). It should be noted that SPMS data does not produce precise mass concentration values of the substances but yields

chemical information on a single-particle level. Isobaric substances, however, cannot be distinguished (*e.g.* phenanthrene *vs.* anthracene).

Analysis of SPMS data

Custom MATLAB software (MathWorks Inc.) was used for the conversion of time-of-flight data to mass spectra with nominal mass resolution. The bars reflect the integrated peak area. Because of the different ionization processes, data from LDI and REMPI were individually normalized. The violin plots were created using the "violin plot" tool for matlab.[42] The principal component analysis (PCA) was performed on the time-of-flight data using the Matlab statistics toolbox with the "pca" command. Therefore, only PAH relevant data from REMPI were considered.

Results and discussion

Mass spectrometric pattern from different ship fuels

Fig. 1 shows the sum mass spectra of particles from engine operation with the different fuels during 60 kW (80%) load. The particle composition derived from LDI (black) reveals carbon clusters from soot as the dominant component of diesel exhaust particles (DEP), organic fragments and signals from lube oil constituents, *i.e.* calcium and phosphate.[43–46] The heavy fuel oils (Fig. 1(c) and (d)) produce the typical marker metals vanadium, iron and nickel. However, they appear relatively low due to the very strong Na^+ signal that dominates the normalized spectrum. The MGO and HVO emissions also reveal signals from these metals, however, with much lower peak intensities. They can originate from carry-over effects, *e.g. via* lube oil, and from redispersed particles from the inner surfaces of the manifold and exhaust.[44,45] Note that iron is resonantly ionized in our instrument, leading to substantial signal enhancements of the Fe^+ signal,[37,47] but also increased Ni^+ and V^+ peaks.[31] Due to their high sulfur content, heavy fuel oils show stronger sulfate signals compared to MGO and HVO. The difference for $^{97}HSO_4^-$ between the HFO fuels is only moderate due to signal saturation in the SPMS but it is noticeable for $^{80}SO_3^-$. Compared to MGO and HVO, the stronger alkali metal signals (Na^+ and K^+) are also noteworthy. For MGO, the inorganic particle composition from LDI resembles the results from previous studies on heavy-duty vehicles without exhaust filters.[45] For the heavy fuel oils, similar compositions have been reported in laboratory-based and field studies on ship emissions.[29–31,48,49]

The corresponding average PAH mass spectra from REMPI are shown in red in Fig. 1. For all fuels except HVO, these PAH signatures are dominated by series in m/z sequences of 14 Da starting at $m/z = 178$. The peak at $m/z = 178$ more likely stems from phenanthrene than from anthracene because the latter is predominantly formed in the combustion process[50] and associated with fewer alkylated derivatives, whereas alkylated phenanthrenes in the emissions are typical residues of unburned fuel.[35,36,39,51] For MGO, $m/z = 178$ is the dominant peak and the signals decrease with increasing degree of alkylation. This pattern has been described in detail in our previous study.[36] About 50% of the characterized particles from MGO combustion reveal clear PAH signals in their REMPI spectra.

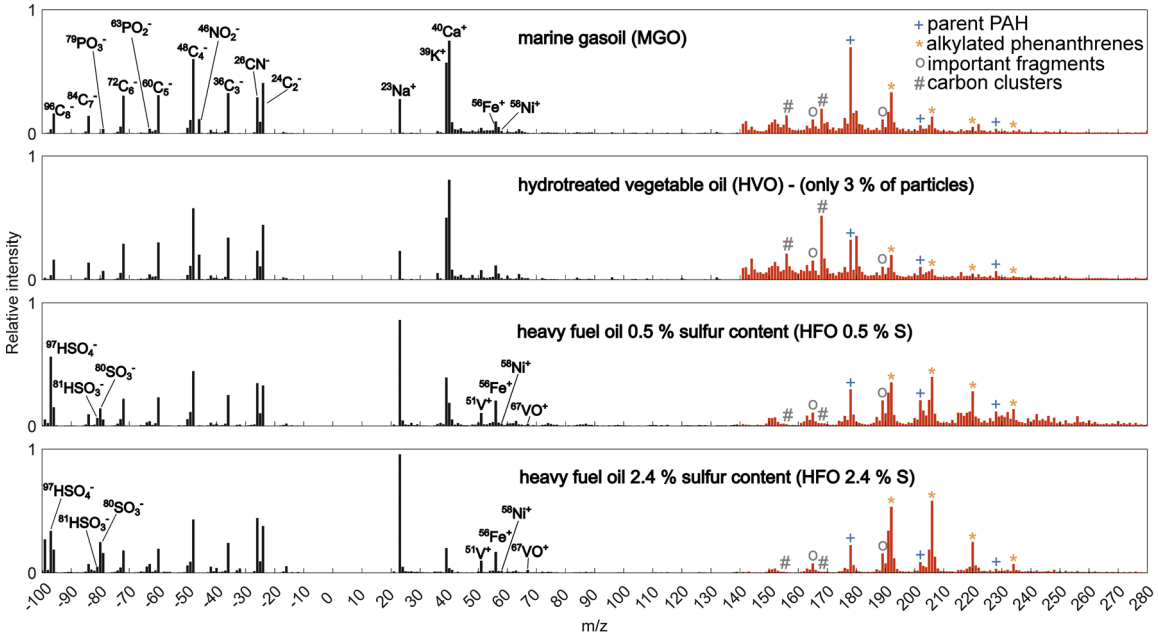

Fig. 1 Sum mass spectra ($n = 10\,000$) from laser desorption/ionization (LDI, black) and resonance-enhanced multiphoton ionization (REMPI, red) of particles from four marine fuels (75% engine load). The inorganic particle composition from the residual fuels exhibits the well-known signals of transition metals and sulfur. The PAH signals from MGO and HVO combustion show comparable pattern, while the total PAH signals for HVO are much smaller (balanced by normalization in the figure, see Fig. S1† for a comparison without normalization). For the HFO fuels, PAHs of higher mass are more pronounced and a higher degree of alkylation is observed, resulting in a shift of the maximum towards the C_2-phenanthrenes. The respective mass spectra for 25% engine load are shown in Fig. S2†.

This value is comparable to the method's hit rate for PAHs[37] indicating that most particles contain PAHs, which is reasonable due to uniform condensation of semi-volatile organics on the particles in the exhaust. For the HVO combustion, the signal strength of PAHs and the fraction of PAH-containing particles is much smaller, with only 3% of particles showing a PAH signal well above the noise level. The signature of this small fraction of particles is comparable to that of the MGO particles (Fig. 1(b)), indicating that these signals result probably from resuspended particles from the exhaust rather than from the HVO combustion or fuel residues. This assumption is supported by fuel sample analyses, where PAHs in HVO were below the limits of detection, see Fig. S3.† Due to the HVO particle's low PAH content, high-mass carbon clusters are more pronounced in the normalized mass spectrum in Fig. 1(b). Similar to the MGO emissions, the particles from HFO combustion are characterized by a dominant series of alkylated phenanthrenes, however, the series extends to larger masses and its maximum is shifted to the C_2-phenanthrenes, resulting in a remarkably different pattern. There are also variations among the HFO fuels, *i.e.* stronger contributions from parent PAHs and high mass species for the low-sulfur HFO. However, compared to MGO, both HFO fuels share the distinct shift of the maximum towards the C_2-phenanthrenes.

The homogeneity of PAH signatures over the particle ensemble

For their use as a marker, it is crucial for the PAH signature to be stable across all emitted particles from one fuel. Although the inorganic composition of individual particles in engine emissions can vary significantly,[44,45] PAHs in ship emission particles from MGO combustion have already shown a higher degree of similarity.[36] Fig. 2 illustrates the distribution of congruence coefficients (r_c) as a measure of the similarity between the individual mass spectra. For each fuel, the congruence coefficient has been calculated for 5000 particles according to

$$r_c = \frac{\sum_{i,j} x_{i,j}^2 y_{i,j}^2}{\sqrt{\left(\sum_{i,j} x_{i,j}^2\right)\left(\sum_{i,j} y_{i,j}^2\right)}}$$

with x and y representing the single particle mass spectra. The median r_c value from REMPI signals represents the PAHs and is higher than the r_c from LDI signals that reveal the particle's inorganic composition, as evident from the violin plots in Fig. 2. For a direct comparison between the r_c values of all LDI and REMPI data at different engine loadings see Fig. S5 and S6.† Furthermore, the distribution of REMPI signals is notably denser for all fuels when compared to the signals in the LDI spectra and the interquartile range is small, demonstrating a high level of similarity for the PAH signatures. This supports the marker characteristics of PAHs in particle emissions from marine fuels.

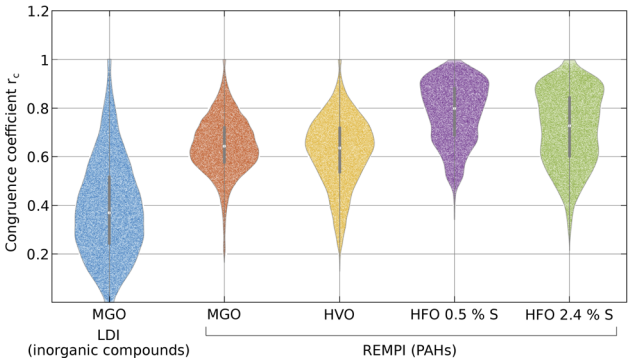

Fig. 2 Distribution of the congruence coefficients r_c between single-particle mass spectra of four different shipping fuels. The violin plot of r_c from the inorganic particle composition (LDI) of MGO particles reflects the heterogeneity of different particle types. In contrast, the REMPI signatures (mainly from PAHs) of the same particles from MGO combustion are more homogeneous. Also, for HVO, HFO with 0.5% sulfur, and HFO with 2.4% sulfur, the respective PAH patterns show a high homogeneity, which is a prerequisite for their use as a ship fuel marker. The width illustrates the number of particles in a bin. The interquartile range (n = 5000) that represents half of the particles is shown as a grey bar with its median in white.

Effect of the particle size

In addition to information on the particle composition, SPMS provides the individual particle size in vacuum aerodynamic diameter. The overall detection efficiency of the SPMS decreases rapidly for particles smaller than 200 nm, mainly due to the Mie scattering limit, which is strongly dependent on the wavelength of the continuous wave lasers in the optical sizing system.[52] To address this inherent bias of SPMS towards the largest size modes of combustion particles, we conducted additional measurements in the so-called 'free-running mode'. Ultrafine particles can be measured using this mode, which deactivates the optical detection and sizing unit while increasing the repetition rate of the desorption-and ionization lasers to 100 Hz in our experiment. The size limit for measured particles is reduced to approximately 50 nm at the expense of lost size information.[53,54] Fig. 3 illustrates the particle composition for different particle sizes. The averaged mass spectra of each 5000 particles are compared for both the free-running mode (including ultrafine particles, blue shaded) and the standard sizing mode ($\gtrsim$150 nm, red shaded). The respective particle size distributions were measured with a scanning mobility particle sizer (SMPS). For MGO and HVO, the measurements in free-running mode include the maximum of the size distribution and soot signatures are slightly increased relative to the larger particles measured in the sizing mode. Mass spectra obtained in the sizing mode show a phosphate signal that is 2 to 4 times more intense, an indication of a larger contribution from the lube oil. The particle size distributions of the heavy fuel oils are dominated by sulfate and soot particles,[55] which are too small to produce mass spectra in the instrument. Therefore, carbon clusters are not enhanced in the free-running mode. Consistent with our previous study,[36] the PAH patterns are not substantially affected by the particle size and retain their fuel-dependent signatures due to the uniform condensation of PAHs on the particles during cooling in the exhaust pipe. The size distribution data for each fuel under different load conditions can be found in the ESI in Fig. S4.†

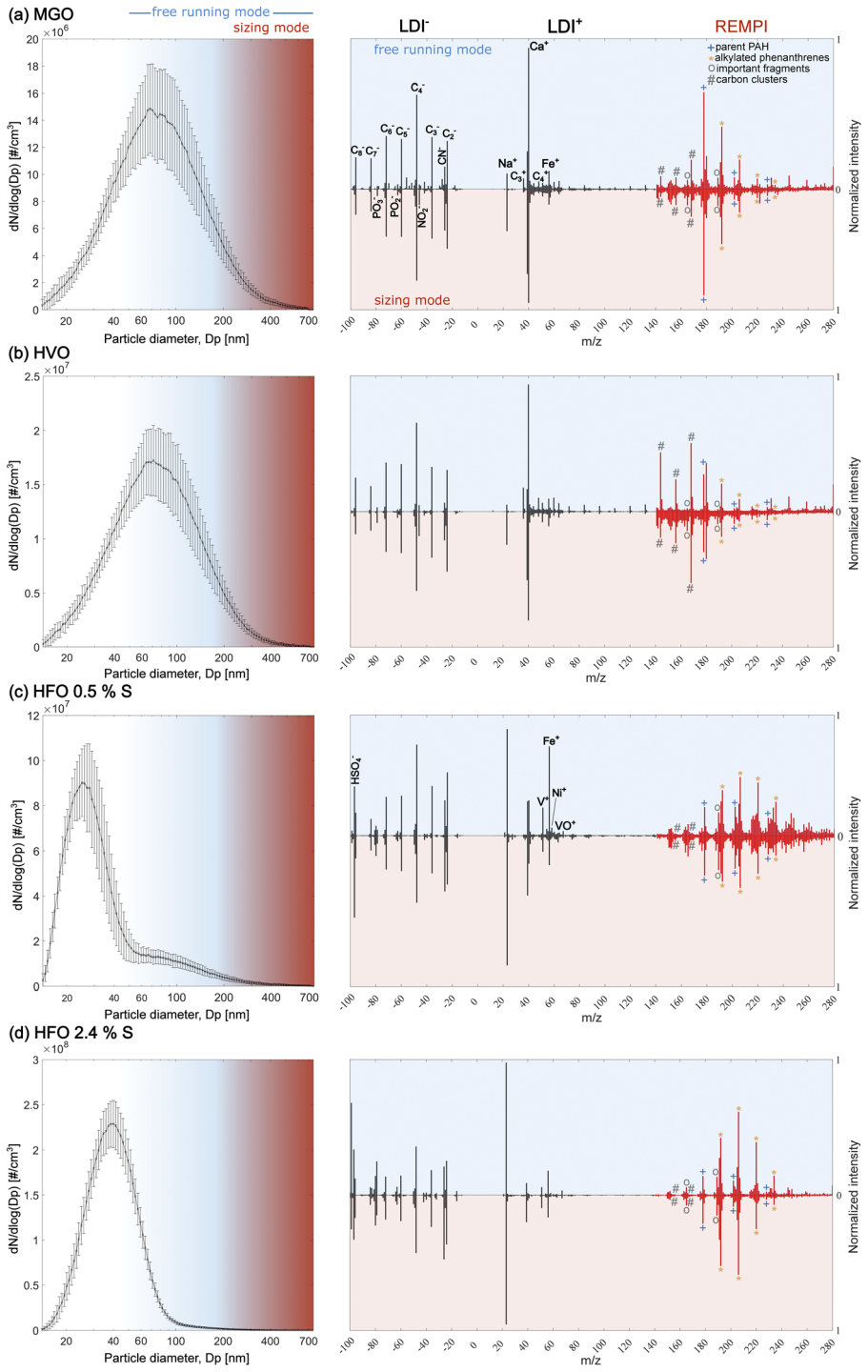

Fig. 3 (Left) Size distributions of (a) MGO, (b) HVO, (c) HFO 0.5% S, (d) HFO 2.4% S, measured using the scanning mobility particle sizer. The particle detection range of the single-particle mass spectrometer in free running mode is indicated by the blue shaded area. In this mode, particles of all sizes are hit at random and size information is not available. The red area indicates the coverage in normal sizing mode. The right side shows the normalized sum spectra of each 5000 particles, respectively, in both the free-running mode (blue shaded) and sizing mode (red shaded). The free-running mode includes smaller particles and reveals more pronounced contributions from soot (see MGO and HVO) while the sizing mode covers only large particles ($\gtrsim$150 nm) and exhibits 2–4 times stronger phosphate signals from lube oil. The PAH mass spectra are hardly affected by the particle size and reveal their distinct patterns for each individual fuel.

Fuel-specific characteristics of PAH signatures

To investigate a measure of fuel differentiation and the influence of load conditions, a principal component analysis (PCA) was performed on the PAH mass spectra of the particles from all fuels at two different engine loads. As an exploratory analysis, the first two principal components were considered, covering

57% of the total variance. The biplot (Fig. 4) illustrates the relation between the factors "fuel" and "load" from PC scores and provide information on the variables responsible for grouping from the PC loadings. A separation along the first PC into HFO and the fuels MGO and HVO can be noticed. HFO contains longer alkylated alkyl chains in the homologue series of phenanthrene, which is the driver of the fuel separation because unburned fuel is the main contributor to aromatic compounds in particulate emissions. Peaks of C_2- to-C_4-alkylated phenanthrenes appear at m/z = 206, 220 and 234, while the peak at m/z = 189 denotes a common fragment of angled PAH with larger degrees of alkylation.[56,57] Except for MGO and HVO, the variances within the two fuel types, highlighted by the 95% confident ellipses, were apparently lower than between them, thus supporting the use of this signature for ship fuel identification. Note that the HVO in this study only serves as the "cleanest" possible hydrocarbon fuel. Engine operation at lower loads causes emissions with a higher contribution of unburned fuel than higher loads. In the PCA biplot, the effect of engine load appears in the vertical direction on the second PC for all fuels, although minor in the case of HVO. Emissions at higher engine loads contain more aromatics from high-temperature pyrosynthesis inside the combustion chamber, such as by the hydrogen-abstraction carbon-addition (HACA) mechanism.[58] Variables pulling in the positive direction of PC2 are m/z = 178 and m/z = 192, *i.e.* phenanthrenes of no or low degree of alkylation, indicating pyrosynthesis and a lower contribution of unburned fuel. Conversely, alkylated phenanthrenes at m/z = 206, 220 and 234 show contributions in the negative direction of PC2, thus towards low engine loads. Nevertheless, variances added by the actor "load" are lower than for the factor "fuel", hence the fuel type has a stronger effect on the mass spectral signatures in the particle ensemble, emphasizing the identification of the used ship fuel by our SPMS approach.

Potential and limitations for the PAHs as fuel markers in SPMS

Our study shows that many of the conditions are in place for the use of single-particle PAH signatures as a future marine fuel marker. In particular, the characteristic PAH pattern unique to the fuel is evident for most particles and is consistent with particle size and engine load. The HVO emissions are difficult to identify due to the low number of particles with PAHs and the similarity to the MGO pattern, but the relevance of HVO for the future shipping industry is questionable.[59,60] The inorganic particle composition remains detectable with our SPMS-method. In a screening approach it can further help to distinguish between *e.g.* high sulfur and low sulfur blends or between metal-containing residual fuels and distillates, which are often named "hybrid" fuels. Higher confidence in identification may be achieved with our complementary PAH analysis. One aspect that is difficult to investigate is the effect of engine type and engine size. However, as fuel residues are a major determinant of the PAH signal, the inevitable emission of unburnt fuel will contribute to signal consistency between different ships. In a previous study, we discussed potential interferences between MGO combustion and terrestrial emissions and concluded that,

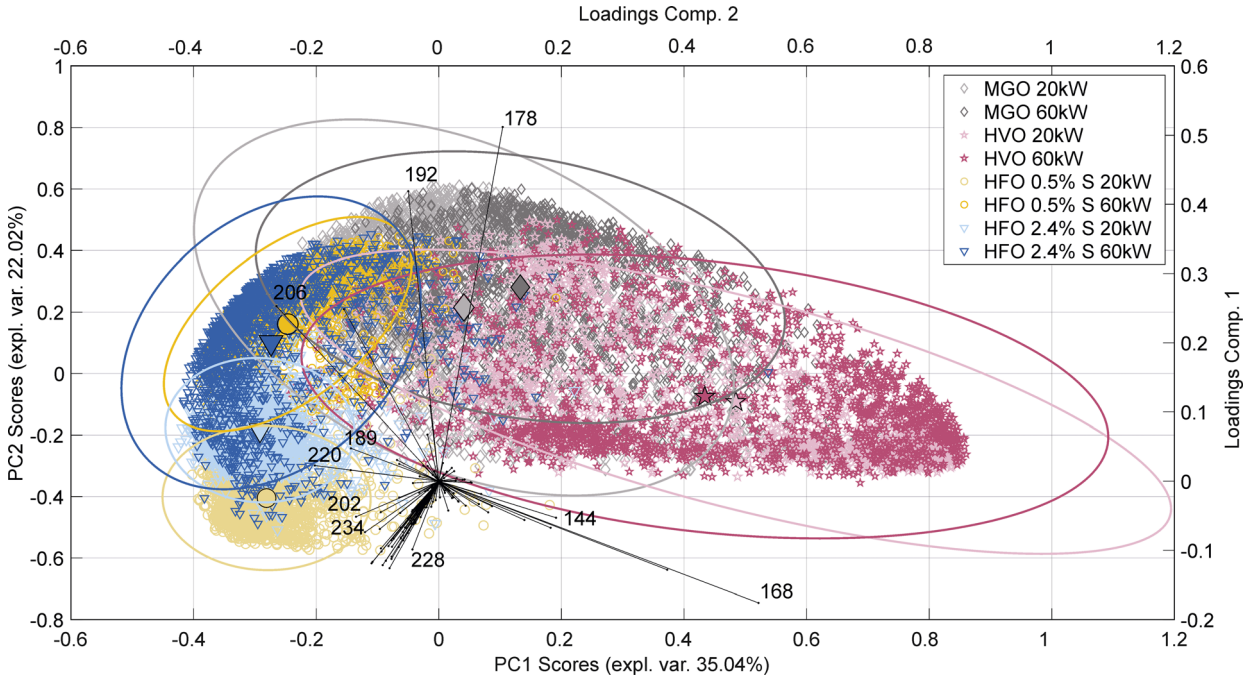

Fig. 4 Principal component analysis of single-particle PAH mass spectra from marine gasoil (grey), hydrotreated vegetable oil (red), heavy fuel oil 0.5% sulfur (blue) and heavy fuel oil 2.4% sulfur (yellow) at 20 kW load and 60 kW load, respectively. The length of the eigenvectors represents the contribution of signals at different mass-to-charge ratios to the mass spectral differences. The ellipses depict the 95% confidence interval for the principal component scores of each cluster. While the clusters are well separated for the low load conditions (light colors), the mass spectral signatures approach each other at higher load (dark colors), but remain distinguishable. N = 1670 for each of the fuels and loads.

due to the widespread use of filter technologies, only a few land-based sources with comparable PAH emission patterns remain, namely diesel engines without exhaust filters, *e.g.* at power generators, construction machines, and old vehicles.[36] The same interferences can also be expected for the HFO emissions with their alkylated PAHs of higher masses. An important terrestrial PAH source is wood combustion. In comparison to ship emission particles, SPMS mass spectra from wood combustion show much stronger parent PAH signals (see *e.g.* ESI† in Anders *et al.* 2023 (ref. 36)). The series of alkylated phenanthrenes in the PAH spectra from HFO shows some similarities to emissions from the smouldering combustion of biomass material.[61] However, while the decomposition of resin acids in wood burning typically results in a (local) maximum of the phenanthrenes at $m/z = 234$,[62,63] the HFO produces a smooth distribution with its maximum at lower masses, see Fig. 1. Nevertheless, with the additional information about the particle's inorganic composition, a straightforward differentiation between the fossil residual fuel (strong sulfur and metal signals) and the biomass fuel (dominant potassium signal[64–66]) is possible. In a field study of PAHs in aerosols using the same method at the Swedish coast, we found no PAH signatures similar to the HFO pattern in >290 000 particles, of which >4000 had detailed PAH mass spectra.[38] Given the large distance to the SECA outer boundary (>1000 km) and the high fuel compliance within the Baltic SECA,[67] this may not be surprising, but it also indicates the absence of other sources with a similar PAH signature.

Another source of ambiguity is related to the degradation of PAHs. Substance-specific rates introduce an important limitation to the diagnostic ratio concept in source apportionment.[68,69] The degradation of PAHs may not be an important factor in the detection and monitoring of individual ship plumes, as the plumes disintegrate within minutes to a few hours.[70] For assessments of the contribution of shipping to background air pollution and for studies of long-range transport, PAH degradation may be a major limitation of the approach. However, PAHs have often been shown to persist in the atmosphere for much longer than suggested by laboratory experiments,[69] *e.g.* because of weather conditions and slower dark ageing[71] or due to shielding effects.[72,73]

Conclusion and outlook

Having introduced the concept of single-particle PAH pattern as a marker for ship emissions from distillate fuel combustion,[36] here we extend this approach to other relevant ship fuels. As unburnt fuel residues contribute significantly to the PAH signatures, the patterns retain their fuel-characteristic profiles under different conditions and are also expected to have a high degree of similarity between different marine engines. The basic field-applicability of the PAH marker approach could already be shown,[36] however, field studies should demonstrate the differentiability of the various fuels for a larger number of ship plumes. This is a challenging task due to fuel uniformity and high compliance rates in SECAs,[67] and it may require open-sea measurements outside the SECA to get data from a sufficient number of ships with different fuels.[74] However, previous research and this study demonstrate the potential of PAHs as fuel markers for ships in the area of source apportionment, where it is difficult to find a long-range method to ensure compliance in emission control areas.

Author contributions

L. A., J. S. and I.-E. R. performed the SPMS experiments. L. A. and H. C. analyzed the data. R. I. provided technical assistance. U. K. and T. G. analyzed the fuel samples. U. E., S. J., M. R. S. B. and J. B. performed the aerosol characterization experiments at the engine. U. E. and B. B. provided the research ship engine and operated it. T. S., B. B. and R. Z. developed and managed the project and raised funding. J. S., M. S., H. C., T. A. and R. Z. gave scientific discussions. J. P. conceived the study. L. A. and J. P. wrote the manuscript.

Conflicts of interest

There are no conflicts to declare.

Acknowledgements

This research has been supported by the German Federal Ministry for Economic Affairs and Climate Action (SAARUS project, grant no. 03SX483D), and by the Helmholtz Association (International Laboratory aeroHEALTH – Interlabs-0005). Funded by the Deutsche Forschungsgemeinschaft (DFG, German Research Foundation) – SFB 1477 "Light–Matter Interactions at Interfaces", project number 441234705.

References

1 J. Fuglestvedt, T. Berntsen, V. Eyring, I. Isaksen, D. S. Lee and R. Sausen, Shipping emissions: from cooling to warming of climate-and reducing impacts on health, *Environ. Sci. Technol.*, 2009, **43**, 9057–9062.
2 E. Ytreberg, S. Åström and E. Fridell, Valuating environmental impacts from ship emissions – The marine perspective, *J. Environ. Manage.*, 2021, **282**, 111958.
3 J. J. Corbett, J. J. Winebrake, E. H. Green, P. Kasibhatla, V. Eyring and A. Lauer, Mortality from ship emissions: a global assessment, *Environ. Sci. Technol.*, 2007, **41**, 8512–8518.
4 V. Eyring, J. J. Corbett, D. S. Lee and J. J. Winebrake, Brief summary of the impact of ship emissions on atmospheric composition, climate, and human health, 2024, **http://www.pa.op.dlr.de/~VeronikaEyring/Eyringetal_IMOBriefSummary_FINAL.pdf**, accessed 7 May.
5 N. Mueller, M. Westerby and M. Nieuwenhuijsen, Health impact assessments of shipping and port-sourced air pollution on a global scale: A scoping literature review, *Environ. Res.*, 2023, **216**, 114460.
6 C. Geels, M. Winther, C. Andersson, J.-P. Jalkanen, J. Brandt, L. M. Frohn, U. Im, W. Leung and J. H. Christensen, Projections of shipping emissions and the related impact

on air pollution and human health in the Nordic region, *Atmos. Chem. Phys.*, 2021, **21**, 12495–12519.
7 Facts about maritime shipping and its environmental impact, 2024, **https://www.umweltbundesamt.de/en/topics/water/seas/maritime-shipping#facts-about-maritime-shipping-and-its-environmental-impact**, accessed 9 February.
8 E. Commission, CE_Delft_7M92_Study_on_methods_and_considerations_for_the_determination_of_greenhouse_gas_Def, 2024, **https://cedelft.eu/wp-content/uploads/sites/2/2021/03/CE_Delft_7M92_Study_on_methods_and_considerations_for_the_determination_of_greenhouse_gas_Def.pdf**, accessed 9 February.
9 Ships face lower sulphur fuel requirements in emission control areas from 1 January 2015, 2024, **https://www.imo.org/en/MediaCentre/PressBriefings/Pages/44-ECA-sulphur.aspx**, accessed 9 February.
10 J. E. Jonson, M. Gauss, M. Schulz, J.-P. Jalkanen and H. Fagerli, Effects of global ship emissions on European air pollution levels, *Atmos. Chem. Phys.*, 2020, **20**, 11399–11422.
11 J. Antturi, O. Hänninen, J.-P. Jalkanen, L. Johansson, M. Prank, M. Sofiev and M. Ollikainen, Costs and benefits of low-sulphur fuel standard for Baltic Sea shipping, *J. Environ. Manage.*, 2016, **184**, 431–440.
12 T. Chu Van, J. Ramirez, T. Rainey, Z. Ristovski and R. J. Brown, Global impacts of recent IMO regulations on marine fuel oil refining processes and ship emissions, *Transp. Res. D: Transp. Environ.*, 2019, **70**, 123–134.
13 S. D. Seppälä, J. Kuula, A.-P. Hyvärinen, S. Saarikoski, T. Rönkkö, J. Keskinen, J.-P. Jalkanen and H. Timonen, Effects of marine fuel sulfur restrictions on particle number concentrations and size distributions in ship plumes in the Baltic Sea, *Atmos. Chem. Phys.*, 2021, **21**, 3215–3234.
14 S. Oeder, T. Kanashova, O. Sippula, S. C. Sapcariu, T. Streibel, J. M. Arteaga-Salas, J. Passig, M. Dilger, H.-R. Paur, C. Schlager, S. Mülhopt, S. Diabaté, C. Weiss, B. Stengel, R. Rabe, H. Harndorf, T. Torvela, J. K. Jokiniemi, M.-R. Hirvonen, C. Schmidt-Weber, C. Traidl-Hoffmann, K. A. BéruBé, A. J. Wlodarczyk, Z. Prytherch, B. Michalke, T. Krebs, A. S. H. Prévôt, M. Kelbg, J. Tiggesbäumker, E. Karg, G. Jakobi, S. Scholtes, J. Schnelle-Kreis, J. Lintelmann, G. Matuschek, M. Sklorz, S. Klingbeil, J. Orasche, P. Richthammer, L. Müller, M. Elsasser, A. Reda, T. Gröger, B. Weggler, T. Schwemer, H. Czech, C. P. Rüger, G. Abbaszade, C. Radischat, K. Hiller, J. T. M. Buters, G. Dittmar and R. Zimmermann, Particulate matter from both heavy fuel oil and diesel fuel shipping emissions show strong biological effects on human lung cells at realistic and comparable in vitro exposure conditions, *PLoS One*, 2015, **10**, e0126536.
15 N. Rajput and A. Lakhani, PAHs and their Carcinogenic Potencies in Diesel Fuel and Diesel Generator Exhaust, *Hum. Ecol. Risk Assess.*, 2009, **15**, 201–213.
16 S. Zhou, J. Zhou and Y. Zhu, Chemical composition and size distribution of particulate matters from marine diesel engines with different fuel oils, *Fuel*, 2019, **235**, 972–983.
17 L. Benbrahim-Tallaa, R. A. Baan, Y. Grosse, B. Lauby-Secretan, F. El Ghissassi, V. Bouvard, N. Guha, D. Loomis and K. Straif, Carcinogenicity of diesel-engine and gasoline-engine exhausts and some nitroarenes, *Lancet Oncol.*, 2012, **13**, 663–664.
18 D. Wu, Q. Li, X. Ding, J. Sun, D. Li, H. Fu, M. Teich, X. Ye and J. Chen, Primary Particulate Matter Emitted from Heavy Fuel and Diesel Oil Combustion in a Typical Container Ship: Characteristics and Toxicity, *Environ. Sci. Technol.*, 2018, **52**, 12943–12951.
19 L. Osipova, E. Georgeff and B. Comer, Global scrubber washwater discharges under IMO's 2020 fuel sulfur limit, 2024, **https://theicct.org/wp-content/uploads/2021/06/scrubber-discharges-Apr2021.pdf**, accessed 9 January.
20 J. E. Jonson, M. Gauss, J.-P. Jalkanen and L. Johansson, Effects of strengthening the Baltic Sea ECA regulations, *Atmos. Chem. Phys.*, 2019, **19**, 13469–13487.
21 M. Viana, V. Rizza, A. Tobías, E. Carr, J. Corbett, M. Sofiev, A. Karanasiou, G. Buonanno and N. Fann, Estimated health impacts from maritime transport in the Mediterranean region and benefits from the use of cleaner fuels, *Environ. Int.*, 2020, **138**, 105670.
22 V. Zisi, H. N. Psaraftis and T. Zis, The impact of the 2020 global sulfur cap on maritime CO2 emissions, *Marit. Bus. Rev.*, 2021, **6**, 339–357.
23 A. Lunde Hermansson, I.-M. Hassellöv, J. Moldanová and E. Ytreberg, Comparing emissions of polyaromatic hydrocarbons and metals from marine fuels and scrubbers, *Transp. Res. D: Transp. Environ.*, 2021, **97**, 102912.
24 H. Winnes, E. Fridell and J. Moldanová, Effects of Marine Exhaust Gas Scrubbers on Gas and Particle Emissions, *J. Manuf. Sci. Eng.*, 2020, **8**, 299.
25 S. Ushakov and N. Lefebvre, Assessment of Hydrotreated Vegetable Oil (HVO) Applicability as an Alternative Marine Fuel Based on Its Performance and Emissions Characteristics, *SAE Int. J. Fuels Lubr.*, 2019, **12**(2), 109–120.
26 T. Solakivi, A. Paimander and L. Ojala, Cost competitiveness of alternative maritime fuels in the new regulatory framework, *Transp. Res. D: Transp. Environ.*, 2022, **113**, 103500.
27 Rotterdam Bunker Prices, 2024, **https://shipandbunker.com/prices/emea/nwe/nl-rtm-rotterdam#ULSFO**, accessed 9 February.
28 H. Czech, J. Schnelle-Kreis, T. Streibel and R. Zimmermann, New directions: Beyond sulphur, vanadium and nickel – About source apportionment of ship emissions in emission control areas, *Atmos. Environ.*, 2017, **163**, 190–191.
29 R. M. Healy, I. P. O'Connor, S. Hellebust, A. Allanic, J. R. Sodeau and J. C. Wenger, Characterisation of single particles from in-port ship emissions, *Atmos. Environ.*, 2009, **43**, 6408–6414.
30 A. P. Ault, C. I. Gaston, Y. Wang, G. Dominguez, M. H. Thiemens and K. A. Prather, Characterization of the single particle mixing state of individual ship plume events

measured at the Port of Los Angeles, *Environ. Sci. Technol.*, 2010, **44**, 1954–1961.

31 J. Passig, J. Schade, R. Irsig, L. Li, X. Li, Z. Zhou, T. Adam and R. Zimmermann, Detection of ship plumes from residual fuel operation in emission control areas using single-particle mass spectrometry, *Atmos. Meas. Tech.*, 2021, **14**, 4171–4185.

32 J. Zhao, Y. Zhang, H. Xu, S. Tao, R. Wang, Q. Yu, Y. Chen, Z. Zou and W. Ma, Trace Elements From Ocean-Going Vessels in East Asia: Vanadium and Nickel Emissions and Their Impacts on Air Quality, *J. Geophys. Res.: Atmos.*, 2021, **126**(8), DOI: **10.1029/2020JD033984**.

33 X. Xiong, Z. Wang, C. Cheng, M. Li, L. Yun, S. Liu, L. Mao and Z. Zhou, Long-Term Observation of Mixing States and Sources of Vanadium-Containing Single Particles from 2020 to 2021 in Guangzhou, China, *Toxics*, 2023, **11**(4), 339.

34 E. I. Rosewig, J. Schade, J. Passig, H. Osterholz, R. Irsig, D. Smok, N. Gawlitta, J. Schnelle-Kreis, J. Hovorka, D. Schulz-Bull, R. Zimmermann and T. W. Adam, Remote Detection of Different Marine Fuels in Exhaust Plumes by Onboard Measurements in the Baltic Sea Using Single-Particle Mass Spectrometry, *Atmosphere*, 2023, **14**, 849.

35 H. Czech, B. Stengel, T. Adam, M. Sklorz, T. Streibel and R. Zimmermann, A chemometric investigation of aromatic emission profiles from a marine engine in comparison with residential wood combustion and road traffic: Implications for source apportionment inside and outside sulphur emission control areas, *Atmos. Environ.*, 2017, **167**, 212–222.

36 L. Anders, J. Schade, E. I. Rosewig, T. Kröger-Badge, R. Irsig, S. Jeong, J. Bendl, M. R. Saraji-Bozorgzad, J.-H. Huang, F.-Y. Zhang, C. C. Wang, T. Adam, M. Sklorz, U. Etzien, B. Buchholz, H. Czech, T. Streibel, J. Passig and R. Zimmermann, Detection of ship emissions from distillate fuel operation via single-particle profiling of polycyclic aromatic hydrocarbons, *Environ. Sci.: Atmos.*, 2023, **3**, 1134–1144.

37 J. Schade, J. Passig, R. Irsig, S. Ehlert, M. Sklorz, T. Adam, C. Li, Y. Rudich and R. Zimmermann, Spatially Shaped Laser Pulses for the Simultaneous Detection of Polycyclic Aromatic Hydrocarbons as well as Positive and Negative Inorganic Ions in Single Particle Mass Spectrometry, *Anal. Chem.*, 2019, **91**, 10282–10288.

38 J. Passig, J. Schade, R. Irsig, T. Kröger-Badge, H. Czech, T. Adam, H. Fallgren, J. Moldanova, M. Sklorz, T. Streibel and R. Zimmermann, Single-particle characterization of polycyclic aromatic hydrocarbons in background air in northern Europe, *Atmos. Chem. Phys.*, 2022, **22**, 1495–1514.

39 T. Streibel, J. Schnelle-Kreis, H. Czech, H. Harndorf, G. Jakobi, J. Jokiniemi, E. Karg, J. Lintelmann, G. Matuschek, B. Michalke, L. Müller, J. Orasche, J. Passig, C. Radischat, R. Rabe, A. Reda, C. Rüger, T. Schwemer, O. Sippula, B. Stengel, M. Sklorz, T. Torvela, B. Weggler and R. Zimmermann, Aerosol emissions of a ship diesel engine operated with diesel fuel or heavy fuel oil, *Environ. Sci. Pollut. Res. Int.*, 2017, **24**, 10976–10991.

40 S. Jeong, J. Bendl, M. Saraji-Bozorgzad, U. Käfer, U. Etzien, J. Schade, M. Bauer, G. Jakobi, J. Orasche, K. Fisch, P. P. Cwierz, C. P. Rüger, H. Czech, E. Karg, G. Heyen, M. Krausnick, A. Geissler, C. Geipel, T. Streibel, J. Schnelle-Kreis, M. Sklorz, D. E. Schulz-Bull, B. Buchholz, T. Adam and R. Zimmermann, Aerosol emissions from a marine diesel engine running on different fuels and effects of exhaust gas cleaning measures, *Environ. Pollut.*, 2023, **316**, 120526.

41 C. Gehm, T. Streibel, J. Passig and R. Zimmermann, Determination of Relative Ionization Cross Sections for Resonance Enhanced Multiphoton Ionization of Polycyclic Aromatic Hydrocarbons, *Appl. Sci.*, 2018, **8**(9), 1617.

42 H. Hoffmann, *Violin Plot. MATLAB Central File Exchange*, 2024, **https://de.mathworks.com/matlabcentral/fileexchange/45134-violin-plot**, accessed 7 May.

43 D. A. Sodeman, S. M. Toner and K. A. Prather, Determination of single particle mass spectral signatures from light-duty vehicle emissions, *Environ. Sci. Technol.*, 2005, **39**, 4569–4580.

44 S. M. Toner, D. A. Sodeman and K. A. Prather, Single particle characterization of ultrafine and accumulation mode particles from heavy duty diesel vehicles using aerosol time-of-flight mass spectrometry, *Environ. Sci. Technol.*, 2006, **40**, 3912–3921.

45 L. G. Shields, D. T. Suess and K. A. Prather, Determination of single particle mass spectral signatures from heavy-duty diesel vehicle emissions for PM2.5 source apportionment, *Atmos. Environ.*, 2007, **41**, 3841–3852.

46 M. T. Spencer, L. G. Shields, D. A. Sodeman, S. M. Toner and K. A. Prather, Comparison of oil and fuel particle chemical signatures with particle emissions from heavy and light duty vehicles, *Atmos. Environ.*, 2006, **40**, 5224–5235.

47 J. Passig, J. Schade, E. I. Rosewig, R. Irsig, T. Kröger-Badge, H. Czech, M. Sklorz, T. Streibel, L. Li, X. Li, Z. Zhou, H. Fallgren, J. Moldanova and R. Zimmermann, Resonance-enhanced detection of metals in aerosols using single-particle mass spectrometry, *Atmos. Chem. Phys.*, 2020, **20**, 7139–7152.

48 Z. Liu, X. Lu, J. Feng, Q. Fan, Y. Zhang and X. Yang, Influence of Ship Emissions on Urban Air Quality: A Comprehensive Study Using Highly Time-Resolved Online Measurements and Numerical Simulation in Shanghai, *Environ. Sci. Technol.*, 2017, **51**, 202–211.

49 L. Zhou, M. Li, C. Cheng, Z. Zhou, H. Nian, R. Tang and C. K. Chan, Real-time chemical characterization of single ambient particles at a port city in Chinese domestic emission control area - Impacts of ship emissions on urban air quality, *Sci. Total Environ.*, 2022, **819**, 153117.

50 J. T. Andersson and C. Achten, Time to Say Goodbye to the 16 EPA PAHs? Toward an Up-to-Date Use of PACs for Environmental Purposes, *Polycycl. Aromat. Comp.*, 2015, **35**, 330–354.

51 C. Radischat, O. Sippula, B. Stengel, S. Klingbeil, M. Sklorz, R. Rabe, T. Streibel, H. Harndorf and R. Zimmermann, Real-time analysis of organic compounds in ship engine aerosol emissions using resonance-enhanced multiphoton ionisation and proton transfer mass spectrometry, *Anal. Bioanal. Chem.*, 2015, **407**, 5939–5951.

52 G. S. He, H.-Y. Qin and Q. Zheng, Rayleigh, Mie, and Tyndall scatterings of polystyrene microspheres in water: Wavelength, size, and angle dependences, *J. Appl. Phys.*, 2009, **105**, 023110.
53 Y. Su, M. F. Sipin, H. Furutani and K. A. Prather, Development and characterization of an aerosol time-of-flight mass spectrometer with increased detection efficiency, *Anal. Chem.*, 2004, **76**, 712–719.
54 W. D. Reents and Z. Ge, Simultaneous Elemental Composition and Size Distributions of Submicron Particles in Real Time Using Laser Atomization/Ionization Mass Spectrometry, *Aerosol Sci. Technol.*, 2010, **33**, 122–134.
55 Q. Xiao, M. Li, H. Liu, M. Fu, F. Deng, Z. Lv, H. Man, X. Jin, S. Liu and K. He, Characteristics of marine shipping emissions at berth: profiles for particulate matter and volatile organic compounds, *Atmos. Chem. Phys.*, 2018, **18**, 9527–9545.
56 Y. Zhao, B. Hong, Y. Fan, M. Wen and X. Han, Accurate analysis of polycyclic aromatic hydrocarbons (PAHs) and alkylated PAHs homologs in crude oil for improving the gas chromatography/mass spectrometry performance, *Ecotoxicol. Environ. Saf.*, 2014, **100**, 242–250.
57 C. Kruth, H. Czech, M. Sklorz, J. Passig, S. Ehlert, A. Cappiello and R. Zimmermann, Direct Infusion Resonance-Enhanced Multiphoton Ionization Mass Spectrometry of Liquid Samples under Vacuum Conditions, *Anal. Chem.*, 2017, **89**, 10917–10923.
58 M. Frenklach, Reaction mechanism of soot formation in flames, *Phys. Chem. Chem. Phys.*, 2002, **4**, 2028–2037.
59 R. McGill, W. Remley and K. Winther, Alternative Fuels for Marine Applications, 2024, **https://www.methanol.org/wp-content/uploads/2016/07/AMF_Annex_41-Alt-Fuels-for-Marine-May-2013.pdf**, accessed 10 January.
60 M. Aarnio, *Cruise Ship Handbook*, Springer International Publishing; Imprint Springer, Cham, 1st edn, 2023.
61 C. Li, Q. He, J. Schade, J. Passig, R. Zimmermann, D. Meidan, A. Laskin and Y. Rudich, Dynamic changes in optical and chemical properties of tar ball aerosols by atmospheric photochemical aging, *Atmos. Chem. Phys.*, 2019, **19**, 139–163.
62 P. Martens, H. Czech, J. Orasche, G. Abbaszade, M. Sklorz, B. Michalke, J. Tissari, T. Bizjak, M. Ihalainen, H. Suhonen, P. Yli-Pirilä, J. Jokiniemi, O. Sippula and R. Zimmermann, Brown Coal and Logwood Combustion in a Modern Heating Appliance: The Impact of Combustion Quality and Fuel on Organic Aerosol Composition, *Environ. Sci. Technol.*, 2023, **57**, 5532–5543.
63 H. Czech, T. Miersch, J. Orasche, G. Abbaszade, O. Sippula, J. Tissari, B. Michalke, J. Schnelle-Kreis, T. Streibel, J. Jokiniemi and R. Zimmermann, Chemical composition and speciation of particulate organic matter from modern residential small-scale wood combustion appliances, *Sci. Total Environ.*, 2018, **612**, 636–648.
64 J. Arndt, J. Sciare, M. Mallet, G. C. Roberts, N. Marchand, K. Sartelet, K. Sellegri, F. Dulac, R. M. Healy and J. C. Wenger, Sources and mixing state of summertime background aerosol in the north-western Mediterranean basin, *Atmos. Chem. Phys.*, 2017, **17**, 6975–7001.
65 M. Dall'Osto, D. C. S. Beddows, E. J. McGillicuddy, J. K. Esser-Gietl, R. M. Harrison and J. C. Wenger, On the simultaneous deployment of two single-particle mass spectrometers at an urban background and a roadside site during SAPUSS, *Atmos. Chem. Phys.*, 2016, **16**, 9693–9710.
66 F. Köllner, J. Schneider, M. D. Willis, T. Klimach, F. Helleis, H. Bozem, D. Kunkel, P. Hoor, J. Burkart, W. R. Leaitch, A. A. Aliabadi, J. P. D. Abbatt, A. B. Herber and S. Borrmann, Particulate trimethylamine in the summertime Canadian high Arctic lower troposphere, *Atmos. Chem. Phys.*, 2017, **17**, 13747–13766.
67 A. Lähteenmäki-Uutela, J. Yliskylä-Peuralahti, S. Repka and J. Mellqvist, What explains SECA compliance: rational calculation or moral judgment?, *WMU J. Marit. Aff.*, 2019, **18**, 61–78.
68 M. Tobiszewski and J. Namieśnik, PAH diagnostic ratios for the identification of pollution emission sources, *Environ. Pollut.*, 2012, **162**, 110–119.
69 I. J. Keyte, R. M. Harrison and G. Lammel, Chemical reactivity and long-range transport potential of polycyclic aromatic hydrocarbons – a review, *Chem. Soc. Rev.*, 2013, **42**, 9333–9391.
70 A. Petzold, J. Hasselbach, P. Lauer, R. Baumann, K. Franke, C. Gurk, H. Schlager and E. Weingartner, Experimental studies on particle emissions from cruising ship, their characteristic properties, transformation and atmospheric lifetime in the marine boundary layer, *Atmos. Chem. Phys.*, 2008, **8**, 2387–2403.
71 U. Pöschl, T. Letzel, C. Schauer and R. Niessner, Interaction of Ozone and Water Vapor with Spark Discharge Soot Aerosol Particles Coated with Benzo[a]pyrene: O 3 and H 2 O Adsorption, Benzo[a]pyrene Degradation, and Atmospheric Implications, *J. Phys. Chem. A*, 2001, **105**, 4029–4041.
72 S. Zhou, A. K. Y. Lee, R. D. McWhinney and J. P. D. Abbatt, Burial effects of organic coatings on the heterogeneous reactivity of particle-borne benzoapyrene (BaP) toward ozone, *J. Phys. Chem. A*, 2012, **116**, 7050–7056.
73 M. Shrivastava, S. Lou, A. Zelenyuk, R. C. Easter, R. A. Corley, B. D. Thrall, P. J. Rasch, J. D. Fast, S. L. Massey Simonich, H. Shen and S. Tao, Global long-range transport and lung cancer risk from polycyclic aromatic hydrocarbons shielded by coatings of organic aerosol, *Proc. Natl. Acad. Sci. U. S. A.*, 2017, **114**, 1246–1251.
74 S. Celik, F. Drewnick, F. Fachinger, J. Brooks, E. Darbyshire, H. Coe, J.-D. Paris, P. G. Eger, J. Schuladen, I. Tadic, N. Friedrich, D. Dienhart, B. Hottmann, H. Fischer, J. N. Crowley, H. Harder and S. Borrmann, Influence of vessel characteristics and atmospheric processes on the gas and particle phase of ship emission plumes: in situ measurements in the Mediterranean Sea and around the Arabian Peninsula, *Atmos. Chem. Phys.*, 2020, **20**, 4713–4734.

Environmental Chemistry Letters
https://doi.org/10.1007/s10311-025-01830-x

ORIGINAL ARTICLE

Limited efficiency of wet scrubbers in reducing the environmental impact of ship-emitted particles

Lukas Anders[1,2] · Martin Bauer[1] · Seongho Jeong[3] · Marco Schmidt[1,2] · Haseeb Hakkim[1,2] · Aleksandrs Kalamašņikovs[1,2] · Ellen Iva Rosewig[1,2] · Julian Schade[3] · Robert Irsig[4] · Sven Ehlert[4] · Jan Bendl[3] · Mohammad Reza Saraji-Bozorgzad[1,3,4] · Barbara Giocastro[3] · Uwe Käfer[1,7] · Uwe Etzien[5] · Bert Buchholz[5] · Thomas Adam[3] · Martin Sklorz[1,2] · Thorsten Streibel[1,2] · Hendryk Czech[1,6] · Johannes Passig[1,2,6] · Ralf Zimmermann[1,2]

Received: 5 November 2024 / Accepted: 19 February 2025

Abstract

Sulfur dioxide pollution by ship emissions can be efficiently decreased by using exhaust gas scrubbers, yet particles can pass through the scrubber and be released into the atmosphere. Here, we studied the impact of using a wet scrubber on the composition of particle emissions, by single-particle analysis. At low engine loads, results show no significant changes in particle composition of metals, salts, and polycyclic aromatic hydrocarbons (PAH). At high engine loads, the scrubber reduced soot and PAH signatures about fourfold. Particles passing through the scrubber undergo minimal chemical changes, except for sulfate uptake. The cleaning effect of wet scrubbers is attributed to the removal of water-soluble gas-phase compounds, diffusion-dominated uptake of ultrafine particles, and wet deposition of coarse particles. The scrubber has little effect on reducing the health and environmental impacts of the remaining particles that pass through it. These emitted particles, primarily in the 60–200 nm size range, constitute a significant portion of the inhalable particle mass and have the potential for long-range transport.

Keywords Ship emissions · Air pollution · Scrubber · Polycyclic aromatic hydrocarbons · Exhaust cleaning · Inhalable particles

Introduction

The shipping industry is a major source of global air pollution [1, 31]. To mitigate its environmental and health impacts, the International Maritime Organization has introduced a global regulation, limiting the fuel sulfur content to a maximum of 0.5% (w/w). In Sulfur Emission Control Areas, such as the North Sea, Baltic Sea, and coastal waters along the U.S. coast, the limit is set at 0.1% (w/w). As an alternative to cleaner fuels, ships are permitted to use cheaper high-sulfur bunker fuels, provided that exhaust scrubbers are used to remove the SOx from emissions. Wet scrubbers can impact the environment when wash water is discharged during so-called open-loop operation [9, 32]. In addition to the efficient removal of SOx, which also reduces secondary sulfate aerosol formation, the air quality benefits include partial scrubbing of water-soluble organic gases, such as carbonyls, thereby reducing the ozone-forming potential of the emissions [7].

✉ Johannes Passig
johannes.passig@uni-rostock.de

1 Joint Mass Spectrometry Centre, Analytical Chemistry, University of Rostock, 18059 Rostock, Germany

2 Department Life, Light & Matter, University of Rostock, 18059 Rostock, Germany

3 Faculty for Mechanical Engineering, Institute of Chemistry and Environmental Engineering, University of the Bundeswehr Munich, 85577 Neubiberg, Germany

4 Photonion GmbH, 19061 Schwerin, Germany

5 Chair of Piston Machines and Internal Combustion Engines, University of Rostock, Rostock, Germany

6 Helmholtz Centre Munich, Comprehensive Molecular Analytics, 85764 Neuherberg, Germany

7 Present Address: Atmospheric Chemistry, Leibniz Institute for Tropospheric Research, Leipzig, Germany

Published online: 17 March 2025

The reduction in particulate emissions depends on fuel, engine, and scrubber parameters, and consequently, it varies in the literature [33, 35] with the majority of the studies indicating only little to moderate effects of the scrubber on particle number and mass emission factors [11, 13]. Changes in the particle size distribution are primarily linked to the diffusion-driven uptake of ultrafine particles, wet deposition of coarse particles, and variations in soot morphology [13, 15]. Additionally, new particle formation and particle growth through the conversion of SO_2 to sulfate play a significant role [14].

Although the chemical composition is a crucial factor in determining the particle's environmental and health impacts [23], the effect of scrubbers on this composition remains poorly studied. Possible scrubber-induced changes in the bulk chemical composition can result, e.g., from the size-selective removal of particles, but also from hygroscopic growth of particles with water-soluble components [14].

However, while data on the scrubber's effect on particulate matter bulk composition are already limited, even less is known at the single-particle level. It has been shown that the mixing state of particles significantly affects their environmental impact [25]. For example, the distribution of components across individual particles plays a role in determining the cloud condensation nuclei potential of the particle ensemble [26, 36]. In terms of biological effects, the concentration of pollutants on individual particles is important, as is the particle's acidity, which influences the bioavailability of transition metals [8].

In addition to changes in bulk composition caused by the scrubber, any alterations in the distribution of pollutants within the aerosol ensemble can impact the emissions' environmental effects, including long-range transport potential, cloud condensation behavior, and biological effects. In this study, we investigate the effect of a wet scrubber on the aerosol composition from a research ship engine at the single-particle level. The single-particle mass spectrometer is sensitive to particles larger than approximately 100 nm [19], which typically constitute the majority of the lung-deposited particle mass [12], also for ship emissions [18] and are capable of long-range transport [29]. Using recently developed technologies, the instrument detects key aerosol components relevant to environmental and health effects, including transition metals [20] and carcinogenic polycyclic aromatic hydrocarbons (PAHs) [2, 17, 27]. The single-particle mass spectra of PAHs can provide indications of the particle source, such as the dominant presence of alkylated phenanthrenes in ship emission particles [4]. In contrast to analyses of the aerosol's bulk composition, single-particle analysis is capable of revealing changes in the distribution of pollutants across the aerosol ensemble. This allows for a deeper understanding of the removal mechanisms in the scrubber and provides an estimate of the potential environmental and health effects of the remaining particles.

Experimental

A single-cylinder, four-stroke, 80-kW research ship engine with common rail injection was operated using heavy fuel oil with 2.4% (m/m) fuel sulfur content, and, for run-in and comparison, marine gas oil with 0.001% fuel sulfur content. With a large displacement of 3.18 L and the capability to run on all marine fuels, this engine is a well-established model for ship propulsion systems [30]. The two investigated loads of 60 kW (75%) and 20 kW (25%) are representative of cruising and maneuvering conditions, respectively. Measurements began after a 20-min stabilization phase to avoid instabilities in the emissions that often occur during the start-up and warm-up phases. A downscaled research wet scrubber (SAACKE, Germany) with a total wash tower volume of 0.9 m^3 was specifically designed and adapted for the 80-kW research ship engine. Due to facility constraints, only open-loop operation was possible. Consequently, Baltic Sea water with a salinity of 10.5 ± 3.6 practical salinity unit and a pH of approximately 8 was used. The aerosol was sampled at 200 °C before the scrubber and at 60 °C downstream the scrubber to avoid condensation, diluted by a factor of 1:100, dried (Model MD-700-12S-1, Perma Pure LLC, U.S.) and guided to the single-particle mass spectrometer. For engine, fuel, and sampling details, see [11] and [3]. In the single-particle mass spectrometer (PhotonLIZA, Photonion GmbH, Germany), individual particles are optically detected, sized and exposed to laser pulses for ion formation. The bipolar time-of-flight mass analyzer detects both anions and cations, providing a chemical profile for individual particles [19, 27]. The instrument utilizes a novel laser excitation scheme, addressing refractory and inorganic components via laser desorption/ionization (LDI) and PAHs via laser desorption/resonance-enhanced multiphoton ionization (LD/REMPI). For details, we refer to [27]. Single-particle mass spectrometry data do not provide exact mass concentration values but instead offers chemical insights at the single-particle level, which enables comparative experiments and identifies characteristic chemical patterns.

Results and discussion

Sum signals and mass spectral signatures

Figure 1 shows the sum mass spectra of each 2000 particles sampled before and after the scrubber for 20 kW load (Fig. 1a) and 60 kW load (Fig. 1c), respectively. The spectra from laser desorption/ionization (LDI, blue) reveal the

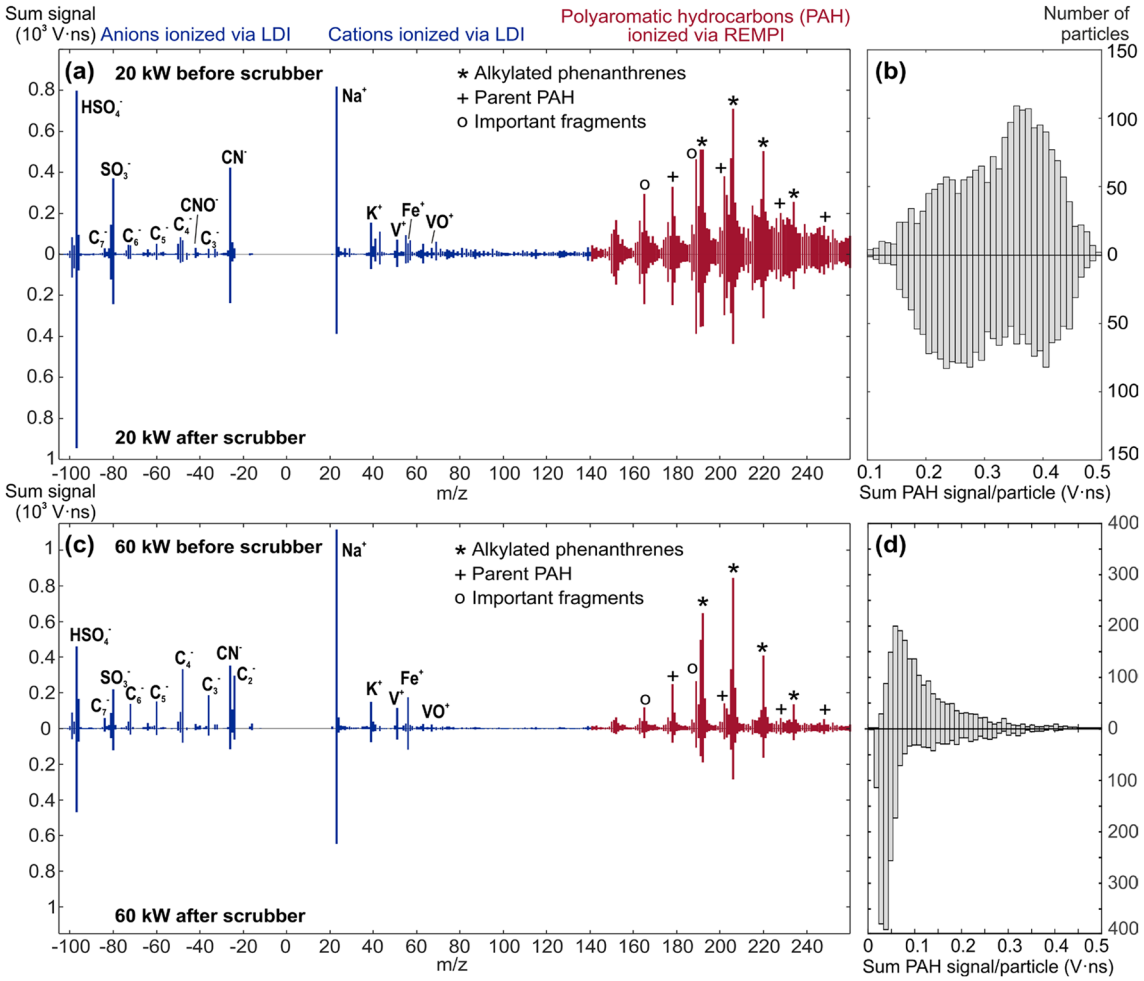

Fig. 1 **a** The summed mass spectra comparison for an equal number of particles (n = 2,000) from heavy fuel oil combustion, measured before (top) and after (bottom) the scrubber at low engine loads, shows no discernible changes in particle composition for either inorganics (ionized via laser desorption/ionization, LDI) or polycyclic aromatic hydrocarbons (PAHs, ionized via resonance-enhanced multiphoton ionization, REMPI). **b** Likewise, the single-particle distribution of total PAH signals remains unchanged after the scrubber. **c-d** At high engine load, the emissions are more soot-dominated. The scrubber reduces predominantly soot and PAH signals, however, without changing the PAH pattern

dominant particle components: sulfate, alkali metals, soot, organic carbon fragments and the typical ship emission markers vanadium and iron [5, 10, 16, 34]. The iron signal is enhanced by resonant laser desorption/ionization [20]. The PAH signatures obtained through LD/REMPI ionization (in red) can serve as an indicator of the particle source [22]. In ship emissions, PAHs primarily originate from unburnt fuel and can therefore be used as a fuel marker, independent of transition metals [3]. The PAH pattern in Fig. 1(a) and (c) is dominated by alkylated phenanthrenes, with its maximum at m/z = 206, which has been linked to heavy fuel oil emissions [4]. Comparing the mass spectra at 20 kW and 60 kW loads reveals stronger contributions of organic carbon and PAHs at 20 kW, while soot signatures are more prominent at 60 kW due to more complete combustion [14]. For comparison, the results for marine gas oil are presented in Supplementary Material (Fig. S1). Size distributions are shown in Fig. S2.

At a 20 kW load, the mass spectra before (Fig. 1(a), up) and after (Fig. 1(a), down) the scrubber are highly comparable. Since the same number of particles is analyzed before and after the scrubber, the mass spectra reveal changes in aerosol composition but not the reduction in particle number concentrations (25% at 20 kW and 38% at 60 kW load; for details, see [11]). Therefore, a slight signal reduction across the entire spectrum after the scrubber may be attributed to instrument performance. The HSO_4^- peak shows a small increase, but due to saturation effects in this mass channel, the SO_3^- signal serves as a more reliable indicator of sulfate content, and it is also reduced. The spectra show no signals of water-soluble organic acids, which can be detected in negative mode with single-particle mass spectrometers

in cases such as aged biomass burning aerosols [37]. The water-insoluble fraction of organic carbon can be assessed through the PAHs. The histogram on the right illustrates the PAH mixing state through the distribution of the summed PAH signals across the particles. Both the distribution and the PAH pattern remain nearly unaffected by the scrubber.

For the elemental carbon (soot)-dominated emissions at a 60 kW engine load (Fig. 1(c)), the scrubber has limited impact on the mass spectra, showing a marked reduction in soot signatures while sulfate signals persist. This aligns with aerosol bulk measurements from the same experiment, which show a reduction in elemental carbon due to the scrubber, while sulfate levels increase [11]. SO_2 is dissolved in the wash water, followed by its conversion to sulfuric acid and ultimately secondary sulfate in the particle phase [6]. The decrease in elemental carbon can be attributed to more effective removal of smaller particles through diffusion-driven coagulation [11, 24], as these smaller particles are often soot particles (see Supplementary Information, Fig. S2(d) and [33]). Alternatively, improved scrubbing efficiency for elemental carbon has been linked to increased soot particle growth from the formation of hygroscopic sulfate on these particles [14]. Nonetheless, this would lead to an increase in elemental carbon signatures in the spectra, given that the instrument is more sensitive to larger particles, which is not observed in this case.

The mass spectral pattern of the PAHs remains unchanged, supporting their effectiveness as fuel marker [4]. However, the histogram in Fig. 1(d) shows a decrease in total PAH signals after the scrubber at higher engine loads, consistent with previously reported PAH reductions in scrubbers [13]. Both the stability of the marker signatures as well as the reduction in PAH levels are confirmed by offline measurements (see Supplementary Material, Fig. S3). The close association between PAHs and elemental carbon indicates that the removal mechanisms for PAHs are likely the same as those for soot.

In summary, for the organic carbon-dominated, relatively large particles emitted at low loads, no substantial changes are observed for the chemical aerosol composition when comparing the same number of particles before and after the scrubber. For the elemental carbon-dominated emissions at high engine load, soot and PAHs are more efficiently removed than other aerosol components, likely due to the smaller particle size of the soot particles [33].

Single-particle analysis

While the summed mass spectra show only little to moderate effects from the scrubber, potential changes in the mixing state and distribution of particle components within the ensemble could alter the environmental effects of aerosol emissions [25] and influence marker-based approaches for source apportionment [4]. In order to analyze the variance of the aerosol composition on a single-particle level, an exploratory principle component analysis was conducted on the mass spectra from LDI (inorganics) and REMPI (PAHs), respectively (see Fig. 2). Data from marine gas oil combustion, sampled before the scrubber, were included for comparison (shown in gray). For both ionization techniques, the first two principal components explained about 70% of the total variance, and thus it creates a representative description of the dataset and variation of mass spectral signatures for different emission scenarios in only two dimensions.

In the scores from the first principal component, heavy fuel oil emissions are well separated from marine gas oil emissions regardless the engine load or sulfur scrubber operation, so single-particle mass spectrometry with LDI at 248 nm is still able to differentiate between these two fuels, mainly by different signatures of Na, Ca, V, Fe and sulfate. The effect of wet scrubber operation on the particle composition exceeds the variation of the engine load by increasing sulfate-related relative ion signals ($m/z = -97$) from hydrolysis-driven gas-to-particle conversion of SO_2. However, the ellipsoids representing the 68% confidence interval of the scores still overlap, highlighting the similarity in particle composition beyond sulfate. In the PAH mass spectra, the impact of wet scrubber operation on heavy fuel oil emission composition is less pronounced, as the distribution of polyaromatic hydrocarbons remains unaffected, and variations in emission composition are typical for all heavy fuel oil combustion emissions.

Moreover, engine load has a greater impact on aromatic emissions from marine gas oil compared to heavy fuel oil, significantly increasing the abundance of alkylated phenanthrenes [3]. However, despite their closer resemblance to heavy fuel oil particle emissions, polycyclic aromatic emissions from marine gas oil combustion at a 20 kW load can still be differentiated from heavy fuel oil emissions using PAH-sensitive single-particle mass spectrometry.

Conclusion

Our single-particle analysis indicates that changes in the chemical composition of particles passing through the scrubber are primarily linked to sulfate uptake. Moreover, our findings suggest that variations in the overall aerosol composition can be attributed to the size-dependent nature of the removal effects: Ultrafine particles with a diameter lower than 100 nm are efficiently removed through diffusion-driven coagulation. As these particles primarily consist of elemental carbon and PAHs, their emissions are notably reduced, especially under high-load conditions during steaming. At low loads, when the aerosol contains high amounts of organics, and for larger particles, no significant

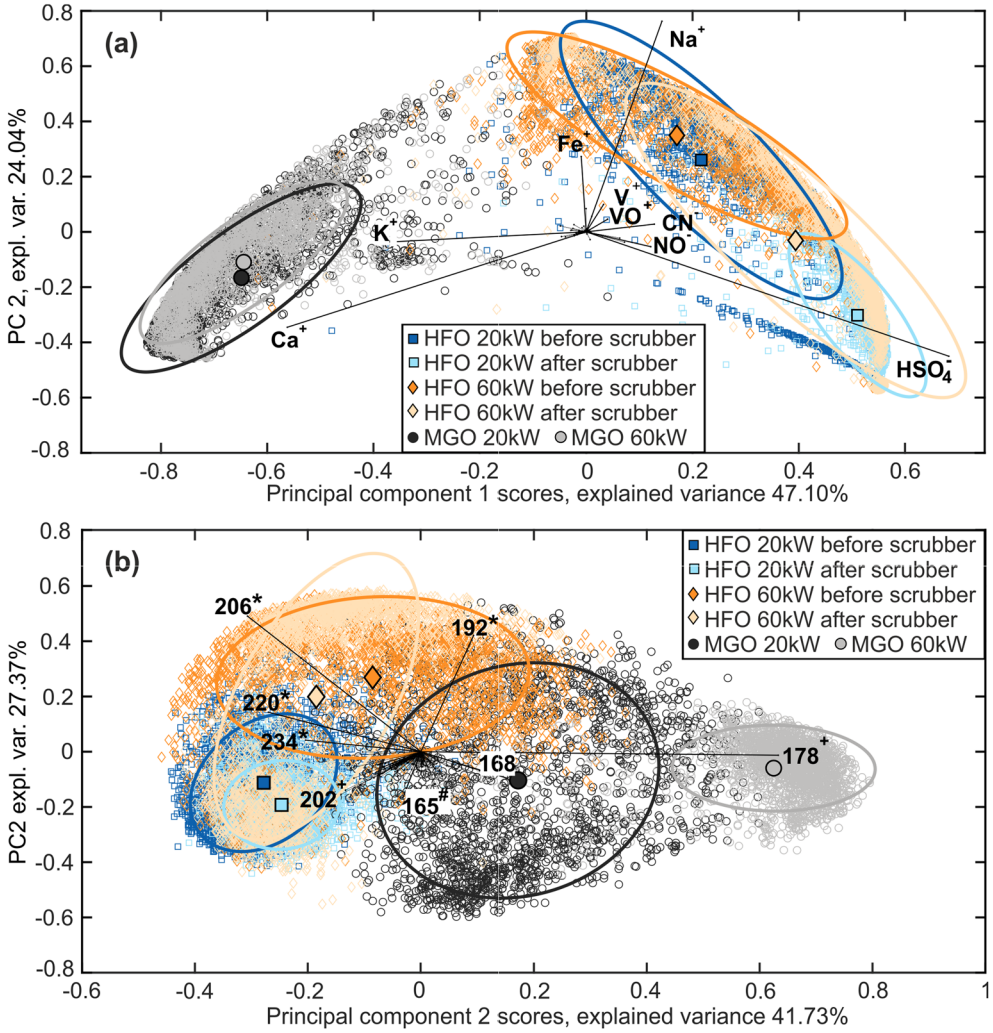

Fig. 2 **a** Principal component analysis of single-particle mass spectra from laser desorption/ionization for 20 kW and 60 kW engine loads, measured before and after the scrubber during operation with heavy fuel oil (HFO). Eigenvector lengths represent the contribution of signals at different m/z ratios to the mass spectral differences. The ellipses depict the 68% confidence interval for the principal component scores of each cluster. For comparison, results from marine gas oil (MGO) combustion, sampled before the scrubber, are shown in gray. The fuel clusters are distinctly separated, with Na, Ca, sulfate, and transition metal signals contributing most to this separation. The only clear effect of the scrubber when comparing the same number of particles is an increase in sulfate signals, due to the gas-to-particle conversion of SO_2. **b** For the polycyclic aromatic hydrocarbons (PAH), small load-dependent effects are observed, but no significant impact from the scrubber is detected. The fuel-specific PAH signatures remain distinguishable. m/z channels: * alkylated Phenanthrenes, $^{+}$ parent PAHs, $^{\#}$ fragment. For each fuel and load condition, n = 2,000 particles were analyzed before and after the scrubber, respectively

reduction in emissions was observed, and the scrubber had no noticeable effect on the aerosol's single-particle composition. However, this size fraction is particularly significant as it often contributes the most to inhalable particulate matter mass and is transported over long distances. Furthermore, since harbors—where ships operate at low engine loads—are located in densely populated coastal regions, exposure to these emissions is particularly high.

The novel ionization technology provides single-particle data on key health-relevant components—metals, soot, PAHs, and salts—but does not capture detailed organic composition beyond aromatic compounds. Schneider et al. [28] reported a scrubber-induced reduction in sulfur-containing water-soluble organics in the high molecular mass range and the formation of new elemental compositions from reactive gas chemistry. Additionally, future studies should focus on full-scale scrubber installations on large ships with two-stroke engines.

Another aspect concerns the environmental monitoring of ship emissions. Our study demonstrates that neither traditional ship emission markers (V, Fe), nor novel PAH-based approaches are influenced by scrubber operation. In fact, ships equipped with scrubbers have already been

detected by their metal emissions over distances of several kilometers [21].

Our findings suggest that using heavy fuel oil with scrubbers in low-emission zones, as an alternative to compliant low-sulfur fuels, may pose an increased health risk due to the insufficient capture of potentially harmful compounds like heavy metals and PAHs.

Supplementary Information The online version contains supplementary material available at https://doi.org/10.1007/s10311-025-01830-x.

Author contributions Lukas Anders: Investigation, Data curation, Visualization, Writing-Original draft preparation. Martin Bauer: Investigation, Data curation, Visualization. Seongho Jeong: Investigation. Marco Schmidt: Data curation, Visualization. Haseeb Hakkim: Writing-Original draft preparation, Supervision. Aleksandrs Kalamašņikovs: Visualization. Ellen Iva Rosewig: Investigation. Julian Schade: Investigation. Robert Irsig: Software. Sven Ehlert: Software, Supervision. Jan Bendl: Investigation. Mohammad Reza Saraji-Bozorgzad: Investigation. Barbara Giocastro: Investigation. Uwe Käfer: Investigation. Martin Sklorz: Investigation, Supervision. Uwe Etzien: Investigation, Supervision. Bert Buchholz: Funding acquisition, Resources. Thomas Adam: Funding acquisition. Thorsten Streibel: Funding acquisition, Project administration. Hendryk Czech: Supervision, Writing- Original draft preparation. Johannes Passig: Conceptualization, Methodology, Writing- Original draft preparation, Writing- Reviewing and Editing, Supervision. Ralf Zimmermann: Funding acquisition, Supervision.

Funding Open Access funding enabled and organized by Projekt DEAL. This work was supported by the German Federal Ministry for Economic Affairs and Climate Action by the project SAARUS (grant number 03SX483D) as well as by the dtec.bw-Digitalization and Technology Research Center of the Bundeswehr (projects "LUKAS" and "MORE"). dtec.bw is funded by the European Union – NextGenerationEU. H.C. acknowledges funding from the Helmholtz Association by the International Lab aeroHEALTH (InterLabs-0005). Funded by the Deutsche Forschungsgemeinschaft (DFG, German Research Foundation)—SFB 1477 "Light-Matter Interactions at Interfaces", project number 441234705.

Data availability The data that support the findings of this study are available from the corresponding author upon reasonable request.

Declarations

Competing Interests The authors have no relevant financial or non-financial interests to disclose.

References

1. Aakko-Saksa PT, Lehtoranta K, Kuittinen N, Järvinen A, Jalkanen J-P, Johnson K, Jung H, Ntziachristos L, Gagné S, Takahashi C, Karjalainen P, Rönkkö T, Timonen H (2023) Reduction in greenhouse gas and other emissions from ship engines: Current trends and future options. Prog Energy Combust Sci 94:101055. https://doi.org/10.1016/j.pecs.2022.101055
2. Abbas I, Badran G, Verdin A, Ledoux F, Roumié M, Courcot D, Garçon G (2018) Polycyclic aromatic hydrocarbon derivatives in airborne particulate matter: sources, analysis and toxicity. Environ Chem Lett 16:439–475. https://doi.org/10.1007/s10311-017-0697-0
3. Anders L, Schade J, Rosewig EI, Kröger-Badge T, Irsig R, Jeong S, Bendl J, Saraji-Bozorgzad MR, Huang J-H, Zhang F-Y, Wang CC, Adam T, Sklorz M, Etzien U, Buchholz B, Czech H, Streibel T, Passig J, Zimmermann R (2023) Detection of ship emissions from distillate fuel operation via single-particle profiling of polycyclic aromatic hydrocarbons. Environ Sci: Atmos 3(8):1134–1144. https://doi.org/10.1039/D3EA00056G
4. Anders L, Schade J, Rosewig EI, Schmidt M, Irsig R, Jeong S, Käfer U, Gröger T, Bendl J, Saraji-Bozorgzad MR, Adam T, Etzien U, Czech H, Buchholz B, Streibel T, Passig J, Zimmermann R (2024) Polycyclic aromatic hydrocarbons as fuel-dependent markers in ship engine emissions using single-particle mass spectrometry. Environ Sci: Atmos. https://doi.org/10.1039/D4EA00035H
5. Arndt J, Sciare J, Mallet M, Roberts GC, Marchand N, Sartelet K, Sellegri K, Dulac F, Healy RM, Wenger JC (2017) Sources and mixing state of summertime background aerosol in the northwestern Mediterranean basin. Atmos Chem Phys 17:6975–7001. https://doi.org/10.5194/acp-17-6975-2017
6. Ault AP, Gaston CI, Wang Y, Dominguez G, Thiemens MH, Prather KA (2010) Characterization of the single particle mixing state of individual ship plume events measured at the Port of Los Angeles. Environ Sci Technol 44:1954–1961. https://doi.org/10.1021/es902985h
7. Bendl J, Saraji-Bozorgzad MR, Käfer U, Padoan S, Mudan A, Etzien U, Giocastro B, Schade J, Jeong S, Kuhn E, Sklorz M, Grimmer C, Streibel T, Buchholz B, Zimmermann R, Adam T (2024) How do different marine engine fuels and wet scrubbing affect gaseous air pollutants and ozone formation potential from ship emissions? Environ Res 260:119609. https://doi.org/10.1016/j.envres.2024.119609
8. Fang T, Guo H, Zeng L, Verma V, Nenes A, Weber RJ (2017) Highly Acidic Ambient Particles, Soluble Metals, and Oxidative Potential: A Link between Sulfate and Aerosol Toxicity. Environ Sci Technol 51:2611–2620. https://doi.org/10.1021/acs.est.6b06151
9. García-Gómez E, Gkotsis G, Nika MC, Hassellöv IM, Salo K, Hermansson AL, Ytreberg E, Thomaidis NS, Gros M, Petrović M (2023) Characterization of scrubber water discharges from ships using comprehensive suspect screening strategies based on GC-APCI-HRMS. Chemosphere 343:140296. https://doi.org/10.1016/j.chemosphere.2023.140296
10. Healy RM, O'Connor IP, Hellebust S, Allanic A, Sodeau JR, Wenger JC (2009) Characterisation of single particles from in-port ship emissions. Atmos Environ 43:6408–6414. https://doi.org/10.1016/j.atmosenv.2009.07.039
11. Jeong S, Bendl J, Saraji-Bozorgzad M, Käfer U, Etzien U, Schade J, Bauer M, Jakobi G, Orasche J, Fisch K, Cwierz PP, Rüger CP, Czech H, Karg E, Heyen G, Krausnick M, Geissler A, Geipel C, Streibel T, Schnelle-Kreis J, Sklorz M, Schulz-Bull DE, Buchholz B, Adam T, Zimmermann R (2023) Aerosol emissions from a marine diesel engine running on different fuels and effects

of exhaust gas cleaning measures. Environ Pollut 316:120526. https://doi.org/10.1016/j.envpol.2022.120526
12. Karg EW, Ferron GA, Bauer S, Di Bucchianico S, Zimmermann R (2020) Is the particle deposition in a cell exposure facility comparable to the lungs? A computer model approach. Aerosol Sci Technol 54:668–684. https://doi.org/10.1080/02786826.2020.1724868
13. Kuittinen N, Timonen H, Karjalainen P, Murtonen T, Vesala H, Bloss M, Honkanen M, Lehtoranta K, Aakko-Saksa P, Rönkkö T (2024) In-depth characterization of exhaust particles performed on-board a modern cruise ship applying a scrubber. Sci Total Environ 946:174052. https://doi.org/10.1016/j.scitotenv.2024.174052
14. Lack DA, Corbett JJ (2012) Black carbon from ships: a review of the effects of ship speed, fuel quality and exhaust gas scrubbing. Atmos Chem Phys 12:3985–4000. https://doi.org/10.5194/acp-12-3985-2012
15. Lieke KI, Rosenørn T, Pedersen J, Larsson D, Kling J, Fuglsang K, Bilde M (2013) Micro- and Nanostructural Characteristics of Particles Before and After an Exhaust Gas Recirculation System Scrubber. Aerosol Sci Technol 47:1038–1046. https://doi.org/10.1080/02786826.2013.813012
16. Liu Z, Lu X, Feng J, Fan Q, Zhang Y, Yang X (2017) Influence of Ship Emissions on Urban Air Quality: A Comprehensive Study Using Highly Time-Resolved Online Measurements and Numerical Simulation in Shanghai. Environ Sci Technol 51:202–211. https://doi.org/10.1021/acs.est.6b03834
17. Mille T, Graindorge P-H, Morel C, Paoli J, Lichtfouse E, Schroeder H, Grova N (2024) The overlooked toxicity of non-carcinogenic polycyclic aromatic hydrocarbons. Environ Chem Lett 22. https://doi.org/10.1007/s10311-024-01719-1
18. Moldanová J, Fridell E, Popovicheva O, Demirdjian B, Tishkova V, Faccinetto A, Focsa C (2009) Characterisation of particulate matter and gaseous emissions from a large ship diesel engine. Atmos Environ 43:2632–2641. https://doi.org/10.1016/j.atmosenv.2009.02.008
19. Passig J, Zimmermann R (2020) Laser Ionization in Single-Particle Mass Spectrometry. In: Zimmermann R, Hanley L (eds) Photoionization and Photo-Induced Processes in Mass Spectrometry: Fundamentals and Applications. Wiley-VCH, Weinheim. https://doi.org/10.1002/9783527682201.ch11
20. Passig J, Schade J, Rosewig EI, Irsig R, Kröger-Badge T, Czech H, Sklorz M, Streibel T, Li L, Li X, Zhou Z, Fallgren H, Moldanova J, Zimmermann R (2020) Resonance-enhanced detection of metals in aerosols using single-particle mass spectrometry. Atmos Chem Phys 20:7139–7152. https://doi.org/10.5194/acp-20-7139-2020
21. Passig J, Schade J, Irsig R, Li L, Li X, Zhou Z, Adam T, Zimmermann R (2021) Detection of ship plumes from residual fuel operation in emission control areas using single-particle mass spectrometry. Atmos Meas Tech 14:4171–4185. https://doi.org/10.5194/amt-14-4171-2021
22. Passig J, Schade J, Irsig R, Kröger-Badge T, Czech H, Adam T, Fallgren H, Moldanova J, Sklorz M, Streibel T, Zimmermann R (2022) Single-particle characterization of polycyclic aromatic hydrocarbons in background air in northern Europe. Atmos Chem Phys 22:1495–1514. https://doi.org/10.5194/acp-22-1495-2022
23. Petzold A, Weingartner E, Hasselbach J, Lauer P, Kurok C, Fleischer F (2010) Physical Properties, Chemical Composition, and Cloud Forming Potential of Particulate Emissions from a Marine Diesel Engine at Various Load Conditions. Environ Sci Technol 44:3800–3805. https://doi.org/10.1021/es903681z
24. Pratsinis SE, Kim K-S (1989) Particle coagulation, diffusion and thermophoresis in laminar tube flows. J Aerosol Sci 20:101–111. https://doi.org/10.1016/0021-8502(89)90034-7
25. Riemer N, Ault AP, West M, Craig RL, Curtis JH (2019) Aerosol Mixing State: Measurements, Modeling, and Impacts. Rev Geophys 57:187–249. https://doi.org/10.1029/2018RG000615
26. Riemer N, West M (2024) The state of the aerosol: Musings on mixing state. Aerosol Sci Technol 58:721–726. https://doi.org/10.1080/02786826.2024.2346220
27. Schade J, Passig J, Irsig R, Ehlert S, Sklorz M, Adam T, Li C, Rudich Y, Zimmermann R (2019) Spatially Shaped Laser Pulses for the Simultaneous Detection of Polycyclic Aromatic Hydrocarbons as well as Positive and Negative Inorganic Ions in Single Particle Mass Spectrometry. Anal Chem 91:10282–10288. https://doi.org/10.1021/acs.analchem.9b02477
28. Schneider E, Czech H, Hansen HJ, Jeong S, Bendl J, Saraji-Bozorgzad M, Sklorz M, Etzien U, Buchholz B, Streibel T, Adam TW (2023) Humic-like substances (HULIS) in ship engine emissions: molecular composition effected by fuel type, engine mode, and wet scrubber usage. Environ Sci Technol 57(37):13948–13958. https://doi.org/10.1021/acs.est.3c04390
29. Seinfeld JH, Pandis SN (2016) Atmospheric Chemistry and Physics: From Air Pollution to Climate Change. Wiley
30. Streibel T, Schnelle-Kreis J, Czech H, Harndorf H, Jakobi G, Jokiniemi J, Karg E, Lintelmann J, Matuschek G, Michalke B, Müller L, Orasche J, Passig J, Radischat C, Rabe R, Reda A, Rüger C, Schwemer T, Sippula O, Stengel B, Sklorz M, Torvela T, Weggler B, Zimmermann R (2017) Aerosol emissions of a ship diesel engine operated with diesel fuel or heavy fuel oil. Environ Sci Pollut Res Int 24:10976–10991. https://doi.org/10.1007/s11356-016-6724-z
31. Tang L, Ramacher MOP, Moldanová J, Matthias V, Karl M, Johansson L, Jalkanen J-P, Yaramenka K, Aulinger A, Gustafsson M (2020) The impact of ship emissions on air quality and human health in the Gothenburg area – Part 1: 2012 emissions. Atmos Chem Phys 20:7509–7530. https://doi.org/10.5194/acp-20-7509-2020
32. Thor P, Granberg ME, Winnes H, Magnusson K (2021) Severe Toxic Effects on Pelagic Copepods from Maritime Exhaust Gas Scrubber Effluents. Environ Sci Technol 55:5826–5835. https://doi.org/10.1021/acs.est.0c07805
33. Winnes H, Fridell E, Moldanová J (2020) Effects of Marine Exhaust Gas Scrubbers on Gas and Particle Emissions. JMSE 8:299. https://doi.org/10.3390/jmse8040299
34. Xiao Q, Li M, Liu H, Fu M, Deng F, Lv Z, Man H, Jin X, Liu S, He K (2018) Characteristics of marine shipping emissions at berth: profiles for particulate matter and volatile organic compounds. Atmos Chem Phys 18:9527–9545. https://doi.org/10.5194/acp-18-9527-2018
35. Yang J, Tang T, Jiang Y, Karavalakis G, Durbin TD, Wayne Miller J, Cocker DR, Johnson KC (2021) Controlling emissions from an ocean-going container vessel with a wet scrubber system. Fuel 304:121323. https://doi.org/10.1016/j.fuel.2021.121323
36. Yuan L, Zhao C (2023) Quantifying particle-to-particle heterogeneity in aerosol hygroscopicity. Atmos Chem Phys 23:3195–3205. https://doi.org/10.5194/acp-23-3195-2023
37. Zauscher MD, Wang Y, Moore MJK, Gaston CJ, Prather KA (2013) Air Quality Impact and Physicochemical Aging of Biomass Burning Aerosols during the 2007 San Diego Wildfires. Environ Sci Technol 47:7633–7643. https://doi.org/10.1021/es4004137

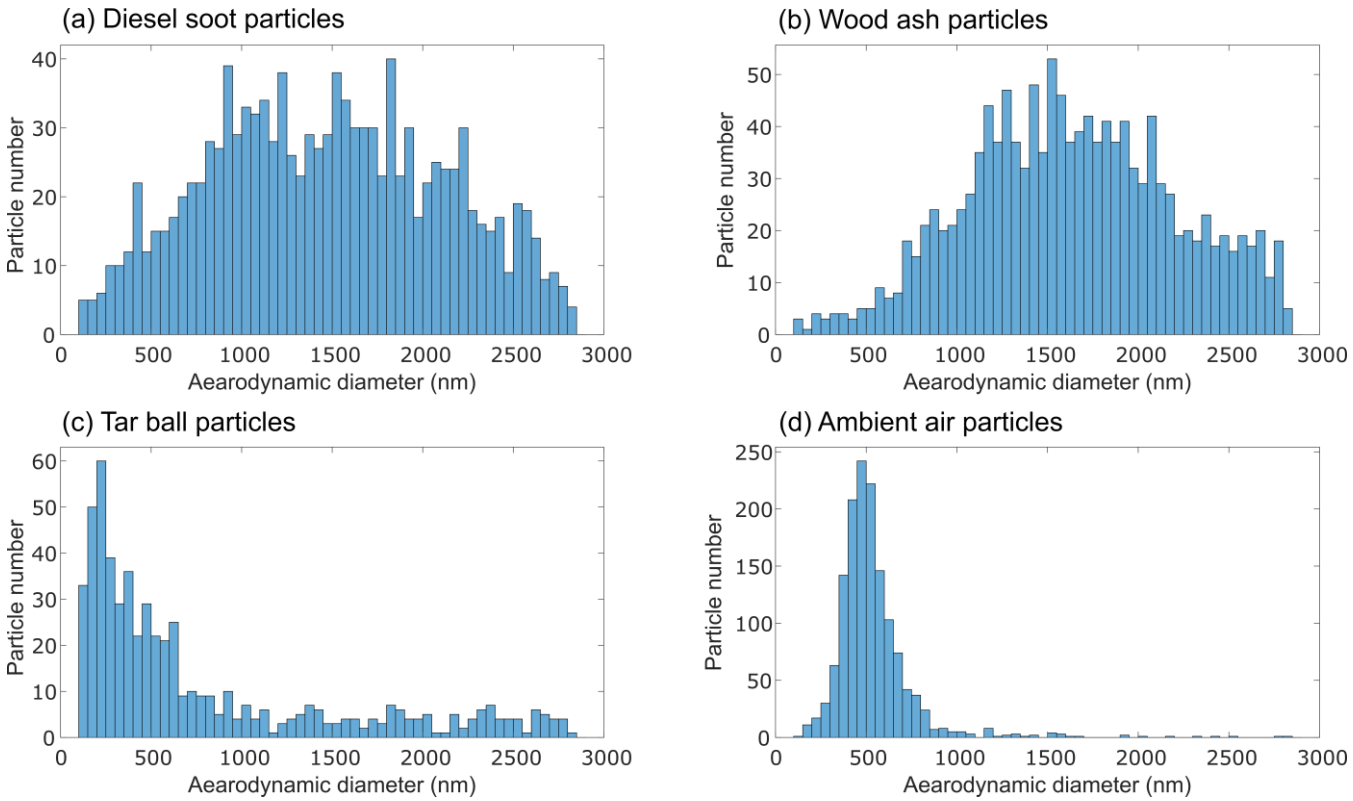

Figure S1 Particle size distributions, each n = 1200, of the laboratory and ambient air particles measured using the optical sizing unit of the SPMS: **(a**) Diesel soot particles; **(b)** Wood ash particles; **(c**) Tar ball particles; and **(d)** Ambient air particles.

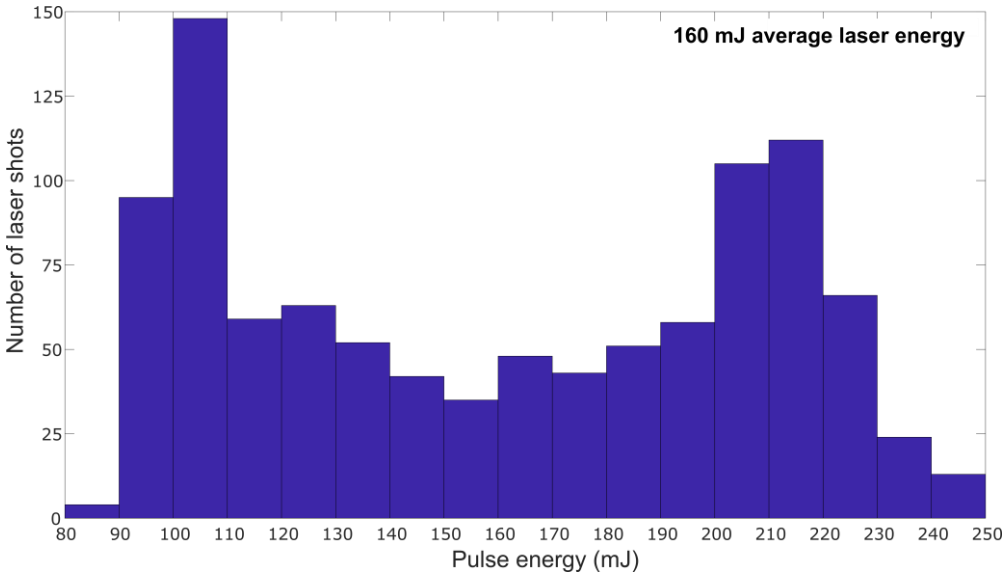

Figure S2 Pulse energies of 1022 laser pulses from the Er:YAG laser. The observed high fluctuation is attributed to the random nature of particle events inducing thermal lensing effects in the laser resonator; the average pulse energy was determined to be 160 mJ.

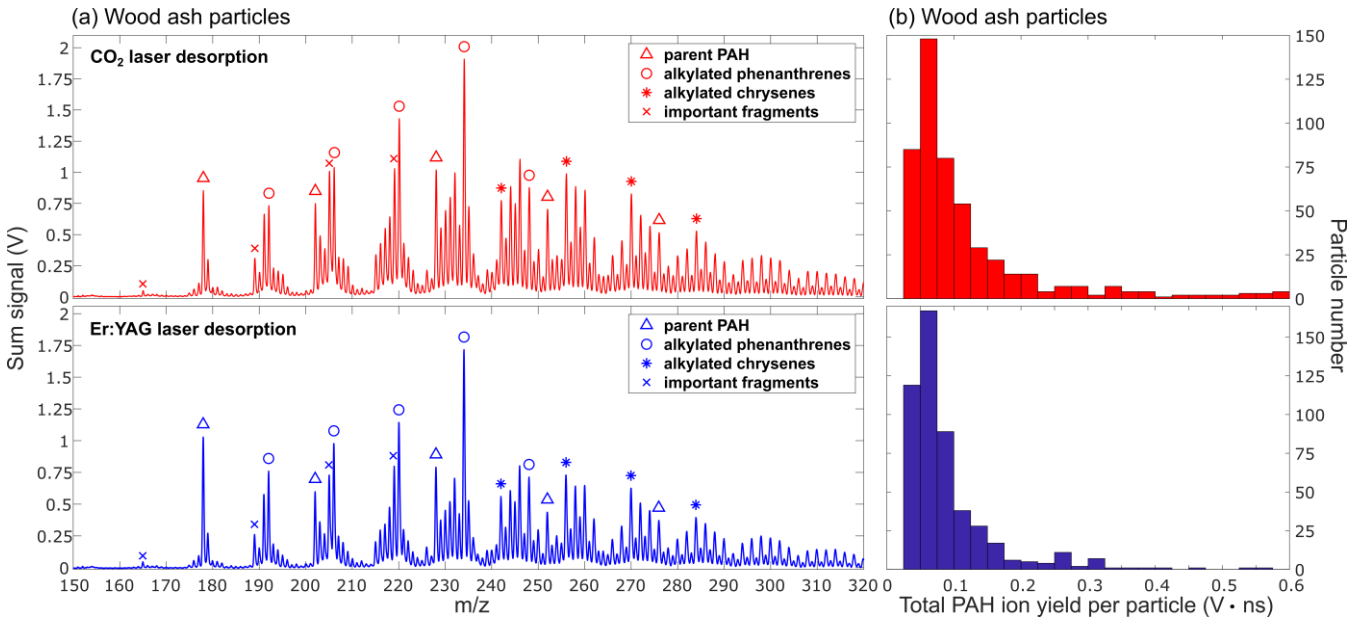

Figure S3 (a) Wood ash particles (n = 500 each) exhibit a very different PAH profile in the LD-REMPI ionization than diesel soot particles, and they show the softwood combustion marker retene (m/z = 234), a thermal degradation product of resin acids. There are also some signals from higher-mass molecules, possibly from oxidized PAHs and other combustion products with aromatic rings, which can be ionized in the LD-REMPI scheme. However, in direct comparison, there are almost no differences between the CO_2 laser and the Er:YAG laser for LD. **(b)** The single-particle signal intensity of PAHs again shows a few more particles with strong PAH signals for the CO_2 laser. The hit rate for PAHs was low, with only 2 % (4 %) of the optically detected particles showing a PAH spectrum when the CO_2 laser (Er:YAG laser) was used due to the nature of the sample, which contains many burnt ash particles and fewer OC/soot particles containing PAHs (Dall'Osto et al., 2016; Healy et al., 2015).

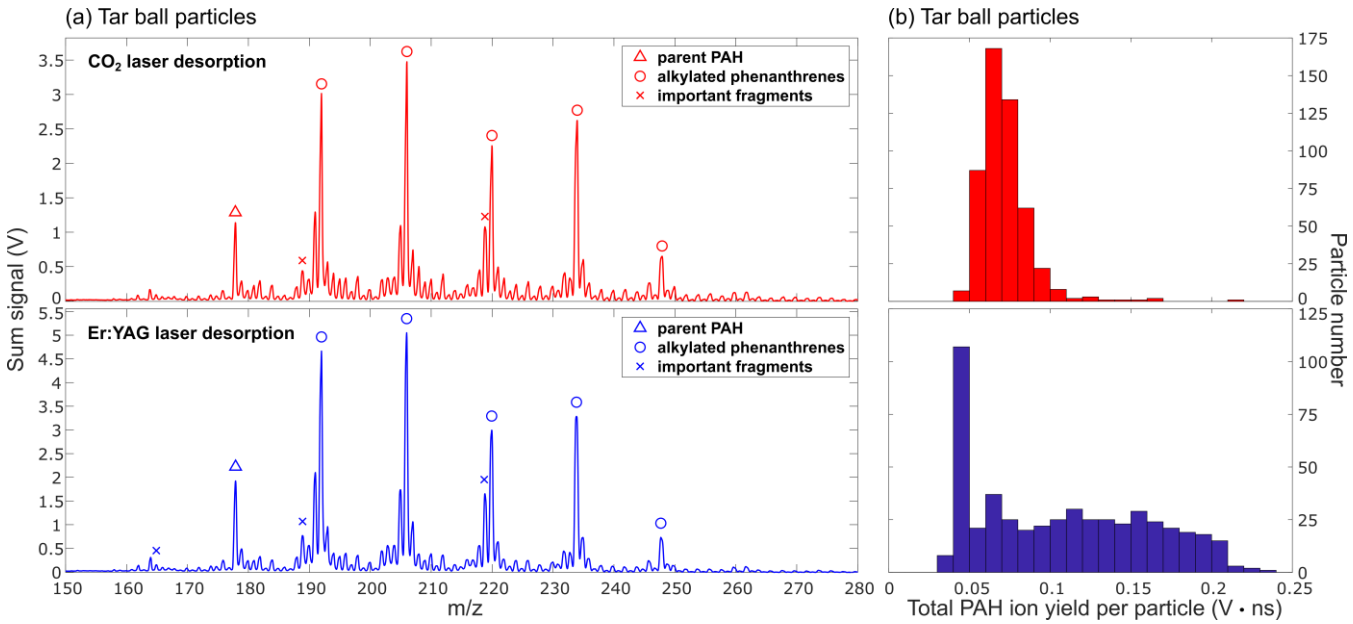

Figure S4 In our case of sprayed wood tar as a proxy for organic aerosols from wood combustion, the sum PAH spectra (n = 500 each) show almost exclusively alkylated phenanthrenes, in contrast to a more sophisticated tar ball model that we analyzed in a previous study using the

same LD-REMPI technique (Li et al., 2019). However, they appear to be an appropriate and easier to generate model to study LD for the highly relevant organic aerosols from wood combustion, as they have comparable physical properties such as high viscosity, low volatility, and a brown color with high absorption in the UV-VIS due to their PAH content (Jacobson, 2012; Brege et al., 2021; Li et al., 2019). While there are no qualitative differences in the mass spectra between the two lasers used for LD, the Er:YAG laser produced intense PAH spectra more often for this particle type. This can be explained by the strong absorption of the solvent methanol at the 3 µm wavelength of the Er:YAG laser. In addition, it was difficult to determine the hit rate in these experiments, because there was a small background of the PAH signature from particle evaporation effects in the inlet, even when no particle was hit. A particle hit was defined when the sum of the peak areas exceeded 30 mV · ns, based on the distribution of signal intensities per laser shot. This results in a hit rate of 54 % (49 %) for the CO_2 laser (Er:YAG laser).

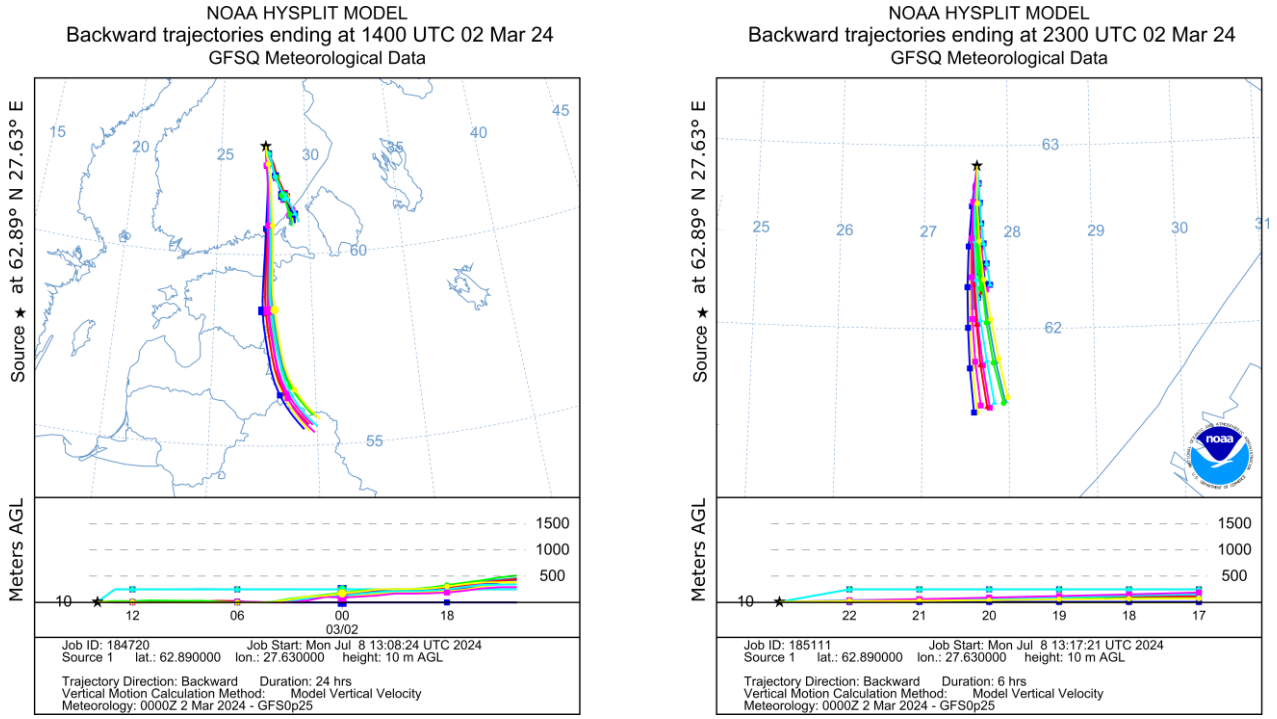

Figure S5 HYSPLIT backward trajectories for 24 h run time (left) for the ambient air experiments with the LD-REMPI approach and with 6 h run time for the subsequent experiments with the combined LD-REMPI/LDI approach (right), both ending at the measurement location.

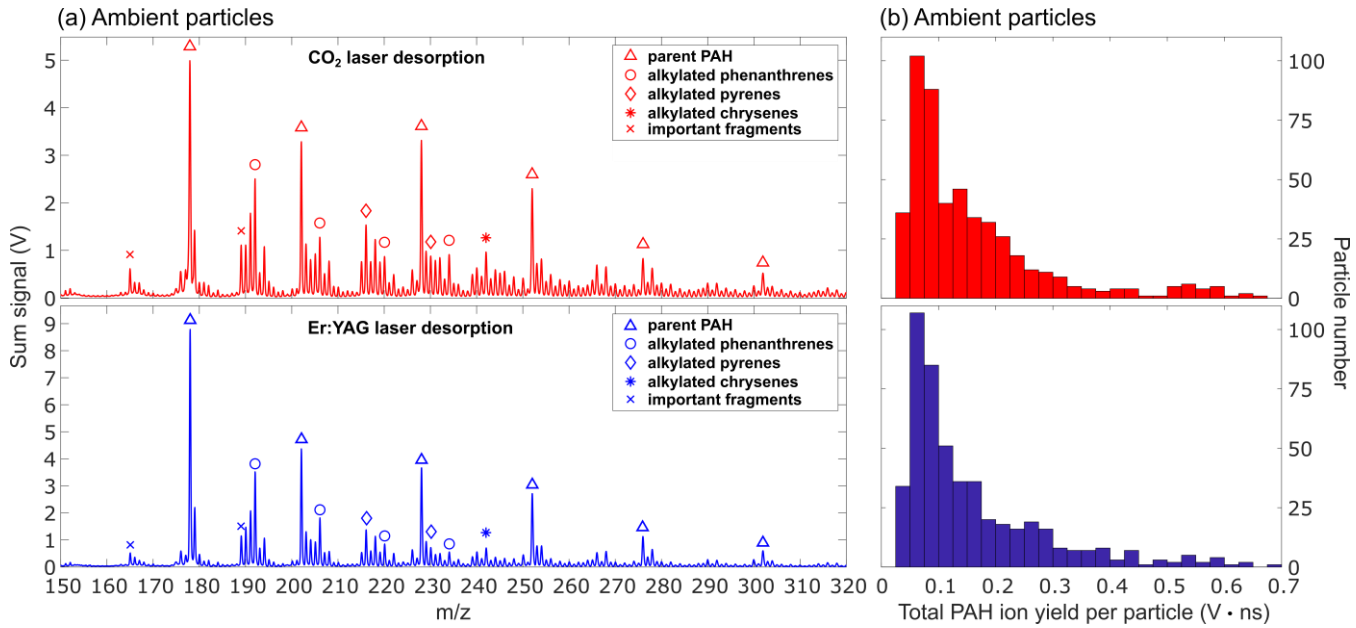

Figure S6 (a) Sum PAH mass spectra from ambient air particles (n = 500 each) measured in the LD-REMPI ionization approach. In direct comparison, the mass spectral signatures are similar between the CO_2 laser and the Er:YAG laser for LD. The Er:YAG produces slightly higher signal intensities for parent PAH, especially for m/z = 178, as discussed before. **(b)** The single-particle signal intensities of PAHs are also comparable for both lasers.

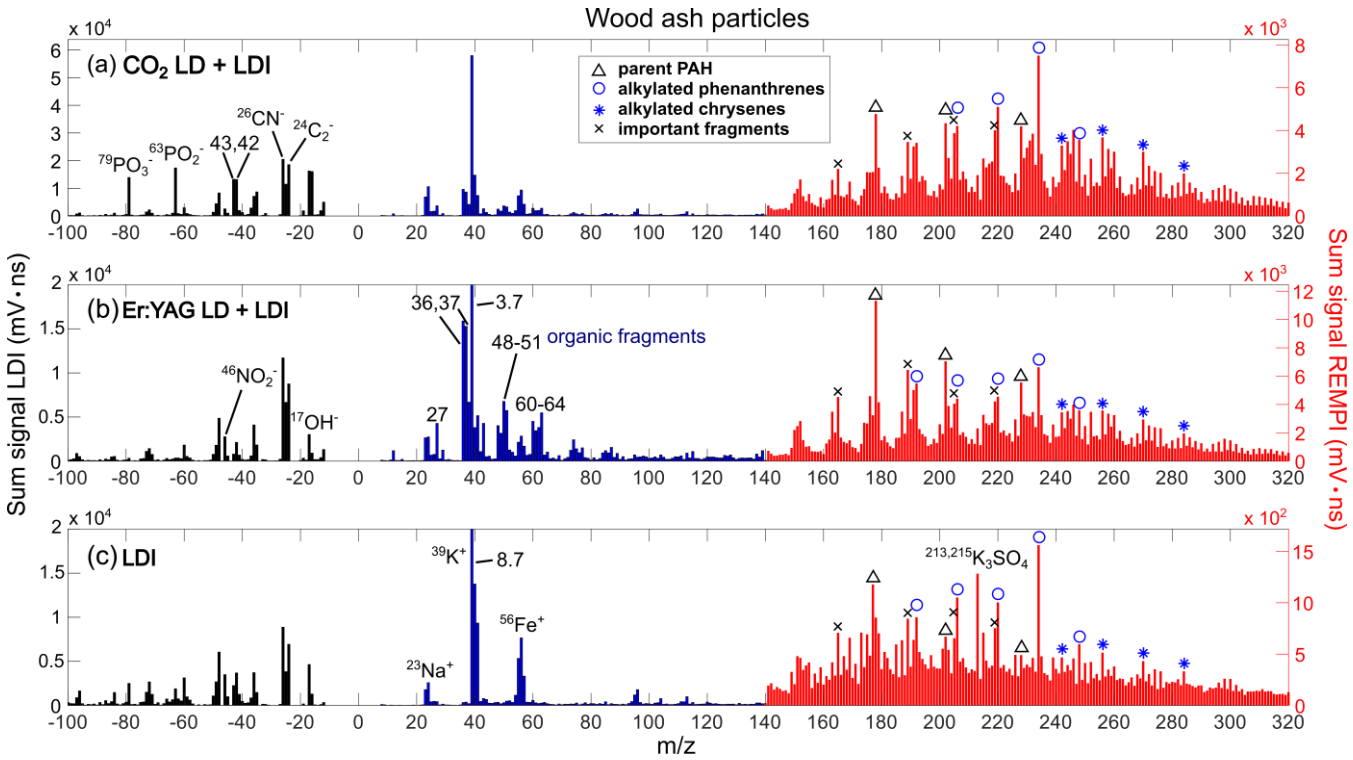

Figure S7 For wood ash particles, the combined method yields comparable results for **(a)** the CO_2 laser and **(b)** the Er:YAG laser applied for LD. Due to the nature of these particles, the single-step LDI method also produces clear PAH signatures, but with a lower sensitivity (compare the Y-axes on the right), n = 500 each.

(a) Cluster analysis of LD/LDI mass spectra with CO_2 laser

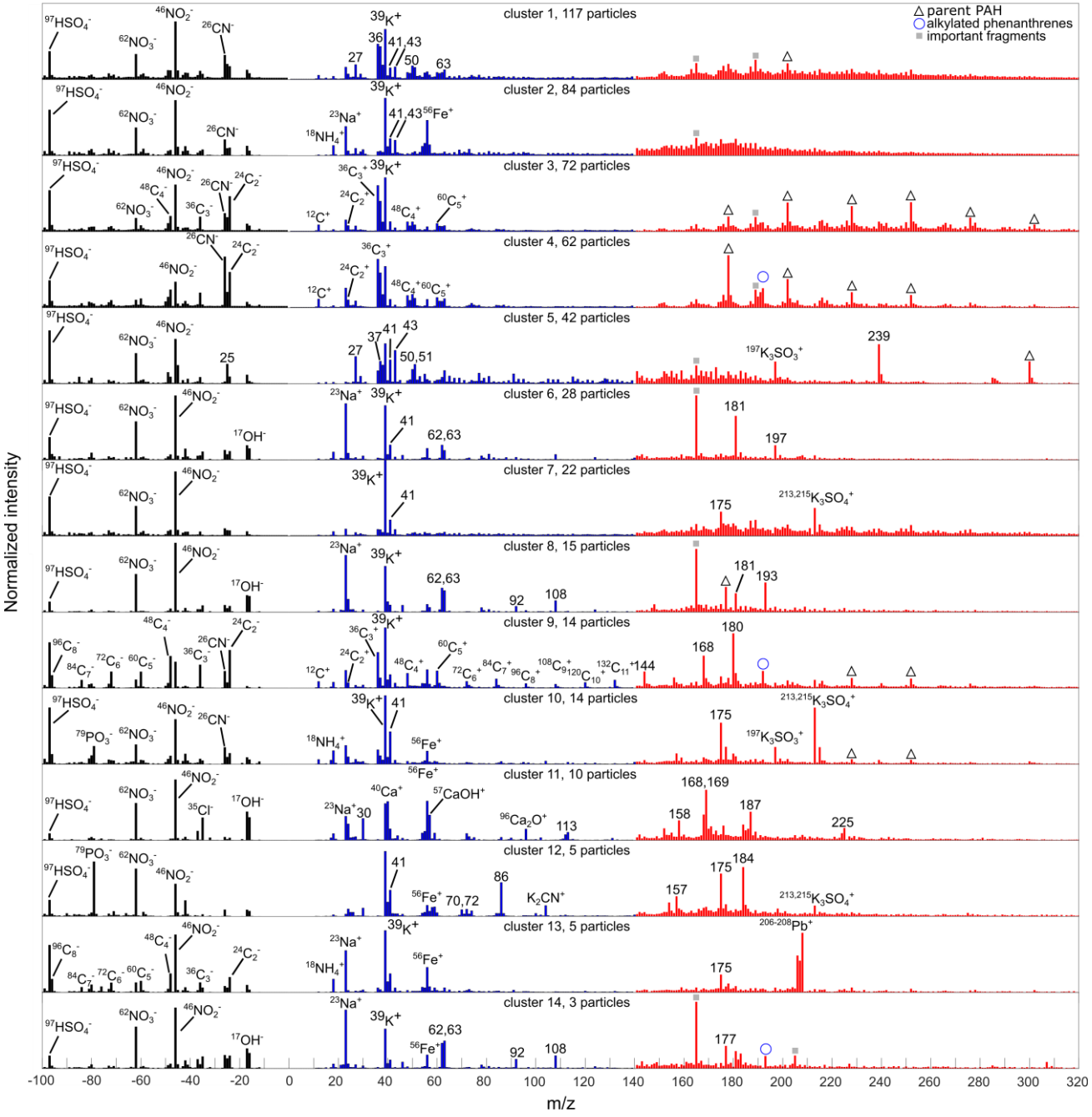

(b) Cluster analysis of LD/LDI mass spectra with Er:YAG laser

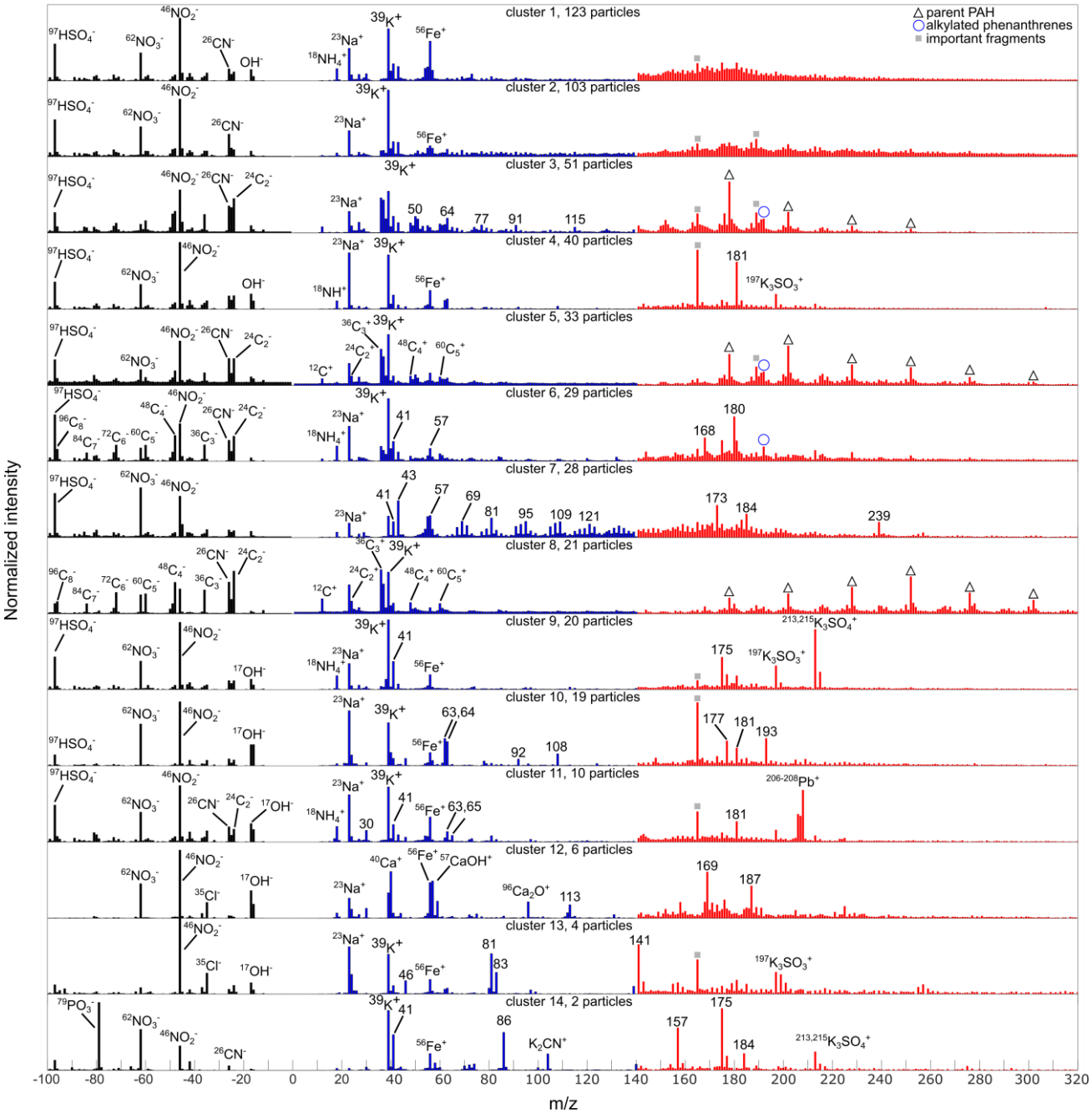

45

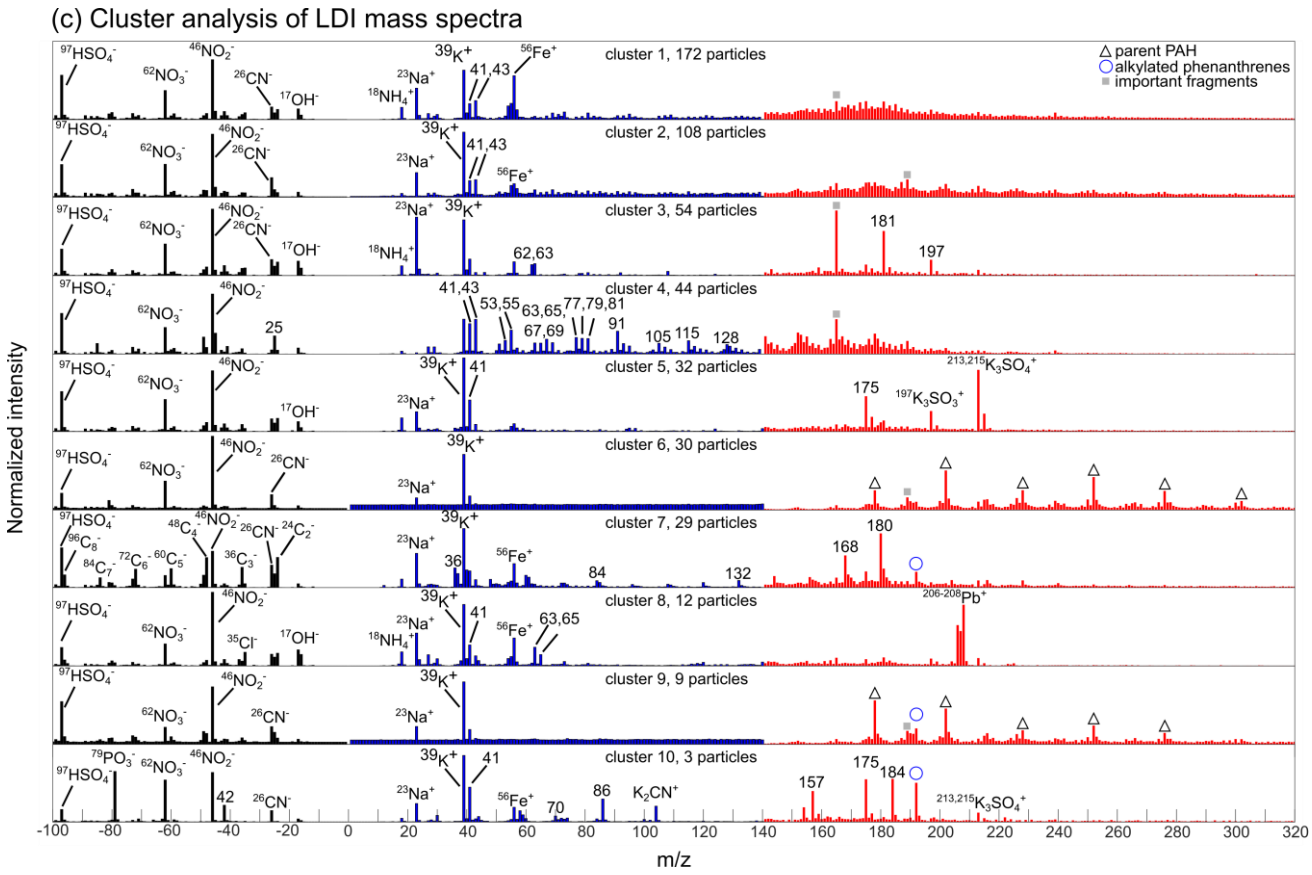

Figure S8 Results of the ART-2a cluster analyses, each including 500 PAH mass spectra from the respective ionization scheme. The combined LD-REMPI/LDI scheme yields comparable cluster centers and numbers of particles in each cluster for **(a)** using the CO2 laser and **(b)** using the Er:YAG laser for the LD step. **(c)** The single-step LDI scheme yields fewer clusters due to its higher fragmentation and lower sensitivity. The most abundant clusters are dominated by unidentified fragment signals. Only 39 out of 500 particles show clear PAH signatures for LDI.

References

Brege, M. A., China, S., Schum, S., Zelenyuk, A., and Mazzoleni, L. R.: Extreme Molecular Complexity Resulting in a Continuum of Carbonaceous Species in Biomass Burning Tar Balls from Wildfire Smoke, ACS Earth Space Chem., 5, 2729–2739, https://doi.org/10.1021/acsearthspacechem.1c00141, 2021.

Dall'Osto, M., Beddows, D. C. S., McGillicuddy, E. J., Esser-Gietl, J. K., Harrison, R. M., and Wenger, J. C.: On the simultaneous deployment of two single-particle mass spectrometers at an urban background and a roadside site during SAPUSS, Atmos. Chem. Phys., 16, 9693–9710, https://doi.org/10.5194/acp-16-9693-2016, 2016.

Healy, R. M., Evans, G. J., Murphy, M., Sierau, B., Arndt, J., McGillicuddy, E., O'Connor, I. P., Sodeau, J. R., and Wenger, J. C.: Single-particle speciation of alkylamines in ambient aerosol at five European sites, Analytical and bioanalytical chemistry, 407, 5899–5909, https://doi.org/10.1007/s00216-014-8092-1, 2015.

Jacobson, M. Z.: Investigating cloud absorption effects: Global absorption properties of black carbon, tar balls, and soil dust in clouds and aerosols, J. Geophys. Res., 117, https://doi.org/10.1029/2011JD017218, 2012.

Li, C., He, Q., Schade, J., Passig, J., Zimmermann, R., Meidan, D., Laskin, A., and Rudich, Y.: Dynamic changes in optical and chemical properties of tar ball aerosols by atmospheric photochemical aging, Atmos. Chem. Phys., 19, 139–163, https://doi.org/10.5194/acp-19-139-2019, 2019.

npj | climate and atmospheric science

Article

Published in partnership with CECCR at King Abdulaziz University

https://doi.org/10.1038/s41612-024-00838-4

Impact of fuel sulfur regulations on carbonaceous particle emission from a marine engine

Martin Bauer[1], Hendryk Czech[1,2] ✉, Lukas Anders[1], Johannes Passig[1,2], Uwe Etzien[3], Jan Bendl[2,4], Thorsten Streibel[1,2], Thomas W. Adam[2,4], Bert Buchholz[3] & Ralf Zimmermann[1,2]

Ship traffic substantially contributes to air pollution, thus affecting climate and human health. Recently introduced regulations by the International Maritime Organization (IMO) on the fuel sulfur content (FSC) caused a shift in marine fuel onsumption from heavy fuel oils (HFO) to diesel-like distillate fuels, but also to alternative hybrid fuels and the operation of sulfur scrubbers. Using multi-wavelength thermal-optical carbon analysis (MW-TOCA), our study provides emission factors (EF) of carbonaceous aerosol particles and link the fuel composition to features observed in the soot microstructure, which may be exploited in online monitoring by single-particle mass spectrometry (SPMS). Particulate matter from distillate fuels absorbs stronger light of the visible UV and near-infrared range than HFO. However, Simple Forcing Efficiency (SFE) of absorption weighted by EF of total carbon compensated the effect, leading to a net reduction by >50% when changing form HFO to distillate fuels.

Worldwide about 90% of goods are transported by ships, thereby releasing in 2011 about 0.2 million tons of fine particulate matter (PM2.5) per year in European waters[1], which has been associated with increased mortality by cardiopulmonary diseases and lung cancer[2]. Before 2020, the vast majority of ocean-going vessels were operated on heavy fuel oil (HFO), which is produced from blending the vacuum residue from crude oil refining with middle distillate. HFO is commonly defined by either a density >900 kg m^{-3} or a kinematic viscosity of >180 mm^2 s^{-1} at 15 °C. The oil consists of high-molecular weight hydrocarbon structures and contains sulfur in the range of few percent by mass[3] as well as substantial amounts of transition metals, such as vanadium, nickel and iron, which are emitted in the PM2.5 fraction[4]. In contrast to diesel cars and trucks, ships are usually not equipped with aftertreatment devices common in road traffic, such as particle filters or oxidation catalysts. Moreover, the upper limits for the fuel sulfur content (FSC) for ships are orders of magnitude higher compared to road traffic, hence ships exhibit high emission per mass of consumed fuel or generated amount of energy especially for SO_x and PM2.5[5,6]. Furthermore, ships typically have either one large slow-speed two-stroke engine and several auxiliary medium-speed four-stroke engines, or several four-stroke engines for propulsion and power generation with different emission patterns[7].

In order to reduce the environmental burden of maritime traffic, the International Maritime organization (IMO) introduced a global FSC cap of 0.5% beginning in 2020. In addition to that measure, previously defined Sulfur Emission Control Areas (SECA) have been introduced, where only fuels with a maximum FSC of 0.1% are allowed[8]. Furthermore, a new measure starting in July 2024 set an upper limit for fuel viscosity in the Arctic[9]. The sulfur cap *de facto* prohibited the use of most HFO and led to a shift in the marine fuel market towards distillate fuels, such as marine gas oil (MGO), and hybrid fuels containing minor amounts of high-molecular weight hydrocarbons above the boiling point range of middle distillate[10]. Alternatively, ships may be still operated on HFO, but only combined with sulfur scrubbing aftertreatment technology, titrating SO_x with sea water (in open-loop mode) or an alkaline solution (in closed-loop mode)[11,12].

Modeling and epidemiological studies have quantified significant public health benefits from the switch to low-sulfur fuels in terms of reductions in air pollutants, such as PM2.5, sulfate, metals and SO_x[13,14]. As a drawback, increased NO_x values have been observed in the North and Baltic Sea[15]. Furthermore, a substitution of HFO by diesel-like fuel reduces acute toxicity in human lung epithelial cells[16], but PM2.5 from diesel fuel combustion affected several essential pathways of lung cell metabolism even stronger[17].

Beyond public health, ship emissions directly or indirectly affect the climate. Direct effects include the release of greenhouse gases, such as carbon dioxide, methane and nitrous oxide, and modification of the Earth's

[1]Chair of Analytical Chemistry, Institute of Chemistry, University Rostock, 18059 Rostock, Germany. [2]Cooperation Group "Comprehensive Molecular Analytics", Helmholtz Centre Munich, 85764 Neuherberg, Germany. [3]Chair of Piston Machines and Internal Combustion Engines (LKV), Faculty of Mechanical Engineering and Marine Technology, University of Rostock, 18059 Rostock, Germany. [4]Institute of Chemistry and Environmental Engineering, University of the Bundeswehr Munich, 85579 Neubiberg, Germany. ✉e-mail: hendryk.czech@uni-rostock.de

radiative forcing by PM2.5 components, predominantly black carbon (BC) but also brown carbon (BrC) including tar[18,19]. Indirect effects comprise the ability of PM2.5 to initiate cloud formation, which increases the albedo of the atmosphere, associated with a cooling effect[20]. Lower FSC leads to lower emissions of hygroscopic sulfate particles but higher fraction of hydrophobic soot particles, which reduces the cloud formation ability of the emissions and thus the cooling effect. Therefore, benefits for public health achieved by regulating the FSC are associated with increasing radiative forcing[21].

Our study examines different emission scenarios from a marine four-stroke engine operated on non-compliant fuels (representing emissions before 2020), globally compliant fuels as well as fuels compliant with current FSC limits in SECA (Supplementary Table S1). Despite its comparably low power of 80 kW, the engine was shown to produce emission representative for larger ocean-going vessels[22]. Filter samples of PM2.5 were measured by a multi-wavelength thermal-optical carbon analyzer, combining established carbonaceous aerosol quantities of organic carbon (OC) and elemental carbon (EC) with their optical properties[23] for comparing emission factors (EF) and changes in physical-chemical properties of the particulate emissions. Finally, distinct differences in the structure of EC is exploited in single-particle mass spectrometry (SPMS) as an extension of recent progress in remote online identification of marine fuels from ship plume analysis based on ultrasensitive detection of transition metals[24] and the pattern of polycyclic aromatic hydrocarbons (PAH)[25].

Results

Emission factors of OC and EC

Emission factors of OC and EC from individual engine loads (Supplementary Table S2) were calculated as weighted averages according to the IMO engine test cycle E2 for six marine fuels: hydro-treated vegetable oil (HVO), marine gas oil (MGO), ultra-low-sulfur aromatic rich heavy fuel oil (ULS-HFO$_{ar}$), low-sulfur heavy fuel oil (LS-HFO), synthetic high-sulfur heavy fuel oil (HS-HFO$_{syn}$), and high-sulfur heavy fuel oil (HS-HFO) (Fig. 1). HFO with high FSC (HS-HFO and HS-HFO$_{syn}$), which were widely used before 2020, led to emission factors for OC and EC in the order of 200 to 500 mg kWh^{-1}, agreeing with previous studies on research engines and ongoing vessels[12,26,27]. Compliant LS-HFO did not show any significant emission reduction for neither OC nor EC compared to HS-HFO$_{syn}$ or HS-HFO. Therefore, the chemical composition of the used HFO is the driving force for carbonaceous particulate emissions, while the FSC alone had no substantial effect.

In SECA, most ships are operated on distillate fuels such as MGO[28], which has been shown to produce significantly lower emissions of both OC and EC than heavy fuels in our study, while the ratio of OC to EC remains around unity. Since only the FSC is regulated, SECA-compliant fuels can also be obtained from alternative production methods. ULS-HFO$_{ar}$ originates from a cycle oil, a side product of the crude oil refining, which is rich in two- to four-ring aromatic hydrocarbons but low in sulfur due to hydrocracking of heavy crude oil fractions. Operating the engine on this hybrid fuel, with properties in between conventional HFO and MGO, has implications for the toxicological properties of the emissions due to its high content of PAH[29], but does not significantly increase emissions of OC and EC compared to MGO. In view of potentially carbon-neutral fuels, hydro-treated vegetable oil (HVO) inherently having a low FSC may be used in the future as an alternative fuel in SECA. Carbonaceous emissions from engine operation on HVO did not drop below emissions from MGO engine operation, so additional costs for fuel did not lead to a reduction in PM emissions. However, engine conditions in this study were optimized for operation of HFO, thus optimized operation of HVO may still lead to a reduction of unexpectedly high OC and EC emissions in this study.

The individual engine loads cause different EF for both OC and EC (Supplementary Table S2). In all HFO-labeled fuels, the average EF of carbonaceous emissions consistently decreased as engine loads increased, whereas this trend was less apparent for distillate fuels. Generally, limitation of the FSC to 0.5% had small effects on the carbonaceous emissions if conventional HFO of proper fuel quality is used (LS-HFO and HS-HFO). The observed reduction in emissions related to the IMO engine test cycle E2 (Fig. 1) by switching from heavy to distillate fuels are mainly caused by lower emissions at 25% engine load.

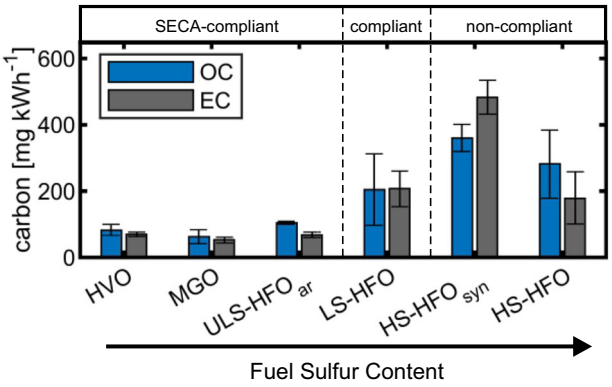

Fig. 1 | Emission factor of OC and EC. Emission factors of organic and elemental carbon (OC, EC), weighted according IMO engine test cycle E2, for marine fuels of different fuel sulfur compliance levels. Error bars denote the standard deviation from $n = 5$.

Composition of carbonaceous aerosol particles

Thermal-optical carbon analysis (TOCA) allows speciation of carbonaceous aerosol particles according to thermal fractions in the temperature protocol *ImproveA*, defining four fractions of OC (OC1-OC4) and three fractions of EC (EC1-EC3) as well as pyrolytic OC (OC$_{pyro}$) from the optical correction of charring. In this study, the approach by Han et al. (2007)[30] is used, dividing EC into char-EC (referring to EC1) and soot-EC (referring to the sum of EC2 and EC3), which accounts for differences in thermal refractiveness and consequently in soot microstructure.

For most carbonaceous emissions, the relative OC content of the total carbonaceous emissions occurred in a moderately small range of 0.425 to 0.75 regardless the fuel (Fig. 2), which is equivalent to ratios of OC to EC (OC/EC) from 3 to 0.74. The majority of all individual sample measurements appeared in the OC content range of 0.36 to 0.8 equivalent to OC/EC from 4 to 0.56 (Supplementary Fig. S1). At higher engine loads, the share of fractions OC1 and OC2 with the lowest thermal refractiveness decreased, while OC fractions of higher thermal refractiveness increased towards higher loads, but trends for fuels can be identified (Supplementary Fig. S2). However, a higher contribution of soot-EC is striking for the diesel-like fuels MGO and HVO, whereas a higher percentage of char-EC can be observed for conventional HFO usage. This also holds for HS-HFO and HS-HFO$_{syn}$ emissions after exhaust gas treatment by an open-loop sulfur scrubber, which enables cruising with FSC larger than 0.5% outside SECA[11]. The aromatic-rich but low-viscous HFO (ULS-HFO$_{ar}$) belongs to the group of so-called "hybrid fuels". It features both properties of distillate fuel and conventional HFO and also the ratio of char-EC to soot-EC appear between those fuel classes with approximately 0.5 (Fig. 2).

Connecting the operationally defined quantities char- and soot-EC from TOCA[30] with the re-classification of light-absorbing carbon by Corbin et al.[19] and fuel properties (Supplementary Table S1), the observations may be explained as following. HFO refers to a dense, highly viscous and low-volatile fuel, which may have a kinematic viscosity of up to 380 mm^2 s^{-1} at 50 °C and a density of up to 0.990 g cm^{-3} at 15 °C, compared to 2 mm^2 s^{-1} and 0.835 g cm^{-3} for MGO in this study (Supplementary Table S1). Hence, during fuel injection, droplets do not fully vaporize and cause locally fuel-rich mixtures, thus surface graphitization occurs by fuel droplet pyrolysis[19,31]. Droplets from spray injection of diesel-like fuels quickly evaporate, so hydrocarbons of the diesel-like fuels thermally decompose into radicals and form soot particles. Hence, engine operation with HVO and MGO generates soot structures different from HFO engine operation.

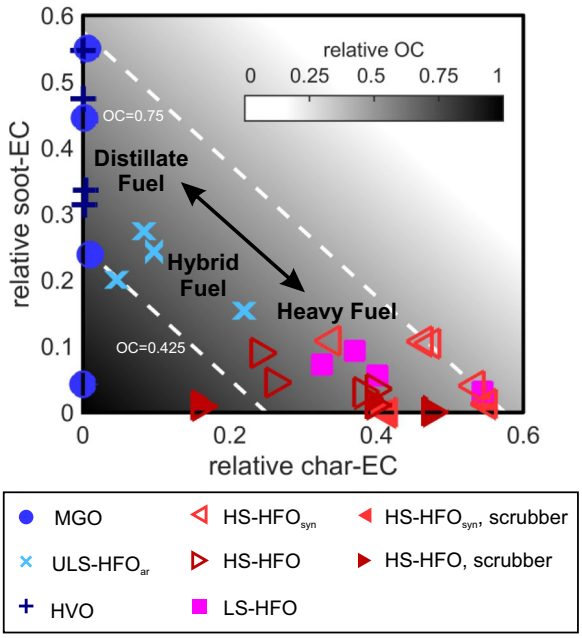

Fig. 2 | Distributions of OC, char-EC and soot-EC. Fractions of OC, char-EC (EC1) and soot-EC (EC2 + EC3) of all 24 fuel/engine load combinations. Two branches of the diesel-like fuels HVO and MGO with low char to EC ratio on the one hand and LS-HFO, HS-HFO$_{syn}$ and HS-HFO with high char to EC on the other are apparent, with ULS-HFO$_{ar}$ in between. Dashed lines denote the space of relative OC from 42.5 to 75% where 90% of the experiments fall in. Filled red triangles refer to HS-HFO$_{syn}$ and HS-HFO emissions after open-loop wet scrubber from Jeong et al.[11].

In TOCA during *ImproveA* temperature protocol, graphite layers of char-EC are immediately oxidized along with pyrolytic OC when oxygen is added to the helium atmosphere due to the porous structure and thus larger surface area[32]. Moreover, tar from partial pyrolysis of fuel droplets may also account for EC1, especially in engine operation with HFO, and contains a lower degree of graphitization than in char[19]. In contrast, soot-EC originates from radical reactions in the flame (flame synthesis), building up graphitized soot from hydrocarbon radicals via soot inception. Those soot particles are smaller and more compact, thus less prone to oxidation[32] and quantified at higher temperatures in EC2 and EC3 during TOCA with *ImproveA*.

ULS-HFO$_{ar}$ refer to a SECA-compliant HFO with high aromatic content, but a density similar to conventional HFO and a viscosity as low as diesel-like fuels. In agreement with that, emissions of EC were comprised of comparable char- and soot-EC content. On the one hand, the low viscosity of ULS-HFO$_{ar}$ compared to conventional HFO generates smaller and faster evaporating fuel droplets after injection. It improves the decomposition of the fuel into small hydrocarbon radicals, leading to soot formation by flame synthesis instead of char formation by droplet pyrolysis. Moreover, the small aromatic hydrocarbons in the fuel are intermediate products during flame synthesis and enhance the soot particle formation further. On the other hand, the high fuel density may cause locally fuel-rich zones through slower droplet vaporization, as indicated by the poor ignition ability and limited use at higher engine load of the ULS-HFO$_{ar}$[11], generating char particles by pyrolysis. Based on the obtained result of EC, both processes appear at comparable importance.

An alternative explanation for the observed abundancies of char- and soot-EC may be the content of metals and sulfur, which inversely correlates with the detection of soot-EC except for HS-HFO$_{syn}$ (Supplementary Fig. S3). Metals and oxygen-containing anions, such as sulfate, are known to promote EC oxidation in thermal analysis[33] but also suppress the formation of soot and soot precursors already during the combustion[34,35]. When ships change their fuels at crossing the border into a SECA, it requires time until the fuel has been completely exchanged in all parts of the fuel system and injection pumps, including metal-containing residues of previously used heavy fuels. Khan et al.[36] reported 84 and 90 min until SO_2 emission concentrations have decreased by 95% after changing from HFO to MGO for an ocean-going vessel. However, the metal content between HFO and MGO differs by two orders of magnitude, hence even a longer switching time would be necessary for metal concentrations approaching those of MGO, assuming that metals exhibit the same behavior as sulfur. As the metal content of the particulate emissions depends on the fuel metal content, fuel switching times likely shift the distribution of evolving carbon to less refractive carbon fractions[37].

In addition to shifts in EC oxidation, the water content of the filter samples as well as the high load of organics proved challenging for the exact determination of EC in PM emissions of ships, affecting the split between OC and EC[37,38]. However, the detected amount of pyrolytic OC was low compared to EC1, hence the ratio of soot-to-char EC cannot be significantly smaller.

EC in slow-speed two-stroke engine emissions are dominated by char-EC regardless of the fuel, while only medium-speed four-stroke engines operated on distillate fuel reveal significant contributions by soot-EC[27,39,40], which agrees with the findings of this study. Hence, the EC fractions may provide an additional fuel-sensitive indicator for ship emissions from auxiliary engines regardless of sulfur scrubber operation. However, at the borders of SECA when fuel switching is required, residues of bunker fuel might affect the EC classification of the emission although distillate fuel is used.

Optical aerosol properties

For allocating absorption of PM2.5 (represented by TC) from the marine engine into BC and BrC, an Angström Absorption Exponent (AAE) of unity and that absorption by BC only happens in the near infrared (NIR) was assumed. For HFO, BrC-related absorption (>5% of total absorption at 405 nm and 450 nm) was only detected at 25% engine load, which is in agreement with previous studies[18,19] and illustrated by AAE larger than unity with the exception of HVO (Fig. 3 top). However, the observed contribution to light absorption by BrC in MGO emissions at 25% engine load, as indicated by an AAE of 1.6, was likely caused by no measurable content of EC. Largest contributions of BrC to total absorption at 405 and 450 nm were found for ULS-HFO$_{ar}$ and HS-HFO with 30% and 15%, respectively. Nevertheless, the majority of absorption in the spectral range from 405 to 980 nm could be explained by BC for all fuels.

Owing to the differences in soot structure, engine operation on diesel-like fuels HVO and MGO generates stronger absorbing particles, indicated by the mass absorption efficiency (MAE$_{TC}(\lambda)$) integrated over wavelengths from 405 to 980 nm (Fig. 3 top). The MAE$_{TC,\lambda}$ of the seven individual wavelengths of the MW-TOCA may be found in Supplementary Table S3. Interestingly, ULS-HFO$_{ar}$ revealed the largest AAE among all fuels, but comparably low MAE$_{TC,\lambda}$. Overall, marine fuels compliant with the global sulfur limit may have manifold effects on light-absorbing properties of ship particulate emissions, driven by various physical and chemical fuel properties.

The Simple Forcing Efficiency (SFE) was introduced by Chen & Bond (2010)[41] to obtain the quantitative radiative effect of aerosol particles per mass in [W g^{-1}]. Here, a reduced approached of SFE is used without the effect of aerosol particles on scattering and integrated from 405 to 980 nm according to:

$$SFE_{405}^{980} = \tau_{atm}^2 \times (1 - F_c) \times a_s \times \int_{405nm}^{980nm} MAE_{TC}(\lambda) \times \frac{S(\lambda)}{4} d\lambda \quad (1)$$

where S(λ) is the solar radiation spectrum at 37° angle of incidence (AM15G) in W m^{-2} in steps of 1 nm, τ_{atm} is the atmospheric transmission, F_c is the cloud fraction, and a_s is the surface albedo. The same atmospheric scenario for τ_{atm}, F_c, and a_s was used as in Tian et al. [42], which denotes global averages of 0.79, 0.6 and 0.19, respectively. Other climate scenarios can be

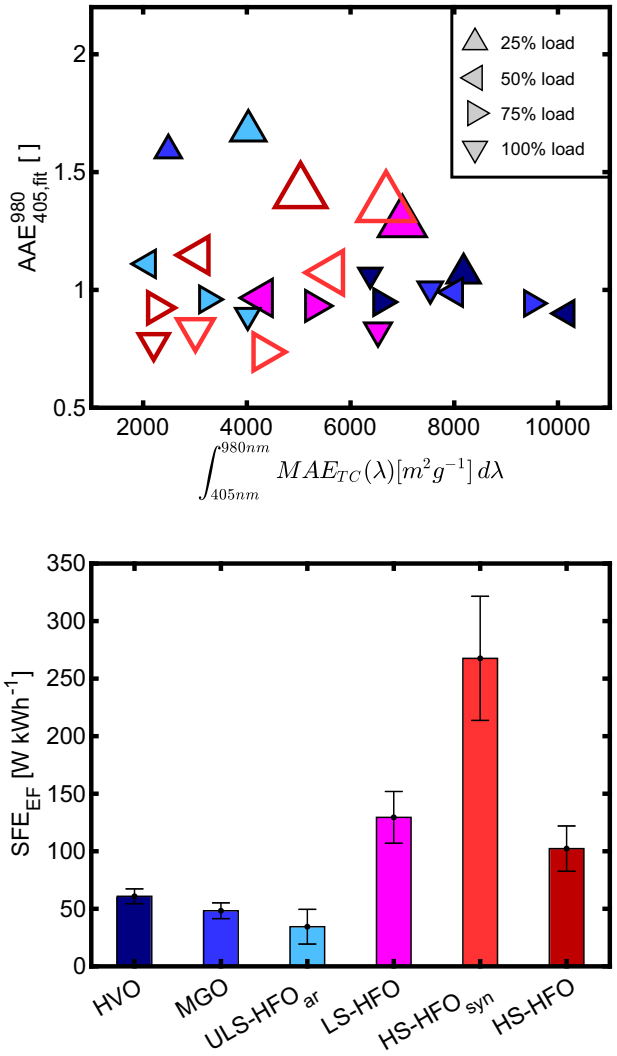

Fig. 3 | Absorption weighted by EF_{TC}. Top: Angström Absorption Exponent (AAE) from exponential fit vs. the integrated mass absorption efficiencies related to total carbon (MAE_{TC}) from 405 to 980 nm for individual engine loads. Marker sizes increase with emission factor of total carbon (EF_{TC}). Open symbol indicates non-compliant fuels with colors as labeled below. Bottom: Sime Forcing Efficiency Emission Factor (SFE_{EF}) integrated from 405 to 980 nm and weighted according to the IMO cycle E2. Errorbars were derived from the integrated 95% confidence prediction band from λ vs. $MAE_{TC}(\lambda)\times EF_{TC}$ (Supplementary Fig. S4).

easily adapted to change quantitative SFE, however, the consequences of fuel switching remain unaffected in this approach.

In order to take quantitative emission data for light-absorption into account, $MAE_{TC}(\lambda)$ in $m^2\ g^{-1}$, obtained from a power law fit of λ vs $MAE_{TC}(\lambda)$ (Supplementary Fig. S4), were multiplied with EF_{TC} in g kWh^{-1} and weighted according to the IMO cycle E2.

$$SFE_{EF} = SFE^{980}_{405} \times EF_{TC} \quad (2)$$

The SFE_{EF} shows a similar pattern (Fig. 3 bottom) to the emission factors for OC and EC (Fig. 1). Switching from the three HFO to SECA-compliant fuels reduced the SFE_{EF} by a factor of two to seven, depending on the individual considered fuel. Particularly engine operation on low-grade HFO, such as HS-HFO_{syn} of this study, generates the most intense light absorption in the spectral range from 405 to 980 nm per kWh of produced energy. LS-HFO and HS-HFO comprising of compounds with a smoother volatility continuum show similar SFE_{EF} despite a difference in FSC of 1.7 percentage points.

Although ULS-HFO_{ar} as a hybrid fuel appeared in between typical HFO and diesel-like fuels, it features the lowest SFE_{EF}. Similar to typical HFO, the $MAE_{TC,\lambda}$ for ULS-HFO_{ar} was lower than for MGO and HVO, but emission factors appeared closer to the diesel-like fuels. Therefore, considering light absorption of its carbonaceous material, ULS-HFO_{ar} has the lowest immediate climate effects among the six studied fuels. However, other criteria including direct climate effects by light scattering, indirect climate effects by induced cloud formation[20], and possibly more health-relevant emissions through the enhanced release of PAH and sustainable engine operation must be considered for an evaluation of the benefit from lower SFE_{EF}.

Identification of marine fuel operation by elemental carbon analysis

Based on EC fractions in the *ImproveA protocol*, fuel classes of HFO, diesel-like fuels and hybrid fuels may be distinguished in the laboratory. Due to the distinct effect of the fuel properties on the nature of EC, it was hypothesized that the EC structure of those particles is reflected in the distribution of carbon clusters produced by laser desorption/ionization in single-particle mass spectrometry (SPMS). This information may increase the confidence in the identification of ship particulate emissions based on traces of transition metals[24] and the molecular signatures of PAH using resonance-enhanced multiphoton ionization (REMPI)[43,44], providing ship fuel identification in real-time. In fact, the clustering algorithm applied to 5000 LDI anion mass spectra of carbon fragment ions $^{12}C_n^-$ for $n = 2, 3, \ldots, 9$ for compliant fuels MGO, LS-HFO and ULS-HFO_{ar} at 75% engine load generated 7 distinct cluster centers, which were dominated by one of the three fuels (Fig. 4). Dependent on the fuel, the pattern of the cluster centers show the highest relative contribution of small ($1 < n < 4$), medium ($3 < n < 7$) and large ($6 < n < 10$) $^{12}C_n^-$ for LS-HFO, MGO and ULS-HFO_{ar}, respectively. Char particles, which are mainly associated with conventional HFO emissions, might decompose to smaller carbon fragment ions on a larger scale because of their porous morphology compared to the more compact soot particles, which are mainly associated with MGO emissions (Fig. 4). Specifically, clusters with highest contribution by ULS-HFO_{ar} particles contained large ($6 < n < 10$) C_n^-, which might be a result of higher initial availability of soot particle precursors and consequently more intense soot inception, but these clusters contribute less to the total cluster weights. However, a larger dataset and complementary measurements of ongoing ships are necessary to confirm the findings and to demonstrate the applicability for remote fuel identification from mid-range transport of ship plumes.

Discussion

Regulations of the FSC by the IMO in the past decade led to an overall shift of marine fuels from HFO, or generally called bunker fuels, to distillate fuels with an intrinsically lower FSC, such as MGO[10]. However, due to the higher price of distillate fuels, other solutions for ship owners became attractive, including low-sulfur bunker fuels, hybrid fuels with properties between typical HFO and MGO but compliant with FSC limits, and the installation of sulfur scrubbers, still enabling engine operation with high-sulfur bunker fuels. Sulfur scrubbers are an investment, which have to redeem for the ship owner, hence sulfur scrubbers are most attractive if the price spread between MGO and HFO is large and especially for ships of a higher lifespan[45]. For older ships, low-sulfur fuels are economically more favorable, but they span a broad range of chemical composition due to its different manufacturing process[3], which complicates an assessment of possible benefits and drawbacks from FSC regulations on public health and climate. Furthermore, it requires a reassessment and further development of markers for the detection of ship emission in the atmospheric environment.

Regarding carbonaceous emissions, our study demonstrates that the FSC is not the determining factor. LS-HFO and HS-HFO of similar quality had comparable EF, whereas the HS-HFO_{syn} with discontinuous boiling behavior caused significantly higher EF for both OC and EC. Therefore, the global sulfur cap to FSC of 0.5% does not seem to affect OC and EC emissions if heavy fuels are still used, but ULS fuels with an FSC < 0.1% lead

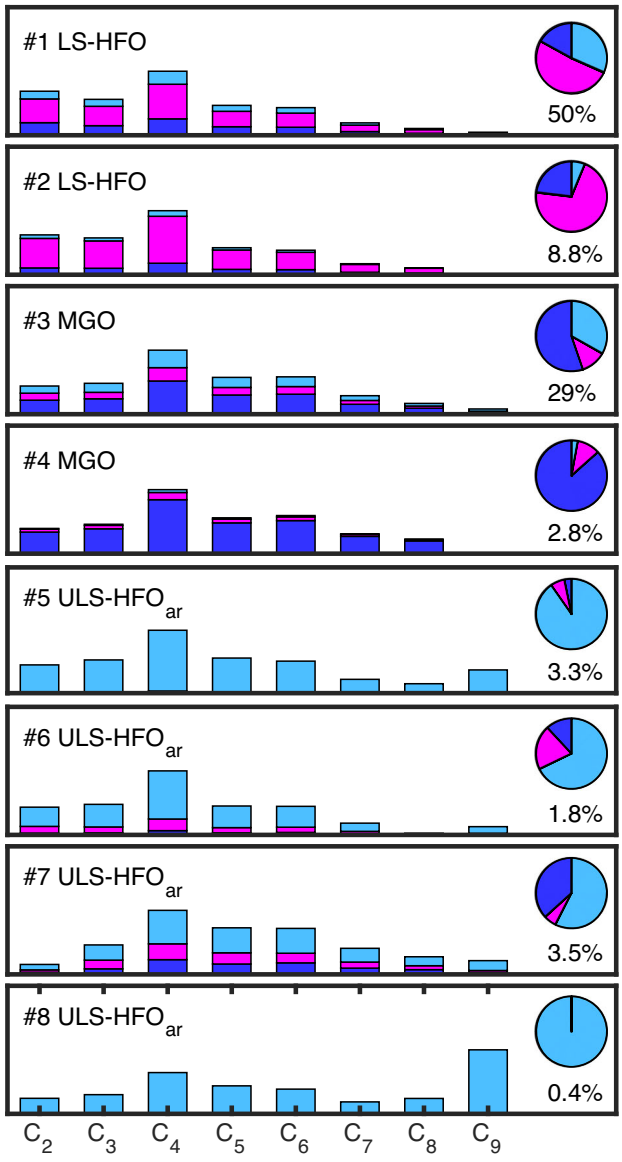

Fig. 4 | Eight clusters of typical C_n distributions in the mass spectra of anions from 5000 single particles for each of the three fuels. Cluster names are derived from the fuel that contributes most to the cluster. The particle number contributions of the fuels are shown as pie charts while the signal contribution is color-coded. Percentages denote the contribution of the individual cluster to the total number of detected particles. Apparently, the bunker fuel LS-HFO with a dominant char content produces smaller carbon fragments while the soot-dominated particles from distillate fuels lead to larger carbon fragments with the ULS-HFO$_{ar}$ in between. (0.5% FSC compliant fuel: LS-HFO (magenta) and SECA compliant fuels: MGO (dark blue) and ULS-HFO$_{ar}$ (light blue)).

to a significant reduction in EF for both OC and EC by a factor of 2–2.5 compared to LS-HFO and HS-HFO, regardless their differences in chemical fuel composition. Therefore, the introduction of SECA has basically a benefit for public health by lower OC and EC emissions, assuming equal toxicity of PM2.5 from all fuels. However, a recent study exposing human lung cells to PM2.5 from marine fuels demonstrates that this is not a justified assumption[29] and may be used to refine health benefits from FSC regulation.

Only an upper FSC limit of 0.1% as currently applicable in SECA shows a decrease in OC and EC emissions because it shrinks the range of compliant bunker fuels to an extend that lighter fuels with lower EF prevail. However, even in SECA this may be circumvented by using sulfur scrubbers, which do not significantly affect the quantitative emissions of PM2.5 but EC or equivalent BC[11] and the composition of high-molecular weight compounds[46].

For the Arctic, new measures become into force in July 2024, prohibiting fuels with a kinematic viscosity larger than 180 mm^2 s^{-1}, and thus banning engine operation on conventional HFO. However, emerging hybrid fuels, such as ULS-HFO$_{ar}$, are not covered by this legislation. Considering that unburned fuel is a major contributor to organic ship emissions[47], the combustion of ULS-HFO$_{ar}$ releases large amounts of two- to four-ring PAH, which are potent precursors of secondary organic aerosol (SOA). Therefore, to reduce secondary PM2.5 from ships and especially to protect sensitive environments such as the Arctic region, a more precise regulation would be required.

Among all three SECA-compliant fuels, the EF of TC were not significantly different despite their distinct difference in origin and chemical composition as well as in market price. Moreover, considering the EF and absorption properties of the carbonaceous emissions in SFE$_{EF}$, a similar ranking of the fuels is obtained as for EF. Therefore, from an economic perspective and for the effect on direct radiative forcing, ULS-HFO$_{ar}$ has the lowest cost/benefit ratio when disregarding its unfavorable ignition behavior and incapability for operation at full engine load. However, particularly PAH-derived health effects and enhanced SOA formation from intermediate-volatile PAH may cancel out low costs and low SFE$_{EF}$. Without considering direct light scattering and indirect effects with a negative effect on radiative forcing, differences between the SFE$_{EF}$ of ULS fuels and LS-/HS-HFO is supposedly smaller. Overall, since 2020 there is evidence for microphysical changes of clouds, also driven by the release and formation of primary and secondary sulfate, and increased radiative warming caused by fuel sulfur legislation on FSC[48,49].

In order to identify marine fuels for operation in ocean-going vessels, SPMS has been shown to provide relevant information from online ship plume measurements in real-time. In addition to the traditional markers vanadium and nickel together with sulfur-related ions[50], the evaluation of polycyclic aromatic compounds[51], and the ultra-sensitive detection of metals by resonant ionization[52] have been developed and used for ship emission studies. This distribution of char- and soot-EC from MW-TOCA is resembled in the pattern of carbon clusters in negative LDI ions where char-EC tends to generate slightly smaller C_n ions than soot-EC. However, the aromatic-rich fuel ULS-HFO$_{ar}$ had distinct contributions from larger C_n, possibly owing to a different soot microstructure than from predominantly aliphatic fuels, such as observed for benzene and n-hexane combustion in diffusion flames[53]. Combining the abundance of sulfur species, PAH pattern, and signature of transition metals with carbon clusters, SPMS is able to identify marine fuels from plume measurements in greater detail, offering a technology for monitoring fuel compliance concerning FSC and potentially beyond.

The main limitation of the findings of this study are their restriction to a four-stroke marine engine, which are typically either used as main engines of smaller ships or as auxiliary engines on larger ones. Main engines of large cargo vessels or tanker are two-stroke engines with different operation principles, fuel requirements and emission pattern. Therefore, further research on two-stroke engine is required to understand indirect effects for climate and public health from latest IMO regulations on FSC and fuel viscosity in the Arctic.

Similar to other transportation sectors, marine traffic is heading for decarbonization or shifts to carbon-neutral fuels from biogenic feedstock, recycling or reusing[7]. Particularly those which are carbon-free, including hydrogen and ammonia, or burned together with a carbon-based pilot fuel necessary for improved ignition, will change the physical-chemical properties of particulate emissions and consequently bring up new challenges for source identification of marine combustion engines and consequences for climate and health.

Methods

Engine operation, marine fuels and PM2.5 sampling

Particulate emissions were investigated from a direct injection four-stroke, single-cylinder research marine engine of 80 kW nominal power, which was operated at four individual loads (25, 50, 75 and 100%) and six marine fuels with different levels of sulfur compliance. Five independent repetitions were

conducted for each combination of engine load and fuel, so 120 samples were collected in total.

High-sulfur heavy fuel oils (HS-HFO and HS-HFO_{syn}) exceed the maximum FSC of 0.5% and are therefore not compliant anymore since 2020 without exhaust aftertreatment. The subscript "syn" indicates that this fuel was produced by artificial blending of vacuum distillation residue with middle distillate fuel, in order to generate a boiling gap and thus a low-grade fuel; HS-HFO denotes a commercial marine bunker fuel. LS-HFO also refers to a commercial HFO, but with a FSC of 0.5%, so it can be used outside SECA. Inside SECA, marine gas oil (MGO) is a commercial compliant fuel, which has high similarity to diesel and a FSC of 10 ppm. Furthermore, hydrotreated vegetable oil (HVO, FSC < 10 ppm) and ultralow-sulfur aromatic-rich heavy fuel oil (ULS-HFO_{ar}, FSC of 0.06%) were tested as alternative SECA-compliant fuels. HVO is obtained from the hydrogenation of vegetable oil. It is chemically composed of alkanes, lighter than MGO and has an intrinsically lower level of impurities including heteroatoms and metals, hence regarded as "clean" fuel. Since the engine was operated with optimized settings for bunker fuels, there is still potential to lower emissions from HVO combustion. Despite being classified as HFO due to its high density, ULS-HFO_{ar} is highly similar to distillate fuels like MGO in terms of sulfur, metal content, viscosity, and flash point. This cycle oil is produced from the fluid catalytic cracking of crude oil and predominantly composed of alkylated 2- to 4-ring aromatics. As expected from the high calculated carbon aromaticity index (CCAI) of 907, slightly exceeding the common range from 800 to 880, ULS-HFO_{ar} has a relatively poor ignition property by means of ignition delay, leading to abrupt energy conversion and high combustion temperatures. Consequently, the engine could not be operated safely at full load, so the maximum engine load for ULS-HFO_{ar} was reduced from 80 kW (100%) to 68 kW (85%). Fuel properties are listed in Supplementary Table S1, further information of the setup and experiments may be found in Jeong et al.[29].

Prior to the experiments, the engine received a major overhaul and exchange of fuel injector nozzles, sleeve and piston skirt among other. Each change of fuel was accompanied by a change of lubrication oil to enhance the detectability of fuel change on the emissions.

For each combination of fuel and engine load, five samples of PM2.5 were collected at a dilution from 25 to 100, achieved by a two-stage dilution system (eDilutor, Dekati Ltd., Finland), on quartz fiber filters (QFF) for offline analysis. The dilution decreases the exhaust gas temperature and let gas-particle partitioning approach ambient equilibrium. Although different dilution ratios affect the condensation of semi-volatile compounds, the net effect is considered to be small because of generally low contribution of OC1 to TC (Supplementary Table S2). Due to low sampling times of 20 min, revolatilization of sampled PM2.5 ("filter blow-off") is negligible. Conversion to emission factors (EF) was based on exhaust gas flow and engine power as described in Mueller et al.[22].

Multi-wavelength Thermal-optical Carbon Analysis (MW-TOCA)

A punch of 0.5 cm^2 from the QFF was analyzed by a thermo-optical carbon analyzer (DRI TOCA 2001A; Reno, NV, USA) using the temperature protocol *ImproveA*, defining five fractions of organic (OC1-OC4 and OCpyro) and three fractions of elemental carbon (EC1-EC3)[54]. Precisions of the carbon analysis is sample-dependent and range between 2 and 6% for TC and 5 to 10% of the split between OC and EC, according to the manufacturer's manual, but may be larger for high content of OC[37,38]. Laser transmittance (LT) at 635 nm was used to correct apparent EC by pyrolytic OC formed by charring. Furthermore, the TOCA was retrofitted with seven light emitting diodes at 405, 450, 532, 780, 808 and 980 nm[23]. The multi-wavelength TOCA (MW-TOCA) was used to measure the light attenuation (ATN) at individual wavelengths λ, which was obtained from ratio of LT of the untreated filter sample and LT at the end of the TOCA. LT measurement artifacts were corrected considering multiple scattering and shadowing effect by factors R(ATN) including f = 1.1 and C of 2.14[55]. In order to compare the absorptivity of PM2.5 from different marine fuels and loads, the mass absorption efficiency (MAE_λ) was calculated for the quantified total carbon (TC = OC + EC) by relating ATN at seven wavelengths to the TC filter load [TC], assuming no non-carbonaceous particle components do significantly absorb light:

$$MAE_{TC,\lambda} = \frac{ATN}{R(ATN)\cdot C\cdot[TC]} \quad (3)$$

The uncertainty of the $MAE_{TC,\lambda}$ varies with filter load, wavelength and composition of TC. Median uncertainties for MAE_λ in the visible UV and near-infrared range are 25 and 50%, respectively, at 95% confidence.

The spectral MAE(λ) dependence on the wavelength follows a power law

$$MAE(\lambda) = \beta \cdot \lambda^{-\alpha} \quad (4)$$

where α is also called Angström Absorption Exponent (AAE) and β denotes a fitting coefficient. For a wavelength pair, e.g. 405 and 808 nm, the uncertainty of the AAE determination is within ±15% at 95% confidence based on the average precision of 8% for the LT measurement[23], while for the exponential fit, 95% of the individual AAE had an uncertainty within ±50%. All data from MW-TOCA represented mean values of five individually collected filter samples.

Single-particle mass spectrometry

Particulate emissions from the marine engine were fed into a cyclone with a cut-off of 10 µm at a temperature of 200 °C and diluted with an eDiluter (Dekati Ltd.; Kangasala, Finland) before entering a single-particle mass spectrometer (SPMS; Photonion GmbH, Schwerin, Germany). In order to mitigate different concentrations of PM10 in the emissions, dilutions were set to 25 (MGO), 100 (LS-HFO) and 50 (ULS-HFO_{ar}).

From a total flow of 1 L min^{-1}, 0.1 L min^{-1} entered the SPMS. Common SPMS system have a steep drop in optical particle detection efficiency below 200 nm. Therefore, to enable the detection range to ultrafine particles (PM0.1), the ionization laser (KrF excimer laser at 248 nm wavelength, pulse energy of 6mJ; PhotonEX, Photonion GmbH, Schwerin, Germany) was operated unsynchronized to optical particle detection at 100 Hz repetition rate[43]. In this so-called free-running mode, particles were randomly hit for laser desorption/ionization (LDI)[51] by the cost of missing particle size information. The spectra were recorded using a 14-bit digitizer (ADQ14, Teledyne SP Devices AB, Sweden) and a customized Labview software., In this study, only carbon clusters (C_n with $n = 2\ldots9$) from negative LDI were considered.

Statistical data analysis

If not otherwise stated, ranges of uncertainty refers to single standard deviations.

The clustering of SPMS data were conducted by adaptive resonance theory neural network algorithm, ART-2a[56]. The program code was taken from the open-source toolkit FATES[57] and embedded in custom MATLAB software (MathWorks Inc.). Carbon cluster related m/z of LDI mass spectra in negative mode were L_2-normalized and clustered using a vigilance factor of 0.8, a learning rate of 0.05, and 20 iterations, followed by a regrouping algorithm to form mean clusters[58].

Data availability

The datasets used and/or analyzed during the current study is partially included the supplementary information and available from the corresponding author on reasonable request.

Received: 9 July 2024; Accepted: 11 November 2024;
Published online: 22 November 2024

References

1. Jalkanen, J.-P., Johansson, L. & Kukkonen, J. A comprehensive inventory of ship traffic exhaust emissions in the European sea areas in 2011. *Atmos. Chem. Phys.* **16**, 71–84 (2016).

2. Corbett, J. J. et al. Mortality from Ship Emissions. A Global Assessment. *Environ. Sci. Technol.* **41**, 8512–8518 (2007).
3. Ershov, M. A. et al. Technological Potential Analysis and Vacant Technology Forecasting in Properties and Composition of Low-Sulfur Marine Fuel Oil (VLSFO and ULSFO) Bunkered in Key World Ports. *J. Mar. Sci. Eng*. **10**, 1828 (2022).
4. Corbin, J. C. et al. Trace Metals in Soot and PM2.5 from Heavy-Fuel-Oil Combustion in a Marine Engine. *Environ. Sci. Technol.* **52**, 6714–6722 (2018).
5. Moldanová, J. et al. Physical and chemical characterisation of PM emissions from two ships operating in European Emission Control Areas. *Atmos. Meas. Tech.* **6**, 3577–3596 (2013).
6. Huang, C. et al. Emission factors of particulate and gaseous compounds from a large cargo vessel operated under real-world conditions. *Environ. Pollut.* **242**, 667–674 (2018).
7. Aakko-Saksa, P. T. et al. Reduction in greenhouse gas and other emissions from ship engines: Current trends and future options. *Prog. Energy Combust. Sci.* **94**, 101055, https://doi.org/10.1016/j.pecs.2022.101055 (2023).
8. The Marine Environment Protection Committee (MEPC). Resolution mepc.192 (61). 2010 guidelines for monitoring the worldwide average sulphur content of fuel oils supplied for use on board ships (2010).
9. The Marine Environment Protection Committee (MEPC). Resolution mepc.329(76). Amendments to the annex of the international convention for the prevention of pollution from ships, 1973, as modified by the protocol of 1978 relating thereto (2021).
10. Chu Van, T., Ramirez, J., Rainey, T., Ristovski, Z. & Brown, R. J. Global impacts of recent IMO regulations on marine fuel oil refining processes and ship emissions. *Transp. Res. D.* **70**, 123–134 (2019).
11. Jeong, S. et al. Aerosol emissions from a marine diesel engine running on different fuels and effects of exhaust gas cleaning measures. *Environ. Pollut.* **316**, 120526 (2023).
12. Lehtoranta, K. et al. Particulate Mass and Nonvolatile Particle Number Emissions from Marine Engines Using Low-Sulfur Fuels, Natural Gas, or Scrubbers. *Environ. Sci. Technol.* **53**, 3315–3322 (2019).
13. Jang, E., Choi, S., Yoo, E., Hyun, S. & An, J. Impact of shipping emissions regulation on urban aerosol composition changes revealed by receptor and numerical modelling. *NPJ Clim. Atmos. Sci.* **6**, 52 (2023).
14. Repka, S. et al. Assessing the costs and environmental benefits of IMO regulations of ship-originated SOx and NOx emissions in the Baltic Sea. *Ambio* **50**, 1718–1730 (2021).
15. van Roy, W. et al. International maritime regulation decreases sulfur dioxide but increases nitrogen oxide emissions in the North and Baltic Sea. *Commun. Earth Environ*. **4**, https://doi.org/10.1038/s43247-023-01050-7 (2023).
16. Wu, D. et al. Primary Particulate Matter Emitted from Heavy Fuel and Diesel Oil Combustion in a Typical Container Ship: Characteristics and Toxicity. *Environ. Sci. Technol.* **52**, 12943–12951 (2018).
17. Oeder, S. et al. Particulate matter from both heavy fuel oil and diesel fuel shipping emissions show strong biological effects on human lung cells at realistic and comparable in vitro exposure conditions. *PLOS ONE* **10**, e0126536 (2015).
18. Corbin, J. C. et al. Brown and Black Carbon Emitted by a Marine Engine Operated on Heavy Fuel Oil and Distillate Fuels: Optical Properties, Size Distributions, and Emission Factors. *J. Geophys. Res. Atmos.* **123**, 6175–6195 (2018).
19. Corbin, J. C. et al. Infrared-absorbing carbonaceous tar can dominate light absorption by marine-engine exhaust. *NPJ Clim. Atmos. Sci.* **2**, 3985–3994 (2019).
20. Santos, L. F. E. D. et al. Marine Fuel Regulations and Engine Emissions: Impacts on Physicochemical Properties, Cloud Activity and Emission Factors. *J. Geophys. Res. Atmos*. **129**, https://doi.org/10.1029/2023JD040389 (2024).
21. Sofiev, M. et al. Cleaner fuels for ships provide public health benefits with climate tradeoffs. *Nat. Commun.* **9**, 406 (2018).
22. Mueller, L. et al. Characteristics and temporal evolution of particulate emissions from a ship diesel engine. *Appl. Energy* **155**, 204–217 (2015).
23. Chen, L.-W. A. et al. Multi-wavelength optical measurement to enhance thermal/optical analysis for carbonaceous aerosol. *Atmos. Meas. Techn.* **8**, 451–461 (2015).
24. Passig, J. et al. Detection of ship plumes from residual fuel operation in emission control areas using single-particle mass spectrometry. *Atmos. Meas. Tech.* **14**, 4171–4185 (2021).
25. Anders, L. et al. Polycyclic aromatic hydrocarbons as fuel-dependent markers in ship engine emissions using single-particle mass spectrometry. *Environ. Sci. Atmos*. https://doi.org/10.1039/D4EA00035H (2024).
26. Zhang, F. et al. Emission factors for gaseous and particulate pollutants from offshore diesel engine vessels in China. *Atmos. Chem. Phys.* **16**, 6319–6334 (2016).
27. Hou, W. et al. On-board measurements of OC/EC ratio, mixing state, and light absorption of ship-emitted particles. *Sci. Tot. Environ.* **904**, 166692 (2023).
28. Lähteenmäki-Uutela, A., Yliskylä-Peuralahti, J., Repka, S. & Mellqvist, J. What explains SECA compliance: rational calculation or moral judgment? *WMU J. Marit. Aff.* **18**, 61–78 (2019).
29. Jeong, S. et al. In vitro genotoxic and mutagenic potentials of combustion particles from marine fuels with different sulfur contents. *bioRxiv,* https://doi.org/10.1101/2024.06.27.601016 (2024).
30. Han, Y. et al. Evaluation of the thermal/optical reflectance method for discrimination between char- and soot-EC. *Chemosphere* **69**, 569–574 (2007).
31. Zhu, J., Lee, K. O., Yozgatligil, A. & Choi, M. Y. Effects of engine operating conditions on morphology, microstructure, and fractal geometry of light-duty diesel engine particulates. *Proc. Combust. Inst.* **30**, 2781–2789 (2005).
32. Elmquist, M., Cornelissen, G., Kukulska, Z. & Gustafsson, Ö. Distinct oxidative stabilities of char versus soot black carbon: Implications for quantification and environmental recalcitrance. *Glob. Biogeochem. Cycl*. **20**, https://doi.org/10.1029/2005GB002629 (2006).
33. Zhao, B. et al. Impact of sulfur functional groups on physicochemical properties and oxidation reactivity of diesel soot particles. *Fuel* **327**, 125041 (2022).
34. Zhang, Z.-H. & Balasubramanian, R. Effects of Cerium Oxide and Ferrocene Nanoparticles Addition As Fuel-Borne Catalysts on Diesel Engine Particulate Emissions: Environmental and Health Implications. *Environ. Sci. Technol.* **51**, 4248–4258 (2017).
35. Streibel, T. et al. Influence of sulphur addition on emissions of polycyclic aromatic hydrocarbons during biomass combustion. *Proc. Combust. Inst.* **35**, 1771–1777 (2015).
36. Khan, M. Y. et al. Benefits of two mitigation strategies for container vessels: cleaner engines and cleaner fuels. *Environ. Sci. Technol.* **46**, 5049–5056 (2012).
37. Aakko-Saksa, P. et al. Considerations in analysing elemental carbon from marine engine exhaust using residual, distillate and biofuels. *J. Aerosol Sci.* **126**, 191–204 (2018).
38. Momenimovahed, A. et al. Comparison of black carbon measurement techniques for marine engine emissions using three marine fuel types. *Aerosol Sci. Technol*. **56**, 46–62 (2022).
39. Zhang, Y., Zhao, K., Lou, D. & Fang, L. Study on the real-world emission characteristics of gaseous and particulate pollutants from an inland ship using a portable emission measurement system. *Mar. Pollut. Bull.* **184**, 114205 (2022).
40. Zhang, F. et al. Size-segregated characteristics of organic carbon (OC), elemental carbon (EC) and organic matter in particulate matter (PM) emitted from different types of ships in China. *Atmos. Chem. Phys.* **20**, 1549–1564 (2020).
41. Chen, Y. & Bond, T. C. Light absorption by organic carbon from wood combustion. *Atmos. Chem. Phys.* **10**, 1773–1787 (2010).

42. Tian, J. et al. Impacts of biomass burning and photochemical processing on the light absorption of brown carbon in the southeastern Tibetan Plateau. *Atmos. Chem. Phys.* **23**, 1879–1892 (2023).
43. Anders, L. et al. Detection of ship emissions from distillate fuel operation via single-particle profiling of polycyclic aromatic hydrocarbons. *Environ. Sci.: Atmos.* **3**, 1134–1144 (2023).
44. Passig, J. et al. Single-particle characterization of polycyclic aromatic hydrocarbons in background air in northern Europe. *Atmos. Chem. Phys.* **22**, 1495–1514 (2022).
45. Jiang, L., Kronbak, J. & Christensen, L. P. The costs and benefits of sulphur reduction measures. Sulphur scrubbers versus marine gas oil. *Transp. Res. D.* **28**, 19–27 (2014).
46. Schneider, E. et al. Humic-like Substances (HULIS) in Ship Engine Emissions: Molecular Composition Effected by Fuel Type, Engine Mode, and Wet Scrubber Usage. *Environ. Sci. Technol.* **57**, 13948–13958 (2023).
47. Sippula, O. et al. Particle emissions from a marine engine: chemical composition and aromatic emission profiles under various operating conditions. *Environ. Sci. Technol.* **48**, 11721–11729 (2014).
48. Diamond, M. S. Detection of large-scale cloud microphysical changes within a major shipping corridor after implementation of the International Maritime Organization 2020 fuel sulfur regulations. *Atmos. Chem. Phys.* **23**, 8259–8269 (2023).
49. Yuan, T. et al. Abrupt reduction in shipping emission as an inadvertent geoengineering termination shock produces substantial radiative warming. *Commun. Earth Environ.* **5**, 281 (2024).
50. Ault, A. P. et al. Characterization of the single particle mixing state of individual ship plume events measured at the Port of Los Angeles. *Environ. Sci. Technol.* **44**, 1954–1961 (2010).
51. Zimmermann, R. & Hanley, L. Photoionization and Photo-Induced Processes in Mass Spectrometry. In *Fundamentals and Applications* (Wiley-VCH, 2021).
52. Passig, J. et al. Resonance-enhanced detection of metals in aerosols using single-particle mass spectrometry. *Atmos. Chem. Phys.* **20**, 7139–7152 (2020).
53. Kobayashi, Y., Furuhata, T., Amagai, K. & Arai, M. Soot precursor measurements in benzene and hexane diffusion flames. *Combust. Flame* **154**, 346–355 (2008).
54. Chow, J. C. et al. The IMPROVE_A Temperature Protocol for Thermal/Optical Carbon Analysis. Maintaining Consistency with a Long-Term Database. *J. Air Waste Manag. Assoc.* **57**, 1014–1023 (2007).
55. Weingartner, E. et al. Absorption of light by soot particles. Determination of the absorption coefficient by means of aethalometers. *J. Aerosol Sci.* **34**, 1445–1463 (2003).
56. Carpenter, G., Grossberg, S. & Rosen, D. B. ART 2-A. An Adaptive Resonance Algorithm for Rapid Category Learning and Recognition. *Neural Netw.* **4**, 493–504 (1991).
57. Sultana, C. M., Cornwell, G. C., Rodriguez, P. & Prather, K. A. FATES. A flexible analysis toolkit for the exploration of single-particle mass spectrometer data. *Atmos. Meas. Tech.* **10**, 1323–1334 (2017).
58. Zhao, W., Hopke, P. K. & Prather, K. A. Comparison of two cluster analysis methods using single particle mass spectra. *Atmos. Environ.* **42**, 881–892 (2008).

Acknowledgements

This study was funded by the Federal Ministry for Economic Affairs and Climate Action (project “SAARUS”, grant number 03SX483D), dtec.bw-Digitalization and Technology Research Center of the Bundeswehr (funded by the European Union – NextGenerationEU, projects “LUKAS” and “MORE”), and the German Science Foundation (Project "PlumeBaSe" ZI 764/32-1; SFB 1477 “Light-Matter Interactions at Interfaces” 441234705). Hendryk Czech ackowledges funding from the Helmholtz Association (Helmholtz International Laboratory aeroHEALTH, grant number InterLabs-0005). We would like to acknowledge Seongho Jeong, Mohammad Saraji-Bozorgzad, Martin Sklorz, and the staff at LKV for their support in the construction of the experimental setup and sample collection.

Author contributions

M.B. conducted the thermal-optical carbon analysis, data processing and evaluation, interpretation of the results and contributed to the manuscript draft. H.C. conceived the study, interpreted the results, performed the statistical data analysis and wrote the manuscript draft. L.A. and J.P. operated the SPMS, conducted its data processing and evaluation. U.E. supervised the experiments, constructed the experimental setup, collected metadata, operated the engine and monitored its performance. J.B. supervised the experiments, constructed the experimental setup, and collected metadata and filter samples. T.S. conceived the study and supervised the experiments. T.W.A., B.B. and R.Z. acquired funding, conceived the study and provided resources. All authors contributed in editing and approved the manuscript.

Funding

Open Access funding enabled and organized by Projekt DEAL.

Competing interests

The authors declare no competing interests.

Additional information

Supplementary information The online version contains supplementary material available at https://doi.org/10.1038/s41612-024-00838-4.

Correspondence and requests for materials should be addressed to Hendryk Czech.

https://doi.org/10.5194/egusphere-2024-2587
Preprint. Discussion started: 12 September 2024

A solid-state IR laser for two-step desorption/ionization processes in single-particle mass spectrometry

Marco Schmidt[1,2,3], Haseeb Hakkim[1,2,3], Lukas Anders[1,2,3], Aleksandrs Kalamašņikovs[1,2,3], Thomas Kröger-Badge[1,2,3], Robert Irsig[3,4], Norbert Graf[5], Reinhard Kelnberger†[5], Johannes Passig[1,2,3] and Ralf Zimmermann[1,2,3]

[1]Joint Mass Spectrometry Centre, Analytical Chemistry, University Rostock, 18059 Rostock, Germany
[2]Joint Mass Spectrometry Centre, Helmholtz Zentrum München, 85764 Neuherberg, Germany
[3]Department Life, Light & Matter, University of Rostock, 18051 Rostock, Germany
[4]Photonion GmbH, 19061 Schwerin, Germany
[5]InnoLas Laser GmbH, 82152 Krailling, Germany
† deceased

Correspondence to: Johannes Passig (Johannes.Passig@uni-rostock.de)

Abstract. Recent advancements in single-particle mass spectrometry (SPMS) have enabled the detection of aromatic hydrocarbons at the individual particle level in conjunction with inorganic/refractory particle components. However, the laser desorption (LD) of organic material from particles prior to their ionization in a two-step process necessitates pulsed infrared lasers with adequate pulse energy that can be irregularly triggered on detected particles. Pulsed CO_2 lasers with a 10.6 µm wavelength have been traditionally utilized, yet these lasers are bulky, costly, and require regular maintenance, including gas exchange or a continuous laser gas supply. In this study, we present the application of a prototype solid-state laser based on an erbium-doped yttrium aluminum garnet (Er:YAG) crystal, emitting long pulses of 200 µs at 3 µm wavelength as a compact, cost-effective, and user-friendly alternative for LD. We directly compared the new laser with a commonly used CO_2 laser and found similar performance in LD for both laboratory particles and ambient air experiments. With the exception of slightly increased fragmentation observed with the CO_2 laser due to its beam profile, no qualitative differences were noted in the resulting mass spectra. Additionally, we compared the novel two-step ionization scheme for the combined detection of aromatic molecules and inorganics with conventional single-step laser desorption/ionization (LDI) for the detection of polycyclic aromatic hydrocarbons (PAH) in laboratory and field experiments. The combined methods demonstrated superior performance in the detection of PAHs, for both the CO_2 and the new Er:YAG laser. In addition to its higher sensitivity and lower fragmentation for PAHs when compared to single-step LDI, it is less dependent on the particle matrix, sharing the benefits of traditional two-step methods but extending its capability to combine PAH measurements with the LDI-based detection of inorganic particle compounds.

https://doi.org/10.5194/egusphere-2024-2587
Preprint. Discussion started: 12 September 2024

1 Introduction

Single-particle mass spectrometry (SPMS) has significantly expanded our understanding of aerosols and atmospheric processes due to two inherent characteristics of the technique. (I) By desorbing and ionizing individual particles using laser pulses, SPMS reveals the mixing state of the particle ensemble, i.e., the distribution of chemicals within individual particles. This allows the detection of subpopulations of particles, their sources, and the investigation of atmospheric processes in complex aerosols. (II) Unlike prevalent bulk methods based on thermal desorption, such as the Aerodyne Aerosol Mass Spectrometer (AMS) or proton transfer reaction-based methods for aerosols (Reinecke et al., 2024a, 2024b), SPMS also captures refractory particle compounds like metals and mineral dust components (Pratt and Prather, 2012; Passig and Zimmermann, 2021; Laskin et al., 2018; Marsden et al., 2019; Zawadowicz et al., 2017; Passig et al., 2020).

In most SPMS instruments, particles are hit by intense, focused UV laser pulses to create a sufficient ion signal for less abundant particle components via laser desorption/ionization (LDI). With few exceptions, organic molecules are fragmented in this process, making their speciation difficult. In contrast to the use of single UV laser pulses for LDI, so-called two-step approaches first use an IR laser pulse to vaporize the organic matter from the particle, and a second UV laser pulse to hit the resulting plume and ionize the molecules in the gas phase. The separation of laser desorption (LD) and ionization allows the independent optimization of both processes. This has several advantages: while LD alone is still a complex process resulting in the vaporization of molecules at high temperatures, the laser intensities and photon energies can be much lower compared to LDI, reducing fragmentation (Schmidt et al., 2023). Because ionization occurs in the gas phase, matrix effects are reduced which is beneficial for quantifying approaches (Woods et al., 2001). In addition, gas-phase ionization allows for very soft ionization techniques such as single-photon ionization (SPI) (Nash et al., 2005; Hanna et al., 2009) or resonance-enhanced multiphoton ionization (REMPI) (Gehm et al., 2018). The latter is particularly useful for SPMS because the involved resonances make it very sensitive – a key characteristic when dealing with such small sample volumes as plumes surrounding tiny particles – and it selectively ionizes aromatic molecules with very high efficiency. This is of great benefit for aerosol studies because it detects carcinogenic polycyclic aromatic hydrocarbons (PAHs), ubiquitous air pollutants from combustion processes, and major contributors to the health effects of aerosols (Agudelo-Castañeda et al., 2017; Holme et al., 2019). The two-step LD-REMPI method, introduced in SPMS by Morrical et al. (1998), has been used by a few groups to study PAHs at the single-particle level, e.g., to identify sources of PAHs in ambient air pollution (Bente et al., 2009) or to analyze particles for studying aging effects (Li et al., 2019). One significant disadvantage of these two-step approaches is the missing particle composition from LDI, i.e., the metals, salts, etc.

This constraint has been successfully addressed, first by implementing a series of three laser pulses for LD, REMPI, and LDI in a rather complex setup that enables the measurement of only positive ions (Passig et al., 2017). Meanwhile, a novel technique has been devised to leverage the spatial segregation of the gas plume from the particle residue, enabling the integration of REMPI and LDI into a single laser pulse with a customized radial profile and yielding bipolar LDI spectra in addition to the

https://doi.org/10.5194/egusphere-2024-2587
Preprint. Discussion started: 12 September 2024

PAH signatures (Schade et al., 2019; Zimmermann et al., 2019). The latter method has been successfully applied in ambient air studies and laboratory experiments, showing its potential for source apportionment, new monitoring concepts, and investigations of atmospheric processes (Passig et al., 2022; Anders et al., 2023; Anders et al., 2024). There are also hybrid approaches where LD is applied prior to LDI at 193 nm to reduce fragmentation of organics while providing LDI mass spectra comparable to many other instruments (Zelenyuk et al., 2015).

To date, all two-step methods in SPMS are based on transversely excited atmospheric pressure (TEA) CO_2 lasers, because these systems provide relatively strong and short mid-IR pulses (multi-mJ, ≈ 50–500 ns duration, 10.6 µm wavelength). These lasers are relatively large and expensive, and they have one major disadvantage: they require regular gas changes or even operation with a constant gas flow. The required gas supply limits the use of CO_2-TEA lasers in field studies, especially in situations where aerosol measurements are urgently needed: in arctic regions, on the open sea, in remote areas with limited infrastructure, and for remote controlled long-term operation. For the ionization step in two-step approaches, frequency-quadrupled Nd:YAG lasers at 266 nm offer a low-cost, robust, and maintenance-free alternative to excimer gas lasers. However, a similar solution is still lacking for the LD step.

Here we report on experiments to replace the CO_2 lasers with a prototype Er:YAG solid-state laser at 3 µm wavelength. We evaluate its performance in direct comparison experiments and discuss its potential and limitations in future applications. Besides, we performed comparative experiments and demonstrated superior detection of PAHs using two-step approaches compared to conventional LDI, regardless of the type of laser used for LD.

2 Experimental Section

2.1 Model Particles and Sampling

Laboratory experiments were performed for three different types of PAH-containing particles. (I) Diesel exhaust particles were collected from an old van (VW Transporter type 3, 1.7 D, no exhaust aftertreatment), directly scratched from the inner surface of the exhaust pipe. These particles have a uniform chemical distribution of PAHs from regular exposure to the hot exhaust gas (Passig et al., 2017; Schade et al., 2019). (II) Wood ash particles were collected from an ash sink in the chimney of a 20 kW wood combustion furnace (Bente et al., 2008). Using a small-scale powder disperser (model 3433 SSPD, TSI Inc., St. Paul, MN), diesel soot and wood ash particles were redispersed into a synthetic air stream of 2.5 L min^{-1}, from which 100 mL min^{-1} was introduced into the SPMS system. (III) Tar ball particles were used as a proxy for organic aerosols (Li et al., 2019). The term tar ball refers to near-spherical, homogeneous particles resulting from the combustion of biomass and biofuels and consisting of amorphous carbonaceous species (Pósfai et al., 2004; Hand et al., 2005; Alexander et al., 2008). To produce the tar ball particles, beechwood tar from a hunting supply store was dissolved in methanol, sprayed with an aerosol generator

https://doi.org/10.5194/egusphere-2024-2587
Preprint. Discussion started: 12 September 2024

(ATM 221, Topas GmbH, Germany), and dried using a custom diffusion dryer with a silica gel-filled cartridge. Size distributions of the particles are shown in the supplementary information, Fig. S1.

The ambient air experiments were performed at the ILMARI laboratory of the University of Eastern Finland in the timeframe from March 1, 2024 to March 3, 2024. To record a sufficient number of single-particle spectra from the relatively clean air ($PM_{10} < 4.0$ µg m^{-3} in average), ambient air particles were sampled using an aerosol concentrator (AC-250 v1.0, ParteQ GmbH, Germany). The instrument is based on an advanced design of the discontinued Model 4240 (MSP Corp., now part of TSI Inc., U.S.A.) and concentrates particles in the size range of approximately 0.5–10 µm from a 250 L min^{-1} inlet flow into a 1 L min^{-1} sample stream (Romay et al., 2002). After passing through a dryer (model MD-700-12S-1, Perma Pure LLC, USA), the aerosols underwent additional concentration to 0.1 L/min through a further virtual impactor at the SPMS aerodynamic lens (Zhuo, Z., Su, B., Xie, Q., Li, L., Huang, Z., Zhou, Z., Mai, 2021). The instrument's overall detection efficiencies for the particles used in this study were not determined (Shen et al., 2019).

2.2 SPMS Instrumentation

The basic principle of SPMS systems relies on the optical detection and sizing of aerodynamically accelerated particles before LDI and ion detection in a bipolar time-of-flight mass spectrometry setup (Passig and Zimmermann, 2021; Pratt and Prather, 2012).

The instrument utilized here has been previously described (Schade et al., 2019) and roughly corresponds to the setup commercialized as PhotonLIZA (Photonion GmbH, Germany). A KrF excimer laser (248 nm, PhotonEx, Photonion GmbH, Germany) is used for ionization after laser desorption. The ion signals, from both cations and anions, were recorded by a 14-bit digitizer card (ADQ14, Teledyne SP Devices AB, Sweden) and were analyzed using custom Matlab software, including preprocessing and peak area integration. Classification of the PAH mass spectra from ambient air particles was performed using the adaptive resonance theory neural network ART-2a (Song et al., 1999) from the open-source toolkit FATES (Sultana et al., 2017) using a vigilance factor of 0.75, a learning rate of 0.05, and 20 iterations.

2.3 Optical setup and triggering

In the two-step mode, the particles entering the ion source are exposed to an IR laser pulse for LD, and the gaseous plume is then irradiated with an unfocused UV pulse of medium intensity for soft REMPI of aromatic species. This layout is illustrated in Fig. 1a and was used to study the LD with the Er:YAG laser in comparison to the CO_2 laser for the laboratory particles and the first of two ambient air experiments. To allow a direct comparison of the prototype Er:YAG laser (Er:YAG 1000 FQ, InnoLas Laser GmbH, Germany) with the standard CO_2 laser (Model EX5, GAM Laser Inc., USA), the setup was modified as follows: the two IR lasers were alternately fired from opposite sides of the ion source at the incoming particles; see Fig. 1a and the time cycle included therein. A noise signal characteristic for each laser was imprinted in the mass spectra to ensure the

https://doi.org/10.5194/egusphere-2024-2587
Preprint. Discussion started: 12 September 2024

assignment of each laser to the resulting single-particle spectrum. Notable, that the instrument in this configuration could not record individual particle size information but only average size distributions.

The CO_2 laser and the Er:YAG laser vary not only in their wavelengths but also by several orders of magnitude in their pulse lengths; see Table 1 for detailed optical parameters. This is due to the lack of Q-switching. Within the 200 µs pulse duration, the particles travel a distance of approximately 1-2 cm. Therefore, the laser is not focused but sent, with its full spot size of 5 mm, into the region above the ion source. The reduced spatial and temporal accuracy requirements facilitate alignment in comparison to the CO_2 laser. The lower power density of the Er:YAG pulse is compensated for by the longer exposure time for each individual particle and by the 10 times higher pulse energy. It should be noted, that the pulse-to-pulse energy variation of the Er:YAG laser was large (up to ± 50 % calculated on the average pulse energy, see Fig. S2). This is a result of unstable thermal lensing in the resonator, as this prototype laser was not optimized for random triggering from the incoming particle events. To reduce this, a regular signal of 5 Hz was mixed into the trigger input. The total reduction in hit rate resulting from the combined loss in duty cycle and pulse-to-pulse variations is estimated to be ≈ 30–50 %, compared to a hypothetical stable Er:YAG laser to be developed for irregular triggering in SPMS. However, this is only a rough estimation because the pulse energy required to generate a sufficient plume is highly dependent on the particle properties and composition.

2.4 Implementation in the combined ionization scheme for PAHs and inorganics

At the end of this paper, we present an additional experiment on ambient aerosols to demonstrate the suitability of the Er:YAG laser for the newly developed ionization in SPMS that combines REMPI and LDI in a single laser pulse (Schade et al., 2019), and we compare this method directly with a conventional LDI-based setup. In the combined setup (Fig. 1b), the unfocused beam inducing REMPI with moderate laser intensity is reflected by 180°, is focused, and sent back into the ion source. There, it hits the refractory particle residue, inducing LDI at virtually the same time as the PAHs are ionized in the gas plume via REMPI. The comparison with conventional LDI was realized as follows (Fig. 1, bottom): One particle event triggered the CO_2 laser for LD, followed by the excimer laser for combined ionization. The second particle triggered the same scheme with the Er:YAG laser instead of the CO_2 laser for comparison. The third particle triggered none of the LD lasers but only the excimer laser. As no LD occurred and no gas plume was produced, only the back-reflected beam induced LDI, similar to conventional LDI ionization, with an excimer laser focused by a lens. All triggering schemes were realized using a Complex Programmable Logic Device (CPLD) microcontroller and custom software.

https://doi.org/10.5194/egusphere-2024-2587
Preprint. Discussion started: 12 September 2024

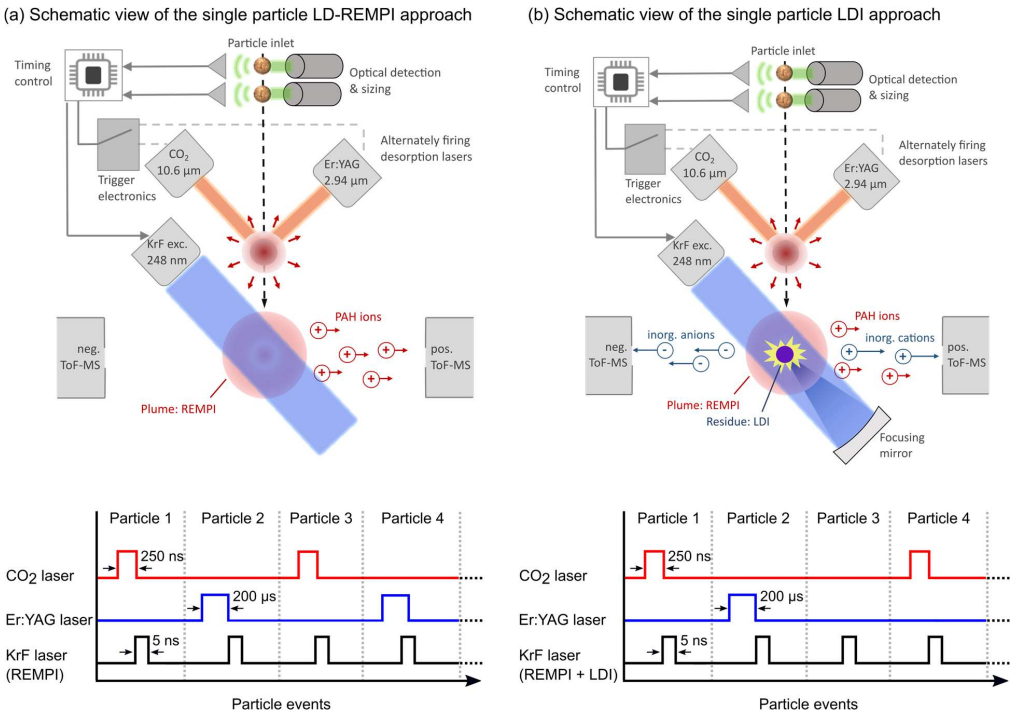

Figure 1 (a) Schematic representation of the single-particle, two-step ionization setup in alternating mode for direct comparison of the two desorption lasers. The particles are optically detected, initiating the SPMS time cycle. The two desorption lasers, i.e., the "standard" CO_2 laser and the experimental Er:YAG laser, are alternately fired at the respective particles, generating a small gas plume for each particle. The subsequent unfocused UV laser pulse ionizes the PAHs in the expanding plume via REMPI. Scheme **(b)** shows the combined method to ionize PAHs by REMPI in the unfocused beam and inorganics by LDI in the back-reflected and focused beam, both from the same laser. In addition to the comparison of the CO_2 laser and the Er:YAG laser for LD in this method, every third particle was not exposed to LD. In this case, only the intense back-reflected UV pulse interacted with the particle, inducing LDI without prior LD, allowing a direct comparison of the combined method with conventional LDI – also for ambient aerosols and on the same instrument.

https://doi.org/10.5194/egusphere-2024-2587
Preprint. Discussion started: 12 September 2024

Table 1 Optical parameters and lasers systems used in the experiments.

	Laser desorption		**REMPI**	**LDI**
Laser type, medium	Gas, CO_2	Solid-state, Er:YAG	Gas-Excimer, KrF	Gas-Excimer, KrF
Wavelength (nm)	10600	2940	248	248
Beam diameter (mm)	1 x 1 (Gaussian)	5 x 5 (Flat top)	5 x 10 (Gaussian x flat top)	0.2 x 0.4 (Gaussian x flat top)
Pulse energy (mJ)	15	160	4	4
Pulse duration	250 ns	200 µs	5 ns	5 ns
Peak irradiance (W cm^{-2})	1.5 x 10^7	3.2 x 10^3	1.6 x 10^6	1.0 x 10^9

3 Results and discussion

3.1. Two-step LD-REMPI for laboratory particles

First, we investigated the suitability of the Er:YAG laser for the LD-REMPI scheme (Fig. 1a) in laboratory experiments for three different PAH-containing particle types, named diesel soot particles, wood ash particles, and tar ball particles. The most probable PAHs reflected in the mass spectra are listed in Table 2. Note that isobar substances, *e.g.,* phenanthrene *vs.* anthracene, *cannot be distinguished.* Figure 2a shows the sum PAH mass spectra of each 500 diesel soot particles, above with LD using the CO_2 laser and below with the Er:YAG laser. The mass spectrometric patterns for both LD lasers are very similar, showing detailed PAH signatures with dominant parent PAHs of low molecular weight from the combustion process (Frenklach, 2002) and some alkylated species, partly consisting of residues from unburned fuel (Spencer et al., 2006; Anders et al., 2023). Note, that the fragments are virtually unrecognizable, underscoring the soft nature of the LD-REMPI approach. The histograms on the right show the distribution of PAH signal intensities among the particles for the two lasers. The CO_2 laser produces very intense PAH mass spectra more frequently, while with the Er:YAG laser more particles with low to moderate signals are observed. This can be attributed to the laser spot geometry: The Er:YAG laser has a large spot and hits the particle with high probability but relatively low intensity, whereas the focused Gaussian profile of the CO_2 laser can result in very high signal intensities when a particle is fully hit. However, the difference is rather moderate, also because of a comparable hit rate for both lasers: 38 % (49 %) of the optically detected particles produced a clear PAH spectrum in this LD-REMPI approach with the CO_2 laser (Er:YAG laser). It is also remarkable, that the signal intensities for the summed mass spectra of the same number of particles are comparable for both lasers, despite the very different laser intensities, durations, and wavelengths. The high degree of similarity can be explained by the underlying physical mechanisms of LD, where the energy transferred to the particle eventually results in thermal desorption for laser pulses longer than a few picoseconds (Schmidt et al., 2023).

https://doi.org/10.5194/egusphere-2024-2587
Preprint. Discussion started: 12 September 2024

Table 2 Polycyclic aromatic hydrocarbons (PAHs) indicated by the measured mass spectra.

PAHs	m/z					
	Number of C in aliphatic side chains					
	0	1	2	3	4	5
Phenanthrene, anthracene	178	192	206	220	234	248
Pyrene, fluoranthene	202	216				
Chrysene(s), benzoanthracene(s), benzophenanthrene(s)	228	242	256	270	284	
Benzopyrene(s), benzofluranthene(s), perylene	252					
Benzo[g,h,i]perylene, indeno[1,2,3-c, d]pyrene	276					
Dibenzophenanthrenes(s), dibenzoanthracene(s)	278					
e.g. Coronen	300					
e.g. Dibenzopyrene(s)	302					
Important fragments	165, 189, 205, 219					

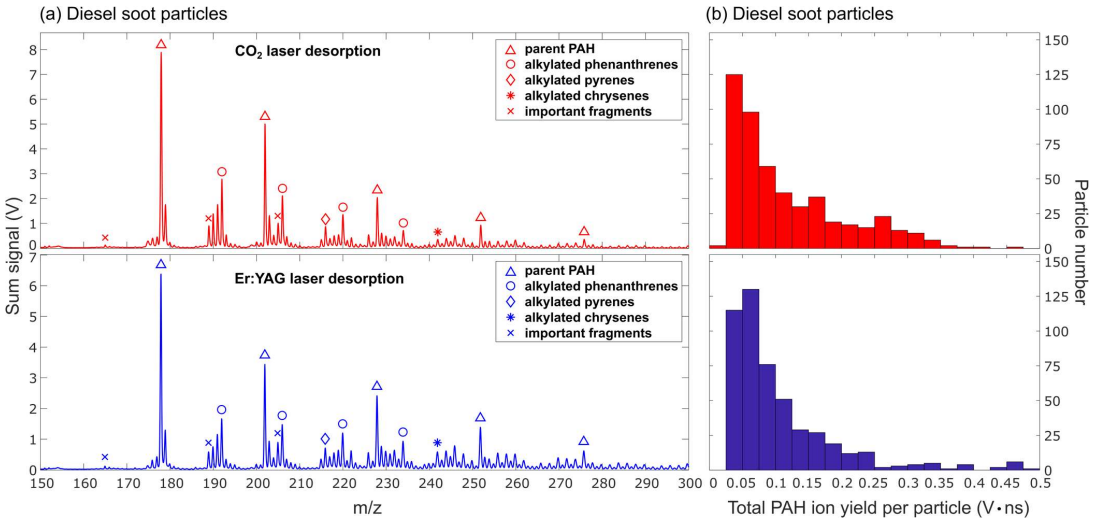

Figure 2 (a) The summed PAH mass spectra of each 500 diesel soot particles exhibit no significant differences when generated by LD-REMPI using a CO_2 laser (top) or the prototype Er:YAG laser (bottom) for the LD step. Note the very low fragmentation of the LD-REMPI method. **(b)** Histogram of the total PAH ion yield per particle. The CO_2 laser produces some more single-particle spectra with very strong PAH signals due to its high peak intensity in its Gaussian beam profile.

https://doi.org/10.5194/egusphere-2024-2587
Preprint. Discussion started: 12 September 2024

As a second representative particle type, wood ash particles were investigated. Here, the hit rate for PAHs was much lower, with only 2 % (4 %) of the optically detected particles showing a PAH spectrum when the CO_2 laser (Er:YAG laser) was used. This is due to the nature of the sample, which contains many burnt ash particles and fewer OC/soot particles containing PAHs (Dall'Osto et al., 2016; Healy et al., 2015). The PAH mass spectra are very different from the PAH signatures of diesel soot particles, highlighting the potential of single-particle PAH detection for source apportionment. Given the completely different fuel, this is not surprising. In addition to parent PAHs as combustion products from the hydrogen-abstraction carbon-addition (HACA) mechanism (Frenklach, 2002), decomposition products from the biomass can also be detected, e.g., a strong signal for retene (m/z = 234). This is a thermal degradation product of resin acids and has often been used as a marker for softwood combustion (Ramdahl, 1983; Shen et al., 2012a) (The stove was mainly fired with spruce logs.). There are also some signals from higher-mass molecules, possibly from oxidized PAHs and other combustion products with aromatic rings, which can be ionized in the LD-REMPI scheme. The comparison between the two LD lasers shows no clear differences. The histogram of single-particle PAH signal strengths on the right indicates again a slightly higher number of particles with very strong PAH signatures, probably due to the beam profile differences discussed above.

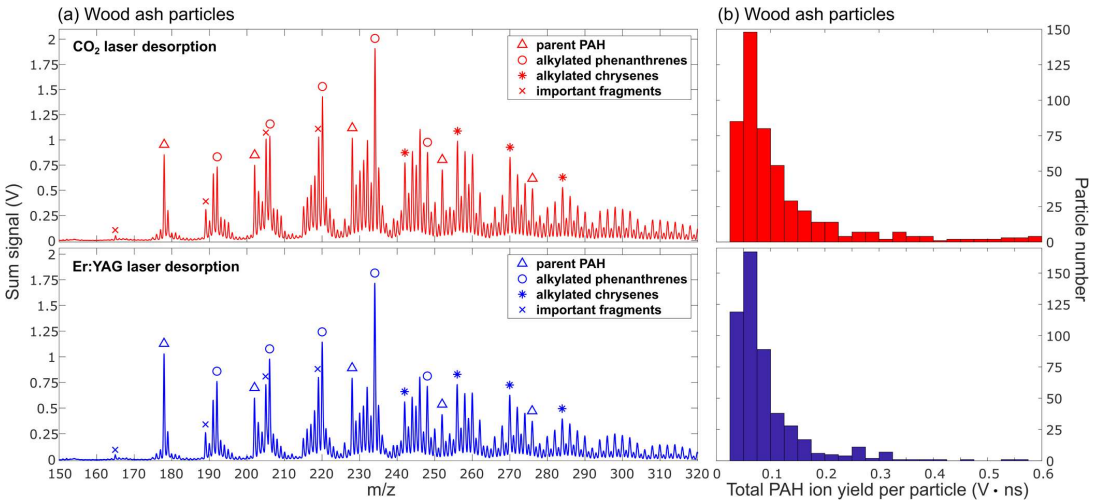

Figure 3 (a) Wood ash particles (n = 500) exhibit a very different PAH profile in the LD-REMPI ionization than diesel soot particles, and they show the softwood combustion marker retene (m/z = 234). However, in direct comparison, there are almost no differences between the CO_2 laser and the Er:YAG laser for LD. **(b)** The single-particle signal intensity of PAHs again shows a few more particles with strong PAH signals for the CO_2 laser.

As a third type of model particle, we focused on tar ball particles. In our case, they were simply sprayed with wood tar and therefore show a signature of only alkylated phenanthrenes (Fig. 4a), in contrast to a more sophisticated tar ball model that we

https://doi.org/10.5194/egusphere-2024-2587
Preprint. Discussion started: 12 September 2024

analyzed in a previous study using the same LD-REMPI technique (Li et al., 2019). However, they appear to be an appropriate and easier to generate model to study LD for the highly relevant organic aerosols from wood combustion, as they have comparable physical properties such as high viscosity, low volatility, and a brown color with high absorption in the UV-VIS due to their PAH content (Jacobson, 2012; Brege et al., 2021; Li et al., 2019). Also, for this particle type, the mass spectral differences between the CO_2 laser and the Er:YAG laser are negligible. Although, the distribution of PAH signal intensities over the particles (Fig. 4b) reveals a higher number of particles with intense PAH signatures for the Er:YAG laser. The reason for this behavior is not known, but we assume that residues of the solvent methanol led to enhancements in the absorption of the Er:YAG laser, since there is a strong absorption band from the O-H stretching vibration in methanol (Linstrom, 1997). In addition, it was difficult to determine the hit rate in these experiments, because there was a small background of the PAH signature from particle evaporation effects in the inlet, even when no particle was hit. A particle hit was defined when the sum of the peak areas exceeded 30 mV · ns, based on the distribution of signal intensities per laser shot; see Fig. 4b. This results in a hit rate of 54 % (49 %) for the CO_2 laser (Er:YAG laser).

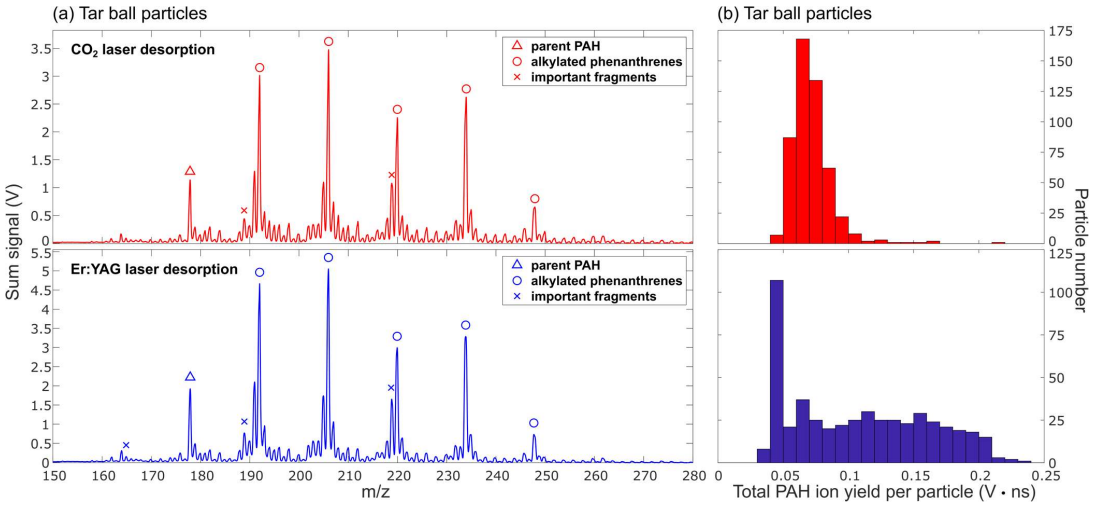

Figure 4 In our case of sprayed wood tar as a proxy for organic aerosols from wood combustion, the sum PAH spectra (n = 500) show almost exclusively alkylated phenanthrenes. While there are no qualitative differences in the mass spectra between the two lasers used for LD, the Er:YAG laser produced intense PAH spectra more often for this particle type. This can be explained by the strong absorption of the solvent methanol at the 3 µm wavelength of the Er:YAG laser.

https://doi.org/10.5194/egusphere-2024-2587
Preprint. Discussion started: 12 September 2024

3.2 Ambient air application of the Er:YAG-based laser desorption

As the laboratory experiments demonstrated the ability of the Er:YAG laser to efficiently desorb organics from different particle types, these results need to be validated in a field study for ambient aerosols. The experiments were conducted at the campus of the University of Eastern Finland in Kuopio, FI (*62.8891° N, 27.6290° E*) from March 1 to 3, 2024. Ambient air masses were sampled at a height of 10 meters above the ground. These air masses came mainly from the south, where the large forests and rural landscapes of Southern Finland and the Baltic States dominate. Backward trajectories were calculated using the HYSPLIT model with GFS 0.25° meteorological fields as the input file (http://www.ready.noaa.gov/HYSPLIT.php, last access: July 8, 2024, see Fig. S3). The average PM_{10} concentration in this winter time period was 4.0 µg m^{-3} and the average $PM_{2.5}$ concentration was 3.4 µg m^{-3} (weather station Kuopio Niirala, https://en.ilmatieteenlaitos.fi/download-observations, last access: July 8, 2024).

Out of 97,063 optically detected particles in 23 hours, 1,450 revealed PAH spectra, defined by the presence of at least five of the peaks listed in Tab. 2. The average mass spectra from each 500 PAH-containing particles are compared in Fig. S4 and show a similar overall pattern for both desorption lasers and a comparable hit rate with slightly higher PAH signals and reduced fragmentation for the Er:YAG laser. As mentioned above, size information is only available at the ensemble average (Fig. S1), but not at the single-particle level.

Beyond performance parameters, these experiments on real-world aerosols should reveal whether different wavelengths and laser parameters affect the results on a single-particle basis. Therefore, the 500 PAH mass spectra from each laser were independently analyzed using the ART-2a clustering algorithm with a vigilance factor of 0.75, 20 iterations, and a learning rate of 0.05 (Sultana et al., 2017). After visual inspection and manual grouping of the 17 (11) ART-2a clusters for the CO_2 laser (Er:YAG laser), four main clusters remained, containing ≈ 95 % of the particles; see Fig. 5. The first three clusters in Fig. 5a and 5b show strong signals from parent PAHs, with distribution maxima at low molecular weight PAHs (LMW, cluster #1), high molecular weight PAHs (HMW, cluster #3), and dominant PAH peaks at m/z = 228 and 252 (cluster #2). Such distributions were previously associated with wood combustion aerosols in ambient air (Passig et al., 2022), and the dominant peaks for benzo[*a*]anthracenes/chrysene (*m/z* = 228) and benzopyrenes (*m/z* = 252) in cluster #2 are an indicator of a higher photochemical age of the particles (Miersch et al., 2019). Of note, not only the mass spectra but also the number of particles in each cluster are comparable for the two desorption lasers, emphasizing a high degree of similarity between the two desorption processes despite the different wavelengths. The main difference between the two lasers is the higher fragmentation of the CO_2 laser, resulting in cluster #4 with dominant fragments, while the fourth cluster produced by the Er:YAG laser again shows parent PAHs as the strongest signals, but with a different intensity distribution.

https://doi.org/10.5194/egusphere-2024-2587
Preprint. Discussion started: 12 September 2024

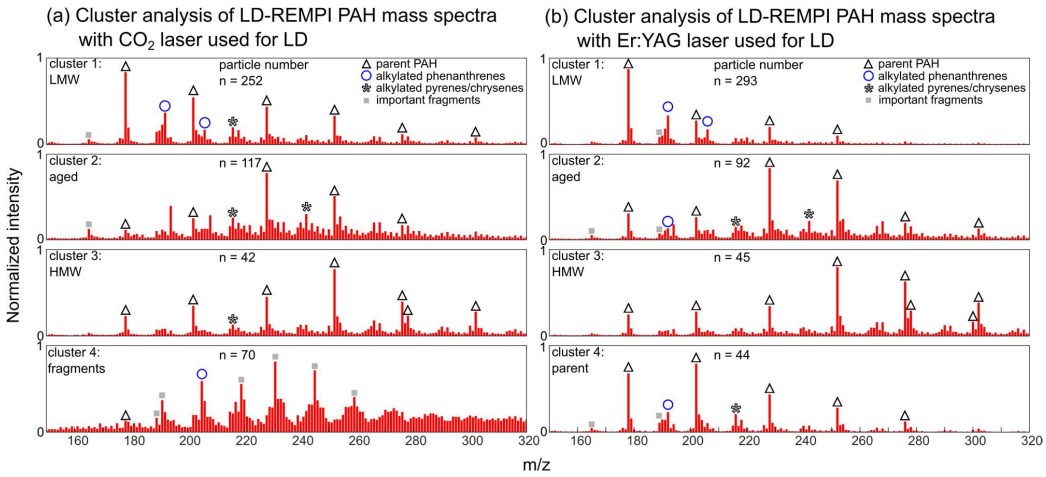

Figure 5 Main ART-2a clusters of each 500 PAH mass spectra from ambient air particles, exposed to **(a)** the CO_2 laser and **(b)** the Er:YAG laser for LD prior to REMPI photoionization. In the first three clusters, containing > 80 % of the particles, not only the mass spectral signatures are similar but also the number of particles in the respective cluster. In the fourth cluster (< 14 % of the particles), significant differences are observed due to the higher fragmentation of the CO_2 laser, which can be explained by its beam profile and higher peak intensity. The results indicate that the compact Er:YAG laser can replace the more commonly used CO_2 lasers for single-particle LD also in ambient air studies.

3.3 Implementation in the combined ionization scheme for PAHs and inorganics – lab experiments

Recent developments using spatially and temporally tailored laser pulses allow the combined analysis of PAHs and inorganic particle constituents by simultaneously inducing REMPI of PAHs in the gaseous plume and LDI of the refractory particle residue (Schade et al., 2019). We investigated the capability of the Er:YAG laser for its implementation in this ionization technique for the same laboratory particles and for ambient air. The back reflection mirror was now used to allow the focused UV beam to be sent back into the ion source for LDI, as shown in Fig. 1b. In addition, the electronics have been modified so that the CO_2 laser and the Er:YAG laser are triggered alternately for LD of the first and second particles as before, and neither of them is triggered for the third particle. In the latter case, the unfocused UV beam does not induce REMPI because no gas plume was previously formed, and the back-reflected UV beam only induces LDI, similar to conventional LDI-based SPMS. This allows a direct comparison of the PAH analysis using the combined ionization scheme with the Er:YAG and CO_2 lasers and with the conventional one-step LDI approach.

Figure 6 shows the results for soot particles, comparing LD with (panel a) the CO_2 laser, (panel b) the Er:YAG laser, and (panel c) one-pulse LDI only. The LDI mass spectra are similar for all three methods, emphasizing that the LD step has no significant effect on the LDI ion formation. For the PAH spectra in Fig. 6a and 6b, a slightly higher fragmentation can be noticed compared to the pure LD-REMPI results shown in Fig. 2. This is due to the back-reflected, narrow, high-intensity

https://doi.org/10.5194/egusphere-2024-2587
Preprint. Discussion started: 12 September 2024

beam for LDI that cuts through a portion of the plume and fragments a fraction of the PAH molecules there. Of note, for the pure LDI process without prior LD, PAH signals are very weak and strongly interfered with molecular fragments (Fig. 6c).

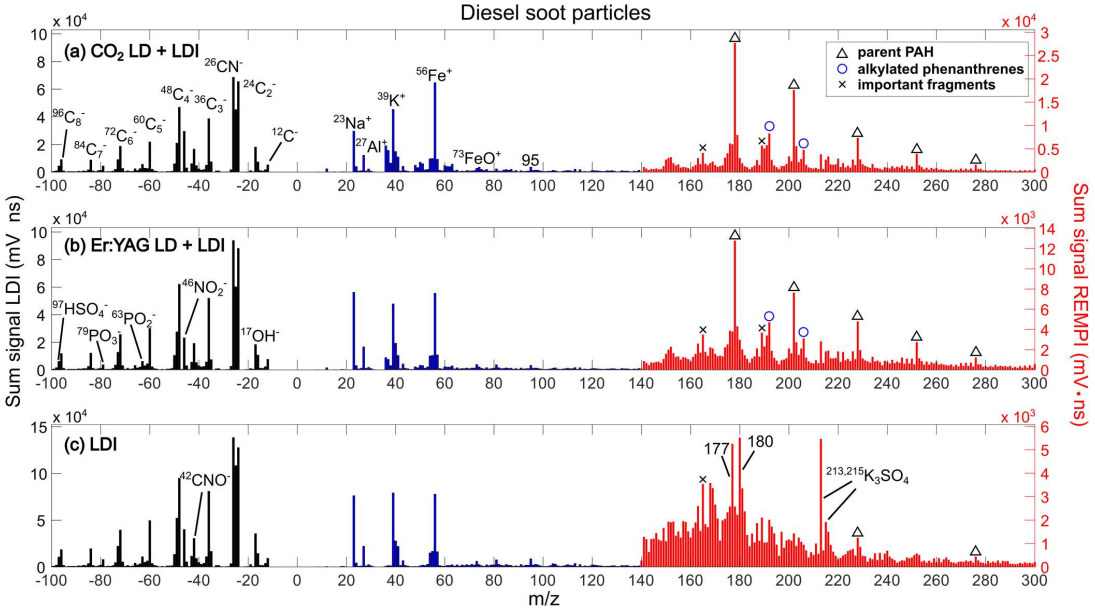

Figure 6 In the combined LD-REMPI/LDI ionization scheme, PAH detection is combined with conventional inorganic characterization via LDI. Neither the PAH signature nor the LDI-derived composition is significantly affected when the CO_2 laser **(a)** is replaced by the Er:YAG laser **(b)** for the LD step. **(c)** In contrast, PAH signatures are barely detectable with conventional single-step LDI ionization. Each n = 500.

For the wood ash particles (Fig. 7), the LDI spectra are comparable, but there are some differences of unknown origin, e.g., enhanced phosphate signals when the CO_2 laser is used for LD. When comparing the PAH signatures in panels (a) and (b), an increased signal at m/z = 178 can be recognized for LD with the Er:YAG laser. This trend is also observed for all other PAH spectra, but to a lesser extent. This may be related to a higher IR absorption of phenanthrene/anthracene at 3 µm compared to the other PAHs (Laurens et al., 2021). In contrast to the diesel soot experiments, PAHs are now also clearly visible for LDI only (Fig. 7c). Obviously, the particle matrix of the wood ash particles supports the ionization of PAHs in LDI. These effects will be discussed in the following sections. Nevertheless, for the combined LD-REMPI/LDI method in Fig. 7a and 7b, the PAH signals are 5–8 times stronger, compare the Y-axes on the right.

https://doi.org/10.5194/egusphere-2024-2587
Preprint. Discussion started: 12 September 2024

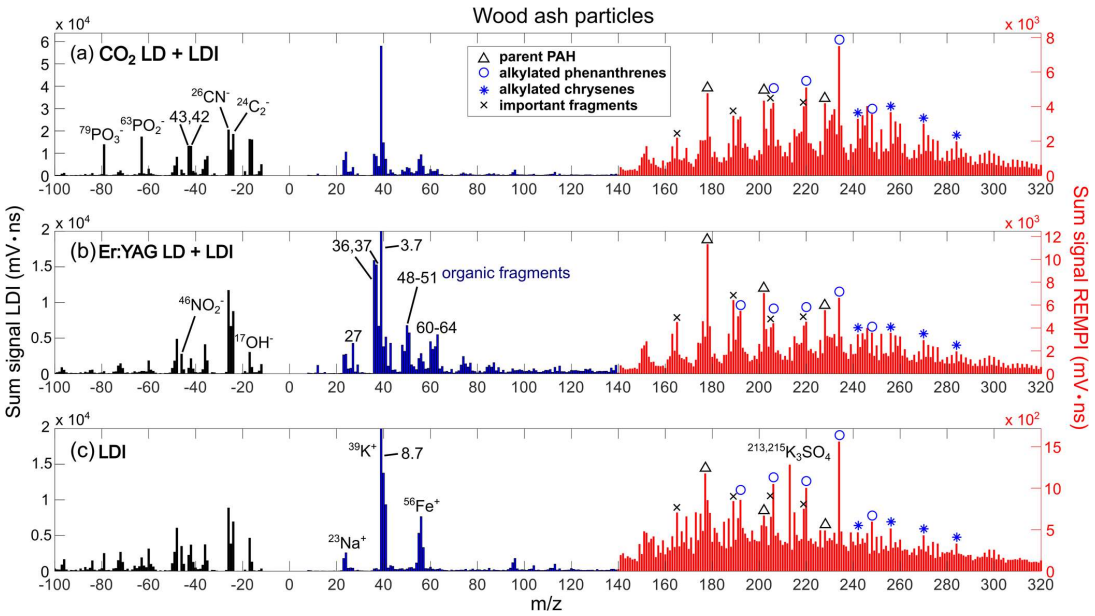

Figure 7 For wood ash particles, the combined method yields comparable results for **(a)** the CO_2 laser and **(b)** the Er:YAG laser applied for LD. Due to the nature of these particles, the single-step LDI method also produces clear PAH signatures, but with a lower sensitivity (compare the Y-axes on the right). Each n = 500.

In the case of tar ball particles, the LDI mass spectra in Fig. 8a and 8b show similar fragmentation patterns. This indicates that resonant excitation of the OH-stretch vibration by the Er:YAG laser does not influence the subsequent LDI when investigating organic aerosols. The PAH signatures are again comparable and approximately four times stronger than the one-step LDI process shown in panel c. Interestingly, the LDI mass spectra in panel c are different, showing stronger signals of soot and inorganic components. This points to the matrix effect of soot: only two types of real-world particles are capable of producing spectra with intact PAHs in one-step LDI: those with strong soot contributions (Zimmermann et al., 2003) and particles with dominant parent PAHs via so-called self-matrix ionization (Zhu et al., 2024). This underlines the superior and more universal PAH detection of two-step methods with LD-REMPI ionization, which is much less dependent on the particle matrix (Woods et al., 2001).

https://doi.org/10.5194/egusphere-2024-2587
Preprint. Discussion started: 12 September 2024

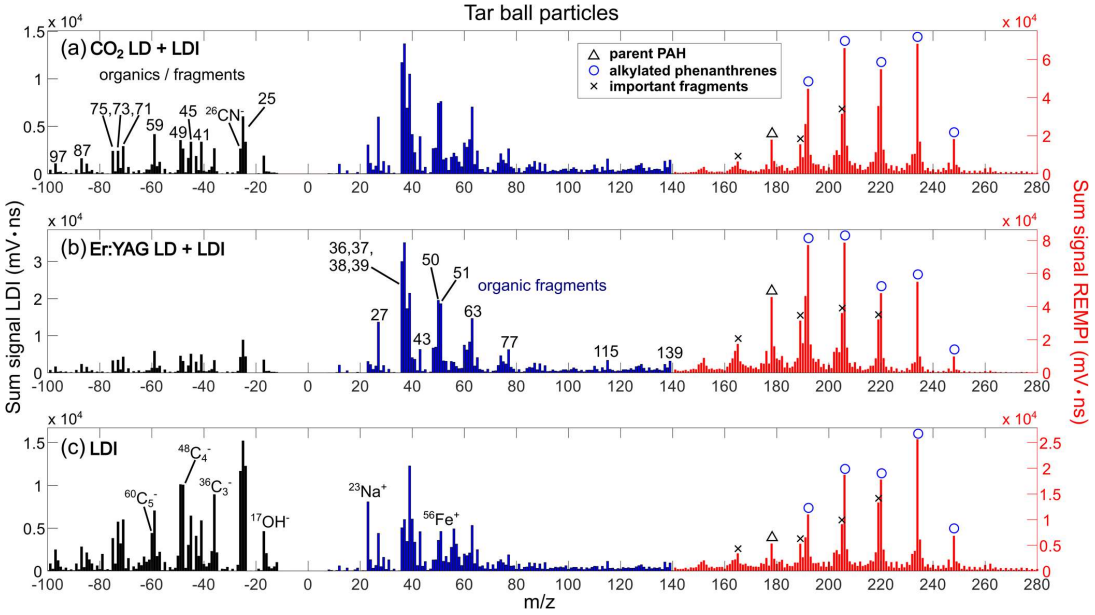

Figure 8 (a) and **(b)** Tar ball particles show comparable behavior in the combined LD-REMPI/LDI scheme, independent of the laser used for LD. **(c)** However, in single-step LDI, only particles with soot signatures and more pronounced signals from inorganics produce PAH mass spectra, underscoring the need for an UV-absorbing and ionization-enhancing matrix in LDI. Each n = 500. LDI anion signals are enhanced three times for better visibility.

3.4 Implementation in the combined ionization scheme for PAHs and inorganics – ambient air experiments

In an extension of the ambient air experiments shown in Sect. 3.2, we continued the measurements for another 6 hours, now with the combined ionization scheme (Fig. 1b). Data analysis is more complex in this case because the signals from inorganics and PAH patterns should be analyzed separately (Passig et al., 2022). From 30,000 optically detected particles, 16,600 produced a cation LDI spectrum and 12,700 revealed bipolar LDI mass spectra, corresponding to a hit rate of about 55 % (42 % bipolar; see X. Shen et al., 2024 for a comparison of hit rates for different LDI-based SPMS instruments). From these particles, 1,846 showed additional PAH signatures as determined by the presence of at least five of the major PAH peaks listed in Tab. 2 (648 particles for the CO_2 laser, 644 for the Er:YAG laser, and 518 for LDI with the Excimer laser only). We selected 500 particles for each laser and analyzed their PAH pattern using ART-2a clustering; see Fig. S5 for the results. A detailed discussion of the particle ensemble is beyond the scope of this paper. In short, the PAH-containing particles were predominantly aged wood combustion particles with strong K^+ peaks and pronounced secondary sulfate and nitrate signals, and sometimes soot signatures. Both the Er:YAG laser and the CO_2 laser produced comparable patterns of PAH mass spectra,

https://doi.org/10.5194/egusphere-2024-2587
Preprint. Discussion started: 12 September 2024

however, with partly different numbers of particles in the respective classes (Fig. S5). For the LDI process only, without previous LD and REMPI ionization in the plume, the vast majority of mass spectra were dominated by fragments. This can be recognized more easily from Fig. 9, where the number of particles with dominant PAH peaks is illustrated for the three different laser excitation schemes.

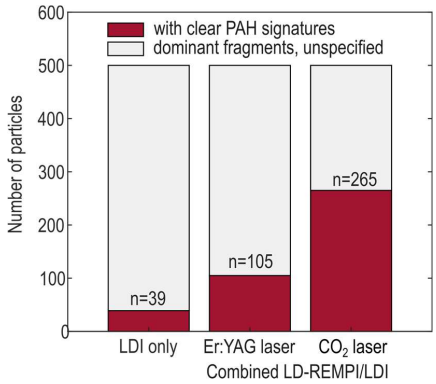

Figure 9 In a direct comparison of ambient air aerosols, the combined LD-REMPI/LDI ionization schemes yield PAH mass spectra with much higher efficiency compared to conventional LDI. In the experiments shown here, the prototype Er:YAG laser suffered from pulse-to-pulse instabilities. For a more stable Er:YAG laser, we expect a similar efficiency in detecting PAHs as for the CO_2 laser in the future. The high prevalence of stable parent PAHs and soot components favors the CO_2 laser and LDI ionization compared to the Er:YAG laser. For some particle types, PAHs are barely detectable with LDI; compare Fig. 6. The mass spectra and a cluster analysis are shown in the Supplement, Fig. S5.

Obviously, the Er:YAG laser was less efficient in producing clear PAH spectra than the CO_2 laser in this experiment. For a given particle type, achieving efficient plume expansion necessitates a specific laser energy threshold. When pulse energy fluctuations are significant, as for the prototype laser used here (refer to Supplementary Fig. S2), low pulse energies can result in inefficient plume expansion, thereby diminishing the hit rate and reducing signal intensities in the mass spectra – a problem that will be solved with a more stable laser in the future. As noticeable from Fig. 9, the pure LDI process also produced some clean and evaluable spectra. Once again, it should be noted that these results are strongly dependent on the experimental conditions and particle type. It is well known that soot can act as an efficient matrix for PAH ionization in LDI, also in SPMS (Zimmermann et al., 2003). Most of the PAH-containing particles detected here reveal also soot signatures by the presence of C_n- clusters in negative LDI spectra (Fig. S5), while in other field studies PAHs were mainly detected on organic carbon particles without clear soot signatures (Passig et al., 2022). Parent PAHs, which are the dominant PAH species in the mass spectra observed here, are also particularly stable to fragmentation, allowing their analysis with LDI via self-matrix ionization (Zhu et al., 2024). In many other cases, other PAHs are important, such as alkylated phenanthrenes from incomplete combustion, which can indicate the particle source (Anders et al., 2023; Anders et al., 2024), or retene, which is a marker for coniferous wood combustion (Shen et al., 2012b). These PAHs are more susceptible to fragmentation than parent PAHs (Passig

https://doi.org/10.5194/egusphere-2024-2587
Preprint. Discussion started: 12 September 2024

et al., 2021; Gehm et al., 2018; Kruth et al., 2017) and could therefore be underrepresented in LDI. In the present data set, aromatics other than the parent PAHs are almost absent for all three laser excitation schemes, so a systematic comparison of the ratios of alkylated/parent PAHs is not possible. In previous tests in Central Europe at warmer temperatures of about 5–10 °C, only the combined two-step excitation scheme was able to detect PAHs in a similar comparison experiment with LDI (not shown due to technical difficulties with the SPMS system). In the experiment shown here, the weaker performance of the Er:YAG laser compared to the CO_2 laser is probably a result of the large shot-to-shot variability of its pulse energy (see Fig. S2). It may also be related to the high abundance of parent PAHs that better resist the higher peak intensities of the CO_2 laser and the LDI laser beam. In general, the combined LD-REMPI/LDI ionization scheme causes more fragmentation than the LD-REMPI approach alone, since part of the gas plume surrounding the particle is hit by the high-intensity LDI beam. Also, interferences between PAHs and inorganics occur more frequently, e.g., with $K_3SO_4^+$ at m/z = 213 and 215. However, it has the advantage of detecting both inorganic components and PAHs of the same particle.

4 Conclusions and Outlook

We have directly compared a prototype solid-state laser with a more conventional CO_2 laser for laser desorption in two-step approaches for ionization in SPMS. Although the wavelengths (3 µm Er:YAG solid-state laser vs. 10.6 µm CO_2 laser) and pulse lengths (200 µs Er:YAG laser and 250 ns CO_2 laser) differ substantially, the resulting PAH mass spectra show a high degree of similarity, and the hit rate is also approximately comparable. This can be explained by the desorption mechanism for laser pulses in the nanosecond to microsecond range, where the laser energy is eventually transferred to thermal energy and the organic material is ejected by thermal vaporization (Schmidt et al., 2023). Solid-state lasers have multiple advantages over gas lasers in terms of reliability, usability, and cost. In particular, the regular gas changes required for CO_2 lasers and the necessary provision of gas cylinders are avoided, which is of great importance for measurements in remote areas, on ships, or in airplanes. This potential can be fully exploited if the excimer laser is also replaced by a (Nd:YAG) solid-state laser, making the two-step process much more flexible and easier to use. However, the large pulse-to-pulse variability of the current prototype Er:YAG laser needs to be overcome by developing a more stable system, and the maximum repetition rate should be increased to allow measurements also in the unsynchronized “free-running” mode for ultrafine particles (Anders et al., 2023; Anders et al., 2024; Erdmann et al., 2005).

We also evaluated the advantages of the recently developed two-step approach with combined ionization for PAHs and inorganics (Schade et al., 2019) by direct comparison with conventional LDI ionization. The combined method clearly showed improvements in the detection of health and environmentally relevant PAHs by spatially separating the LD-REMPI and LDI processes. The technique facilitates detecting clear PAH signatures and inorganic/refractory particle components simultaneously. In addition to the higher detection rates for PAHs, we concluded that the combined technique is universally

https://doi.org/10.5194/egusphere-2024-2587
Preprint. Discussion started: 12 September 2024

applicable to mixed aerosols, which has been demonstrated previously (Passig et al., 2022; Anders et al., 2024), whereas conventional LDI is more limited to soot-containing particles (Zimmermann et al., 2003), pure PAH particles (Zhang et al., 2023), and could potentially introduce a bias toward parent PAHs. Furthermore, we have illustrated that the advantages of two-step processes extend beyond a specific type of desorption laser, as evidenced by comparing a solid-state Er:YAG laser with a CO_2-TEA laser.

Data availability. Data are available on request from Johannes Passig (johannes.passig@uni-rostock.de).

Author contributions. M.S., H.H., and J.P. performed the SPMS experiments. M.S. and J.P. analyzed the data. T.K.B., L.A., A.K., and R.I. provided technical assistance. R.K. and N.G. constructed the Er:YAG laser. M.S. and J.P. wrote the manuscript. J.P. conceived the experiments. J.P. and R.Z. raised funding.

Conflicts of Interest. The authors declare no conflict of interest.

Acknowledgements

Funded by the Deutsche Forschungsgemeinschaft (DFG, German Research Foundation) - SFB 1477 "Light-Matter Interactions at Interfaces", project number 441234705. This research was supported by the Federal Ministry for Education and Research as part of the joint project HazarDust under the funding code 13N15569.

The authors would like to thank Olli Sippula and colleagues at the University of Eastern Finland for hosting the ambient air experiments.

References

Agudelo-Castañeda, D. M., Teixeira, E. C., Schneider, I. L., Lara, S. R., and Silva, L. F. O.: Exposure to polycyclic aromatic hydrocarbons in atmospheric PM1.0 of urban environments: Carcinogenic and mutagenic respiratory health risk by age groups, Environmental pollution (Barking, Essex 1987), 224, 158–170, https://doi.org/10.1016/j.envpol.2017.01.075, 2017.

Alexander, D. T. L., Crozier, P. A., and Anderson, J. R.: Brown carbon spheres in East Asian outflow and their optical properties, Science (New York, N.Y.), 321, 833–836, https://doi.org/10.1126/science.1155296, 2008.

Anders, L., Schade, J., Rosewig, E. I., Schmidt, M., Irsig, R., Jeong, S., Käfer, U., Gröger, T., Bendl, J., Saraji-Bozorgzad, M. R., Adam, T., Etzien, U., Czech, H., Buchholz, B., Streibel, T., Passig, J., and Zimmermann, R.: Polycyclic aromatic hydrocarbons as fuel-dependent markers in ship engine emissions using single-particle mass spectrometry, Environ. Sci.: Atmos., https://doi.org/10.1039/D4EA00035H, 2024.

https://doi.org/10.5194/egusphere-2024-2587
Preprint. Discussion started: 12 September 2024

Anders, L., Schade, J., Rosewig, E. I., Kröger-Badge, T., Irsig, R., Jeong, S., Bendl, J., Saraji-Bozorgzad, M. R., Huang, J.-H., Zhang, F.-Y., Wang, C. C., Adam, T., Sklorz, M., Etzien, U., Buchholz, B., Czech, H., Streibel, T., Passig, J., and Zimmermann, R.: Detection of ship emissions from distillate fuel operation via single-particle profiling of polycyclic aromatic hydrocarbons, Environ. Sci.: Atmos., 3, 1134–1144, https://doi.org/10.1039/D3EA00056G, 2023.

Bente, M., Sklorz, M., Streibel, T., and Zimmermann, R.: Thermal desorption-multiphoton ionization time-of-flight mass spectrometry of individual aerosol particles: a simplified approach for online single-particle analysis of polycyclic aromatic hydrocarbons and their derivatives, Analytical chemistry, 81, 2525–2536, https://doi.org/10.1021/ac802296f, 2009.

Bente, M., Sklorz, M., Streibel, T., and Zimmermann, R.: Online laser desorption-multiphoton postionization mass spectrometry of individual aerosol particles: molecular source indicators for particles emitted from different traffic-related and wood combustion sources, Analytical chemistry, 80, 8991–9004, https://doi.org/10.1021/ac801295f, 2008.

Brege, M. A., China, S., Schum, S., Zelenyuk, A., and Mazzoleni, L. R.: Extreme Molecular Complexity Resulting in a Continuum of Carbonaceous Species in Biomass Burning Tar Balls from Wildfire Smoke, ACS Earth Space Chem., 5, 2729–2739, https://doi.org/10.1021/acsearthspacechem.1c00141, 2021.

Dall'Osto, M., Beddows, D. C. S., McGillicuddy, E. J., Esser-Gietl, J. K., Harrison, R. M., and Wenger, J. C.: On the simultaneous deployment of two single-particle mass spectrometers at an urban background and a roadside site during SAPUSS, Atmos. Chem. Phys., 16, 9693–9710, https://doi.org/10.5194/acp-16-9693-2016, 2016.

Erdmann, N., Dell'Acqua, A., Cavalli, P., Grüning, C., Omenetto, N., Putaud, J.-P., Raes, F., and van Dingenen, R.: Instrument Characterization and First Application of the Single Particle Analysis and Sizing System (SPASS) for Atmospheric Aerosols, Aerosol Science and Technology, 39, 377–393, https://doi.org/10.1080/027868290935696, 2005.

Frenklach, M.: Reaction mechanism of soot formation in flames, Phys. Chem. Chem. Phys., 4, 2028–2037, https://doi.org/10.1039/B110045A, 2002.

Gehm, C., Streibel, T., Passig, J., and Zimmermann, R.: Determination of Relative Ionization Cross Sections for Resonance Enhanced Multiphoton Ionization of Polycyclic Aromatic Hydrocarbons, Applied Sciences, 8, 1617, https://doi.org/10.3390/app8091617, 2018.

Hand, J. L., Malm, W. C., Laskin, A., Day, D., Lee, T., Wang, C., Carrico, C., Carrillo, J., Cowin, J. P., Collett, J., and Iedema, M. J.: Optical, physical, and chemical properties of tar balls observed during the Yosemite Aerosol Characterization Study, J. Geophys. Res., 110, https://doi.org/10.1029/2004JD005728, 2005.

Hanna, S. J., Campuzano-Jost, P., Simpson, E. A., Robb, D. B., Burak, I., Blades, M. W., Hepburn, J. W., and Bertram, A. K.: A new broadly tunable (7.4–10.2eV) laser based VUV light source and its first application to aerosol mass spectrometry, International Journal of Mass Spectrometry, 279, 134–146, https://doi.org/10.1016/j.ijms.2008.10.024, 2009.

https://doi.org/10.5194/egusphere-2024-2587
Preprint. Discussion started: 12 September 2024

Healy, R. M., Evans, G. J., Murphy, M., Sierau, B., Arndt, J., McGillicuddy, E., O'Connor, I. P., Sodeau, J. R., and Wenger, J. C.: Single-particle speciation of alkylamines in ambient aerosol at five European sites, Analytical and bioanalytical chemistry, 407, 5899–5909, https://doi.org/10.1007/s00216-014-8092-1, 2015.

Holme, J. A., Brinchmann, B. C., Refsnes, M., Låg, M., and Øvrevik, J.: Potential role of polycyclic aromatic hydrocarbons as mediators of cardiovascular effects from combustion particles, Environmental health a global access science source, 18, 74, https://doi.org/10.1186/s12940-019-0514-2, 2019.

Jacobson, M. Z.: Investigating cloud absorption effects: Global absorption properties of black carbon, tar balls, and soil dust in clouds and aerosols, J. Geophys. Res., 117, https://doi.org/10.1029/2011JD017218, 2012.

Kruth, C., Czech, H., Sklorz, M., Passig, J., Ehlert, S., Cappiello, A., and Zimmermann, R.: Direct Infusion Resonance-Enhanced Multiphoton Ionization Mass Spectrometry of Liquid Samples under Vacuum Conditions, Analytical chemistry, 89, 10917–10923, https://doi.org/10.1021/acs.analchem.7b02633, 2017.

Laskin, J., Laskin, A., and Nizkorodov, S. A.: Mass Spectrometry Analysis in Atmospheric Chemistry, Analytical chemistry, 90, 166–189, https://doi.org/10.1021/acs.analchem.7b04249, 2018.

Laurens, G., Rabary, M., Lam, J., Peláez, D., and Allouche, A.-R.: Infrared spectra of neutral polycyclic aromatic hydrocarbons based on machine learning potential energy surface and dipole mapping, Theor Chem Acc, 140, https://doi.org/10.1007/s00214-021-02773-6, 2021.

Li, C., He, Q., Schade, J., Passig, J., Zimmermann, R., Meidan, D., Laskin, A., and Rudich, Y.: Dynamic changes in optical and chemical properties of tar ball aerosols by atmospheric photochemical aging, Atmos. Chem. Phys., 19, 139–163, https://doi.org/10.5194/acp-19-139-2019, 2019.

Linstrom, P.: NIST Chemistry WebBook, NIST Standard Reference Database 69, 1997.

Marsden, N. A., Ullrich, R., Möhler, O., Eriksen Hammer, S., Kandler, K., Cui, Z., Williams, P. I., Flynn, M. J., Liu, D., Allan, J. D., and Coe, H.: Mineralogy and mixing state of north African mineral dust by online single-particle mass spectrometry, Atmos. Chem. Phys., 19, 2259–2281, https://doi.org/10.5194/acp-19-2259-2019, 2019.

Miersch, T., Czech, H., Hartikainen, A., Ihalainen, M., Orasche, J., Abbaszade, G., Tissari, J., Streibel, T., Jokiniemi, J., Sippula, O., and Zimmermann, R.: Impact of photochemical ageing on Polycyclic Aromatic Hydrocarbons (PAH) and oxygenated PAH (Oxy-PAH/OH-PAH) in logwood stove emissions, The Science of the total environment, 686, 382–392, https://doi.org/10.1016/j.scitotenv.2019.05.412, 2019.

Morrical, B. D., Fergenson, D. P., and Prather, K. A.: Coupling two-step laser desorption/ionization with aerosol time-of-flight mass spectrometry for the analysis of individual organic particles, J. Am. Soc. Mass Spectrom., 9, 1068–1073, https://doi.org/10.1016/S1044-0305(98)00074-9, 1998.

Nash, D. G., Liu, X. F., Mysak, E. R., and Baer, T.: Aerosol particle mass spectrometry with low photon energy laser ionization, International Journal of Mass Spectrometry, 241, 89–97, https://doi.org/10.1016/j.ijms.2004.12.016, 2005.

https://doi.org/10.5194/egusphere-2024-2587
Preprint. Discussion started: 12 September 2024

Passig, J. and Zimmermann, R.: Laser Ionization in Single-Particle Mass Spectrometry, in: Photoionization and Photo-Induced Processes in Mass Spectrometry, edited by: Zimmermann, R. and Hanley, L., Wiley, 359–411, https://doi.org/10.1002/9783527682201.ch11, 2021.

Passig, J., Schade, J., Irsig, R., Kröger-Badge, T., Czech, H., Adam, T., Fallgren, H., Moldanova, J., Sklorz, M., Streibel, T., and Zimmermann, R.: Single-particle characterization of polycyclic aromatic hydrocarbons in background air in northern Europe, Atmos. Chem. Phys., 22, 1495–1514, https://doi.org/10.5194/acp-22-1495-2022, 2022.

Passig, J., Zimmermann, R., and Fennel, T.: Fundamentals and Mechanisms of Vacuum Photoionization, in: Photoionization and Photo-Induced Processes in Mass Spectrometry, edited by: Zimmermann, R. and Hanley, L., Wiley, 1–21, https://doi.org/10.1002/9783527682201.ch1, 2021.

Passig, J., Schade, J., Rosewig, E. I., Irsig, R., Kröger-Badge, T., Czech, H., Sklorz, M., Streibel, T., Li, L., Li, X., Zhou, Z., Fallgren, H., Moldanova, J., and Zimmermann, R.: Resonance-enhanced detection of metals in aerosols using single-particle mass spectrometry, Atmos. Chem. Phys., 20, 7139–7152, https://doi.org/10.5194/acp-20-7139-2020, 2020.

Passig, J., Schade, J., Oster, M., Fuchs, M., Ehlert, S., Jäger, C., Sklorz, M., and Zimmermann, R.: Aerosol Mass Spectrometer for Simultaneous Detection of Polyaromatic Hydrocarbons and Inorganic Components from Individual Particles, Analytical chemistry, 89, 6341–6345, https://doi.org/10.1021/acs.analchem.7b01207, 2017.

Pósfai, M., Gelencsér, A., Simonics, R., Arató, K., Li, J., Hobbs, P. V., and Buseck, P. R.: Atmospheric tar balls: Particles from biomass and biofuel burning, J. Geophys. Res., 109, https://doi.org/10.1029/2003JD004169, 2004.

Pratt, K. A. and Prather, K. A.: Mass spectrometry of atmospheric aerosols--recent developments and applications. Part II: On-line mass spectrometry techniques, Mass spectrometry reviews, 31, 17–48, https://doi.org/10.1002/mas.20330, 2012.

Ramdahl, T.: Retene—a molecular marker of wood combustion in ambient air, Nature, 306, 580–582, https://doi.org/10.1038/306580a0, 1983.

Reinecke, T., Leiminger, M., Klinger, A., and Müller, M.: Direct detection of condensed particulate polycyclic aromatic hydrocarbons on a molecular composition level at low pg m -3 mass concentrations via proton-transfer-reaction mass-spectrometry, 2024a.

Reinecke, T., Leiminger, M., Klinger, A., and Müller, M.: Direct detection of polycyclic aromatic hydrocarbons on a molecular composition level in summertime ambient aerosol via proton transfer reaction mass spectrometry, Aerosol Research, 2, 225–233, https://doi.org/10.5194/ar-2-225-2024, 2024b.

Romay, F. J., Roberts, D. L., Marple, V. A., Liu, B. Y. H., and Olson, B. A.: A High-Performance Aerosol Concentrator for Biological Agent Detection, Aerosol Science and Technology, 36, 217–226, https://doi.org/10.1080/027868202753504074, 2002.

Schade, J., Passig, J., Irsig, R., Ehlert, S., Sklorz, M., Adam, T., Li, C., Rudich, Y., and Zimmermann, R.: Spatially Shaped Laser Pulses for the Simultaneous Detection of Polycyclic Aromatic Hydrocarbons as well as Positive and Negative

https://doi.org/10.5194/egusphere-2024-2587
Preprint. Discussion started: 12 September 2024

Inorganic Ions in Single Particle Mass Spectrometry, Analytical chemistry, 91, 10282–10288, https://doi.org/10.1021/acs.analchem.9b02477, 2019.

Schmidt, M., Irsig, R., Duca, D., Peltz, C., Passig, J., and Zimmermann, R.: Laser-Pulse-Length Effects in Ultrafast Laser Desorption, Analytical chemistry, 95, 18776–18782, https://doi.org/10.1021/acs.analchem.3c03558, 2023.

Shen, G., Tao, S., Wei, S., Zhang, Y., Wang, R., Wang, B., Li, W., Shen, H., Huang, Y., Chen, Y., Chen, H., Yang, Y., Wang, W., Wang, X., Liu, W., and Simonich, S. L. M.: Emissions of parent, nitro, and oxygenated polycyclic aromatic hydrocarbons from residential wood combustion in rural China, Environmental science & technology, 46, 8123–8130, https://doi.org/10.1021/es301146v, 2012a.

Shen, G., Tao, S., Wei, S., Zhang, Y., Wang, R., Wang, B., Li, W., Shen, H., Huang, Y., Yang, Y., Wang, W., Wang, X., and Simonich, S. L. M.: Retene emission from residential solid fuels in China and evaluation of retene as a unique marker for soft wood combustion, Environmental science & technology, 46, 4666–4672, https://doi.org/10.1021/es300144m, 2012b.

Shen, X., Saathoff, H., Huang, W., Mohr, C., Ramisetty, R., and Leisner, T.: Understanding atmospheric aerosol particles with improved particle identification and quantification by single-particle mass spectrometry, Atmos. Meas. Tech., 12, 2219–2240, https://doi.org/10.5194/amt-12-2219-2019, 2019.

Song, X.-H., Hopke, P. K., Fergenson, D. P., and Prather, K. A.: Classification of Single Particles Analyzed by ATOFMS Using an Artificial Neural Network, ART-2A, Analytical chemistry, 71, 860–865, https://doi.org/10.1021/ac9809682, 1999.

Spencer, M. T., Shields, L. G., Sodeman, D. A., Toner, S. M., and Prather, K. A.: Comparison of oil and fuel particle chemical signatures with particle emissions from heavy and light duty vehicles, Atmospheric Environment, 40, 5224–5235, https://doi.org/10.1016/j.atmosenv.2006.04.011, 2006.

Sultana, C. M., Cornwell, G. C., Rodriguez, P., and Prather, K. A.: FATES: a flexible analysis toolkit for the exploration of single-particle mass spectrometer data, Atmos. Meas. Tech., 10, 1323–1334, https://doi.org/10.5194/amt-10-1323-2017, 2017.

Woods, E., Smith, G. D., Dessiaterik, Y., Baer, T., and Miller, R. E.: Quantitative detection of aromatic compounds in single aerosol particle mass spectrometry, Analytical chemistry, 73, 2317–2322, https://doi.org/10.1021/ac001166l, 2001.

Zawadowicz, M. A., Froyd, K. D., Murphy, D. M., and Cziczo, D. J.: Improved identification of primary biological aerosol particles using single-particle mass spectrometry, Atmos. Chem. Phys., 17, 7193–7212, https://doi.org/10.5194/acp-17-7193-2017, 2017.

Zelenyuk, A., Imre, D., Wilson, J., Zhang, Z., Wang, J., and Mueller, K.: Airborne single particle mass spectrometers (SPLAT II & miniSPLAT) and new software for data visualization and analysis in a geo-spatial context, J. Am. Soc. Mass Spectrom., 26, 257–270, https://doi.org/10.1007/s13361-014-1043-4, 2015.

https://doi.org/10.5194/egusphere-2024-2587
Preprint. Discussion started: 12 September 2024

530 Zhang, Y., Pei, C., Zhang, J., Cheng, C., Lian, X., Chen, M., Huang, B., Fu, Z., Zhou, Z., and Li, M.: Detection of polycyclic aromatic hydrocarbons using a high performance-single particle aerosol mass spectrometer, Journal of environmental sciences (China), 124, 806–822, https://doi.org/10.1016/j.jes.2022.02.003, 2023.

Zhu, Y., Li, J., Zhang, Y., Ji, X., Chen, J., Di Huang, Li, J., Li, M., Chen, C., and Zhao, J.: Distinct Photochemistry of Odd-Carbon PAHs from the Even-Carbon Ones During the Photoaging and Analysis of Soot, Environmental science &
535 technology, 58, 11578–11586, https://doi.org/10.1021/acs.est.4c00764, 2024.

Zhuo, Z., Su, B., Xie, Q., Li, L., Huang, Z., Zhou, Z., Mai: Improved Aerodynamic Particle Con- centrator for Single Particle Aerosol Mass Spectrome- try: A Simulation and Characterization Study, Chinese Journal of Vacuum Science and Technology, 443–449, https://doi.org/10.13922/j.cnki.cjvst.202008026, 2021.

Zimmermann, R., Ferge, T., Gälli, M., and Karlsson, R.: Application of single-particle laser desorption/ionization time-of-
540 flight mass spectrometry for detection of polycyclic aromatic hydrocarbons from soot particles originating from an industrial combustion process, Rapid communications in mass spectrometry RCM, 17, 851–859, https://doi.org/10.1002/rcm.979, 2003.

Zimmermann, R., Passig, J., and Ehlert, S.: DEVICE AND METHOD FOR MASS SPECTROSCOPIC ANALYSIS OF PARTICLES, EP20180171596;WO2019EP58780, H01J49/00;H01J49/02;H01J49/16, 2019.

545